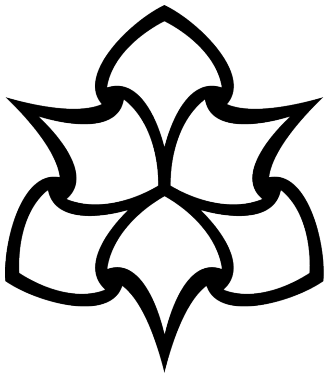

Nanocomposite Zirconium Nitride/Silver Coatings to Combat External Bone Fixation Pin Infections

David John Wickens

Department of Healthcare Sciences

Manchester Metropolitan University Manchester, UK

A Thesis submitted for the degree of

Doctor of Philosophy

Acknowledgements

I would firstly like to thank my director of studies Dr Kathryn Whitehead for her patience, support and technical advice throughout my PhD. I would like to thank Dr Glen West for providing support and instruction on the magnetron sputtering systems as well as theory behind the processes and coating characterisation techniques. I would also like to thank Professor Peter Kelly and Professor Joanna Verran for providing guidance and support throughout my project and Dr Stephen Lynch for his expertise and training on using the MATLAB software. I would also like to thank Dr Natalie Renevier at UcLan for providing access to the scratch tester and pin on disk instrumentation.

A special thank you to my parents who have been hugely supportive and encouraging throughout my whole PhD.

Abstract

External bone fixation provides rehabilitation for severely broken limbs. The nature of the pins compromises the skin at the entry point and creates an interface that is prone to infection by opportunistic pathogens. Pin tract infections possess one of the highest infection rates of implanted devices. Infection induces further physical and psychological stress to the patient as well as increasing healthcare costs. If the infection can be prevented there is the potential to reduce patient distress, related healthcare costs and the overuse of antibiotics. Using magnetron sputtering, zirconium nitride/ silver coatings were co-deposited onto medical grade 316L stainless steel. Combining the hard wearing properties of ZrN and the broad spectrum antimicrobial properties of silver, these nanocomposite coatings displayed the potential to combat pin tract infections. The coatings were characterised in terms of surface topography, morphology, chemical composition, physicochemistry, antimicrobial efficacy and bacterial retention towards *Staphylococcus aureus* and *Staphylococcus epidermidis*.

The Ti-ZrN/Ag coatings displayed an increase in nanotopography in comparison to the underlying stainless steel but no increase in microtopography was observed. The silver was deposited as particles in the coatings and the silver content increased linearly with an increase in magnetron power. The most antimicrobial coating was not necessarily the one with the most silver. The Ti-ZrN-Ag coatings were tested against two of the most commonly isolated bacteria from pin tract infections; *Staphylococcus aureus* and *Staphylococcus epidermidis*. The Ti-ZrN/Ag coatings displayed an effective contact kill towards both microorganisms, with the silver causing multiple bacterial physiological changes, reducing bacterial respiration and compromising the cell membranes. An increase in silver content displayed an increase in short term antimicrobial efficacy (< 1 hour) whereas following 24 hours contact time (humid conditions) no bacteria survived on the surfaces containing silver, regardless of the concentration.

To replicate an *in vivo* environment, the Ti-ZrN/Ag coatings were characterised in the presence of a blood conditioning film. The underlying topography of the surfaces were found to have an effect on the physicochemical properties of the adsorbed conditioning film. The surface chemistry also affected the adsorption of the conditioning film, with differences in surface morphology between the stainless steel and ZrN in comparison to the ZrN/Ag coatings. The short term antimicrobial activity was reduced when the surfaces were dry (similar to the environment the pin will encounter outside the body), however keeping the environment humid (similar to the environment the pin will encounter inside the body) the coatings demonstrated an antimicrobial effect over 24 hours.

Multifractal analysis was used to provide a method to quantify bacterial dispersion and density by analysing the micrographs of retained bacterial cells on the ZrN/Ag surfaces. Multifractal analysis found that with increasing silver content the densities of the retained *S. aureus* cells remained similar whereas the *S. epidermidis* decreased. *S. aureus* demonstrated a more heterogeneous dispersion and *S. epidermidis* a more homogeneous cell spread. Using this quantitative data acquisition method on the retention behaviour of bacteria displays potential to rapidly assess the surface – bacteria interfacial characteristics of biomaterials, thus, aiding improvement of surface characteristics of an implant at early research and development stages.

These results demonstrate the importance of thorough characterisation, microbiological and conditioning film testing when designing new coatings. This work has demonstrated that Ti-ZrN/Ag coatings have the potential to provide an actively antimicrobial pin coating *in situ*.

Thesis Organisation

This thesis is presented in eight chapters and follows a development process through five stages:

1) The production, surface characterisation and antimicrobial testing of the initial ZrN/Ag coatings.

2) Improvement of the coatings using an experimental array.

3) Production, surface characterisation and antimicrobial testing of the new Ti-ZrN/Ag coatings.

4) Investigation into the effect of a medically relevant conditioning film on the surface properties and antimicrobial status of the surfaces.

5) Using multifractal analysis as a method to quantify the density and dispersion characteristics of retained bacteria on the stainless steel, Ti-ZrN and Ti-ZrN/Ag surfaces.

Contents

List of Figures

List of Tables

1 Introduction

1.1 Biomaterial and implant infection

A biomaterial is defined as any type of material that is used to produce a device to replace or aid a function of the body in a safe, reliable and physiologically acceptable manner. The materials used for biomaterials are required to be systemically and pharmacologically inert within the body. However, items that are classed as being in contact with the skin, such as artificial limbs, are not included as a biomaterial because the skin acts as a barrier between the internal bodily systems and the external environments (Lakes and Park, 2007). There are many types of biomaterials, these include; metallic, glass, ceramic, polymeric and natural products such as proteins, that can be used to build these implant materials (Dee *et al.*, 2003). The focus of this work was metal nitride biomaterials, in particular pins used in stabilising broken limbs.

Due to their invasive nature implanted devices are prone to infection. Biomaterial infections, particularly bacterial implant infections, are of high significance in medicine (Chen *et al.*, 2006). In the UK, the cost associated with implant infections is estimated at £7-11 million per year, and in the USA costs were estimated for treatment of at least $50,000 per patient, and overall in excess of $250 million per year (Sculco, 1995, Campoccia *et al.*, 2006, Kazemzadeh-Narbat *et al.*, 2010). With the use of implants increasing indefinitely, in part due to an ageing population, methods to prevent and reduce infection are greatly sought after (Harris and Richards, 2006). The failure of medical implants to resist colonisation by pathogens and the frequency of infection depends on many factors. These include the presence of potentially pathogenic bacteria and commensals surrounding the implant, surrounding tissue necrosis and the surface characteristics and material type used for the construction of the medical implant (Chen et al., 2006). The most common infections are caused by opportunistic pathogens, which are part of the body's natural flora, generally *Staphylococcus spp*. It was stated by Harris and Richards (2006) that *Staphylococcus aureus* infections are

most common in metal biomaterials whilst *Staphylococcus epidermidis* are more frequently associated with polymeric biomaterials. However, *S. epidermidis* is still the second most isolated pathogen from metal implant infections (Darouiche, 2004, Harris and Richards, 2006, Coester *et al.*, 2006) This may be due to surface properties of the bacterial cells and the physicochemical interactions with the substratum.

1.1.1 External Bone Fixation Devices

External bone fixation is a method widely used in orthopaedics for a range of correctional and rehabilitation procedures. External fixation is most commonly used in the repair of severe fractures of the long bones, however it is also applied throughout correctional surgery, for example in bone lengthening and correction of bone deformities from complications such as rickets and brachymetatarsia (stunted growth of a metatarsal) (Gilbody and Nayagam, 2008, Nayagam, 2010, Eralp *et al.*, 2011). The advantages of using external fixation include improved stability for severely comminuted fractures, allowing for weight bearing on the limb, increased bone healing rates, as well as being less invasive than internal fixation structures (Timms *et al.*, 2013) (Figure 1).

There are a range of pin and wire types used for different applications. There are devices which use pins, known as half-pins, which are usually over 3mm in diameter and often screwed into the bone using a thread machined on the end of the pin; these may be self-tapping, follow a drilled pilot hole, or self-drilling (Figure 2). Pins less than 3mm are usually classed as wires and mostly have no thread and are either fixed into the bone using other methods such as clamps, or the wire has a stopper on it which secures it through the drilled hole (Figure 3).

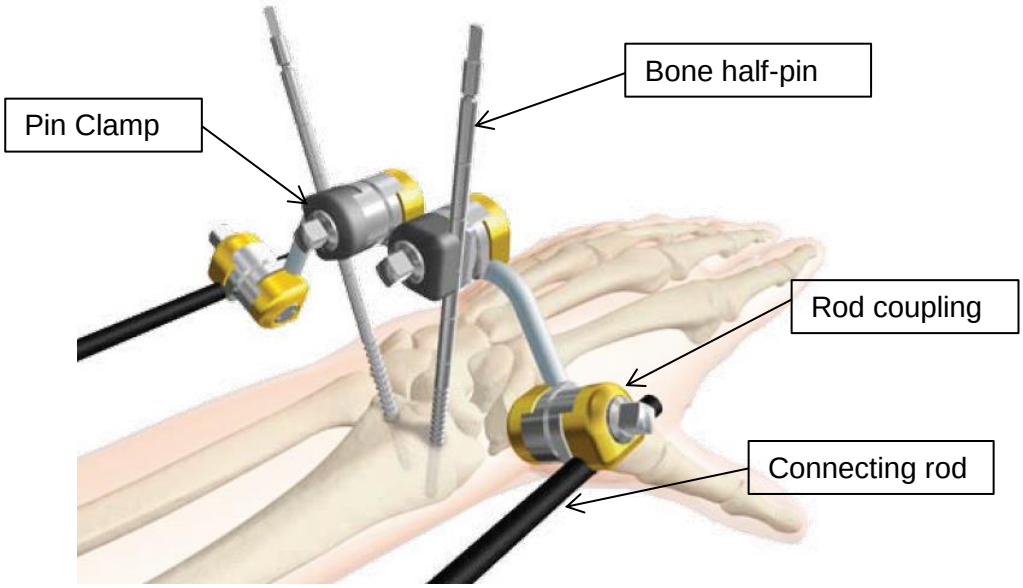

Figure 1: Schematic diagram illustrating the design of an external fixation device (Asche *et al.*, 2006), demonstrating the components used in external bone fixation on an example pin site.

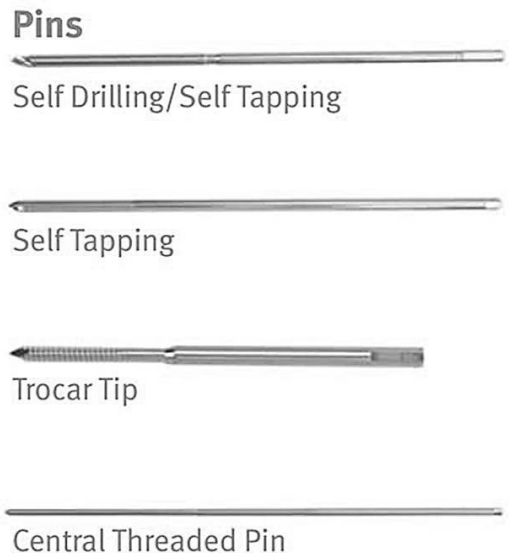

Figure 2: An example of some available external fixation pins and the types of thread (Zimmer, UK). The self-drilling pins do not require pre-drilling, whereas the other types do require drilling. The trocar tip pin is used on a specialised system which the pin is inserted through during drilling to guide the pin and protect the surrounding soft tissue. The central threaded pin allows anchorage to the bone at two sides using one hole.

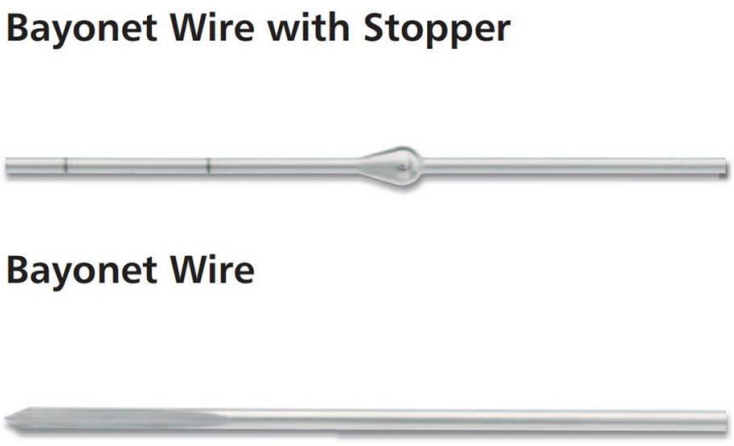

Figure 3: Examples of external fixation wires (Orthofix, USA) which are used by either insertion into or through the bone and often used in conjunction with pins on a spatial frame.

Due to the nature of the procedure, the pin entry sites are prone to infection. The procedure creates an external-internal interface between the body and the environment at the pin entry site that remains exposed for the duration of the implant; partially due to movement of the tissue around the pin and the presence of the pin keeping the wound open. This leaves the wound vulnerable to colonisation of opportunistic pathogens and/or skin commensals surrounding the wound. Pin entry sites are classified as "percutaneous", a term also used to define devices entering the skin, usually for the administration or removal of fluids. Terminology for the entry sites of the pins include; "pin tracks", "pin tracts", "pin (wound) sites", "percutaneous pin sites" and "insertion sites" (Timms *et al.*, 2013).

A pin tract infection will occur at the entry site whereupon, if left untreated, it will spread down the pin into the tissue, causing potential pin loosening and eventually an infection within the deep tissue or bone. This may lead to serious complications such as osteomyelitis (inflammation and infection of the bone) and bacteraemia (bacterial infection of the blood stream) (Harris and Richards, 2006). Many authors state the most effective method of eliminating a pin tract infection is the removal of the device, followed with a course of systemic antibiotics (Coester *et al.*, 2006, Harris and Richards, 2006, Trampuz and Zimmerli, 2006). Although the rate is not specified, Coester *et al.* (2006) states that following treatment re-infection may still occur. Others have suggested that the severity of the infection will indicate whether removal is required or if antibiotic therapy is sufficient to eliminate the infection (Mahan *et al.*, 1991, Checketts *et al.*, 1993, von Eiff *et al.*, 2005), with Ferreira and Marais (2012) stating that removal should occur at Checketts stage '4' or above (Table 1).

There is no single validated measure for pin site infection, however factors that may lead to an incidence of pin tract infection include: the patient's immune status, whether the fracture is open (the bone has penetrated the skin during the break), the methods employed by the surgeons both hygienically and technically, the areas in which the

pins are used, the type of pins used, the techniques used for insertion of the pins and the methods used for pin site after-care following the procedure and throughout the duration of the rehabilitation (Davies *et al.*, 2005). The methods used by the medical staff to assess and classify infection are also important factors in the definition of the severity of the infection and in the control of pin tract infections.

Santy (2010) reviews the methods of infection assessment criteria to recognise infection at pin sites. Six publications of assessment criteria were reviewed and it was found that all methods operate strongly on the opinion of an individual and this undoubtedly varies between people. The most common used grading system is that of Checketts et al. (1993, 2001) utilizing 6 grades: 1-3 denoting minor infections and 4-6, major infections (Table 1). However, despite this classification system being described as the “gold standard” (Streiner, 2003), there is still controversy over the validity of using this and other grading systems to assess infection. Overall, the conclusion of the study by Santy (2010) demonstrated that all techniques of identification were flawed and lacked discriminating criteria to enable the clinicians to identify changes in pin site morphology. Due to the variety of assessment methods, the range of cleaning methods and the many different areas of the body that use external bone fixation, defining an accurate infection rate is difficult, however a short consensus of infection rates given in literature can be compiled (Table 2).

Table 1: The Checketts *et al.* infection grading system (Checketts *et al.*, 1993).

Grade	Appearance
Minor Infections	
1	Slight redness around the pin together with a little discharge and settles with better pin site care.
2	Redness in the skin, discharge from the pin site and pain and tenderness in the soft tissues. Settles with improves pin site care and a short course of appropriate antibiotic which is chosen according to the organism cultured. In almost all cases the organism will be *Staphylococcus aureus*.
3	The same as grade 2 but fails to settle with diligent pin site care and the appropriate antibiotic. The affected pin or pins are re-sited and external fixation can be continued.
Major Infections	
4	Severe soft tissue infection involving several pins, sometimes with loosening of the pins. Re-siting of the pins is impossible and external fixation must be abandoned.
5	There is radiographic evidence of osteomyelitis in addition to severe soft tissue involvement. External fixation must be abandoned and the infection then resolves.
6	Infection occurrs after fixator removal following completion of treatment. The pin heals initially but subsequently at intervals, will break down and discharge. The infection will clear with curettage (instrument used to remove tissue) of the pin track in the soft tissue and bone. Will usually show sequestra (dead bone separated from the living tissue) in the bone with reaction in the adjacent periosteum on the proximal cortex.

Table 2: A short consensus of literature, comparing the infection rate of pin tracts throughout a range of studies.

Author	Subjects (N)	Infection Rate (%)	Location
(W-Dahl, 2003)	50	15%	Knee
(Ward, 1997)	126	10.2-10.7%	N/A
(Sims and Saleh, 2000)	2773	71%	Leg (Femur & Tibia)
(Camathias *et al.*, 2012)*	204	35%	Tibia, Femur, Humerus & Forearm
(Ahlborg, 1999)	314	21%	N/A
(Davies *et al.*, 2005)	120	89% (Regular cleaning) 64% (Ilizarov cleaning)	Radius
(Mahan *et al.*, 1991)+	214	74.8%	N/A
(Grant *et al.*, 1992)	N/A	10%	N/A
(Antoci *et al.*, 2008)×	116	96.6% (Half Pin) 78% (Hybrid) 33% (Fine Wire)	Tibia and Femur
(Parameswaran *et al.*, 2003)	285	11.2%	N/A

N/A: Study did not specify the area the assessed pin sites were located

*Rate described as local inflammation, not explicitly an infection.

+Amount of pins that cultured positive. This does not denote an infection.

×Assessed according to Paley (1990).

The subject of pin site care is a heavily discussed area with vastly differing results and outcomes. Lee-Smith (1999) focussed more on the aftercare and nursing procedures, and defined that the nursing staff should be aware of the patients vulnerability. They also referred to current research in infection control and how it can be used to improve patient care in orthopaedics (and all surgical disciplines for that matter). As there is no general consensus in the literature towards optimal pin care to prevent infection, a blind study was undertaken by Camathias et al. (2012) involving the effect of pin care versus no care at all. The care of the treatment group involved; removing crusts around the pin site, irrigation with sterile saline, drying with sterile swabs and then dressing with iodine pre-soaked dressings applied to the pin site with a dry wrap. The subjects in the group with no treatment were left untouched. They found that 35% of the pin sites demonstrated inflammation but explained that this does not always denote infection and could be just soft tissue irritation following the trauma of the pin or inflammation displayed from normal skin colonisation. This could result in incorrect diagnosing with the Checketts (1993) system if lack of experience of the medical staff was to occur. In addition, microbiological swabs are not always a reliable method to diagnose pin tract infections, as the results may often display what could be normal skin microflora. Thus it was concluded that there was no significant difference in the infection rates between the pin sites that had been cleaned using the Ilizarov technique (Grant *et al.*, 1992) when compared to these pin sites which had no cleaning regimen at all (Table 3). Their concluding remarks were that cleaning regimens do not need to be undertaken to reduce infection rates. However, other publications have found that studies such as Camathias et al. (2012) have not altered the practices of cleaning regimens currently in place, since a questionnaire found that 90% of the participants believed that pins should still be cleaned with chlorhexidine and alcohol. Other studies in this area have also been carried out. Dahl et al. (2003) studied the difference between daily and weekly pin site care. The pins were cleaned in a 0.9% NaCl solution and the infections assessed using the Checketts classification, whereby they concluded that no difference

in infection rate was observed. Ferreira and Marais (2012) found that pin site care did not have a universally recognised protocol and there are many methods and products available to be used on pin sites, which alter from one hospital to another. They also found that the time that pin tract care is to be undertaken varies greatly in literature from twice daily, daily, weekly or 'when required' (Lee-Smith *et al.*, 2001). The author also found that the cleaning solutions vary greatly depending upon the literature and found a range of; sterile water, soap and water, saline, peroxide, polyvinylpyrrolidone iodine, isopropyl alcohol and chlorhexidine. Their findings were that although every effort is made by the medical teams to prevent pin tract infections a standardised pin site care protocol should be designed and adopted that covers all aspects covering pin loosening and infection to help reduce this common complication. Although there are a range of techniques and cleaning solutions used to control pin tract infections, there is still an issue with high infection rates. Thus new measures of control need to be developed to combat this problem.

Table 3: The comparison of the regular and Ilizarov cleaning techniques taken directly from Davies et al. (2005).

Regular Cleaning	**Ilizarov Cleaning**
Normal handling of the wires/pins	Non-touch handling of the wires/pins
Continuous drilling with irrigation	Pulsed drilling (Stop-Start) with irrigation
Bone swarf (bone chips from drilling) removal	Bone swarf removal
Dry dressings used for the pin-site at the completion of the operation	Immediate pin-site dressings in alcoholic solution of chlorhexidine with pressure to reduce haematoma (Localised bleeding/swelling); changed at completion of the operation if bloodstained
Original theatre dressings left undisturbed for 48 hours	Pin sites cleaned daily for three days to ensure blood removal; pin cleaning using a solution of 70% alcohol and dressing moistened with Hydrex (chlorhexidine)
Daily cleaning thereafter with normal saline, crust removal and simple non-adherent dressings only in the presence of exudates, otherwise left uncovered.	Occlusive pressure dressing after the third day; pin cleaning and dressing changes repeated every seven to ten days using the same technique

1.2 Biomaterial Surfaces

1.2.1 Biomaterials

Bodily implants used in modern medicine come in a vast range of materials, containing different textures, surface properties and surface chemistry depending upon the application. The types of materials range from flexible and rigid polymers to stainless steels, titanium and many alloys and ceramic compounds. Ceramic materials have many properties including high tensile strength, being lightweight (in some applications) and having low corrosion and cytotoxicity towards bodily fluids (Ortiz *et al.*, 2011). For orthopaedic implants the majority of biomaterials used in today's applications involve stainless steel, titanium and polymers. External fixation devices are mostly made of stainless steel or titanium. It is suggested that titanium implants can contribute towards a reduction of bacterial infection over stainless steel, due to their surface properties, rendering titanium a more suitable material for the application although in some countries it is not always favoured over medical grade stainless steel (Arens *et al.*, 1996).

1.2.2 Coatings

The method of combatting infection in implants can come from a variety of methods to introduce antibiotics. Some examples include; oral antibiotics, intravenous antibiotics, ceramic beads impregnated with antimicrobials to be inserted locally to the infection site, topical treatments such as creams and lavages, and antimicrobial coatings applied to the implanted material, either polymeric (polyurethane sleeves) or metallic (Forster *et al.*, 2004, Wang *et al.*, 2004, DeVasConCellos *et al.*, 2012, Goodman *et al.*, 2013, Kazemzadeh-Narbat *et al.*, 2013, Liu *et al.*, 2013). The method used in this investigation will be the use of a metal alloy nanocomposite coating, produced using magnetron co-sputtering, to demonstrate potential antimicrobial properties. A putative

antimicrobial alloy that has been studied for use in this work was zirconium nitride/silver.

1.2.2.1 Zirconium (Zr)

Zirconium is a grey/white lustrous metal from the transition metals area of the periodic table. It is a group 4 metal and has an atomic weight of 91.22 (Winter, 2012). Zirconium has desirable corrosion resistant properties towards most agents including sea water, acids and alkalis, so is often used by the chemical industry where the use of corrosive agents is common. Zirconium is also a superconductor at low temperatures and can be used to make superconductive magnets (Emsley, 2011). Due to the properties of zirconium including that is an extremely hard elementmuch like titanium, it can be used as a medical implant material (Guglielmotti *et al.*, 1997). Studies of zirconium used as implants either as thin film coatings on polymers or as a pure solid material display similar osseointegration (allowing of bone growth onto the surface) properties to titanium, with no cytotoxic properties displayed (Wetzel *et al.*, 2008, Mueller *et al.*, 2013).

1.2.2.2 Zirconium nitride (ZrN)

Medical devices, particularly in orthopaedics are prone to wear and damage from contact with bone and other biomaterials, or chemical and mechanical stresses from cleaning, as is the case with external fixation pins. Protecting surfaces from wear and the induction of surface scratches can be performed with the addition of hard wearing ceramic coatings (Kertzman *et al.*, 2008). Zirconium nitride is a hard wearing coating that is commonly deposited onto cutting and forming tools to improve the performance life as well as being a decorative coating in cases due to its gold appearance. (Pilloud *et al.*, 2003, Aouadi *et al.*, 2004, Aouadi *et al.*, 2006, Deng *et al.*, 2008b, Kelly *et al.*, 2010b).

Alongside having an excellent mechanical strength, zirconium nitride has been recognised as a potential biomaterial due to its excellent corrosion resistance and chemical stability as well as good biocompatibility and low cytotoxicity to human cells (Okazaki *et al.*, 1996, Brugnoni *et al.*, 1998, Aouadi *et al.*, 2004, Kertzman *et al.*, 2008). However, from the literature, it is apparent that its application as a coating for medical devices has yet to be fully investigated.

1.2.2.3 Silver (Ag) and its antimicrobial properties

Silver in its bulk metallic form is inert and has no antimicrobial properties; it requires moisture such as bodily fluids or water to ionise from metallic silver (Ag^0) into three possible oxidation states: Ag^+, Ag^{2+} and Ag^{3+}, of which Ag^+ is the most common oxidation state and eminently antimicrobial (Klasen, 2000, Edwards-Jones, 2009, Rai *et al.*, 2009).

Silver has been used in the treatment of chronic wounds and burns for centuries, with evidence found that silver had been used for health improvements as far back as 1000 B.C., to make water potable for drinking (Rai *et al.*, 2009). Silver is more commonly used as an antimicrobial in ion and salt form, for example as silver sulphadiazine, silver nitrate and as metallic incorporation into medical and health products. Metallic silver has been impregnated into wound dressings by either incorporating woven fibres or using physical vapour deposition. These displayed broad-spectrum antimicrobial activity towards many microorganisms which may potentially reduce wound infection and aid healing (Chen *et al.*, 2006, Kim *et al.*, 2007, Necula *et al.*, 2009a). More recently, the application of silver has been brought to other areas of medicine such as the coating of catheters and dental abutments (Kim et al., 2007).

There are many theories concerning the mechanism by which silver ions cause bacterial cell death, and these differ depending upon the organism type, cell physiology, strain and methods used. Many authors have found multiple changes to

bacterial physiology when treated with silver (Modak and Fox, 1973, Schierholz *et al.*, 1998, Darouiche, 1999, Percival *et al.*, 2005, Chen *et al.*, 2006, Allaker, 2010, Radzig *et al.*, 2013). The most common hypothesis for the antimicrobial action of silver involves silver ions binding to the proteins and enzymes in the cell wall, cell membrane and peptidoglycan. This causes structural changes in the cell wall, such as pits. This increases cell permeability, leading to distortion and finally lysis of the cells (Sondi and Salopek-Sondi, 2004, Pal *et al.*, 2007, Edwards-Jones, 2009). Another antimicrobial mechanism of silver is the ability to inter-chelate with the phosphorus elements in DNA, causing it to lose its ability to replicate and express ribosomal subunit proteins and other cellular proteins (Schierholz *et al.*, 1998, Kim *et al.*, 2007, Pal *et al.*, 2007, Edwards-Jones, 2009, Rai *et al.*, 2009). This would be described as a bacteriostatic method of eradication, preventing the bacteria from dividing. Rai et al. (2009) described silver ions as having a high affinity for bacterial cell membranes, tissue proteins, nuclear membrane and respiratory enzymes, the latter resulting in inhibition of respiration and replication. This may be explained since Kim et al. (2007) suggested that a positive charge is required for antimicrobial efficacy, which also allows attraction between the positively charged ions and the negative polarity of the cell membrane of some bacteria. Gram negative bacteria are said to be more susceptible to silver ions than Gram positive bacteria due to the reduced thickness of the peptidoglycan layer just outside the cell membrane (Goering *et al.*, 2008). Gram negative bacteria have a thin (5-10nm) peptidoglycan layer under an additional outer membrane, whereas Gram positive bacteria have a thicker (20-80nm) layer outside the cell membrane. This relationship to cell wall thickness and antimicrobial susceptibility is not the case for all metal ions, antimicrobials or bacteria (Goering *et al.*, 2008).

1.2.3 Zirconium Nitride Silver (ZrN/Ag)

Co-depositing zirconium nitride and silver creates a nanocomposite thin film, which has been shown to combine the hardness and scratch resistance of the metal nitride with

silver nanoparticles embedded in the matrix, the silver acts as the antimicrobial. Silver nanoparticles are formed because reacted silver nitride is thermodynamically unstable, therefore deposits onto the surface as particles embedded in the zirconium nitride matrix. The silver is not deposited in layers because of the deposition rate of the silver and the rotation of the substrates between the silver and zirconium nitride deposition. These coatings produced antimicrobial effects in the form of a surface contact kill, which is relevant and effective in the prevention of pin tract infections (Kelly *et al.*, 2011, Wickens *et al.*, 2012). As discussed previously, zirconium nitride (1.2.2.2) and silver (1.2.2.3) are both materials with desired properties in the field of biomaterial design that may be used to combat infection, reduce bacterial colonisation as well as being hard wearing (having high scratch and high wear resistance) and also the potential to have anti-adhesive properties towards microorganisms. Previous studies have investigated zirconium nitride-silver, titanium nitride-silver and chromium nitride-silver (Kelly *et al.*, 2010a) and results suggested that zirconium nitride-silver displayed the most attractive antimicrobial properties in relation to tribological properties. Thus within this work zirconium nitride and silver were deposited together in a thin film capable of adhering to stainless steel implant surfaces using a physical vapour deposition method called magnetron sputtering. Once developed and generated, this coating was characterised and tested in a number of microbiological assays.

1.3 Physical Sputtering

1.3.1 The Concept of Sputtering

Sputtering has been a long recognised phenomenon since 1852 where it was recorded as the vaporisation and film formation of metals, but was only fully recognised in the press in the later 1890's (Grove, 1852, Crookes, 1891). The phenomenon of sputtering occurs when ions collide with a solid and lead to the ejection of the target (solid) atomic particles during the bombardment process (Šroubek, 1981). This process occurs under a high vacuum (1 x 10^{-3} mBar), approximately 1 million times lower than atmospheric pressure. This is achieved using special pumping groups combining mechanical rotary pumps and molecular pumps using diffusion, turbomolecular or cryogenic pumps. Under vacuum, the amount of molecules in the chamber environment are reduced, to such an extent that the mean free path (distance a molecule can travel before colliding with another) is increased.

The concept of sputtering can be simply described as "a billiard game on an atomic scale", using the momentum transfer of accelerated ions to initiate a collision cascade, which will dislodge and eject atoms of the target material (Figure 4) (Bräuer *et al.*, 2011).

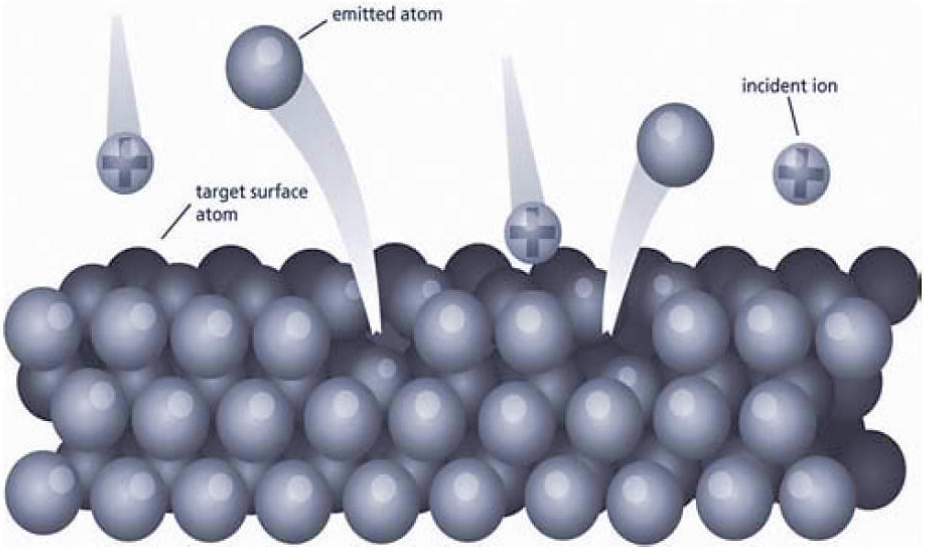

Figure 4: The principal concept of sputtering, demonstrating the incident ions colliding with the target surface and dislodging and emitting atoms of material from the surface (Bräuer *et al.*, 2011).

1.3.1.1 Nucleation and Film Growth

When physical vapour deposition is used to produce a thin solid film three stages occur: 1) under vacuum, the creation of a vapour phase of the deposition material is produced within the vacuum chamber by sputtering 2) the sputtered atoms (vapour phase) are transported from source to substrate through diffusion and 3) condensation of the material as a film growth on the substrate. The coatings are formed on the substrate surface by a succession of occurrences known as nucleation and growth. The nucleation and growth of the thin films depends upon the thermodynamic parameters of the deposition material and the substrate - surface interaction. Three modes of nucleation that will be discussed are 1) the Volmer-Weber model, 2) the Frank-Van der Merwe model and 3) Stranski-Krastanov model (Alfonso *et al.*, 2011). The Volmer-Weber model describes nucleation as three-dimensional crystals forming on the substrate surface while the rest of the substrate is free of any condensed phase. Nucleation occurs in the form of discrete three-dimensional nuclei on the surface of the substrate. The number of nuclei and the size of the nucleus then increase and grow until they intersperse and form a continuous film (Figure 5a). The Frank – van der Merwe model describes coating deposition when nucleation occurs in the form of a monolayer island of the deposit. Eventually these monolayers will grow together to form a complete monolayer and the process then repeats itself (Figure 5b). The Stransky - Krastanov model combines both layer by layer and three-dimensional nucleation, which is most common with metallic and ceramic deposition onto metal substrates. The nucleation and growth usually occurs in a layer by layer deposition and then subsequently begins to form discrete three dimensional nuclei (Figure 5c) (Alfonso *et al.*, 2011).

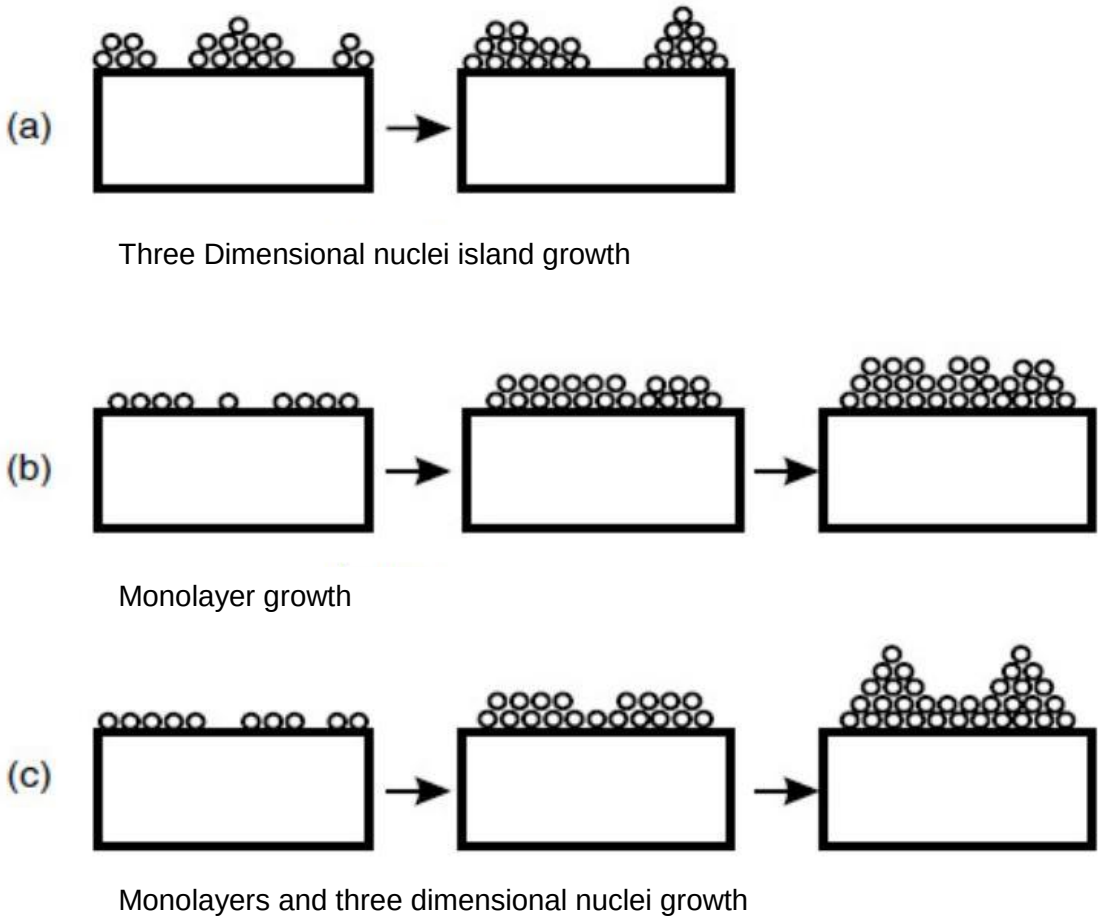

Figure 5: Modes of film nucleation and growth, demonstrating a) Volmer-Weber island growth, b) Frank van der Merwe layer growth and c) Stranski-Krastanov layer and island growth (Harsha, 2005, Alfonso *et al.*, 2011)

1.3.2 Magnetron Sputtering

Magnetron sputtering is a vacuum coating method originating from the physical vapour deposition family, along with evaporative and cathodic arc deposition. Magnetron sputtering has been developed largely since the late 1960s to produce surface coatings and is one of the most rapidly growing methods in the industry and vacuum technology (Nicolaus and Schäpers, 2006). The technique allows the coating of thin metals, alloys and compound films onto most solid substrates. These can be used for applications including tool coatings, aerospace and automotive parts, reflective coatings, data storage devices, for example compact disks (CDs), and to improve the corrosion resistance of materials (Nicolaus and Schäpers, 2006, Kelly and Bradley, 2009).

The magnetron uses the combination of an electrical power source and a magnetic field interacting in a reduced pressure environment to produce and control a plasma. Plasma, known as the fourth state of matter, is a mixture of positive ions, negative electrons, neutral particles and radicals, yet in a magnetron plasma the ions and electrons are of equal concentration it is of a quasi-neutral polarity within its bulk, with electrical fields only developing at the interfaces of other surfaces (Nicolaus and Schäpers, 2006).

During magnetron sputtering, the magnetic field lines confine electrons in the plasma to the vicinity of the cathode, which is usually a metallic plate of the material to be deposited and is referred to as the target (Figure 6a). These electrons ionise particles of inert process gas (most commonly argon). The electric field increases the kinetic energy of the ions, causing them to bombard the target (cathode). These collisions release secondary electrons into the plasma and dislodge atoms of coating material scattering them in different directions, of which some diffuse towards and condense on the substrate (item to be coated) as a thin film. The substrate can be electrically biased (negative voltage) to increase the energy delivered to the growing film through positive ion bombardment and, thereby modify the film structure (Schiller *et al.*, 1993, Nicolaus

and Schäpers, 2006, Kelly and Bradley, 2009). For the deposition of compound films, e.g. metal nitrides, a reactive gas, in this case nitrogen is also introduced into the plasma and the process is known as reactive magnetron sputtering.

A type (II) unbalanced magnetron contains a stronger magnetic field from the outside pole than the inside (type (I) being the opposite) (Figure 6b) (Window and Savvides, 1986b). This alters the field lines by opening them up from the target vicinity allowing some electrons to break away from the confinement of the target (Figure 6). The unbalanced magnetron configuration allows a greater plasma density further away from the target so that items can be coated from a further distance. This type of magnetic configuration for magnetrons is the most common, if not the sole configuration used in all magnetron sputtering situations.

A closed field magnetic configuration occurs when magnetrons have opposing polarities (for example S-N-S and N-S-N). This closes the field lines and directs the electrons in the plasma to the vicinity of the substrate, therefore both plasma density and ion bombardment at the substrate are increased allowing a more dense film to be deposited (Figure 7) (Savvides and Window, 1986).

There are a number of operating parameters that can be varied, including the process and reactive gas flow, substrate bias, power magnitude and the power delivery method to the magnetrons including the pulse frequency. Every parameter change will alter the plasma characteristics, and hence the deposition energy, which can potentially alter the characteristics of the deposition rate and coating morphology. The alterations of the coating structure in relation to the differing parameters can be roughly mapped out using a structure zone model, the most popular example being the Thornton structure zone model. This model demonstrates that with an increase in process gas pressure the coating to be deposited has a dense columnar structure. However an increase in substrate temperature (related to power applied to the magnetron) results in the

columnar structure increasing in size until it is deposited as a granular structure (Figure 8) (Thornton, 1974). By carefully controlling both the process gas pressure and substrate temperature it is theoretically possible to achieve the desired coating morphology.

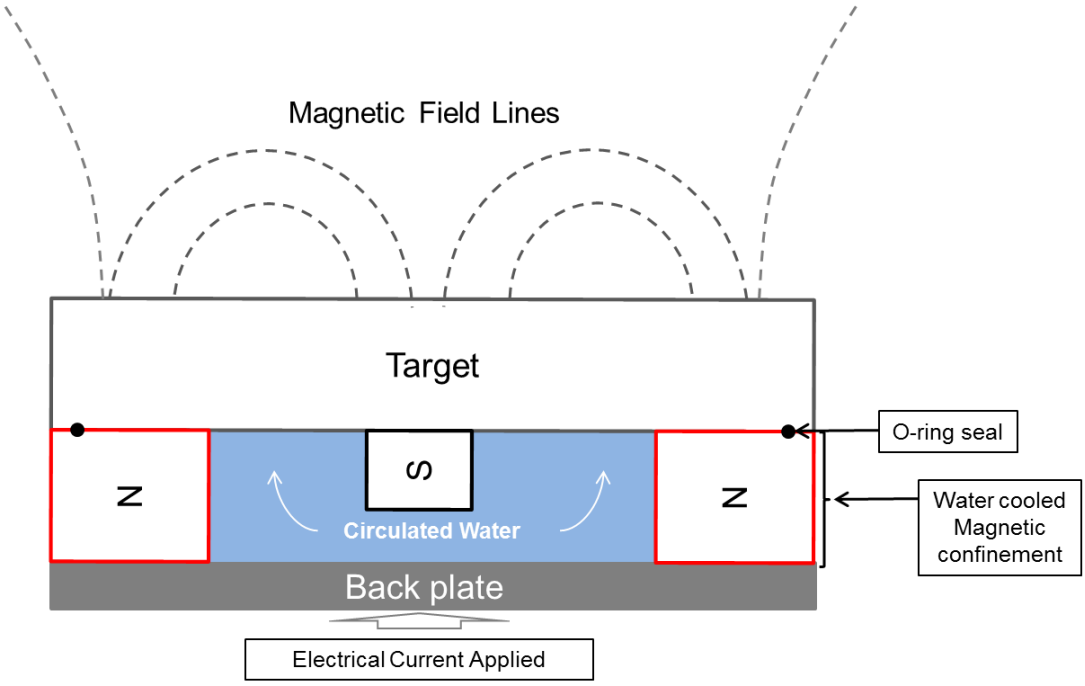

a)

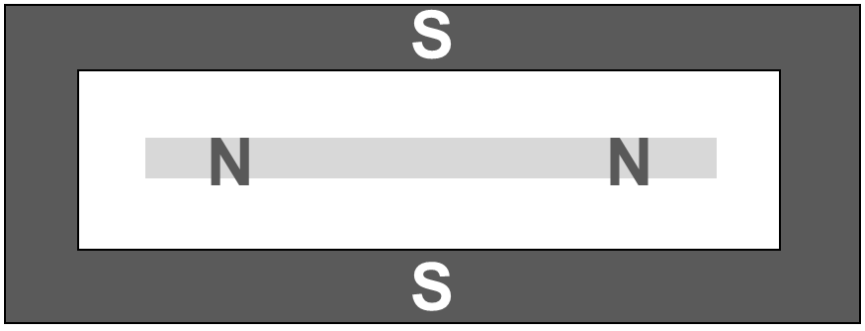

b)

Figure 6: Schematic transverse plane diagram of a) A planar magnetron displaying the positioning of the 'target' of pure metal to be sputtered, the water cooled space behind containing the magnets and the backing plate to which the electrical power is applied, b) The magnetic configuration of the Type (II) unbalanced magnetron from a frontal plane view, the inside magnet being weaker than the outside.

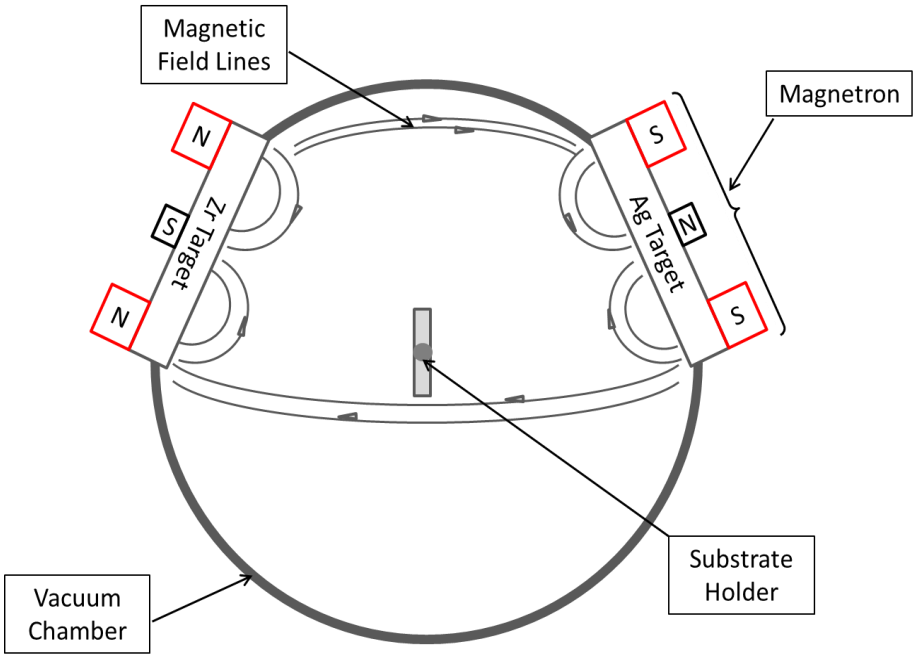

Figure 7: Schematic diagram of a closed field unbalanced magnetron configuration. The central pole magnets are smaller than the outer ring demonstrating an unbalanced configuration. The grey lines represent magnetic field lines that are closed between the magnetrons due to the opposing poles.

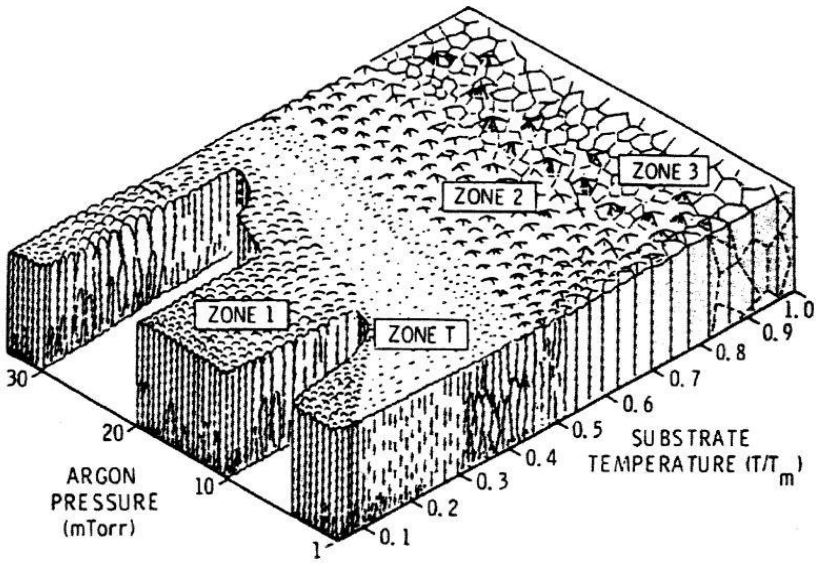

Figure 8: The Thornton Structure Zone Model for sputter deposition. *T* is the substrate temperature, which is relative to the deposition energy and argon pressure which, when increased would increase the probability of particle collision in the plasma (Thornton, 1974, Miao *et al.*, 2003).

1.3.2.1 Process Gas

The process gas is the inert monatomic gas that is introduced into the chamber throughout sputtering and these atoms will be responsible for the sputtering process. Thus, the chosen gas needs to be inert when in the presence of metals because if a gas such as oxygen is used as the process gas, the sputtered particles will react with the oxygen and deposit as different oxygen containing compounds instead of the pure metal. The gas chosen is most commonly one from the noble gases group of the periodic table because they are stable and inert due to their outer electron shell being full. The most common gas used as a process gas is argon because it possesses a heavy molecular weight and is most abundant and cost effective for the user. The heavy molecular weight allows a higher kinetic energy transfer when the ions collide with the cathode (magnetron) target surface, providing a high sputter yield.

1.3.2.2 DC Magnetron Sputtering:

Direct current (DC) power delivery in magnetron sputtering can be argued as one of the most abundant and successful sputtering techniques used, due to the range of applications it can serve. DC magnetron sputtering can be used for industries such as the coating of data storage devices, reflective coatings, such as mirrors and automotive headlamps, corrosion resistant coatings, and hard coatings to improve the life of tools (Savvides and Window, 1986, Window and Savvides, 1986a, Window and Savvides, 1986b, Teer, 1988, Sproul *et al.*, 1990). Deposition of metallic coatings and nitrides can be achieved easily using DC sputtering, however deposition of dielectric coatings or insulating thin films can prove problematic. During reactive sputtering (see 1.3.2.4) the outsides of the target, adjacent to the sputtering erosion path (racetrack) become coated with an insulating layer of the reactive product (most often oxide coatings). This area charges up with positive ions that cannot escape the negative polarity of the magnetron until it breaks down in the form of an arc, where the excess charge releases itself onto a grounded area of the chamber, for example the magnetron shields or the

chamber walls. This is problematic because when an arc occurs, a ‘droplet’ of material is ejected from the target and may condense on the substrate surface causing surface defects. It also makes the process unstable, especially if the plasma emissions are being monitored (1.3.2.4.2).

For a number of years titanium, zirconium and chromium nitrides have been deposited onto cutting and forming tools using DC magnetron sputtering until around the last 20 years, when pulsed magnetron sputtering was developed.

1.3.2.3 Pulsed DC Magnetron Sputtering

Pulsed DC magnetron sputtering is achieved when the power to the magnetron is delivered in a square wave mono-polar format; the power is applied for a set amount of time and the power is off for the rest of the pulse cycle. The proportion of time the power supply is not applying power to the magnetron is known as the ‘off time’ and the amount of time the power is applied to the magnetron in relation to the entire pulse cycle is referred to as ‘duty’ and is displayed as a percentage. A high duty, for example 90% over a 10 µs pulse cycle (100 kHz frequency) would be 9 µs of the power on and 1 µs of the power not applied. An example of a 50% duty pulse cycle is shown (Figure 9). The oscillations displayed on the target current waveform are overshoots, which are an artefact of the power supply electronics. The target voltage is curved and not a square wave due to the combination of the plasma dynamics and the power supply.

The benefits of using pulse DC power over DC power allow the potential charge on the ‘poisoned’ areas of the target surface to be reduced, suppressing the amount of hard arcs occurring. However, using operating conditions which are incorrect can still allow arcs to occur. Further, the use of pulsed DC magnetron sputtering changes the plasma characteristics. This increases the plasma density due to more energetic electrons and changes the structure of the deposited coating (Anonymous, 2005b, Kelly and Arnell, 2000, Kelly and Bradley, 2009). Lin et al (2010) found that pulsed DC deposition of CrN

thin films created a more dense structure that was harder and more wear resistant over DC deposition. Schiller et al (1993) also found that depositing TiN thin films using DC and pulsed DC magnetron sputtering caused the plasma density to rise and the coating structure to become denser and the surface roughness to decrease. They also found that substrate bias (1.3.2.5) caused the morphology of the film to appear almost structureless.

1.3.2.4 Reactive sputtering

Reactive magnetron sputtering is the sputtering of a metallic target in the presence of a reactive gas to produce, most commonly, oxides and nitrides due to the atoms ejected from the target reacting with the gas in the vacuum chamber (Danisman *et al.*, 2009). The reactive gas is either added to the vacuum chamber at a known amount, following a hysteresis study (see 1.3.2.4.1), or is added by a plasma emissions monitoring (PEM) system, which uses a closed-loop system to monitor the plasma and vary the amount of reactive gas added to produce a thin film of the correct composition (see 1.3.2.4.2).

1.3.2.4.1 Hysteresis

Reactive magnetron sputtering can be divided into three modes: 1) metallic, 2) transition and 3) reactive and these three modes depend upon the amount of reactive gas added (Musil *et al.*, 2005, Danisman *et al.*, 2009). At low flow rates of reactive gas the majority of the gas is adsorbed (gettered) by the sputtered material, therefore no significant change in the gas pressure or voltage is seen. This means that the sputtered material is still being deposited in a metallic mode. Following an increase of reactive gas flow rate, there becomes a threshold where the flow rate of the reactive gas to the chamber becomes higher than the amount the sputtered material can getter/adsorb. This leads to an increase in the partial pressure of the reactive gas, which will ‘poison’ the target. Consequently the surface of the target will develop a layer of reacted material on the surface. Leaving the flow rate the same will result in fewer

atoms are being ejected therefore less reactive gas will be consumed and this is known as the ‘reactive mode’. Any addition of reactive gas flow rate will only lead to a linear increase in reactive gas partial pressure. When the flow rate is decreased, the partial pressure will not follow the same trajectory back, because the partial pressure remains high until the compound layer that has formed on the target surface has been sputtered off and the pure metal is once again exposed. The voltage of the target will differ in a similar fashion to the sputtering rate or gas partial pressure; whether the voltage rises or falls depends upon the target material (Mientus and Ellmer, 1999, Musil *et al.*, 2005, Danisman *et al.*, 2009). An example of typical hysteresis curves is shown (Figure 10).

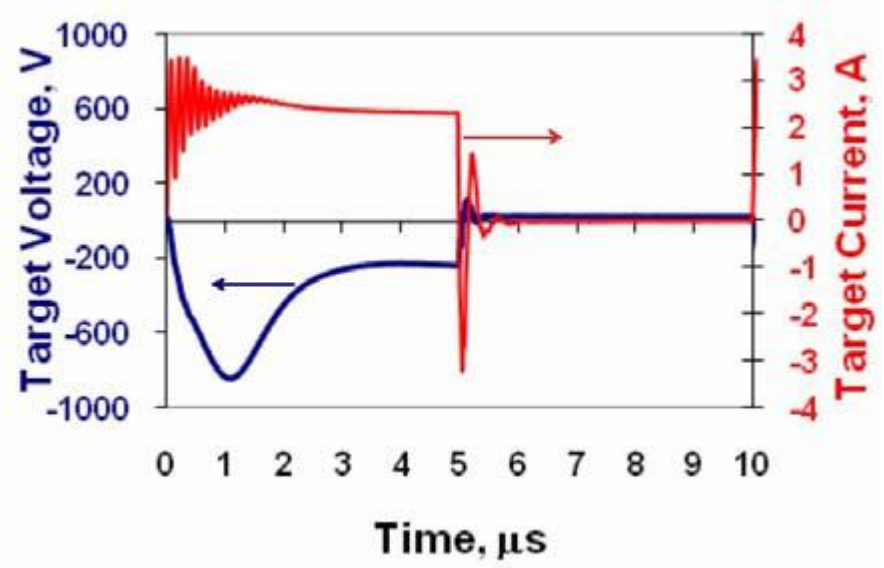

Figure 9: An example of a complete waveform of a DC pulse cycle from a Pinnacle Plus power supply (Advanced Energy, CO, USA) at 50% duty cycle and 100 kHz frequency (Kelly and Bradley, 2009)

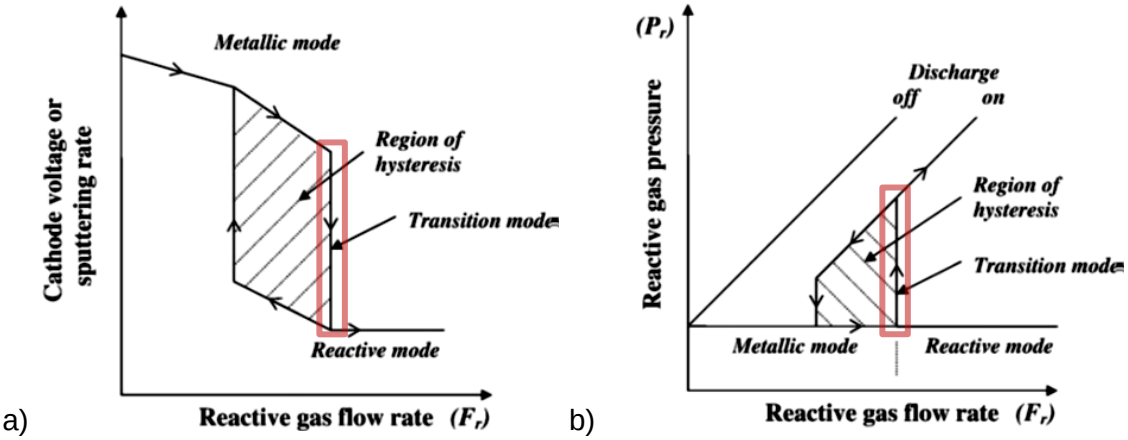

Figure 10: Examples of typical hysteresis curves and the effect of the gas flow rate on a) the cathode (target) voltage and b) the reactive gas pressure. a) Demonstrates as the gas flow increases the voltage drops steeply, known as the transition mode but further increase of gas flow does not typically affect the voltage. b) Demonstrates the effect of the reactive gas partial pressure as the flow rate is increased and following the sharp increase in the transition mode the increase in pressure remains constant. The ideal area for reactive sputtering (stoichiometric and highest deposition rate) is highlighted in red.

1.3.2.4.2 Plasma emissions monitoring (PEM)

To sputter in the desired region of the hysteresis curve as described above, the plasma optical emissions can be monitored and systems have been developed to automatically increase or decrease the reactive gas flow rate depending upon the parameter that is being monitored.. The plasma colour differs with every metal that is sputtered as each emits a different light wavelength characteristic to that metal. The plasma colour can be picked up using a fibre optic cable which leads to a spectrophotometer box, where the intensity of the light at the chosen wavelength is converted into an electrical current that can be fed to a sputter controller. The sputter controller can interpret the intensity of the signal and increase or decrease the flow of gas through a connected piezo valve. An increase in gas flow will alter the plasma emissions which will feed back through the system to alter the gas flow, when one changes it affects the other, acting as a feedback loop. This type of system is known as a closed loop feedback system because once it is running it is self-regulating and does not require user input.

1.3.2.5 Substrate sputter cleaning and bias

Substrate holders in magnetron sputtering systems are usually isolated at the floating potential (the electrical potential of the surrounding plasma), so only carry the floating potential voltage of the plasma. In some instances, the sputtering rigs have the ability to apply a voltage to the holder through a power supply to create a negative potential to the substrate holder, this increases argon ion flux and bombardment of the substrate holder and substrates instead of the chamber walls (anode). This increase in argon ion energy alters the coating characteristics and the way the material is deposited. This usually makes the coating denser, but it also increases the heat to the substrates so this method is more commonly used in the deposition of nitrides for tool coating applications.

Prior to coating, substrates can be subjected to some form of plasma treatment to remove any remaining surface volatiles. Due to the substrates ability to be attached to

a power supply it is possible to use this directly to 'sputter clean' the substrates. Applying a DC or pulsed DC voltage to the substrate holder in a vacuum chamber allowing the charge of the holder to ignite and hold a plasma discharge. This creates bombardment and sputtering of the substrate surfaces with the surrounding ionised gas particles but does not sputter etch the substrate material itself. This application allows the substrate surface to be free from contaminants so that adhesion of the coating is maximised.

1.4 Thin Film Coating Analysis

1.4.1 Scratch Testing

Thin nitride films deposited onto surfaces by physical vapour deposition are designed to improve wear resistance. One of the most important parameters in terms of wear resistance is the strength of adhesion between the substrate and the coating (Attar and Johannesson, 1996). The most commonly used technique to evaluate the coating adhesion is scratch testing. Other less accurate methods include the peel test and modified edge lift off test (Mittal, 2001). A scratch tester is 'an instrument used to rigidly hold the stylus and apply both the normal load and the driving force to produce scratches' in the test film (Anonymous, 2005a) (Figure 11).

Scratch testing, according to the British Standard (2005a), consists of 'drawing a loaded stylus across a coated surface. The load on the stylus is increased until failure of the coating/substrate system occurs'. This load at which the coating fails is recorded as the critical load, L_c. Failure events are detected by the use of acoustic emission monitoring, microscopic examination and friction force measurements. The $L_c(n)$ refers to different critical events at which the coating has failed, which can be examined using an optical microscope (Jacobs *et al.*, 2003).

The instrument used for hard coatings such as the ones investigated was a CSM Revetest (CSM Instruments, Peseux, Switzerland) utilised loading in the macro range

(1-100 N) and can be used to test coatings up to a thickness of 20 μm using a Rockwell-C diamond stylus (Attar and Johannesson, 1996). This can be loaded from 1 N – 100 N but for the tests used in this work the range of 1 N – 60 N was used because of the thickness of the investigated films (1 μm).

The test is designed to assess the mechanical integrity and the adhesion of the coatings to the underlying substrate by drawing a stylus across the surface and evaluating the constituents contributing towards coating failure. Elastic-plastic deformation, frictional force, coefficient of friction and acoustic emissions during testing were measured from the coating. Not only does the L_c depend on the coating adhesion strength but also on other factors, such as the wear of the diamond tip, the surface roughness and the speed and loading rate of the test, so one needs to be mindful of these variables when obtaining data.

The stages of coating failure occur in an order of different events observed on the scratch length (Figure 12). The first damage events are known as plastic deformation, seen before 'L_c1' (Figure 12). The next type of deformation is usually in the form of chevron cracks 'L_c2' (Figure 12) or hertzian cracks which are rounder in shape than the former. This usually follows with an increase in cracks in the surface, which leads to conformal buckling of the surface or spallation (small amounts of coating chipping off) occurring (L_c2 - L_c3) (Figure 12). There are various types of cracking and spallation that occur depending upon the structure, rigidity and strength of the coating (Heinke *et al.*, 1995), which are defined in the British Standard BS1071-3:2005 (Anonymous, 2005a). The final point of failure is when complete perforation of the coating has occurred down to the bare underlying substrate 'L_c3' (Figure 12) usually by either ductile perforation of the coating or large scale interfacial spallation.

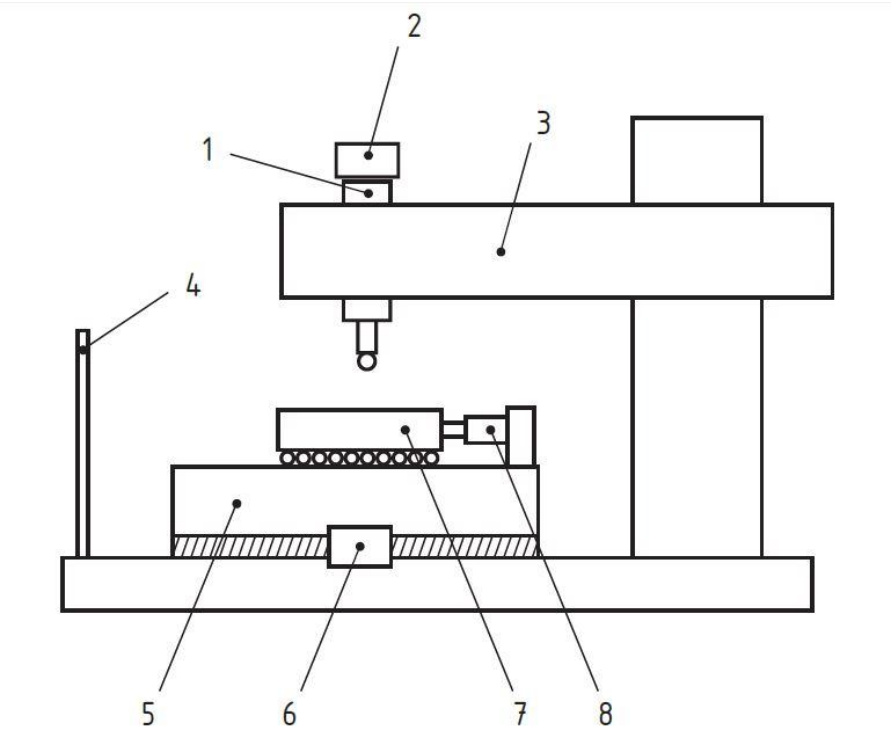

Figure 11: A schematic diagram of a typical scratch tester: 1) Stylus shaft, 2) Vertical load transducer, 3) Upper support assembly, 4) Base reference, 5) XY stage to manoeuvre, 6) XY stage drive arrangement, 7) Low friction sample table and 8) horizontal force transducer (Anonymous, 2005a).

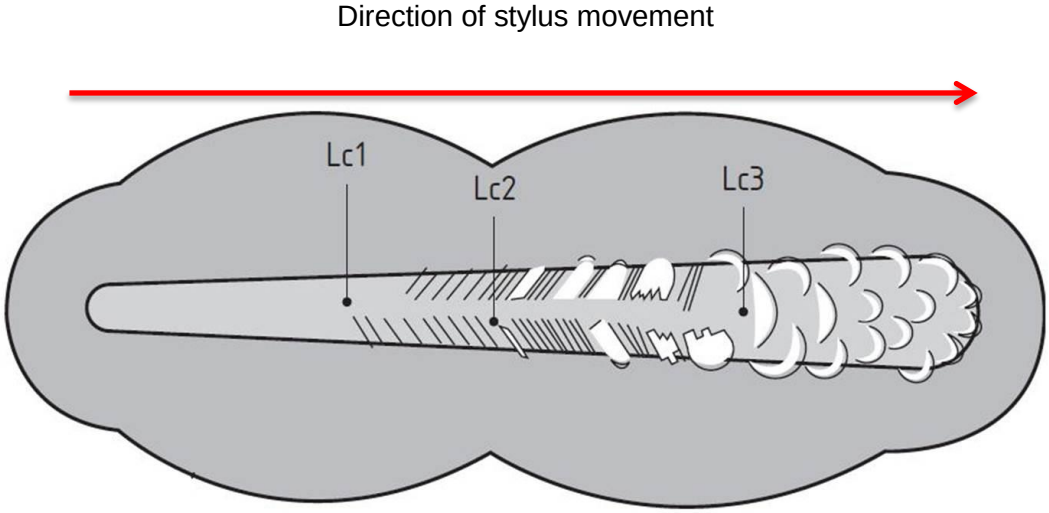

Figure 12: Schematic diagram of an entire scratch length indicating an example of the beginning of cracking (L_c1), spallation (L_c2) and full coating delamination/critical failure (L_c3) (Anonymous, 2005a).

1.4.2 Inductively Coupled Plasma - Atomic Emission Spectroscopy (ICP-AES)

Inductively Coupled Plasma – Atomic Emission Spectroscopy (ICP-AES) is used to rapidly quantify trace elements in liquids, air and particulate matter (Asami and Hashimoto, 2003, Lewen and Nugent, 2010). ICP-AES analysis uses the ion coupled plasma to atomise the sample and subsequently excite electrons in the trace elements, which then emit energy at wavelengths depending upon the element. The electrons in the outer shell of the element are excited, which then emits a photon of light in a wavelength unique to the element. This light emission is picked up by photomultiplier detectors. The more intense the light signal emitted corresponds to a more concentrated sample of the trace element. The software interprets the intensity of the plasma emission and calculates the elemental concentration, in accordance to prior calibration tests of the element standards (USGS, 2013).

In this study ICP-AES was used to quantify silver leaching into the surrounding liquid medium. This method allows the detection of sub-inhibitory concentrations of silver that are being leached from the surface.

1.4.3 Surface Topography and Roughness

The topography of any surface take the form of a series of peaks and valleys which may vary in both height, width and spacing and thus possess a texture which, in terms of properties both physical and aesthetically are typical of the surface components, production processes or the way the surface is being used (Whitehead and Verran, 2006). Magnifying a seemingly smooth surface using methods, such as white light profilometry and atomic force microscopy, reveals a complex structure. These surface structures are called texture (Anonymous, 2010a). The British Standards BS 1134-1:1972 and BS 1134-1:1988 define roughness as ‘the irregularities in the surface texture which are inherent in the production process but excluding waviness and errors of form’ (Anonymous, 1972, Anonymous, 1988, Whitehead and Verran, 2006). Surface

roughness values are categorised into three groups according to functionality. These include; Amplitude parameters, spacing parameters and hybrid parameters. Amplitude parameters are the most widespread and important factors when characterising surface topography and are most commonly used in product hygiene specification of products in the food and medical industries. The amplitude parameters measure the vertical deviations in a surface. According to the British Standard to assess surface texture, 'to control a surface texture (roughness) it first has to be measured' (Anonymous, 2010a).

Substratum surface characteristics play a key role in bacterial adhesion, growth and viability, therefore close attention needs to be paid to surface characterisation. Surface topography and roughness measurements are one on the most important physical factors relating bacterial retention to surfaces, such as biomaterials (BoulangePetermann *et al.*, 1997, Scheuerman *et al.*, 1998, Méndez-Vilas *et al.*, 2006, Choi *et al.*, 2007, Whitehead and Verran, 2007, Anselme *et al.*, 2010, Puckett *et al.*, 2010, Verran *et al.*, 2010).

1.4.3.1 Arithmetic average height (R_a/S_a)

The topography of a surface is quantified using surface roughness amplitudes (*R* values) (Gadelmawla *et al.*, 2002). The most universally utilised roughness parameter is the Arithmetic Average Height, (or R_a). The R_a of a profile is the average absolute deviation in topography from the mean line over one sample length (Gadelmawla et al., 2002). This method provides a description of the overall height deviation throughout the surface. However it is insensitive to small changes in the surface topography due to the nature of averaging the height parameters. The R_a is the benchmark roughness parameter used in microbiological directives and guidelines (Gadelmawla *et al.*, 2002, Whitehead and Verran, 2006). The S_a value is defined the same way as the aforementioned R_a parameter but has been measured by an optical surface quantifying instruments or "areal geometrical specifications" (Anonymous, 2012)

1.4.3.2 Root mean square values (*RMS*)

The root mean square (RMS) or R_q represents roughness values as the standard deviation of the distribution of the surface heights. RMS values are suitable for use in statistical methods, because it has an increased sensitivity to large infrequent deviations than R_a (Anonymous, 2009, Sedlaček *et al.*, 2009, D Antonio *et al.*, 2012)

1.4.3.3 Ten point height value (R_z)

The R_z value is known as the ten-point height because the average difference in height between five highest peaks and the five lowest valleys along the surface profile gives the R_z value (Gadelmawla et al., 2002). This method is used by the Health and Safety Directive RR732 to help assess the slip resistance of floors as it uses multiple surface deviations in the calculation taking into account multiple peaks.

1.4.3.4 Maximum peak height and maximum valley depth (R_p/S_p) (R_v/S_v)

R_p, also sometimes referred to as R_{pk}, is used to describe the maximum height of the surface peaks. The highest peak is defined as the highest topographical characteristic above the mean line within the profile length. R_v describes the lowest point below the mean line of the surface profile (Anonymous, 1998, Gadelmawla *et al.*, 2002).

1.4.3.5 Total height/ maximum profile height (R_t/S_t)

R_t or R_{max} is defined as the maximum height of the profile. This is the overall height of the profile between the lowest valley and the highest peak across the assessment profile. R_t is also equal to R_p + R_v. This parameter is extremely sensitive to surface anomalies such as deep scratches or high peaks (Gadelmawla *et al.*, 2002, Aydin *et al.*, 2013).

1.4.3.6 Average Height and Max Range

The two parameters that follow are not as universally used as those previously stated but are used by instrumentation for this study, such as the atomic force microscope (AFM). The “Average Height” is a calculation defined as the ‘sum of all height values divided by the number of data points’. This term gives a description of the average height of the deviations throughout the scan area.

The “Max Range” parameter relates to the difference between the single largest peak and the single deepest valley, similar to R_t, more commonly seen in literature.

It is important to obtain the values for a range of roughness parameters to assess the surface topography because it has been well documented that the use of just one parameter, such as the most popular R_a, is not sufficient to define the roughness and hygienic status of a surface (Faille *et al.*, 2000).

1.4.3.7 Macro, Micro and Nano-topography

Throughout evaluation of surface roughness it is essential to distinguish the size of the surface topography with reference to microbial sizes and this can be split into three categories:

1. Macrotopography, $R_a \geq 1$ µm - 10 µm
2. Microtopography, $R_a \geq 500$ nm - 1 µm
3. Nanotopography, $R_a < 500$ nm

R_a values in the macro scale are usually found on surfaces where the hygienic status will not have a significant impact (Choi *et al.*, 2007, Verran and Boyd, 2001). It is believed that an increase in roughness will increase the initial accumulation of bacteria in the bottom of the valleys in the topography because of protection from shear stress (Duddridge *et al.*, 1982). Micro roughness R_a values are the most commonly used measurements operative in situations such as finishes of stainless steel surfaces in the

food industry and other applications such as medical equipment and surfaces and implants in the oral cavity and also orthopaedic implants. These are important in terms of bacterial adhesion and retention. It was suggested that an R_a equal to or less than 0.8 μm is recommended for food contact surfaces for them to be hygienic (Curiel, 1993, Faille *et al.*, 2000) and the ISO standard 4287 (1997) recommended an R_a of less than or equal to 1.6 μm The nano-roughness of a surface is extremely important in the field of implants, especially in orthopaedic applications because the nanotopography of a surface can not only affect the behaviour of bacterial cells and how they adhere but the behaviour of the bone cells and their ability to adhere to the surface in a phenomenon known as osseointegration (Anselme *et al.*, 2010). It is suggested in the literature that the method of altering the surface roughness (at the nano scale) to prevent adhesion of bacteria without the use of drugs may be one of the best ways to reduce orthopaedic implant infection (Campoccia *et al.*, 2006, Puckett *et al.*, 2010). It has also been shown that whilst the increase in nanotopography of the biomaterial surface may increase osseointegration by enhancing osteoblasts, it may simultaneously decrease competitive cell integration by such cells as fibroblasts (fibrous tissue that forms around the implanted material) preventing proper bone integration (Miller, 2005, Cohen *et al.*, 2007, Yao *et al.*, 2008, Puckett *et al.*, 2010). Further, increasing the nanoroughness of a surface can also decrease bacterial adhesion (Colon *et al.*, 2006). Xu et al. (2012) found that nano-textured surfaces (sub-micron range, 400/400 nm and 500/500 nm feature size and spacing, respectively) reduced the bacterial adhesion of *S. aureus* and *S epidermidis* by up to 90% under a shear stress situation on polyurethane urea (PUU) substrates.

1.4.4 Atomic Force Microscopy (AFM)

Atomic force microscopy (AFM) was carried out on a type of scanning probe microscope, which used a silicon nitride tip mounted on a cantilever, which may either be in contact with the surface (during contact mode) or non-contact (tapping mode)

(Figure 13). The tip moves in a raster motion across the surface producing feedback from a laser beam, which is deflected off the back of the cantilever and the reflection of the beam is picked up by a photodiode. The data acquired by the photodiode is recorded in the form of a topographical interpretation. AFM imaging produces both qualitative data, for example the image of the surface and quantitative data, such as roughness (*R*) values (Hansma and Pietrasanta, 1998, Gadelmawla et al., 2002).

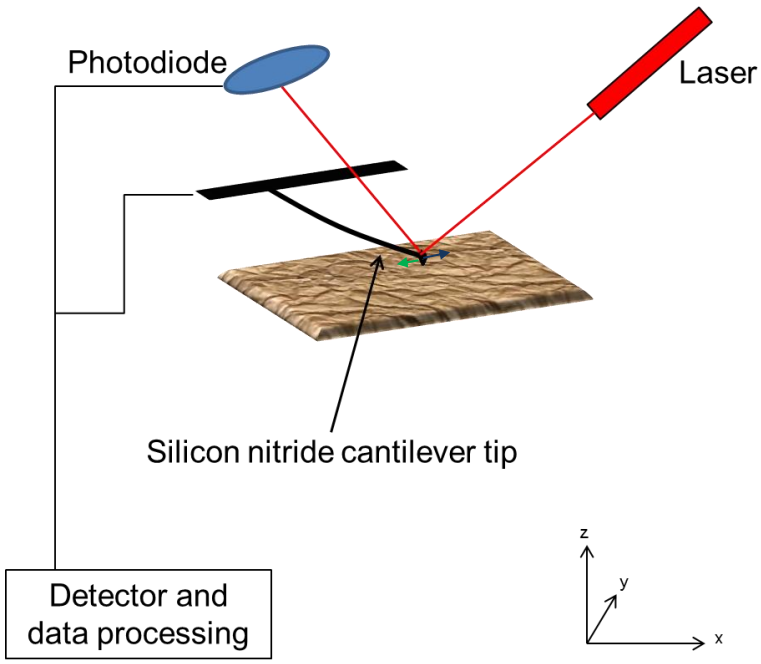

Figure 13: Simplified diagram of an AFM system, displaying how the cantilever tip moves over the surface in a raster pattern whilst reflecting the laser off the tip onto the photodiode.

1.4.5 White Light Profilometry (WLP)

White light profilometry (WLP) also referred to as (Scanning) White Light Interferometry (SWLI) and Vertical Scanning Interferometry (VSI), is a non-contact, optical method used to analyse the 3D topography of a surface using visible light. This method is capable of rapidly providing quantitative and qualitative reproducible roughness measurements (Blunt, 2006). The WLP system works by a source of white light, whereby the beam is split into two parts, so as to hit both a reference mirror, which is a constant optical path, and the sample. This directs the beam of light down the objective lens to reflect off the sample surface and into the lower beam splitter. The combined light from the reference source and the sample surface creates an interference pattern that allows the vertical movement of the lens to be tracked. The piezo drive system moves the beam splitter in a series of steps and the interference pattern is recorded for each step, thus making it possible to construct a three dimensional map of the sample surface (Figure 14) (Lindseth and Bardal, 1999, Blunt, 2006).

The accuracy of results obtained from the WLP is similar to an AFM and have been shown to be comparable at similar scales (Lindseth and Bardal, 1999, Koyuncu *et al.*, 2006, Spencer *et al.*, 2013). However the white light profilometer has some advantage for surface analysis versatility due to the method of data collection, and it has the ability to scan larger areas so provides more comprehensive data on the overall surface topography (Koyuncu *et al.*, 2006).

The main disadvantage of WLP in comparison to AFM is that due to it being an optical technique the lateral resolution has a limit of around 0.35 μm; light may not be able to be reflected off opaque and non-reflective samples so some deeper features may not be detected (Blunt, 2006).

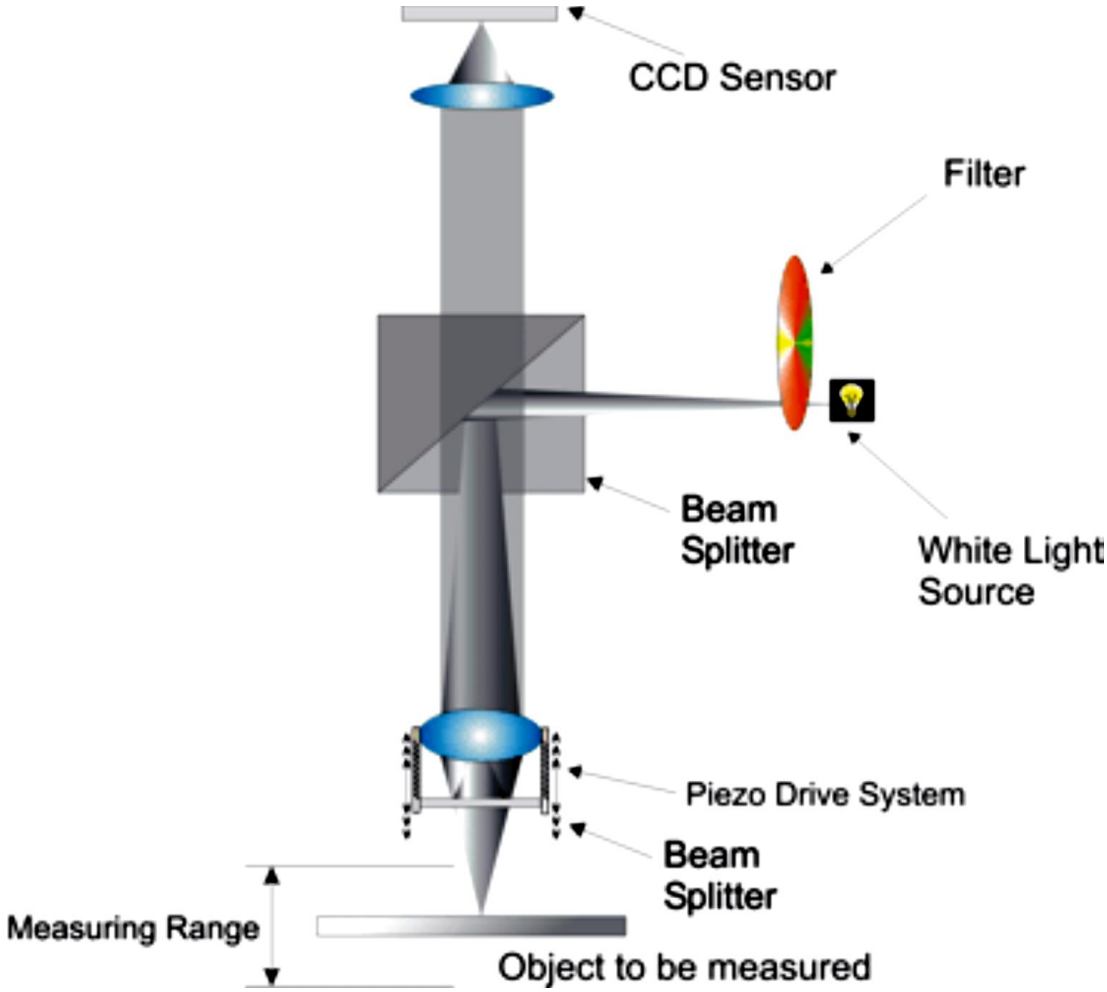

Figure 14: Schematic diagram of a White Light Profilometer (interference microscope) (Blunt, 2006) displaying the path of the light beams from the light source to the sample and up to the sensor.

1.4.6 Surface hydrophobicity

It is well established that physico-chemical properties influence initial microbial attachment. Surface hydrophobicity plays an important role in medical device surface design, as it can be modified to reduce bacterial adhesion (Pereni *et al.*, 2006). Hydrophobic surfaces have been found to attract water with strong binding energies from hydrogen bonding, however it is not to be overlooked that these attractive forces are a lot stronger for hydrophilic interactions (van Oss, 1995). The most common misinterpretation of the term “hydrophobic” is that they do not repel water, as is believed but attract water with heavy binding energies, just not with as much energy as a hydrophilic surface. Hydrophobicity occurs due to the hydrogen-bonding free energy cohesion of the water molecules of the liquid medium in which the hydrophobic subject is immersed (van Oss, 1995). A hydrophilic surface occurs when the difference between the apolar attraction and polar repulsion between the molecules on the surface immersed in water is equal to the cohesive polar attraction between the water molecules themselves (Van Oss and Giese, 1995). It has been said that in biological systems, hydrophobic interactions are the strongest non-covalent interactions. In order to determine the hydrophobicity of surfaces, of the known contact angles of three solvents can be substituted into an equation in order to derive the unknown surface energy values.

The standard method for physicochemical characterisation of surfaces, inert or organic, is measuring contact angles of three liquids, two polar solvents, water and formamide and one non-polar solvent, such as 1-bromonaphthalene (van Oss, 1995, Skovager *et al.*, 2012). The contact angles obtained from the three solvents can be then used to calculate the electron acceptor (γ_s^+), electron donor (γ_s^-), Lifshitz-van der Waals component (γ_s^{LW}) and hydrophobicity (ΔG_{iwi}). There are a number of different terms and symbols used to describe these parameters but throughout this document the previous stated descriptors will be used, as stated by van Oss (1995).

The theory behind hydrophobicity calculations will now be summarised from van-Oss (1995). Free energy of interactions between molecules (*i*) immersed in water (*w*) can be expressed as ΔG_{iwi}

$$\Delta G_{iwi} = -2\gamma_{iw} \quad (1)$$

where γ_{iw} is the interfacial tension between *i* and water. It has been defined that hydrophobic components are said to contain a $\Delta G_{iwi} < 0$ (negative), whereas hydrophilic counterparts display values of $\Delta G_{iwi} > 0$ (positive) (van Oss, 1995). The surface free energy of a solid or a liquid, γ_i, is the sum of the non-polar Lifshitz-van der Waals γ_i^{LW} and polar acid-base interactions, γ_i^{AB}, such that

$$\gamma_i = \gamma_i{}^{LW} + \gamma_i{}^{AB} \quad (2)$$

where γ_i^{AB} comprises of two parameters, the electron donor γ_i^- and the electron acceptor γ_i^+. This is calculated by using the following:

$$\gamma_i{}^{AB} = \sqrt{\gamma_i{}^+}\gamma_i{}^- \quad (3)$$

There are three unknowns to these parameters that will be used in the equations. Using contact angle (θ) measurements of three different liquids, of which two are polar and one apolar, and Young's equation (4) the γ_i^{LW}, γ_i^+ and γ_i^- can be derived.

$$(1 + \cos\theta)\gamma_L = 2\left(\sqrt{\gamma_S^{LW}\gamma_L^{LW}}\sqrt{\gamma_S^{\oplus}\gamma_L^{\ominus}} + \sqrt{\gamma_S^{\ominus}\gamma_L^{\oplus}}\right) \quad (4)$$

Where *L* is the contact angle liquid and *S* is the solid (Figure 15) (van Oss, 1995). Full calculations of the hydrophobicity values were obtained from Bos *et al.* (1999) and van Oss (1995)

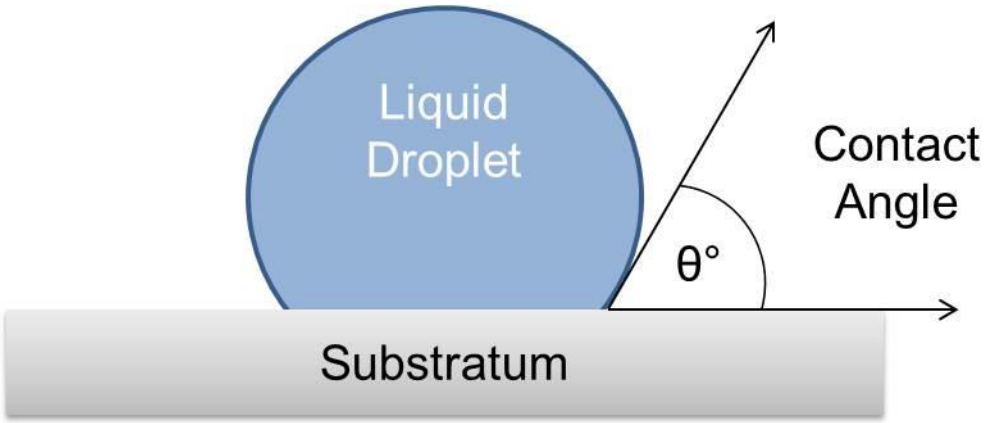

Figure 15: A simplified diagram of a water droplet on a solid surface, displaying the measured contact angle.

1.4.7 Substratum Wettability

Surface wettability is the term used to describe if a surface is wettable or non-wettable and is determined only by using water as the test solvent. There is some confusion over these terms since “wettability” may be used interchangeably with hydrophobicity. Further, many authors have stated that the threshold for hydrophobicity is based on the water contact angle threshold being ≤ 65^0 is hydrophilic and > 65^0 is hydrophobic, sometimes known as the ‘Berg limit’, taken from the name of the author who first defined this hypothesis (Pashley and Kitchener, 1979, Berg *et al.*, 1994, Vogler, 1998, Szlavik *et al.*, 2012). However, other studies use 90º as the threshold between the definitions (Pogorzelski *et al.*, 2013)

One of the most important attributes to the physiology of a bacterium related to interfacial interaction is hydrophobicity and related interactions. There are three types of non-covalent interactions: 1) interfacial interactions, 2) electrostatic interactions and 3) Brownian movement (Van Oss, 1994, van Oss, 1995). Of these three interactions, only interfacial interactions are responsible for hydrophobicity and hydrophilicity (See 1.7.4).

1.5 Implant associated infections

The adhesion of microbes to a surface is an important step towards implant and biomaterial infection (Gristina and Costerton, 1985, Bellon-Fontaine *et al.*, 1996). The bacterial cell surface is a complex structure involving both biological and chemical interactions at the surface to aid its survival. Bacterial adhesion at the initial stages is governed by physico-chemical reactions and the survival of a bacterial cell may be more successful if it is able to attach and form a community on a surface, also known as a biofilm (Pereni *et al.*, 2006). Biofilms are important in pin tract infections because the majority of infections will comprise of biofilm. The presence of a mature biofilm over early attached cells increases the resistance of the bacterial cells towards

antimicrobials by 100-1000 fold higher than planktonic bacteria (Stewart and Costerton, 2001, Hoiby *et al.*, 2010).The prerequisite of biofilm formation is the successful cell attachment, adhesion and retention of the cell/s to a solid surface.

1.5.1 The stages of biofilm formation

The formation of a biofilm is a complex phenomenon, which takes into consideration a number of factors; the material surface properties, the properties of the bacteria and the environment in which the attachment, adhesion and retention take place, the environment pH, the charge of the bacterial cell wall, and flow conditions are some examples of the affecting aspects (Desrousseaux *et al.*, 2013).

Biofilms begin with attraction and attachment of single cells on a surface and lead to mature, complex biofilms over time. This process occurs as stages recognised in literature most commonly as a diagram (Figure 16) which is an oversimplified version of events occurring at the surface interface (Arciola *et al.*, 2012). Initially there is attachment of the cells to the surface, involving hydrophobic interactions and surface charges to attract the cells. The second stage is growth and aggregation of these cells on the surface, leading to adhesion of the cells and multilayers of bacteria. Once the bacteria are retained and mature, the third stage involves production of exopolysaccharides, proteins and eDNA within the matrix of the cells. The final stage of a mature biofilm is the detachment/release of cells from the biofilm into the surrounding phase. The excess of auto inducing peptide (AIP) triggers this phase releasing the cells into the surroundings, most often a liquid medium, allowing newly planktonic cells to disperse and initiate growth on a surface elsewhere in the environment. This work was aimed at determining how the zirconium nitride/silver surfaces affected cell retention on the surfaces, for if this stage can be controlled, hypothetically, biofilm formation cannot occur.

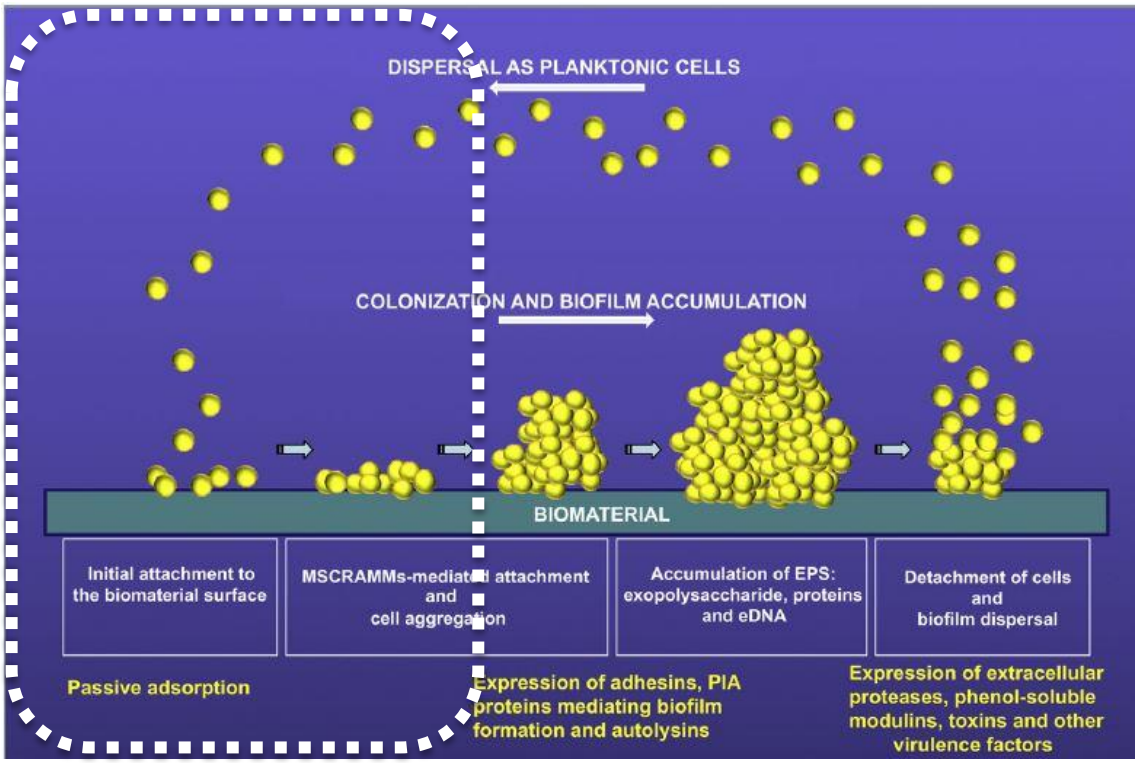

Figure 16: The cycle of a biofilm, demonstrating the early stages of attachment and colonisation, followed by cell aggregation and expression of adhesins from the cells to initiate adhesion to the surface (Arciola *et al.*, 2012). This is followed by the production of extracellular polymeric substances to aid the survival of the mature biofilm and the final stage is the detachment of the cells and the dispersal of the newly planktonic cells in the surrounding environment (Arciola *et al.*, 2012). The stages of biofilm formation that will be investigated in this work are indicated within the white outline.

1.6 Staphylococci

Staphylococcus spp. are the most common pathogens isolated from implant infections (Garvey, 1980, von Eiff *et al.*, 2005, Harris and Richards, 2006, Teterycz *et al.*, 2010). This is due to the majority of infections being transferred from the skin flora to the wound and colonising the area, giving rise to opportunistic infections.

1.6.1 Staphylococcus aureus

Staphylococcus aureus is a non-motile, non-spore forming facultative anaerobe and a natural skin commensal. It is a Gram positive, coagulase positive coccus approximately 1 µm in diameter. *S. aureus* cells grow in clusters and form colonies on nutrient agar that are round and golden in colour from carotenoid pigments, found to potentially play a role in virulence (Liu et al., 2005). *S. aureus* is the most common opportunistic pathogen, well known for causing infections in wounds and includes the antibiotic resistant strain MRSA (Methicillin resistant *Staphylococcus aureus*) known throughout the world via the media describing outbreaks in hospitals and care home communities. The virulence of *S. aureus* is high, although its prevalence is low and the non-antibiotic resistant strains can be treated relatively easily.

1.6.2 Staphylococcus epidermidis

Staphylococcus epidermidis is a less well known microorganism in comparison to *S. aureus*. It is also a Gram positive, non-motile, non-spore forming coccus around 1µm in diameter that grows in clusters, but it is coagulase negative and grows in nutrient agar as white, round colonies. Many authors refer to *S. epidermidis* as “coagulase negative staphylococci” because many other species of coagulase negative staphylococci are rarely found in implant associated infections. *S. epidermidis* is an abundant skin commensal, more common than *S. aureus* yet its virulence is low and it rarely causes infections unless the host is immuno-compromised. Once established, *S. epidermidis*

exhibits a much higher drug resistance than *S. aureus,* requiring more aggressive antibiotic therapy.

1.7 Microbiological and Conditioning Film Assays

1.7.1 Bacterial Attachment, Adhesion and Retention

Biofilm formation primarily consists for four main steps: 1) initial attachment of bacterial cells, 2) cell aggregation, 3) biofilm maturation and 4) detachment of cells from the biofilm. During the first step there are three additional phases the bacterial cells need to go through; attachment, adhesion and retention (Arciola *et al.*, 2012) or two phases; reversible and irreversible (Skovager *et al.*, 2013). The reversible phase of initial adhesion is when a bacterium comes in contact with the substrate surface for a small period of time by forces such as electrostatic or Lifshitz-van der Waals forces. Following the initial phase the bacteria enter an irreversible adhesion phase where the bacterium strengthens its attachment with the surface by bonding such as covalent bonding or hydrogen bonding (Skovager *et al.*, 2013). Bacterial retention occurs when forces such as flow do not remove cells from the surface; they are retained due to variations in surface topography (1.4.3; Page 34), chemical and physicochemical interactions between the bacteria and the surface, such as hydrophobicity (1.4.6; Page 42) and surface charges (Whitehead *et al.*, 2004).

1.7.2 Acridine Orange Retention Assays

An increase in microtopography is found to affect the attachment, adhesion and retention of bacterial cells, especially those that have similar dimensions to the surface topography and defects (Whitehead and Verran, 2007). The micro and nanotopography of a surface can also alter the overall surface charge and the properties of the conditioning film/organic compounds upon the substrata. The properties of the

conditioning film will in turn alter the surface properties and attachment to which the bacteria adhere to the surfaces. This will be discussed more thoroughly in Chapter 7 (Page 214).

Retention assays investigate the interactions of the bacteria and the surface when introduced for a period of time and subjected to a standardised rinse. This assay does not determine cell attachment, adherence or late biofilm formation; the interactions are focussed on the retention of the bacteria onto the substrate. The bacterial suspension is made to a standardised optical density before use and a measured amount of the suspension is added to all sample dishes, to enable comparison and keep the experiment repeatable. The samples are, in this case, incubated at 37ºC, without agitation, for 1 hour. This gives the bacterial cells time to settle on the surfaces. The standardised rinse allows the cells that are not attached to be rinsed away using a gentle shear force. The bacteria then need to be stained for visualisation under a microscope. The cells are often stained for visualisation for the coverage or number of bacteria retained to be counted. However, the pattern of distribution of the cells cannot be measured using this technique. Since the surfaces used in this investigation are opaque, the most suitable stains are those which are fluorescent for use on an epifluorescent microscope. The stain used in this investigation was acridine orange, a universal nucleic acid stain. Acridine orange is capable of staining both ribonucleic acid (RNA) and deoxyribonucleic acid (DNA) and has many biological uses (Traganos *et al.*, 1977). Acridine orange has an excitation/emission spectra of 500/526 nm for DNA and 460/650 nm for RNA (Anonymous, 2013).

1.7.3 SEM of Retention Assays

The scanning electron microscope is a versatile method for visualising the retained bacterial cells on a surface and even the structure of biofilms, if prepared correctly (Camargo *et al.*, 2005, Greif *et al.*, 2010). When the SEM is operated under high vacuum, the cells and extracellular polymeric matrix become reshaped, due to the

initial sample preparation and vacuum dehydrating the organic components. Preparing the samples by using an agent such as gluteraldehyde to fix the cells and an alcohol gradient using absolute ethanol may be used to remove water from the structures and preserve cell integrity (Franson *et al.*, 1984).

1.7.4 Bacterial Hydrophobicity (MATH)

It has been determined that the forces responsible for bacterial adhesion involve electrostatic, van der Waals and Lewis acid-base interactions. There are many more methods to measure cell surface hydrophobicity than there are to determine acid-base properties. One method to calculate acid-base properties uses the "Microbial Adhesion to Solvents" (MATH) assay, developed by Bellon-Fontaine et al. (1996), which uses pairs of both a monopolar and apolar solvent. These pairs include (Bellon-Fontaine *et al.*, 1996):

- Chloroform (an acidic solvent) and hexadecane
- Diethyl ether (a strongly basic solvent) and hexane
- Ethyl acetate (a strongly basic solvent) and decane

Hexadecane, hexane and decane are apolar *n*-alkanes, whereas chloroform is an electron acceptor acidic solvent, diethyl ether is a polar basic solvent and ethyl acetate, a basic, polar electron donating solvent. In the MATH assay, the microbial affinity observed are considered a result of the same electrostatic, van de Waals and Lewis acid-base interactions that would occur at a bacterial-surface interface. The bacterial suspension is made to a known optical density in a phosphate buffer solution. This is vortexted/agitated with the solvents stated above and then the two phases are left to separate. The aqueous solution is removed and the optical density is taken again and the decrease in turbidity is calculated as a percentage of affinity for that particular solvent using the following equation (Rosenberg *et al.*, 1980, Bellon-Fontaine *et al.*, 1996):

$$\%\ adherence = \left(1 - \frac{A}{A_0}\right) \times 100,$$

where A_0 is the original optical density measured at 400 nm prior to mixing and A is the absorbance of the aqueous phase after mixing. It is said that hydrophilic (repulsion) and hydrophobic (attraction) interactions observed in these interfaces are primarily due to Lewis acid-base interactions and the Lifshitz-van der Waals interactions (van Oss, 1993, Bellon-Fontaine *et al.*, 1996). An affinity for the chloroform would indicate that the bacteria are electron donating (basic) and affinity for hexadecane would indicate that the microorganisms are electron accepting (acidic). The other pairs of solvents demonstrate the same, with diethyl-ether and ethyl-acetate being the electron accepting and the hexane and decane being the electron donating, non-polar solvents with a similar intermolecular attraction to the paired solvent (Takahashi *et al.*, 2010).

1.7.5 Efficacy Testing of Antimicrobial Surfaces

1.7.5.1 Retention Assay and LiveDead™ Staining

Staining the bacteria with LiveDead™ cell viability stain allows differentiation between viable and potentially non-viable cells (those with a compromised cell membrane). The stains used in the procedure are propidium iodide and SYTO-9. The excitation and emission ranges for the two products are 480/500 nm for SYTO 9 and 490/635 nm for propidium iodide (Anonymous, 2004). Propidium iodide permeates cells with a damaged membrane, which are assumed to be non-viable. SYTO-9 acts like a counter stain and marks all other bacterial cells green as it has the ability to permeate all cells which are viable and have an intact membrane, which the larger propidium iodide molecule cannot enter (Williams *et al.*, 1998, Whitehead *et al.*, 2011).

1.7.5.2 CTC-DAPI fluorescent staining

Testing the viability of individual bacterial cells through epifluorescent staining has been demonstrated by the use of LiveDead staining, however this tests the bacterial cell membrane integrity and those with a compromised membrane are deemed non-viable. However, some bacterial cells may be viable but not culturable or non-viable with an intact cell membrane or viable with a compromised cell membrane. Therefore the use of a fluorescent redox dye was used in an assay to indicate actively respiring microorganisms. The tetrazolium salt 5-cyano-2,3-ditolyl tetrazolium chloride (CTC) is used as an indicator of bacterial respiration. The action of indication occurs when respiring microorganisms reduce the tetrazolium salts in their electron transport chain producing the insoluble crystal product formazan (Weaver *et al.*, 2008).

1.7.5.3 Antimicrobial leaching and contact kill

The two types of kill that were investigated in terms of the antimicrobial activity of the surfaces were leaching of antimicrobial compounds and contact kill. A contact kill surface is one which on the surface contains an antimicrobial which kills microorganisms on contact (Sawan *et al.*, 1998, Sawan *et al.*, 2000). In this work two types of method were used; the NTV assay, a variation of an experiment designed by Barnes et al., (1996) and a variation on the Japanese Industrial Standard JIS Z 2801 (Kawakami *et al.*, 2008, Anonymous, 2010b). The advantages of a contact kill are that the antimicrobial action is local and there is no risk of release into the surrounding environment and bodily tissues, thus reducing damage to the cells and improving healing. Contact kill is preferred in many biomaterial applications. The disadvantage of a contact kill antimicrobial surface is when a conditioning film such as proteins, bodily fluids and surrounding environmental molecules adsorb onto the surface, they create a chemical barrier and increase the distance between the bare substrate where the antimicrobial elements, thus the surface may become ineffective.

The advantages of antimicrobial leaching are that the efficacious product is not just effective at the surface interface but it is also effective towards surrounding microorganisms, mostly in a liquid or solid medium such as bodily tissue or agar media. The disadvantages of leaching into the surrounding area, especially in terms of biomaterials, is that the release and absorption of the antimicrobial product into surrounding bodily tissues can cause local or potential systemic toxicity if the antimicrobial compound has toxic properties. Hardes *et al.* (2007) found that in literature and the studies conducted in their investigation that silver coatings applied to orthopaedic megaprosthesis do not release enough silver into the body to initiate toxicological side effects.

1.7.5.4 Viability Assay (NTV) (Contact Kill)

Tetrazolium salts are recognised as indicators of respiratory activity in microbial cells. The assay performed uses nitro-tetrazolium violet, which is a redox dye that changes colour when in contact with viable respiring colonies (Barnes *et al.*, 1996). The salts are reduced within the cells when in contact with respiring bacterial colonies changing the pale yellow- colourless tetrazolium salt into irreversible formazan, which is converted to a dark blue-violet colour. The bacterial colonies will be clearly indicated on the surfaces and can be enumerated. Nitro-blue tetrazolium was previously used for the assay (Kelly *et al.*, 2009a), but was changed to nitro-tetrazolium violet due to toxicity safety issues.

1.7.5.5 JIS Standard Assay (Contact Kill)

The Japanese industrial standard test for antimicrobial activity and efficacy is a method to evaluate the efficacy of antimicrobials towards bacteria on the surface. The most common uses of the assay include the testing of metallic antimicrobials and photocatalytic materials with potential antimicrobial properties. The assay involves depositing a constant amount of a known concentration of bacterial suspension and

overlaying it with an inert polymer film. The film ensures complete contact with the surface and also slows evaporation and environmental contamination of the test pieces. After being left in an incubated environment at high humidity (> 90%) for 24h the cells can be recovered and counted to enumerate the antimicrobial activity. Kawakami et al., (2008) used this method to test 21 metallic elements for antimicrobial contact kill efficacy against *Staphylococcus aureus* and *Escherichia coli*. They found cobalt, nickel and aluminium had moderate antimicrobial effects when not expected and gold (Au^{3+}) did not display any contact kill efficacy although it has been previously reported as a strongly 'toxic' antimicrobial, possessing a similar minimum inhibitory concentration (0.2 mM) as Ag^{+} (Nies, 1999). Many studies use the JIS Z 2801 technique to test antimicrobial efficacy, in particular antimicrobial contact surfaces in medical situations, such as TiO_2-Ag to combat Methicillin resistant *S. aureus* (MRSA) (Necula *et al.*, 2009b) and the study of antibacterial activity of cutting boards containing silver against five strains of *S. aureus* (Møretrø *et al.*, 2012). However Moretro *et al.* (2012) believed following their investigation that the JIS standard may overestimate the effects of the test subject in comparison with the cutting boards when used in a real life situation.

Combining the JIS Z 2801 standard test and the NTV assay, which uses the respiration of the viable cells to determine contact kill, gives a more comprehensive vision of the contact kill properties of a test surface.

1.7.5.6 Zones of inhibition assay (Leaching)

Zones of inhibition (ZoI) assays are widely used in medical microbiology to test for susceptibility to antimicrobial agents. The assay employs the diffusion of antimicrobial products into a surrounding microbial 'lawn' and assesses the effectiveness of the antimicrobial agent from the diameter of the clear zone observed around the sample (Zone of inhibition) (Kelly *et al.*, 2011). This can in turn be cross referenced with

standards to work out the minimum inhibitory concentration (MIC) of the compound and give an estimate of the content and efficacy of the antimicrobial, in this case silver.

1.7.6 Testing For Antimicrobial Activity in the Presence of a Conditioning Film

As soon as 'clean' surfaces are exposed to the environment they immediately begin to adsorb material from the surroundings and form what is known as a conditioning film. The presence of organic and inorganic deposits on the surface will affect the surface properties and potentially the hygienic status of the surface because the 'soil' can interfere with cleaning and disinfecting agents and physically and chemically protect microorganisms. This soil also has the potential to provide nutrients for adhered bacteria to grow and re-contaminate following cleaning, if suitable growth conditions are available (Whitehead *et al.*, 2009).Therefore evaluating the surfaces when a relevant fouling material is present gives a more comprehensive insight towards the behaviour of the bacterial cells and the antimicrobial activity of the surfaces in conditions more likely encountered *in vivo*.

Methods to assess the fouling of surfaces by organic material are frequently discussed in literature but a relatively quick and simple method for assessment is rarely seen (Verran *et al.*, 2002). Methods for visualising the effect of conditioning films on microorganisms usually involve epifluorescent microscopy and differentially staining the two counterparts (Verran and Whitehead, 2006). Using methods involving epifluorescent microscopy may have a relatively rapid test time however the investigations into the correct staining technique is time consuming and may not always work when used on different surfaces. Performing the reliable macroscopic methods of; zones of inhibition, NTV tetrazolium assay and the JIS assay in the presence of a suitable conditioning film has the potential to be a viable option to evaluate the effect of conditioning film on the microorganisms. This method can be comparable to the work carried out without conditioning films and may demonstrate the

efficacy of the antimicrobial coatings in the absence and presence of a conditioning film.

In vitro, the choice of conditioning film should be decided to relate to the environment the surface will encounter. In the case of this investigation the end goal is for the coatings to be applied to external bone fixation pins so the fouling of the pins will involve bodily fluids such as blood, plasma, bone and proteins from surrounding tissues.

1.8 Quantitative Assessment of cell Distribution (MATLAB)

When microorganisms are retained on a surface they are usually distributed across the surface in a pattern depending upon the surface properties of the substrate and the bacterial cell surfaces. Measuring the dispersion and density of bacterial cells under a microscope is undertaken using qualitative data and descriptive terms, however the reliability of this data between users and methods mean that it is difficult to gain reliable results.

In other scientific areas measuring the dispersion of objects quantitatively has been achieved by using multifractal analysis (Block *et al.*, 1991, Kropp *et al.*, 1997, Mills *et al.*, 2004). The distribution of points in a multifractal analysis sample can be created from a map, to quantify earthquake distribution (Pastén *et al.*, 2011) or the mapping the dispersion of flame retardant polymer particles in materials (Mills *et al.*, 2002).

Using the mathematical computer program MATLAB programs can be created which analyse images and can be requested to analyse the dispersion or a certain brightness phase in a greyscale image. This is advantageous in microscopic images of bacteria because the bacteria are viewed as distinct points on the image, which the program is commanded to analyse. The analysis method will be described further in Chapter 8.

1.9 Aims and Objectives

The aim of the investigation was to develop a hard wearing antimicrobial coating for surgical applications, in particular external fixation pins, using reactive magnetron sputtering.

1.9.1 Objectives

- Develop novel coatings using magnetron sputtering to produce a zirconium nitride/silver alloy with three different concentrations of silver.
- Deposit the coatings onto medical grade 316L stainless steel with a unique surface finish to replicate the surface of implant biomaterials.
- Deposit the coatings onto silicon wafer substrates for chemical and structural analysis.
- Characterise the morphology, tribology and topography of the coatings on stainless steel.
- Test the coatings against significant implant pathogens for antimicrobial efficacy.
- Optimise the coating tribology and antimicrobial performance for use in medical implants and/or devices.
- Design a method to investigate the antimicrobial effects of the coatings in the presence of a relevant conditioning film.
- Quantify the leaching of silver from the coatings using ICP-AES.
- Determine any physicochemical relationship between the retention of the bacteria and the surfaces.
- Analyse the distribution and density of the retained bacteria using a mathematical analysis package (MATLAB).

2 Characterisation of Nanocomposite ZrN/Ag Coatings

2.1 Introduction

2.1.1 Magnetron co-sputtering of Zirconium Nitride Silver

Magnetron sputtering is a versatile method of metallizing solid surfaces to improve the properties and functionality of a product application. Co-sputtering involves multiple magnetrons with targets of different chemical composition to deposit different metals in either monolayers or a homogenous coating, depending upon the exposure time towards each magnetron. Uses for magnetron co-sputtering include multilayer stacks of TiO_2 and silver for low emissivity optical coatings on glass (Li, 2013) and deposition of Cr-Cu-O for use as an antimicrobial surface with good mechanical properties (Musil *et al.*, 2013). It is also used in many ways to produce antimicrobial coatings such as depositing metallic silver (Baghriche *et al.*, 2012) or copper (Osorio-Vargas *et al.*, 2011) and also producing hard wearing coatings with antimicrobial properties such as TaN-(Ag,Cu) by co-sputtering, (Hsieh *et al.*, 2013), titanium oxide silver (TiO/Ag) (Song *et al.*, 2012) and Cr-Cu-N antimicrobial coatings (Kuo *et al.*, 2007). The zirconium nitride silver (ZrN/Ag) coatings used in this investigation were developed from previous investigations on titanium nitride/silver, zirconium nitride/silver, chromium nitride/silver and chromium nitride/copper thin films deposited using the same method (Kelly, 2009b, Kelly *et al.*, 2010a, Kelly *et al.*, 2010b, Whitehead *et al.*, 2011). ZrN was selected since it had the best antimicrobial properties and very good tribological properties, following CrN (Kelly *et al.*, 2010a).

2.1.2 Scanning Electron Microscopy

Visualisation of the surface morphologies by means of scanning electron microscopy is a versatile method, with the ability to characterise the thin films and understand the coating structure. By looking at fracture cross sections, using energy dispersive x-ray spectroscopy and using backscattered electron detection allowed the characterisation

of the coating structure, the chemical content and qualitative chemical distribution of the sample surface, respectively.

Scanning electron microscopy (SEM) is used to study the surface morphology of specimens. The SEM employs a beam of electrons (Goodhew *et al.*, 2001), which are directed in a raster pattern at the sample through a series of objective and condenser lenses. Secondary electrons and some backscattered primary electrons are emitted from the surface. The secondary electrons are detected and the data is assembled to produce an image.

2.1.3 Energy Dispersive X-Ray Spectroscopy

Energy dispersive X-ray spectroscopy (EDX) can be incorporated onto SEM instruments to determine the atomic percentage composition of the specimen. This employs X-rays that are generated in the specimen following the interaction of the electron beam with the surface. Analysis of the energy and intensity of the emitted X-rays can determine the elements and their amounts present in the specimen structure (Goodhew *et al.*, 2001).

2.1.4 Electron Backscattered imaging

Electron backscattered imaging utilises the primary electrons that are scattered back from the substrate following contact with the electron beam. Backscattered electron micrographs are primarily used for the qualitative assessment of chemical composition because brighter phases on the image relate to heavier elements, and darker phases to atomically lighter elements (Zupanic, 2010).

2.2 Experimental Methodology

ZrN and ZrN/Ag surfaces were produced with silver contents 15.5 at.% and 29.8 at.% for use in subsequent antimicrobial assays. The silver concentrations were chosen by replicating work by Kelly *et al.* (2011). These coatings were characterised using a range of methods.

2.2.1 Substrates

Medical grade 316L stainless steel coupons (Aalco, Bolton, UK) (10 x 10 mm) with a fine polish finish: R_a = 10 ± 2 nm were used as the underlying substratum and thus also as a control for microbiological testing. Coatings were also deposited onto highly polished silicon wafers (Montco Silicon Inc., PA, USA), cut into 10 mm x 10 mm coupons to determine the benchmark surface topography. Both stainless steel coupons and silicon wafers were cleaned using methanol and a clean fibre-free paper towel (Buehler, TEXMET® 1000, IL, USA), prior to sputtering.

2.2.2 Magnetron Sputtering

To produce the coatings for the study a method had been followed from a previously published article (Kelly *et al.*, 2010b). The sputtering rig used was a Teer Coatings UDP 350 magnetron sputtering system in a closed field unbalanced magnetic configured planar cathodes (Figure 6, Figure 7, Figure 17). The substrate holder was placed in the magnetron sputtering chamber with the samples facing away from the zirconium target to avoid deposition during initial target cleaning. The chamber was evacuated to a vacuum below 1.1×10^{-3} Pa. Following the pump down procedure Ar gas (99.99 % purity) was introduced into the chamber using a mass flow controller (MKS Instruments, Altrincham, UK). The substrates were sputter cleaned by increasing the chamber pressure to 0.4 Pa and applying an electrical bias to the substrate holder; -600 V DC for 10 minutes. Throughout the sputtering procedure which followed, the zirconium target (99.95 % purity) was driven with 1.5 kW pulsed DC power with a 20

kHz frequency (90 % duty) and the silver target (99.99 % purity) with powers of; 150 W and 230 W in separate experiments to achieve two different Ag concentrations in the deposited films. The sputter coating procedure took place in a 0.24 Pa argon atmosphere with a -30 V DC substrate bias and the nitrogen was delivered using a reactive sputter controller (Megatech, Staffordshire, UK) to introduce the nitrogen in relation to the optical emission signal of the zirconium plasma, (368 nm) (50% of the full metal signal) using parameters stated in earlier work from Kelly *et al.* (2011). Deposition times varied between 19 minutes and 50 minutes with depending upon the power delivered to the Ag target, higher power caused increased deposition rates. Following deposition the chamber was left for 40 minutes to 1 hour to cool before venting to minimise coating stresses from thermal expansion.

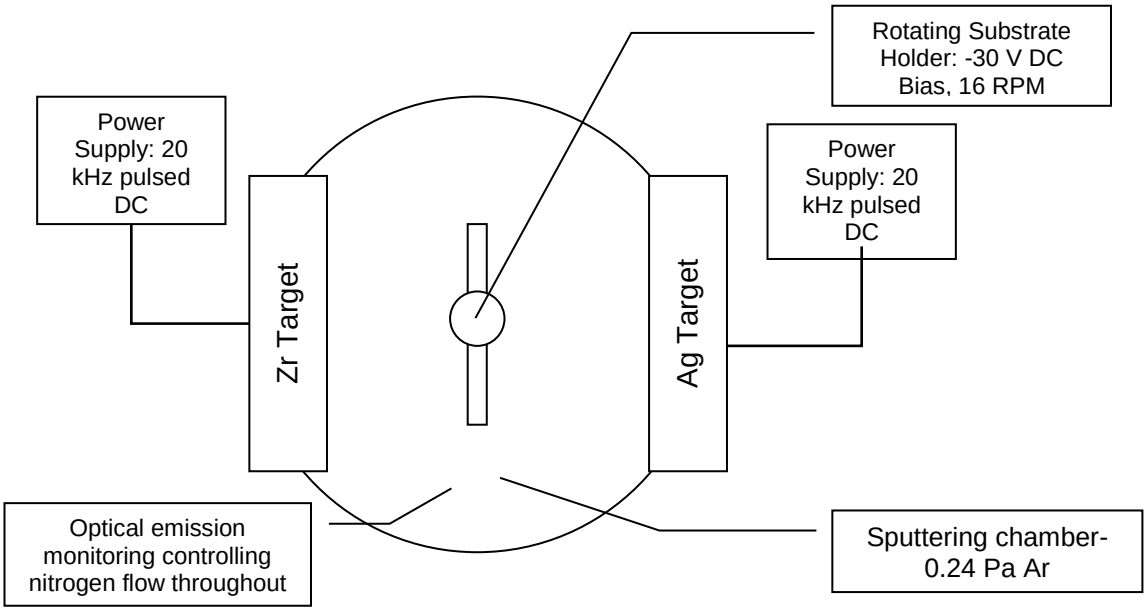

Figure 17: Simplified diagram of the Teer Coatings UDP 350 sputter coating rig. Both targets run simultaneously whilst the substrate holder is rotated at a constant speed (16 RPM). Reactive sputtering is undertaken via optical emissions monitoring to control the nitrogen flow to give a stoichiometric coating.

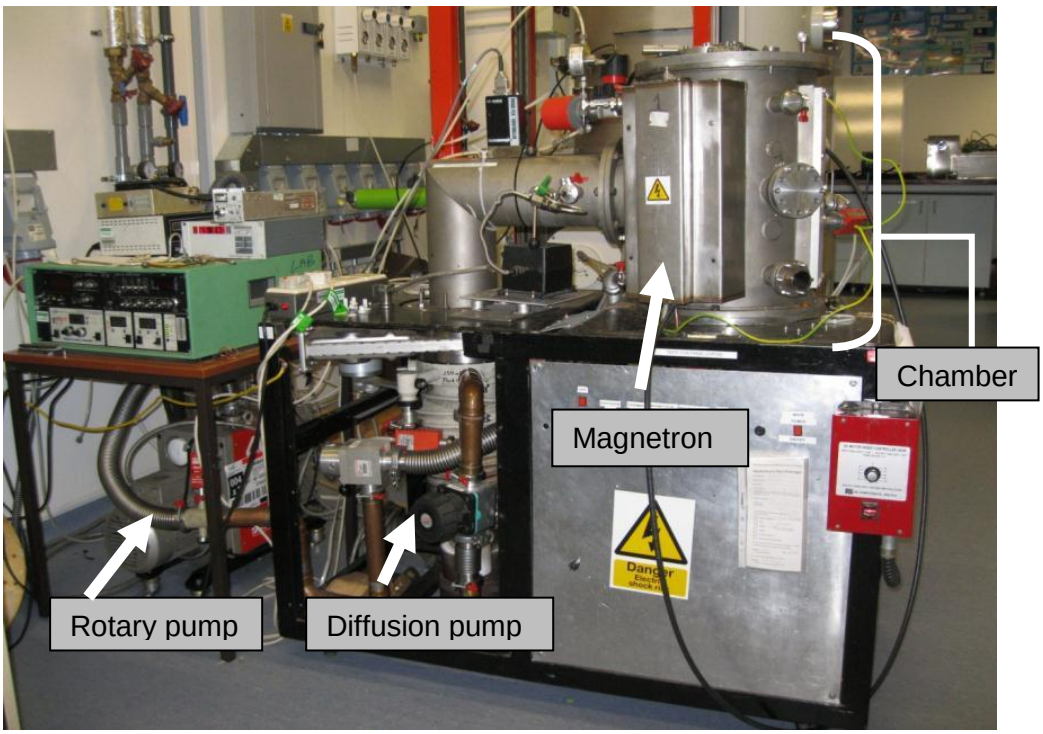

Figure 18: Teer coatings UDP 350 magnetron sputtering rig, displaying the chamber on the right, the pumps on the left (below) and monitoring equipment (above).

2.2.3 SEM and Fractures

Scanning electron microscopy was used to display the coatings morphology and structure using a Zeiss Supra VP40 field emission gun scanning electron microscope (FEG SEM). The coatings that were deposited onto silicon wafer were fractured to obtain cross section images, tilting the SEM stage 45°.

2.2.4 Backscattered electron detector

Electron backscattered imaging spectroscopy was undertaken on the samples to map the silver particle distribution on the substrate (Zeiss, Supra VP40). Electron backscattered detection was performed on the samples to qualitatively display the chemical distribution of the coating morphology. Heavier elements backscatter more primary electrons, therefore they are detected as a brighter phase. This was advantageous as silver has a heavier atomic weight than zirconium, thus the silver particle distribution was displayed as a brighter phase on the image.

2.2.5 Energy Dispersive X-Ray Spectroscopy

EDX was performed on the samples to determine the chemical composition of the coatings (Edax Trident) using an EDAX Sapphire Si (Li) detector, and quantified using a standardless ZAF algorithm. The chemical composition was calculated as an atomic percentage (at.%), giving the percentage of the said atom relative to the total number of atoms in the scan.

2.2.6 Atomic Force Microscopy (AFM) (nanotopography of the ZrN/Ag surfaces)

Two dimensional and 3D images along with roughness parameters were obtained using an explorer AFM (Veeco, CA, USA) operated in contact mode using a force constant of 0.12 Nm^{-1} and a silicon nitride tip. Scans were made of the stainless steel and silicon wafer substrates to measure benchmark topographies. Scans for both the silicon and stainless steel substrates, with the ZrN coating and ZrN/Ag coatings

containing 15.5 at.% and 29.8 at.% silver were performed. Scan sizes were 20 μm^2 and 1 μm^2 for the stainless steel and silicon wafer samples to measure the microtopography and the nanotopography of the surfaces, respectively. Three replicate scans were performed on three separate coupons. R_a roughness parameters were taken from all scans of all substrates and the average value calculated ± the standard error.

2.2.7 White Light Profilometry (microtopography of the ZrN/Ag surfaces)

Five images of three replicates (n = 15) of each surface topography were taken using a MicroXAM (phase shift) surface mapping microscope on the highest magnification setting (x101.61 magnification) with an ADE phase shift (XYZ 4400 ml system) and an AD phase shift controller (Omniscan, Wrexham, UK). The image analysis software used was Mapview AE 2Æ17 (*Z* range 210.5 nm – 1.169 µm) (Omniscan). Analysis was carried out using EX mode. The '*Z* range' is the term used as a height descriptor on a surface topography map. The value determines the maximum height difference throughout the scanned area.

2.3 Results

2.3.1 Chemical Composition (Energy Dispersive X-ray Analysis)

EDX was performed on the stainless steel substrate, the zirconium nitride and the zirconium nitride/silver at two different concentrations of silver that were deposited onto silicon wafer. From the results it is apparent that the zirconium nitride has been deposited as a stoichiometric compound and the two silver containing coatings had concentrations of 15.5 at.% and 29.8 at.% of silver for the target powers of 150 W and 230 W, respectively (Table 4). The carbon and oxygen detected in the sample is from surface contaminants that are unavoidable once the surfaces are removed from the vacuum chamber. The stainless steel used for the biomaterial replica substrate was 316L grade steel, which is most commonly recognised as “medical grade” steel and the EDX demonstrated the composition to have a higher chromium and nickel content, than a food grade 304 stainless steel, along with the addition of molybdenum in this grade of stainless steel (Table 5).

Table 4: EDX data, stating the elemental atomic percentage of ZrN and ZrN/Ag coatings on Si wafers.

Element (at.%)	ZrN	ZrN/150 W Ag	ZrN/230 W Ag
C	7.8 ± 0.3	7.1 ± 0	8.8 ± 1.3
N	44.3 ± 3.0	28.3 ± 0.7	21.3 ± 0.9
O	7.8 ± 3.9	20.7 ± 1.0	20.0 ± 1.3
Zr	39.9 ± 1.2	28.3 ± 0	20.1 ± 0.7
Ag	0.1 ± 0.0	15.5 ± 1.8	29.8 ± 0.2

Table 5: EDX results of the 316L stainless steel chemical composition displaying the weight % (Wt.%) and the atomic % (At.%) compositions.

Element	Wt %	At %
C	1.6	6.8
Fe	61.4	57.9
Ni	15.5	13.9
Al	0.2	0.5
Si	0.6	1.1
Mo	2.2	1.2
CrK	16.5	16.7
MnK	2.1	2.0

2.3.2 Scanning Electron Microscopy (SEM)

SEM micrographs of the 316L stainless steel substrate (Figure 19) with a fine polished surface finish (Ra = 9.5 ± 2 nm) to visualise the surface morphology of the stainless steel. The ZrN and ZrN/Ag coatings deposited onto silicon wafer were used to visualise the coating surface morphology. The coating surface morphology was viewed on the silicon wafer samples for the ZrN coating appeared to have a less dense structure with larger grain sizes than the thin films with added silver (Figure 20). The coatings with higher silver contents displayed bright spots throughout the micrograph, which could potentially be silver particles (Figure 21c, white arrows). This phenomenon was further investigated using the backscattered electron detector.

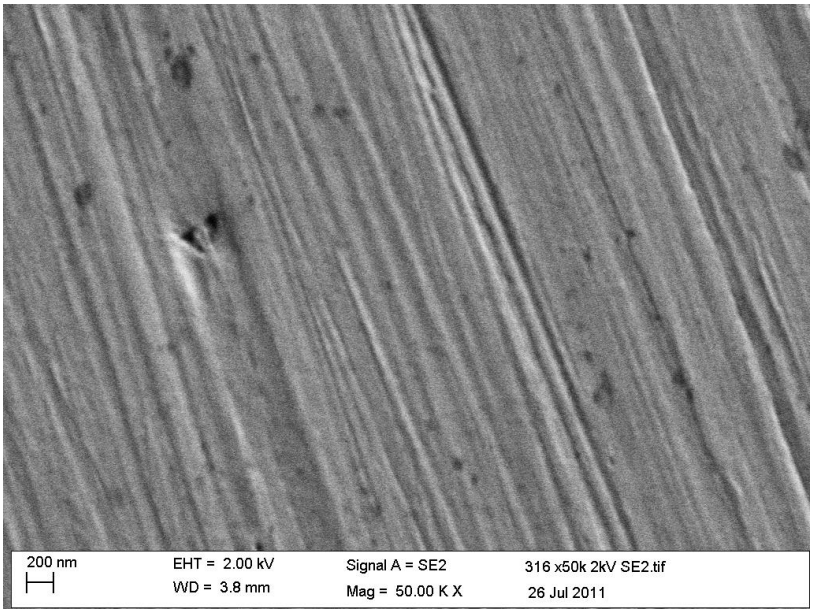

Figure 19: SEM micrograph (X 50,000 magnification) of the polished stainless steel substrate.

a)

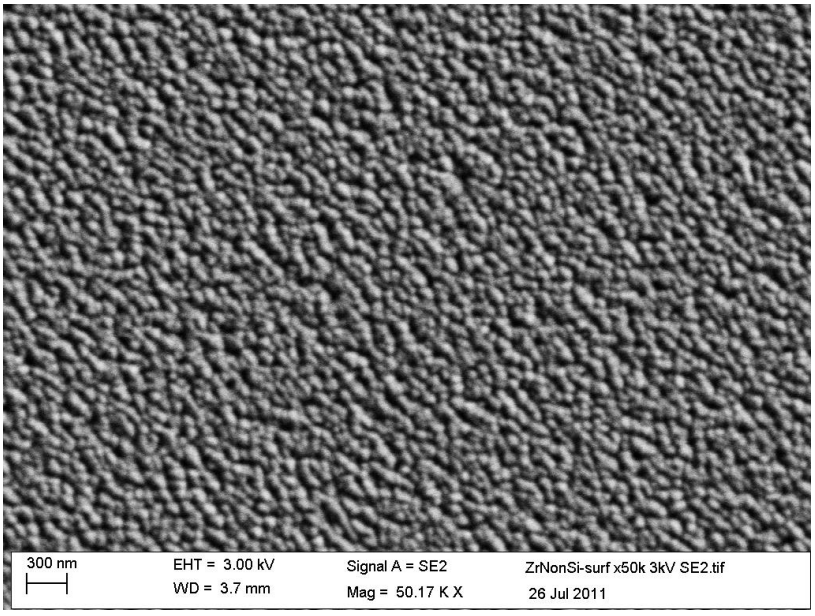

b)

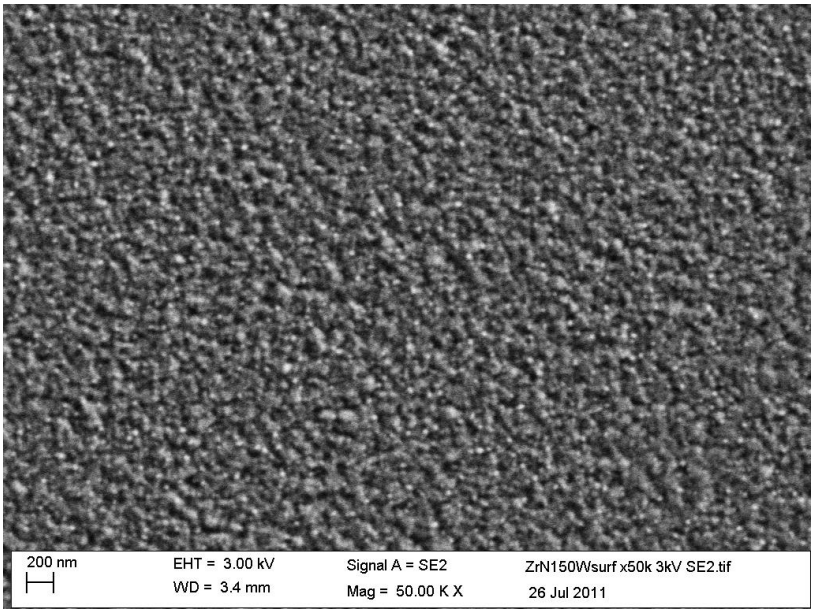

c)

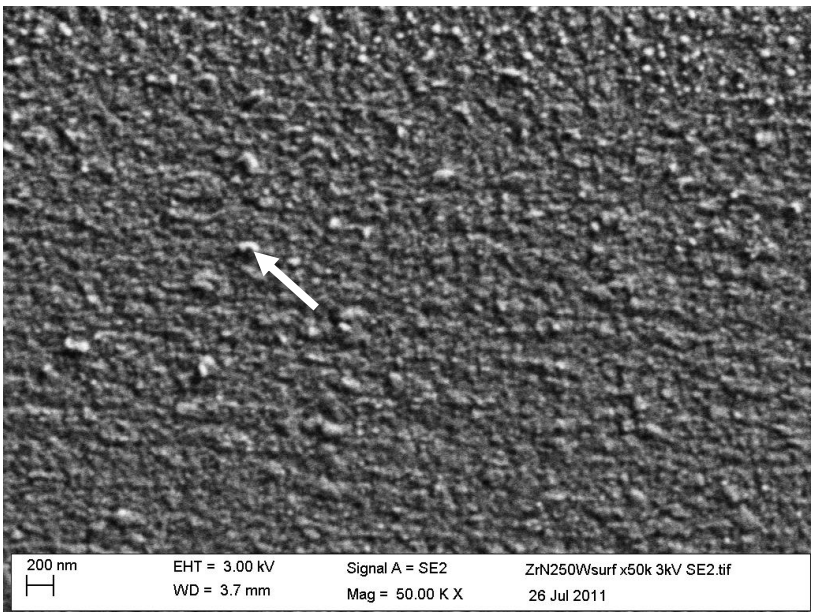

Figure 20: SEM images (x 50,000 mag) of the surface morphology of the coatings in relation to the underlying substratum (silicon wafer) a) ZrN, b) ZrN/15.5 at.% Ag and c) ZrN/29.8 at.% Ag. Coatings containing silver displayed particulate silver on the surfaces, indicated on c), which was confirmed with electron backscatter detection (see below).

2.3.3 Backscattered Electron Imaging

The backscattered electron detector was used to visualise the dispersion of silver in the coatings. There were no observable differences in the coating surface topography in relation to silver content. Given that more backscattered electrons are emitted from heavier elements (i.e. silver), domains of the latter will appear brighter in the images. Silver is the heaviest element in the coating, therefore observations suggest that the co-sputtered zirconium nitride and silver were deposited in a heterogeneous fashion, with silver nanoparticles embedded in a ZrN matrix. As the silver content increased bright particles were visible in the ZrN material with 15.5 at.% Ag and 29.8 at.% Ag content (Figure 21b and c).

2.3.4 SEM Coating Fracture cross Sections

The results displayed the structure of the coating from cross sections of fractures of the substrata using high magnification images of the surfaces. The thin film was columnar in structure and the columnar element reduced as the silver content increased (Figure 22b and c). The 29.8 at.% Ag coating displayed a clear difference in structure as seen in the cross section micrograph with no evidence of columnar deposition (Figure 22c).

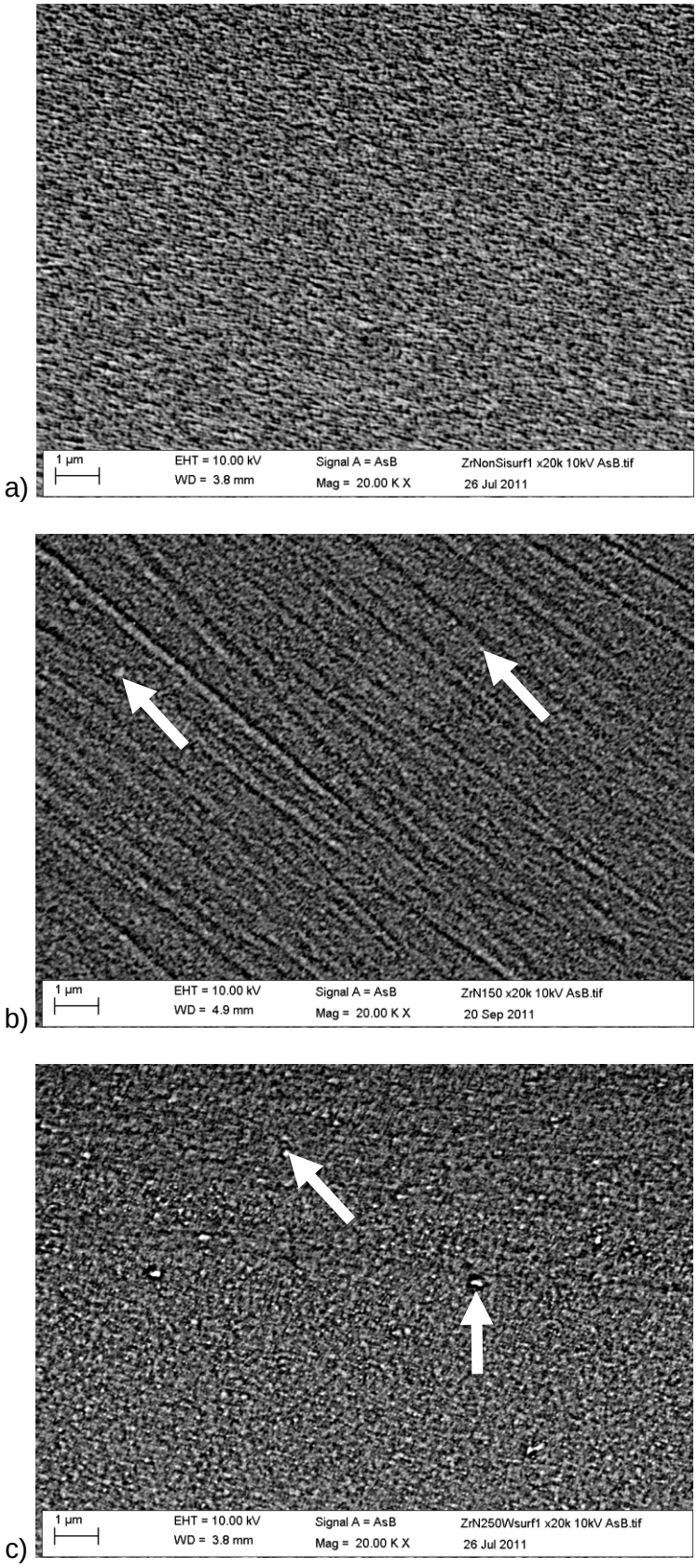

Figure 21: Backscattered electron micrographs of a) ZrN, b) ZrN/15.5 at% Ag, c) ZrN/29.8 at% Ag, displaying silver particle distribution on b) and c) (white arrows).

a)

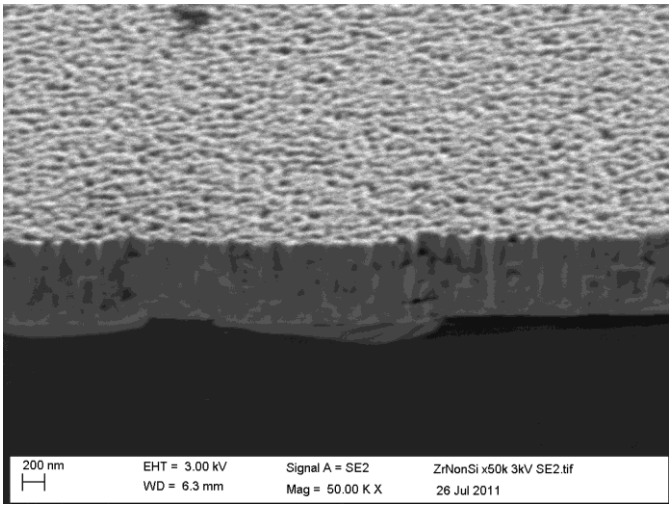

b)

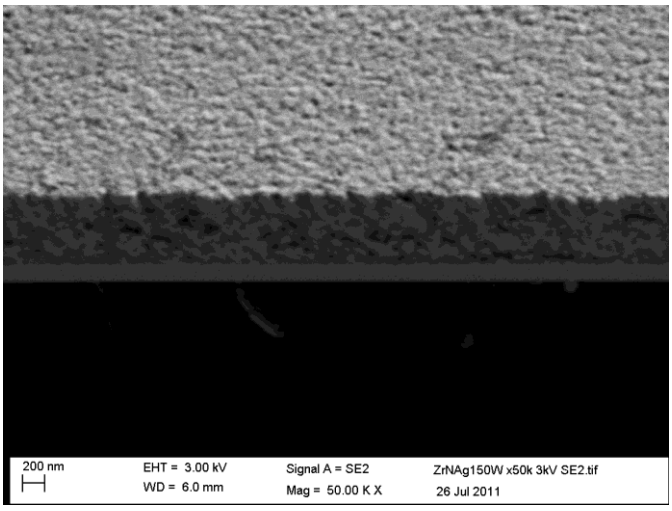

c)

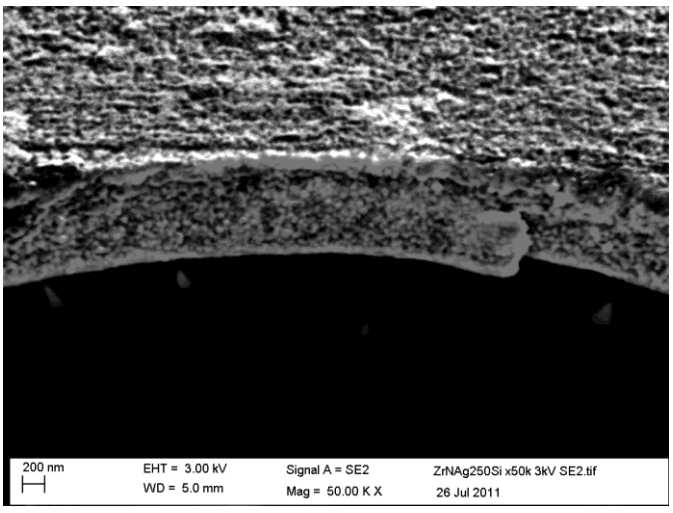

Figure 22: SEM imaging of coatings in cross section on Si wafer (x 50,000 mag) a) ZrN, b) ZrN/15.5 at.% Ag, and c) ZrN/29.8 at.% Ag, demonstrating a loss of columnar structure as the silver content increased until at the highest silver content (29.8 at.% Ag: c) the structure appeared granular.

2.3.5 Atomic Force Microscopy

The nanotopographies of the three coating compositions differed on the atomic force micrographs (Figure 23). The ZrN/15.5 at.% Ag displayed the most unique structure, where the coating surface appeared more homogenous, containing irregular protrusions of a range of sizes (Figure 23b), of which are most likely silver, determined from the backscattered electron imaging (Figure 21b). The ZrN/29.8 at.% Ag coating had a morphology similar to the prior two coatings but with increasingly elongated features and regular large rounded protrusions (Figure 23c).

2.3.6 White Light Profilometry (WLP)

White light profilometry was performed on the coatings deposited onto stainless steel to analyse the microtopography of the coating. 'The real time' scans of the surfaces displayed an increase in overall surface *Z* range in comparison to the stainless steel. The Z heights for the three coatings were 335.8 nm, 270.6 nm 1169 nm, for the ZrN, 15.5 at.% Ag and the 29.8 at.% Ag surfaces respectively. This is due to the silver particles protruding from the surface which caused large sharp peaks in the surface profile, overall increasing the total Z height, (Figure 24d), indicated with a white arrow.

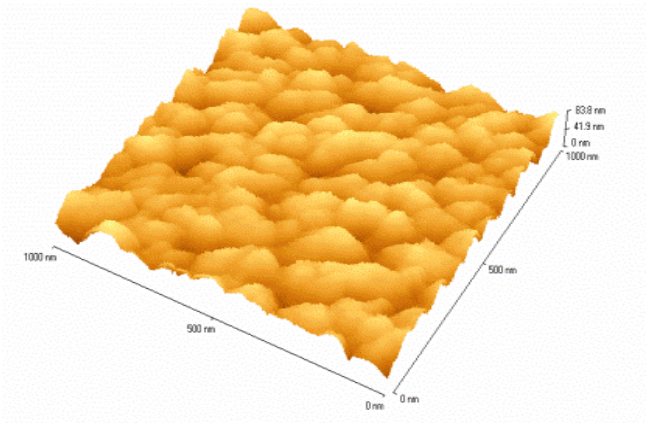

a)

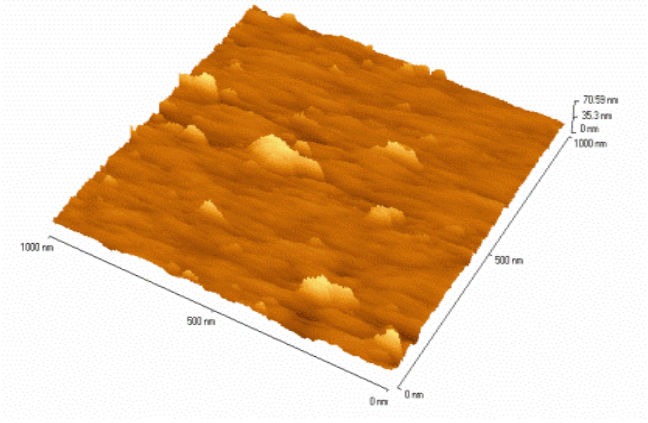

b)

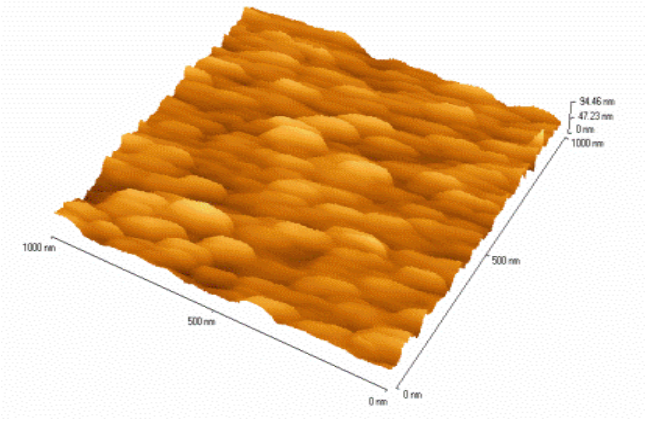

c)

Figure 23: 3D AFM images demonstrating the topographies of a) ZrN, b) ZrN/15.5at.% Ag and c) ZrN/29.8 at.% Ag when deposited onto silicon wafers. Note the variation in *Z* scale for each micrograph (a= 83.8 nm, b= 70.6 nm, c= 94.5 nm).

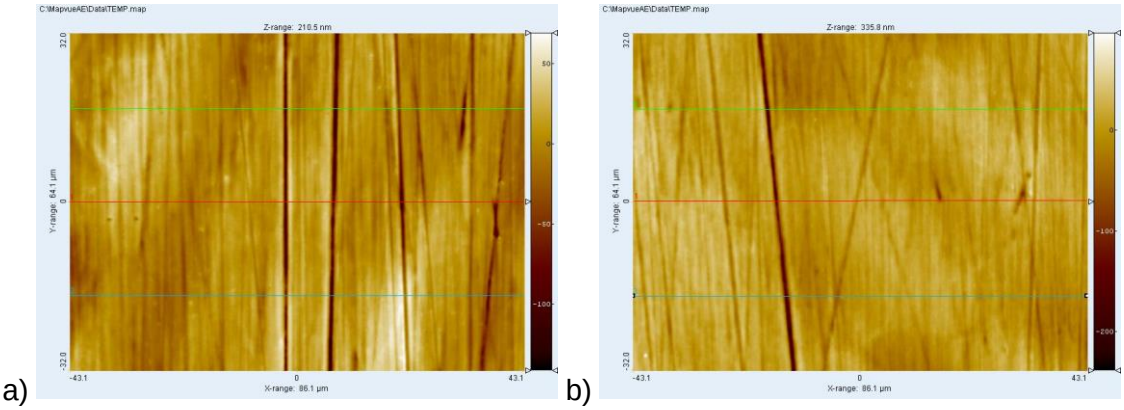

Z range: 210.5 nm *Z* range: 335.8 nm

Z range: 270.6 nm *Z* range: 1169 nm

Figure 24: White light profilometry of the four surfaces (X 101.64 magnification) a) Stainless steel b) ZrN, c) ZrN/15.5 at.% Ag and d) ZrN/29.8 at.% Ag, demonstrating similarities in microtopography between the coated and uncoated samples due to the polishing scratches in the stainless steel surface.

2.3.6.1 Line Profiles from White Light Profilometry

Line profiles were obtained from the two dimensional maps and the cross section is indicated with the red line (centre) (Figure 24). The four line profiles showed differing results from each surface, the stainless steel contained valleys, with irregular spacing of which have an effect on the profile of the deposited coatings hereafter (Figure 25a). The pure ZrN coating demonstrated a similar surface morphology to the stainless steel, still containing the irregular valleys (Figure 25b). The ZrN coating containing 15.5 at.% silver possessed a different surface texture, the large valleys cannot be seen and the texture appears to be constructed of regular spaced and sized features (Figure 25c). The zirconium nitride coating containing 29.8 at.% of silver appeared to have a smoother overall surface with very few large deviations (Figure 25d). However, from the two dimensional 'real time' image it can be seen that the surface looks smoother than the rest of the coatings, apart from the infrequent large peaks, most likely from the silver particles. This is a larger field of view of the coating surfaces in the case of microtopography, in comparison to the AFM scans, which focus primarily on nanotopography and the coating deposition morphology.

Although the line profiles have been described, a quantitative measure gives a more accurate descriptor of the individual surface features, so measurements of individual peaks and valleys were measured. The surface features were measured for height and width and the average, maximum and minimum (obtained from the total measures, not every feature of the surface) feature sizes were obtained from both the AFM and the WLP line profiles. The WLP profiles showed that there was no significant difference (p<0.05) between the entire average surface widths measured. The maximum widths were 60-80 nm (Table 6). The average width and height values from the WLP contained large standard errors, therefore it cannot be established that the addition of the coatings altered the microtopography using WLP (Table 7).

2.3.7 Wettability

Water contact angles were obtained for the four different surfaces to determine surface wettability. The most wettable surface was the pure ZrN, displaying the lowest water contact angle of 60.9º (Figure 26). The least wettable was the stainless steel, with the highest contact angle of 88.8º. This demonstrated that the addition of zirconium nitride coatings reduced the surface wettability. The addition of silver to the ZrN coating, however increased the average contact angles of the surfaces demonstrating that the alteration of surface composition alters the surface wettability and potentially other physicochemical properties of the surfaces.

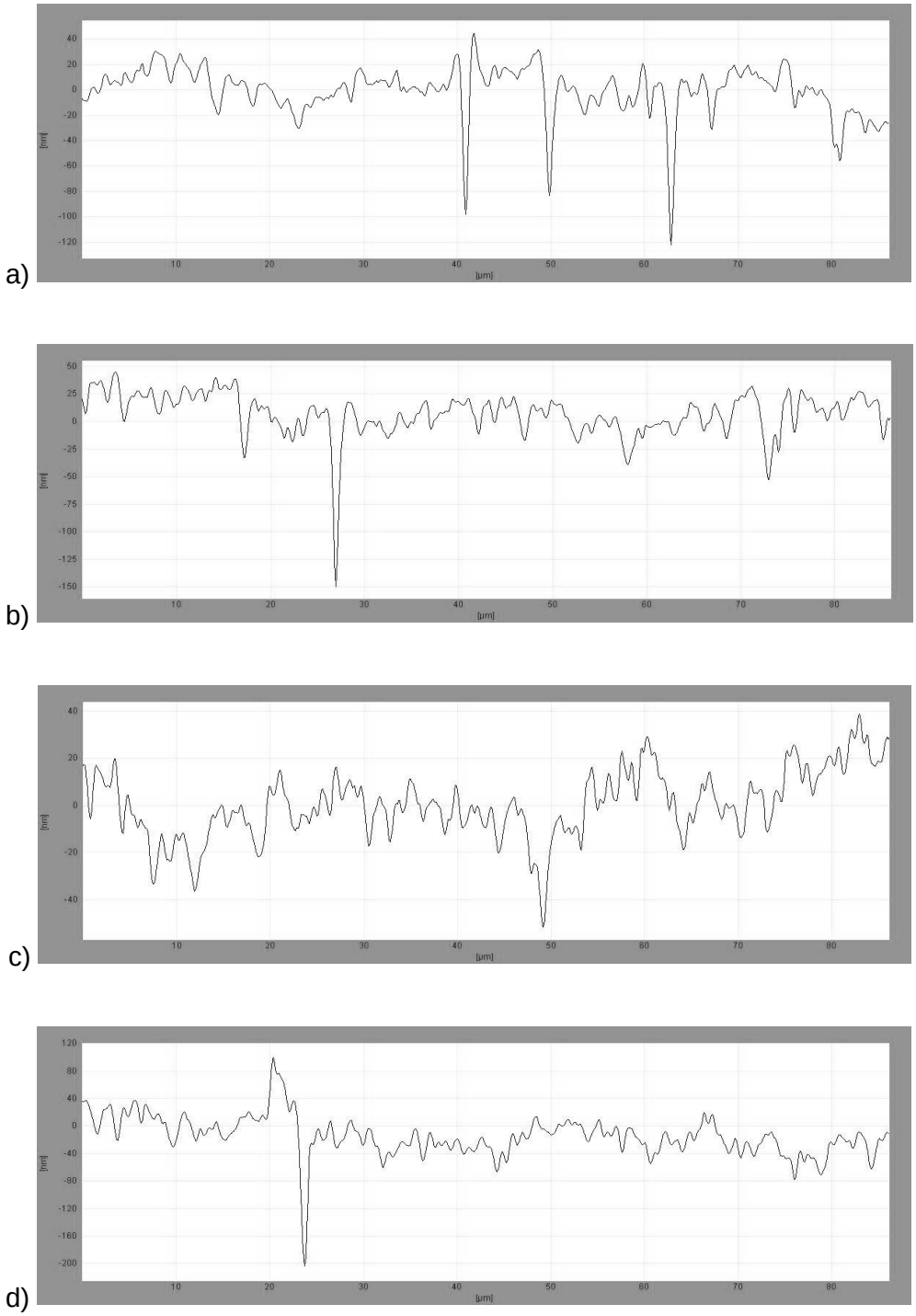

Figure 25: Line profiles of the WLP scans of a) stainless steel, b) ZrN, c) ZrN/15.5 at.% Ag and d) ZrN/29.8 at.% Ag, displaying the width and depth of the peaks and valleys as well as a cross section of the microtopography shown from Figure 24. Note differences in Z scales: a) +40 nm, -120 nm, b) +50 nm, -150 nm, c) +40 nm, -50 nm, d) +120 nm, -200 nm. All Y axes are the same (100 µm).

Table 6: White light profilometer line profile (X 101.64 magnification) peak and valley measurements, displaying the average width and depth ± the standard deviation and the maximum and minimum sized features.

WLP	Stainless Steel			ZrN			ZrN/15.5 at.% Ag			ZrN/29.8 at.% Ag		
(nm)	Average	Max	Min	Average	Max	Min	Average	Max	Min	Average	Max	Min
Width	213 ± 121	776.3	69	186 ± 111	770	77	212 ± 116	654.5	77	186 ± 95	731.5	57.8
Depth	26 ± 26	137.8	5.46	22 ± 27	200	2.1	16 ± 11	66	3.8	32 ± 22	161.7	6

Table 7: AFM line profiles (10 μm x 10 μm) peak and valley measurements, displaying the average width and depth ± the standard deviation and the maximum and minimum sized features.

AFM	Stainless Steel			ZrN			ZrN/15.5 at.% Ag			ZrN/29.8 at.% Ag		
(nm)	Average	Max	Min	Average	Max	Min	Average	Max	Min	Average	Max	Min
Width	412 ± 138	660	227	341 ± 116	460	139	587 ± 298	983	187	702 ± 241	1187	421
Depth	8 ± 7	25.2	1.4	28 ± 10	27.99	11.7	47 ± 31	101.4	13.5	44 ± 18	69	20

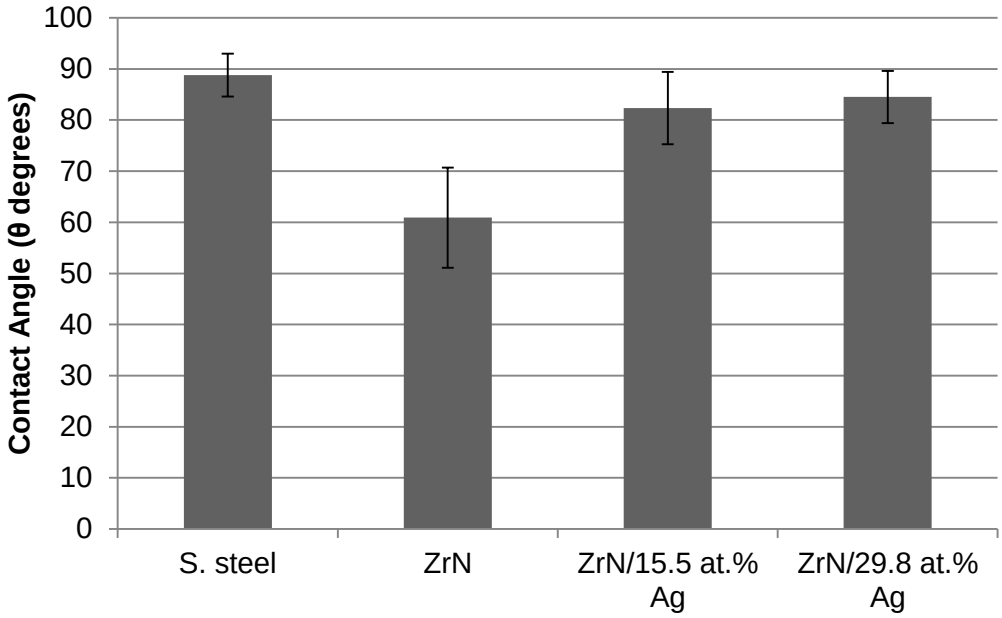

Figure 26: Water contact angles, using the sessile drop method, of the four surfaces investigated. Stainless steel had the highest contact angle and therefore was the least wettable.

2.4 Discussion

The coatings were sputtered onto silicon wafer for morphology, structure and chemical composition analysis and 316L stainless steel coupons for antimicrobial testing, tribological tests and analysis of the surface wettability. The coatings were deposited with a columnar structure which decreased in grain size and became more granular/cuboidal in morphology with an increase in silver content.

The ZrN coatings, in all cases, were deposited stoichiometrically with both elements zirconium and nitrogen being a similar atomic percentage of 44.3 at.% Zr and 39.9 at.% N for ZrN, 28.3 at.% Zr and 28.3 at.% N for ZrN/15.5 at.% Ag coating and 21.3 at.% Zr and 20.1 at.% N for the ZrN/29.8 at.% Ag coating. The silver content within the three samples was not as expected, with the 70 W target power predicted to have around 5 at.% Ag (Kelly *et al.*, 2011), whereas it was found the surfaces contained 0.45 ± 0.6 at.% Ag. This result was most likely due to co-sputtering different materials and the silver target surface becoming coated with zirconium nitride from the opposite target, thus reducing the sputtering rate of the silver. This also makes it harder for the thin layer of zirconium nitride to be sputtered off, as it takes more energy to dislodge the surface ZrN particles. Contamination of the silver target could be decreased if a barrier were to be created between the zirconium target, the substrate and the silver target. This has been developed for use in further work using a thin stainless steel sheet manufactured into screens. Results from Kelly et al. (2010) demonstrated that the 150 W and 230 W target power levels should have given coatings with silver contents of 10.4 ± 0.7 at.% and 25.9 ±0.4 at.% of silver, respectively. However these values are lower than were obtained in this work: 15.5 ± 1.8 at.% and 29.8 ± 0.2 at.% of silver, for powers of 150 W and 230 W, respectively. Backscattered electron images obtained from the SEM suggested that the silver was deposited as nanoparticles embedded within the zirconium nitride matrix.

SEM images of the cross section of the coatings indicated columnar structures, which changed to a denser granular structure as the silver content increased. This observation may be explained by a variety of factors. The Thornton structure zone model (Figure 8) demonstrated that as the energy of the film growth (ion bombardment) increased, the average diameter of the columns decreased, producing a denser coating structure (Thornton, 1974). This phenomenon also occurs as the process gas pressure increases (Miao et al., 2003), meaning a potential method for altering the structure, if needed, could be to decrease the process gas pressure, potentially giving a more dense structure and in turn altering the coating properties (Thornton, 1974, Window and Savvides, 1986). Also the addition of the silver will have altered the deposition of the coating, having a material effect, producing different film structures, as observed in the SEM fractures. Some of the coatings delaminated and stressed, especially when subjected to certain microbiological assays such as the NTV assay, which involved submerging them in molten agar. This problem was addressed in future work (See Chapter 4; Page 111) by improving adhesion and coating properties via modification of the deposition parameters and initial interlayers onto the bare substrate. Zirconium has been known to have a slight immiscibility towards iron and the fact that stainless steel is high in iron content may have affected the coating adhesion. The method of magnetron sputtering is so versatile that it is possible to add and remove magnetrons to the sputtering chamber containing targets of different materials. Thus, in later work an initial interlayer of titanium was investigated, as well as the grading of the nitrogen gas in proportion to the zirconium optical emissions to produce graded layers from the most metallic to fully stoichiometric coatings (Li *et al.*, 2006, Monaghan *et al.*, 1993).

The ZrN coating displayed a brittle structure and a poor adhesion to the underlying substrate following use during the antimicrobial assays (Chapter 3). The poor adhesion will be addressed in future work by investigating sputtering a metallic interlayer prior to

depositing the nitride coating. Sputtering a pure metal interlayer before depositing a nitride has been found to improve adhesion, improve corrosion resistance, relieve stress on the nitride film and potentially change the crystalline texture of the deposition (Huang *et al.*, 2006, Gerth and Wiklund, 2008).

White light profilometry of the ZrN and ZrN/Ag coatings in relation to the underlying bare substrate indicated that the coatings did not alter the surface features but followed the underlying microtopography of the stainless steel. Although some features in the stainless steel may exceed 1 μm in width, the amplitude of the features never exceeded more than 200 nm, which is still shallow enough to be classed as “nanotopography”. The AFM scans were smaller than the WLP to demonstrate more comprehensive detail of the nanotopographies.

Surface defects arise from abrasion and mechanical and chemical cleaning, which are commonly encountered during the life of a medical device; including external bone fixation pins due to the open surface requiring regular cleaning and re-dressing. Therefore the ZrN coating was used to enhance scratch resistance of the surfaces. The difference in the microtopography of coatings, deposited onto stainless steel, were further investigated in the presence of conditioning film (Chapter 7; Page 214). The latter contained organic components such as blood, plasma or fibrinogen expected to be found within the environment in which a bone fixation pin resides. This is an important facet of the research as differences in nanotopography can affect the type and how the conditioning film adheres to the surface.

The roughness of the coatings increased as the silver content increased, which could be due to the silver forming as particles protruding from the ZrN surface. This was visible on the AFM scans of the coatings deposited on the silicon wafer but less so on the stainless steel substrates investigated on the white light profilometer.

The wettabilities of the four surfaces tested were all relatively similar, between 82.3º and 88.8º, apart from the pure ZrN, which was more wettable with an average contact angle of 60.9º. The stainless steel possessed a water contact angle of 88.8°, of which reflects similar findings from Nguyen *et al.* (2011), showing a water contact angle of 87.2 ± 3.3°. The hydrophobicity of the surface and also surface interaction with the cells will affect the bacterial cell adhesion behaviour (Reid, 1999, Whitehead et al., 2005, Yüce and Demirel, 2008). The hydrophobicity and surface free energies of the surfaces are investigated by calculating the contact angles of polar and non-polar solvents with the substrata. However, in this investigation only the surface wettability was investigated, by determining the contact angles of water on the surfaces. The difference between hydrophobicity and wettability is that the unit of hydrophobicity is calculated to quantify the surface charges and the value is given in a quantifiable state (ΔG_{iwi}), whereas wettability just compares the contact angles obtained from water contact on the surface and the relation to qualitative measurements, for example, less wettable and more wettable (Van Oss and Giese, 1995). In further work the hydrophobicities of the surfaces were investigated (5.3.6; Page 173) using two polar solvents (one being water) and one non-polar solvent, and using a method derived from Van Oss (1995) to calculate the ΔG_{iwi} values. These values provided insight into why the bacterial cells were retained on the surfaces.

2.5 Concluding Remarks

Zirconium nitride and zirconium nitride silver coatings with concentrations of 15.5 at.% Ag and 29.8 at.% Ag were deposited onto 316L medical grade stainless steel coupons. Following EDX, SEM, backscattered electron imaging, AFM, white light profilometry and wettability tests it was demonstrated that the coatings were deposited in a columnar formation, reducing in grain size and altering to a more granular/cuboidal morphology with the addition of silver. The increase of silver displayed an increase of the surface roughness. All surfaces, including the stainless steel possessed similar wettabilities, with the pure ZrN being the most wettable and stainless steel being the least. The nanotopography differed for all of the surfaces, the ZrN possessed regular evenly sized grains, the 15.5 at.% Ag displayed smaller grains with protruding larger particles and the 29.8 at.% Ag possessed more elongated grains. These surfaces were tested (Chapter 3) in the presence of bacteria relevant to pin tract infections to determine the antimicrobial efficacy of the coatings and effects on the surface properties on bacterial retention.

3 The Antimicrobial Efficacy of Zirconium Nitride Silver Substrata and Their Effect on Bacterial Retention

3.1 Introduction

3.1.1 Zirconium and Zirconium Alloys

Zirconium is a non-toxic metal that possesses a high tolerance to corrosion and leaching/metal release, even under harsh chemical environments (Emsley, 2011). Its current use as a biomaterial appears limited but its potential is clearly stated. Wetzel et al. (2008) used a PVD method to deposit pure zirconium onto polyurethane flexible surfaces used in biomaterials and tested for biocompatibility and cytotoxicity. They found that the zirconium coated surfaces displayed an enhanced adhesion of human umbilical vein endothelial cells to the surface compared to the uncoated surfaces. They concluded that this is a potential method to adapt polymeric implants towards long-term stability requirements. Primarily, the use of zirconium in medical implants is as zirconia (ZrO_2) ceramic implants in dental surgery. Zirconium compounds, in contrast to titanium, does not undergo electrochemical corrosion from contact with bodily fluids and also has the aesthetic properties in dental applications as it is white in colour (Mueller *et al.*, 2013). Oxidised zirconium, which uses heat (~500ºC) to oxidise zirconium into a ceramic, has been investigated for use in load bearing implants as well as ZrO_2 and it was determined that the surfaces displayed excellent biocompatibility *in vitro* compared to Ti and decreased wear rate over 'as deposited' Zr (Balla *et al.*, 2009).The desirable chemical properties of zirconium and its alloys has the potential to be applied elsewhere, such as zirconium nitride. Literature on zirconium nitride as a biomaterial is scarce but in the literature it is usually investigated alongside relatively similar nitrides such as TiN, NbN, TiAlN and ZrCN (Balaceanu *et al.*, 2010). Aouadi (2004) described the potential for ZrN/Ag in biomedical applications due to:

- Silver and zirconium nitride being two of the most biocompatible materials and possess good corrosion resistance and biocompatibility

- Silver and zirconium nitride being immiscible with each other, therefore form a nanocomposite structure through segregation
- Zirconium nitride is the most stable nitride.

Aouadi investigated the preliminary structural, optical, chemical and mechanical properties of the ceramic film for potential use in biomedical implants but did not perform any *in vitro* assays against any cells to test for histocompatibility. Kertzman et al., (2008) subsequently investigated the same coatings for biocompatibility in their study. It was found that human serum albumin and fibrinogen successfully adsorbed to the coating surfaces deeming them histocompatible and antibacterial activity was observed in the presence of *Staphylococcus aureus, Escherichia coli* and *Staphylococcus epidermidis*. The surfaces were shown to consist of nano-grains of silver embedded in a nanocrystalline ZrN matrix. The combination of desirable properties of corrosion resistance, scratch resistance and antimicrobial efficacy give this type of coating potential for use on implants and in the case of this study orthopaedic implants.

3.2 Methodology

3.2.1 Maintenance of Microorganisms

The microorganisms *Staphylococcus aureus* NCTC 8532 and *Staphylococcus epidermidis* NCTC 11057 were used for this investigation. Stock cultures were stored in the freezer at -80 ^{o}C. When required the cultures were thawed and inoculated onto nutrient agar (Oxoid, UK) media and incubated for 24 h at 37 ^{o}C. The stock cultures were re-frozen following use. The inoculated agar plates were kept refrigerated at 4 ^{o}C and replaced every four weeks to maintain the cells' physiology.

3.2.2 Preparation of Cultures For Use in Microbiological Assays

Sterile brain heart infusion (BHI) broths (Oxoid, UK) (10 ml) were inoculated with *S. aureus* NCTC 8532 or *S. epidermidis* NCTC 11057. These were incubated overnight in an orbital incubator at 37 ^{o}C for 24 hours at 130 RPM. Cultures were removed from incubation and the cells were washed in sterile membrane filtered water (Millipore Elix, MA, USA) (10 ml) by centrifuging at 604 *g* for 8 minutes. The supernatant was removed and the cells were re-suspended in sterile distilled water. Cells were diluted to an optical density (OD) of 1.0 ± 0.05 at 540 nm using a spectrophotometer (Jenway 6305, Bibby Scientific, Essex, UK), using distilled water as a blank. Cell numbers were determined in colony forming units/ml (CFU/ml) using serial dilutions to a dilution of 1 x 10^{-8}. The diluted cell suspension (100µl) was spread and repeated in duplicates on brain heart infusion agar (Oxoid, Basingstoke, UK) and incubated at 37 ^{o}C for 24 h.

3.2.3 Retention Assay

Microorganisms were prepared using the method described previously (3.2.2). Wearing gloves, samples were cleaned with a fibre free cloth (Buehler, IL, USA) by wiping in one direction, linearly with ethanol (2 ml) (Sigma Aldrich, Dorset, UK), then rinsed by

wiping with a piece of fibre free cloth soaked in sterile distilled water (2 ml) and dried in a class II air flow cabinet for 15 minutes before use. The samples were stuck into the bottom of a glass Petri dish with double sided tape (Guilbert Niceday, Hampshire, UK). The prepared cell suspension (30 ml) was poured over the samples in the glass Petri dishes. The lids were placed on the dishes and incubated for one hour at 37^{o}C without agitation. Samples were removed using sterile forceps and rinsed once, gently with 5 cm^{3} distilled water, with the bottle at a 45^{o} angle, and a 3 mm nozzle. Depending upon the staining or fixing procedure used, the surfaces with retained bacteria were treated in different ways following rinsing.

3.2.4 SEM Preparation (Retention Assay)

The method for fixing and preparing the samples for visualisation under the SEM was derived from Whitehead *et al.* (2005b). Following the retention assay procedure (*see* 3.2.3) the substrata plus retained cells were immersed in 4% (v/v) gluteraldehyde for 24 h at 4º C. After fixing, the surfaces were washed gently with distilled water and passed down an ethanol gradient (BDH,UK) of 30 %, 50 %, 70 %, 90 % and 100 % each for 10 min. Prior to examination, samples were stored at room temperature in a desiccator with silica gel (BDH UK). The samples were fixed onto SEM stubs for gold sputter coating, which was carried out using an Emitech SC7460 (East Sussex, UK) SEM sputter coater. Samples were sputter coated at a vacuum of 0.09 mbar, for 3 min, at 2500 V, in argon gas at a power of 18–20 mA. Images of the surfaces including the bacterial cells were obtained using a JEOL JSM 5600LV scanning electron microscope and six field images were collected from the samples (n = 3).

3.2.5 Acridine Orange Staining of Retained Bacteria

Following on from the retention assay method (3.2.3) the cells needed to be stained for visualisation under an epifluorescent microscope. The substrata and subsequent retained cells were allowed to dry in a class II laminar flow hood for 1 hour. The surfaces with retained bacteria were stained for 2 minutes with 0.03% acridine orange

(Sigma, St. Louis, USA) in 2% glacial acetic acid (BDH, Poole, UK), then rinsed with distilled water (3.2.3), and air dried once more in the class II laminar flow hood, in the dark. The substrata plus retained cells were visualised using epifluorescent microscopy (Nikon Eclipse E600 epifluorescence microscope, Tokyo, Japan), at 502 - 526 nm wavelength and Cell-F image visualisation software (Olympus, UK) was used for image capture and analysis.

3.2.6 Retention Assay (LiveDead™)

Following the retention assay (3.2.3) the samples were mounted onto glass slides for air drying in a class II microbiological flow cabinet for 45 minutes before staining. Prepared BacLight bacterial viability LiveDead™ stain (LiveDead™, BacLight™ bacterial viability kit, Invitrogen, Paisley, Scotland) (2.5µl) was added to the samples. Both stains had been individually diluted to a 1:40 stain: water ratio and made up into a 2.5:1 ratio of SYTO9 and propidium iodide respectively. The stain was spread with the end of the pipette tip over the sample and left to dry (approximately 15 minutes) in the dark without rinsing.

Viable and non-viable cells were counted using an epifluoresence microscope (Nikon Eclipse E600, Surrey, UK), through a mounted F-View II black and white digital camera (Soft Imaging System Ltd, Helperby, UK, supplied by Olympus, Hertfordshire, UK) using Cell-F Image analysis program (Olympus, Hertfordshire, UK). The viable bacteria fluoresced green whilst non-viable cells, with a compromised membrane, fluoresced red. The two stains were differentiated by using filters of 590-650 nm for red excitation and emission spectra and 510-560 nm for the green. The samples were observed under a 10x and 100x (oil immersion) objective lenses (Leica Type F immersion oil, Wetzlar, Germany).

3.2.7 Cell Viability (NTV) Assay

This method was derived from Barnes et al. (1996) and modified to suit the application. Cells were prepared as in section 3.2.2. Colonies were counted and a dilution chosen for the assay containing between 10^5 and 10^6 colony forming units per ml (CFU/ml) (Kelly *et al.*, 2011).

The appropriately diluted suspension (10 µl) was deposited onto each coupon and put into a class (II) cabinet for one hour to dry. Following drying, 25 ml of molten brain heart infusion agar (Oxoid, Basingstoke, UK) at a temperature of 50 ^oC was poured over the coupons and once set incubated for 24 hours at 37 ^oC. Following incubation, the surface of each plate was flooded with two ml of 0.3 % filter sterilised Nitro Tetrozolium Violet (Sigma-Aldrich, MO, USA) and incubated for six hours at room temperature. Colonies were visible on the coupons as dark violet colonies, which were counted for quantitative data and photographs were taken for qualitative data.

3.2.8 Zones of Inhibition

One hundred microliters of cell suspension (OD of 1.0) was spread onto brain heart infusion agar using a sterile glass spreader. Stainless steel coupons (10 mm x 10 mm) of: ZrN, ZrN/Ag at 15.5 at.% and 29.8 at.% Ag were sterilised by wiping using 70 % ethanol and air drying in a class (II) cabinet for 15 minutes. Sterile forceps were used to transfer the coupon to the agar where it was placed with the coating (if coated) face down on the bacterial lawn. Three coupons were placed on one agar plate. The agar plates were incubated overnight for 24 h at 37 ^oC. Any clear zones were measured around the coupons (zones of inhibition) using an electronic micrometer (Mitutoyo CD-6”CP, Japan).

3.2.9 Statistical Analysis

All statistical analysis was performed using Microsoft Excel. Two tailed distribution T-tests with two sample homoscedastic variance or ANOVA (ANalysis Of VAriance)

(single factor) analysis of overall variance were carried out on the data. Results were reported as the mean ± standard error. Differences in statistical data were considered to be significant when $p \leq 0.05$ (Whitehead *et al.*, 2010).

3.3 Results

3.3.1 The Effect of Surface Properties on Bacterial Retention

3.3.1.1 SEM of the bacteria on the surface

Following SEM imaging, the *S. epidermidis* cells were shown to have different retention patterns on the surfaces in comparison to the *S. aureus* cells. The *S. aureus* cells were retained in clusters on the stainless steel, (Figure 27a) with large spaces in between, whereas the *S. epidermidis* cells (Figure 28a) attached in a more sparse pattern in groups of two or three cells. On the pure ZrN, *S. aureus* appeared to retain in higher numbers and an increased density pattern (Figure 27b). The *S. epidermidis* also reduced in size and appeared less rounded than *S. aureus* on all surfaces, and have reduced in number as the silver content increased, but not in noticeable terms (Figure 28c and d). The silver may have contributed towards an anti-adhesive effect against *S. aureus*, reducing the number of cells retained and displaying sparse distribution (Figure 27c and d).

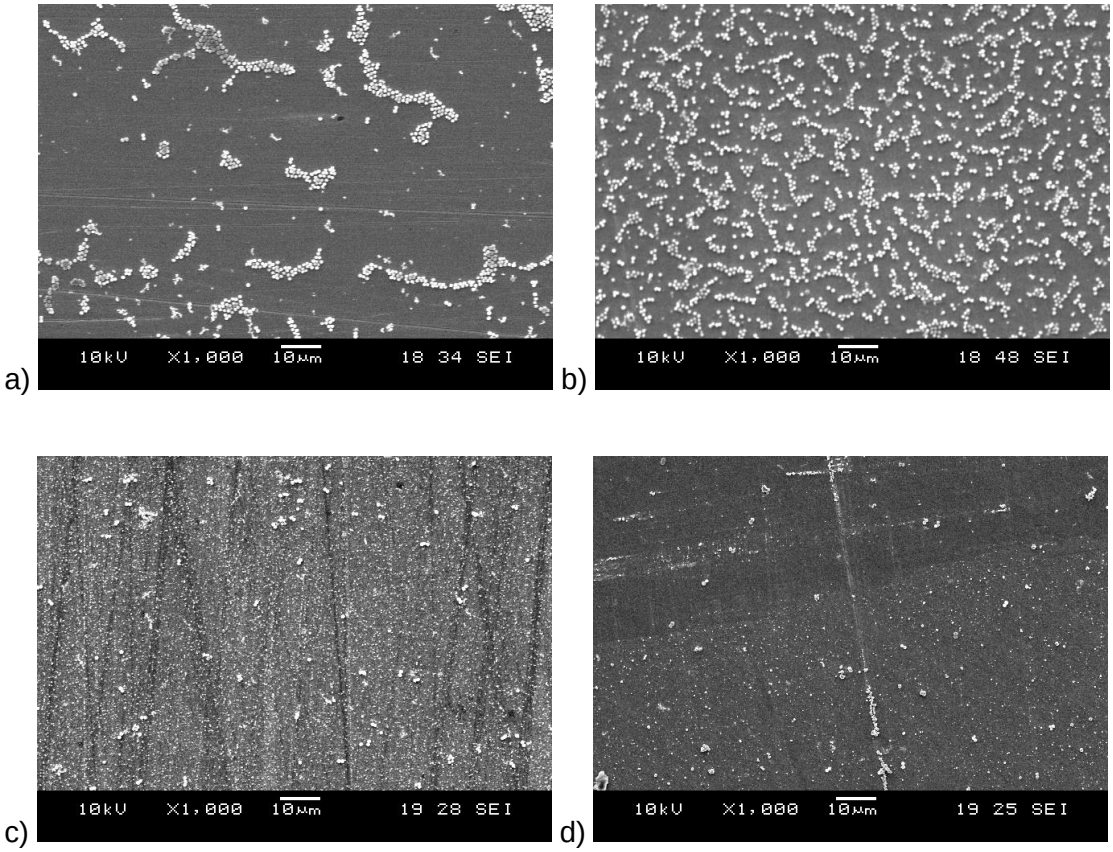

Figure 27: SEM images of *Stapylococcus aureus* (X1000 magnification) on the four investigated surfaces; a) stainless steel, b) ZrN, c) ZrN/15.5 at.% Ag and d) ZrN/29.8 at.% Ag. The surfaces all demonstrated different cell retention morphologies, with the pure ZrN (b) having the highest density retention characteristics. The silver coatings (c and d) displayed potential anti-adhesive properties towards the bacterial cells.

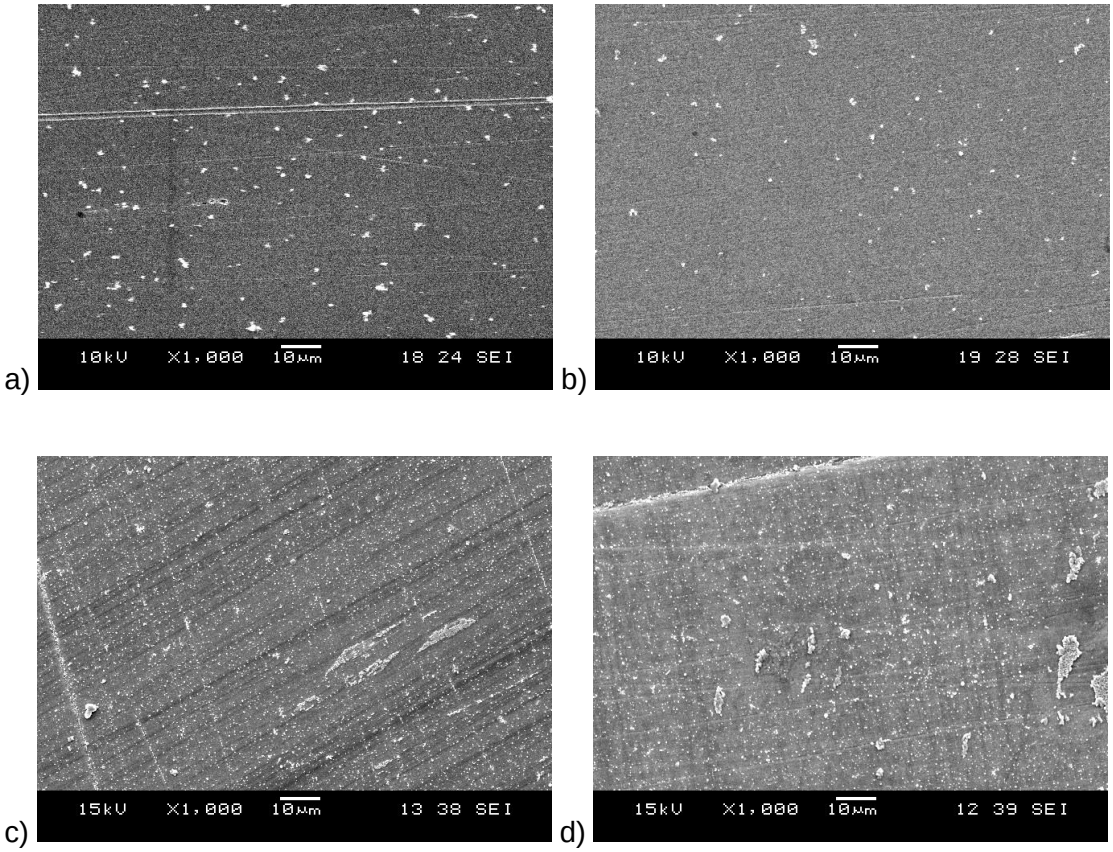

Figure 28: SEM images of *Stapylococcus epidermidis* (X1000 magnification) on the four surfaces; a) stainless steel, b) ZrN, c) ZrN/15.5 at.% Ag and d) ZrN/29.8 at.% Ag. The bacterial cells appeared smaller and less round than the *S. aureus* cells, and it appeared that the retention densities were reduced for all of the coatings in comparison to the *S. aureus* retention characteristics.

3.3.2 Acridine Orange Epifluoresence Microscopy

Acridine orange retention assays were undertaken and viewed under the epifluoresence microscope at 1000X magnification. From the images taken the qualitative distribution of the retained cells was established and the total percentage coverage of cells of the field of view was calculated (Figure 29). The number of bacteria retained increased as the silver content increased and the stainless steel retained the least amount of cells (Figure 29). Both microorganisms displayed an increasing trend throughout with the highest retained cells being on the 29.8 at.% silver coatings.

Visualising the bacteria retained on the surfaces from the epifluorescent microscopy, demonstrated that the distribution of *S. aureus* appeared similar for all four surfaces, however the coverage of bacteria appeared to increase with the increase in silver concentration (Figure 30). The *S. epidermidis* cells were retained in a different pattern and in lower numbers. The *S. epidermidis* tended to be sparsely distributed across the surfaces, with the cells grouping into clusters of less than 5. There was no significant difference ($p<0.05$) between the *S. epidermidis* numbers retained on the stainless steel (Figure 31a), ZrN (Figure 31b) and the ZrN/Ag coatings (Figure 31c and d). However, the average percentage coverage of both the microorganisms tended to increase between the stainless steel and ZrN and the ZrN/Ag surfaces, as they increased in silver content (Figure 29).

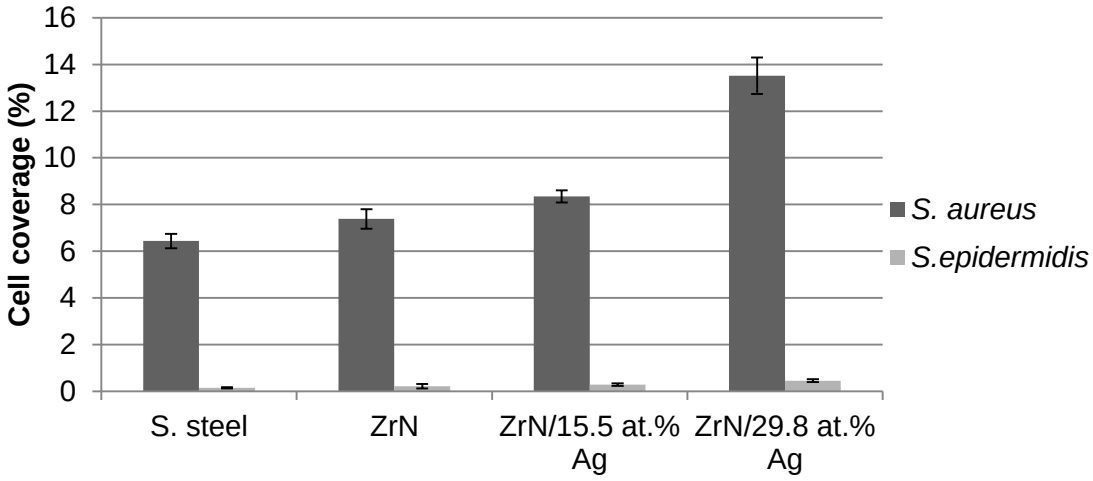

Figure 29: Average percentage coverage of *S. aureus* and *S. epidermidis* cells retained on the four surfaces, from 10 image fields of view of triplicate samples, ± the standard error, demonstrating increased cell coverage over the coatings over both materials. *S. epidermidis* demonstrated lower retention numbers than *S. aureus* cells.

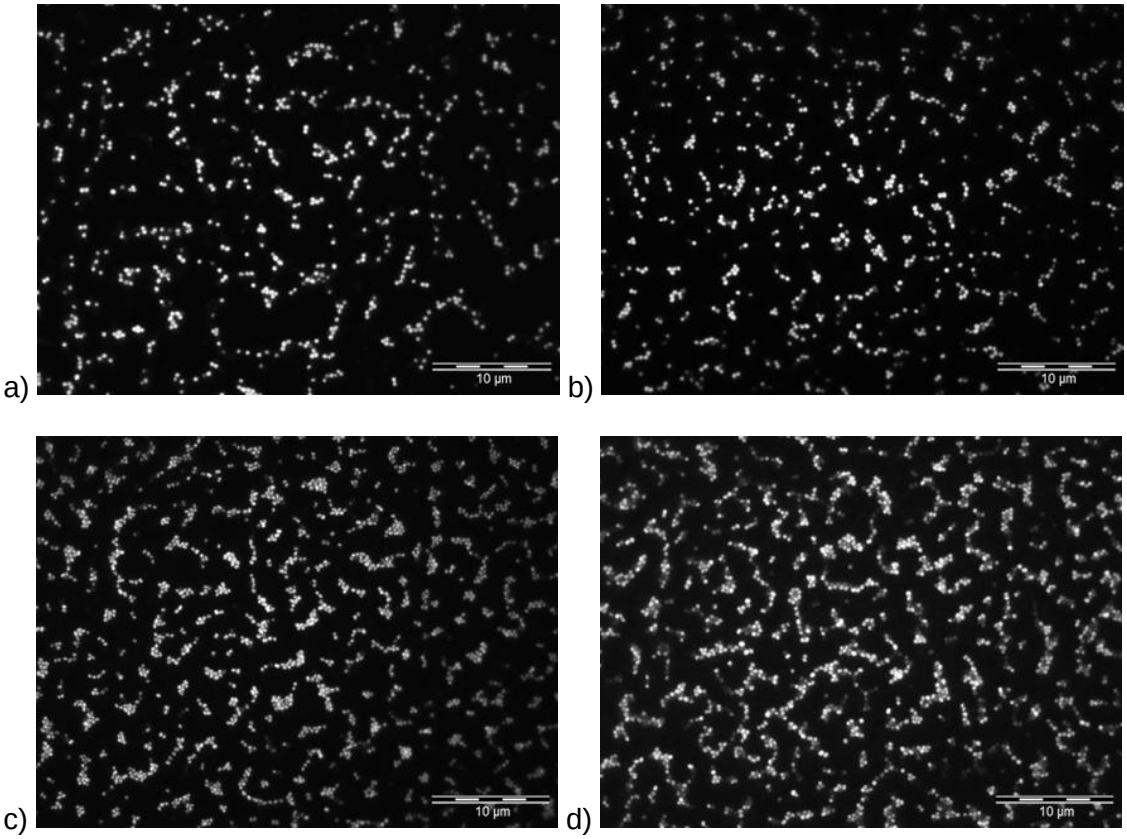

Figure 30: Epifluorescent microscopy images of *S. aureus* (X1000) on a) Stainless steel, b) ZrN, c) ZrN/15.5 at.% Ag, and d) ZrN/29.8 at.% Ag. An increase in bacterial coverage over the surfaces was observed as the silver increased.

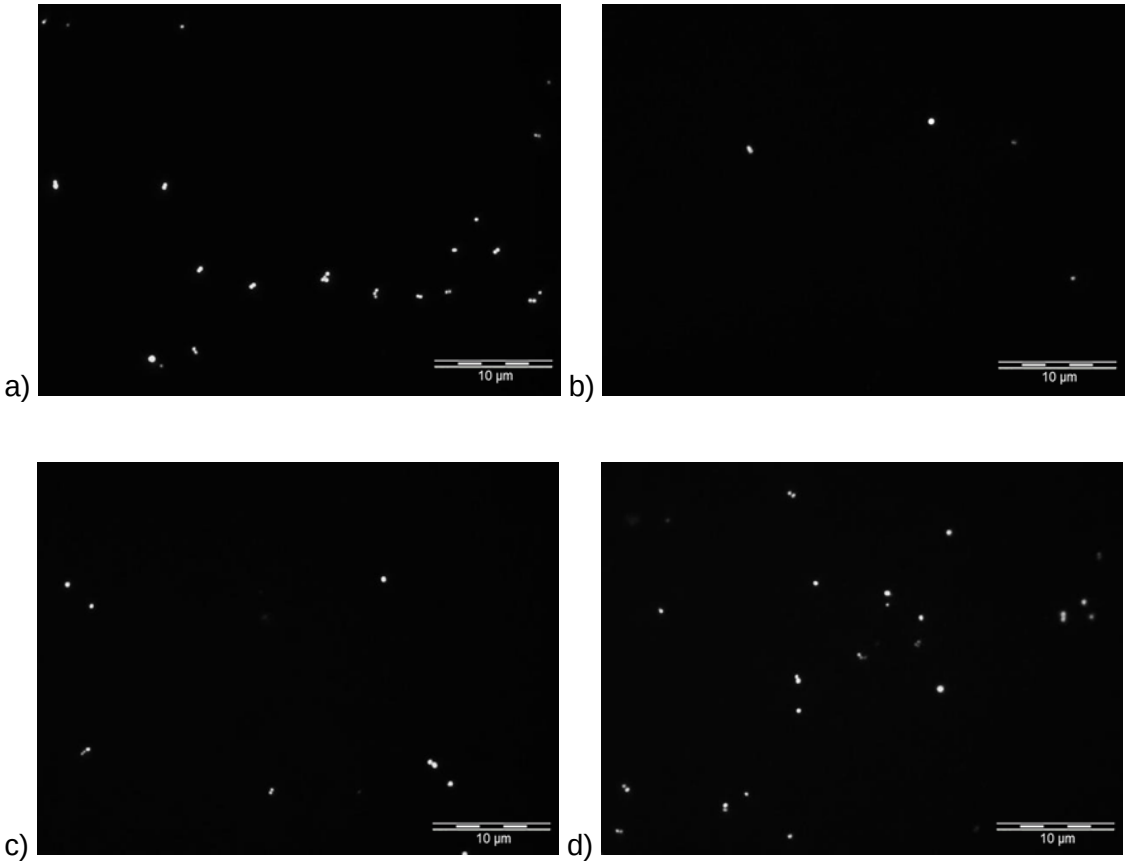

Figure 31: Epifluorescent microscopy images of *S. epidermidis* (X1000) on a) Stainless steel, b) ZrN, c) ZrN/15.5 at.% Ag, and d) ZrN/29.8 at.% Ag. An increase in bacterial coverage over the surfaces can be observed as the silver increased. Fewer cells were observed than *S. aureus* and the bacteria were more widely dispersed.

3.4 Antimicrobial efficacy

3.4.1 Retention (LiveDead™) Assay

The number of cells observed on the LiveDead results demonstrated that the *S. epidermidis* cells were retained in numbers a factor of ten lower than the *S. aureus*.

LiveDead™ staining following retention assays demonstrated that there was a higher number of dead to live *S. aureus* cells on all surfaces, (Figure 32a). The coated samples displayed a trend of increasing dead cells present as the silver content increased. The coatings containing 15.5% at. % Ag and 29.8% at.% Ag both displayed a significant difference ($p<0.05$) between live and dead cells, whereas no significant difference was observed for the ZrN and the stainless steel (Figure 32a).

For the *S. epidermidis* assays, a higher number of dead to live cells for all coatings and the stainless steel were observed (Figure 32b). All the surfaces displayed a significantly higher number of dead cells to viable cells ($p<0.05$), with the higher silver content coatings displaying high significance values ($p<0.005$).

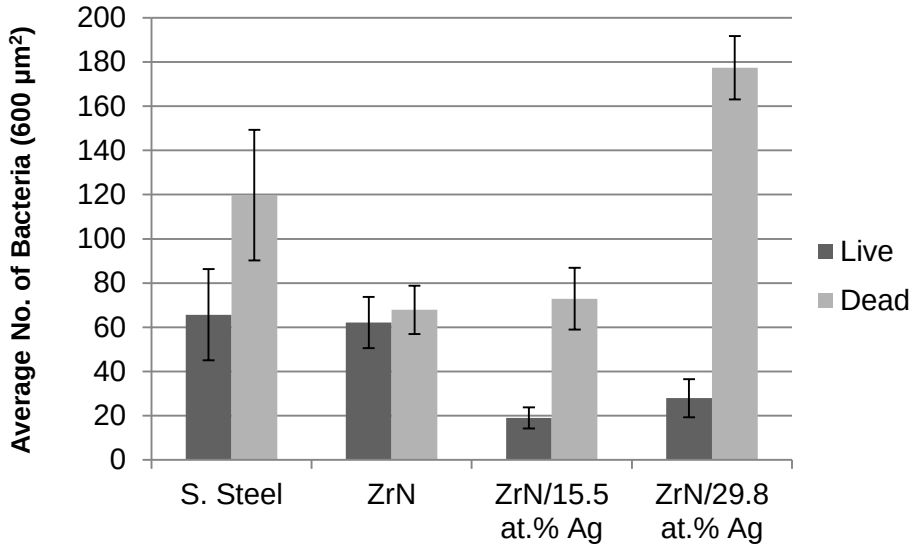

a)

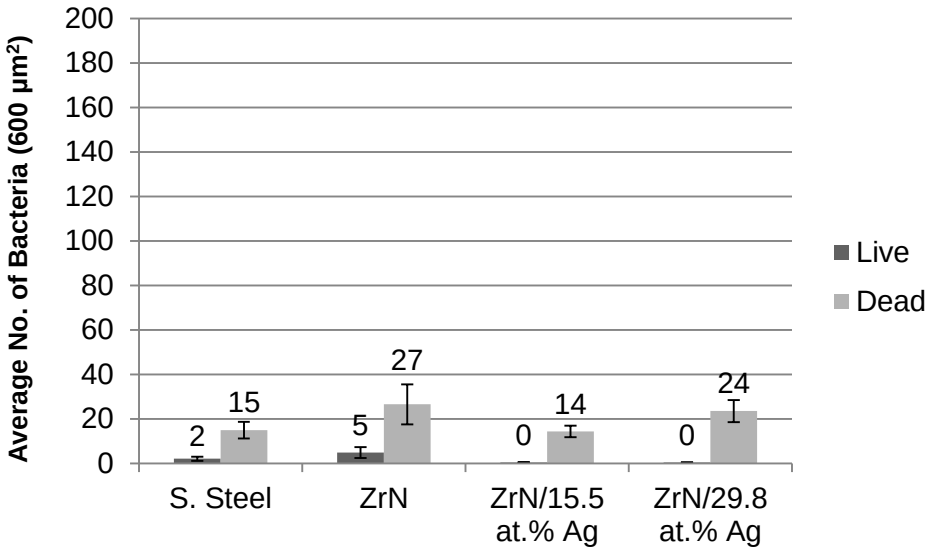

b)

Figure 32: Retention assays and LiveDead™ staining for comparison of the retained bacteria that are viable ('Live') and dead; counted from an average of 10 fields of view at X1000 magnification. Results demonstrated that a) *S. aureus* and b) *S. epidermidis* live cells decreased in on the ZrN/Ag coatings over the non-silver containing surfaces. The number of dead *S. aureus* cells in comparison to live is highest on the 29.8 at.% Ag and similar was observed for *S. epidermidis* demonstrating a successful indication of antimicrobial effect on the silver containing surfaces. Note the difference in scale between a) (200) and b) (50)

3.4.2 Nitro-Tetrazolium Violet Respiratory Assay

As the silver content increased in the ZrN coatings the number of viable colonies decreased in relation to the 'pure ZrN'. Both microorganisms appeared to survive better on the ZrN than the stainless steel surfaces (Figure 33). As viable colonies of *S. aureus* were seen on the ZrN/29.8 at.% Ag surfaces this organism could potentially be more resistant to the antimicrobial properties than *S. epidermidis*. This observation requires further investigation.

The pure zirconium nitride surface displayed a significant increase in viable cells on the surface over stainless steel and ZrN/Ag coatings (*S. aureus*: $p < 0.005$ *S. epidermidis*: $p < 0.05$). However, significantly less viable colony forming units (CFU's) were observed on the silver containing surfaces than the ZrN and the stainless steel (Figure 33). The exception for this was the *S. aureus* on 29.8 at.% Ag which displayed a greater average number than the 15.5 at.% Ag coating. This follows the trend seen with the LiveDead and SEM results. The 15.5 at.% Ag surface could have possessed improved efficacy over the 29.8 at.% Ag coating as the silver deposited possessed a larger particle size/shape, which may have affected its antimicrobial efficacy. Also the 15.5 at.% Ag was shown to display the most efficacy towards the *S. aureus* cells and the 29.8 at.% towards the *S. epidermidis* (Figure 33). This could mean alterations in silver content changes silver particle size and shape therefore potentially affect different microorganisms in different ways.

3.4.3 Zones of inhibition

Zones of inhibition assays were carried out to determine whether the coatings leached inhibitory amounts of silver into the surrounding area. It was determined that none of the surfaces showed any sign of inhibitory leaching of silver using this method (Figure 34), which would have been displayed as a clear zone surrounding the test coupon where the bacterial cells have been inhibited/killed.

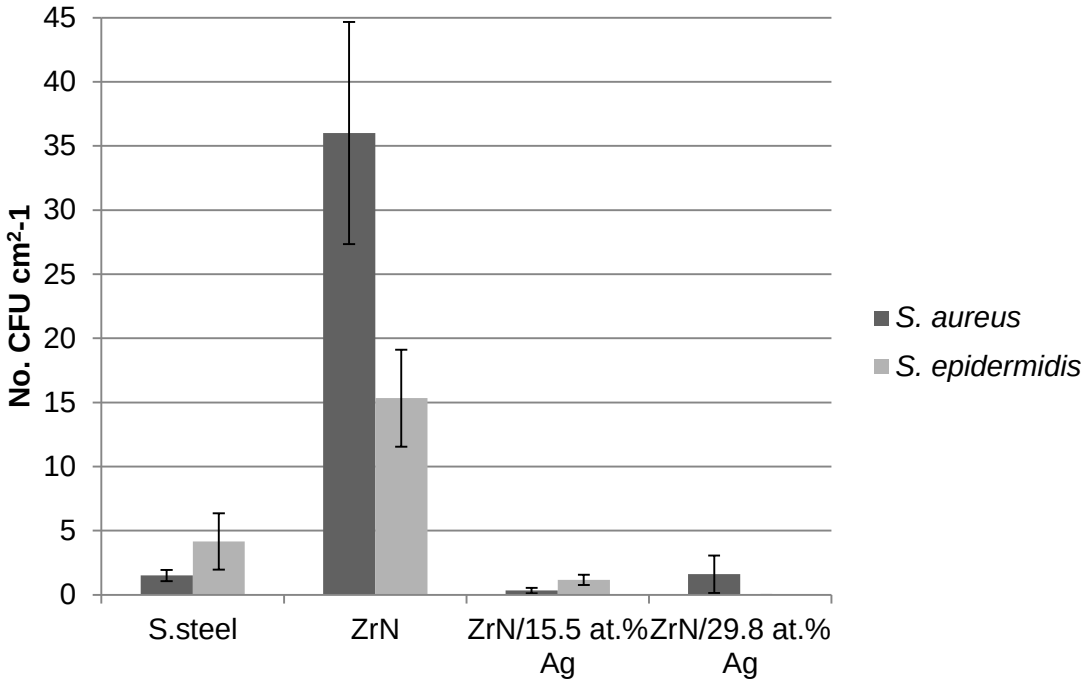

Figure 33: NTV assay performed using *S. aureus* and *S. epidermidis* on stainless steel, ZrN, ZrN/15.5 at.% Ag and ZrN/29.8 at.% Ag, displaying a contact kill occurred from the silver surfaces. The 15.5 at.% Ag proved more efficacious for the *S. aureus* and the 29.8 at.% for the *S. epidermidis*.

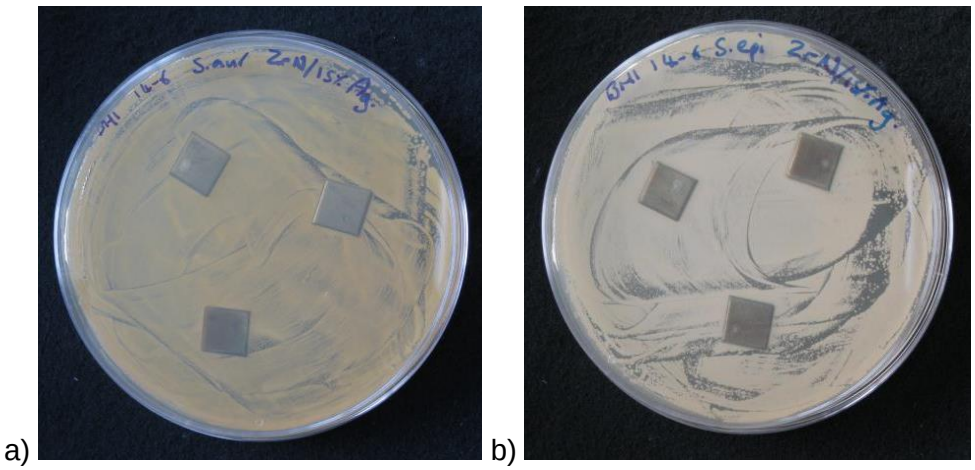

Figure 34: Zone of inhibition assay displaying no kill zones for the ZrN/29.8 at.% Ag surfaces on a) *S. aureus* and b) *S. epidermidis*. All other surfaces also had no inhibitory zones towards both bacterial species (results not shown).

3.5 Discussion

SEM results displayed the physical spread of the bacterial cells on the surfaces at high magnification. SEM can visualise the structure of the cells and the surrounding organic matter adsorbed on the surface. The disadvantages of the SEM method is that the samples have to be dehydrated to fix and prepare for the gold sputter coating, so as to maintain the original cell physiology and not damage the cell integrity. This fixing process may have affected the *S. epidermidis* cells, which appeared to have reduced in size and were no longer spherical. Staining the microorganisms with a fluorescent stain to view under an epifluorescent microscope is a faster and simpler method to enumerate the bacterial retention.

From the images obtained from the SEM it was seen that all four surfaces caused different bacterial retention morphologies. There were larger groups of *S. aureus* cells on the stainless steel surface, but the most bacterial retention occurred on the pure ZrN. The silver containing coatings retained the least amount of bacteria retained on the surfaces with no noticeable difference in retention morphology between them, preliminarily suggesting the silver in the coatings may have displayed an anti-adhesive effect. The *S. epidermidis* results displayed the highest number of bacteria retained on the stainless steel. The least amount of bacteria appeared to have been on the 15.5 at.% silver coating and the 29.8 at.% silver coating.

Following acridine orange staining of the retained bacterial cells, it was shown that *S. aureus* was retained on all of the surfaces in greater numbers than *S. epidermidis*. Both bacteria displayed a trend of increasing retention as the silver content increased and more coverage on the ZrN surfaces over the stainless steel. This result was found to have little relation to the micro surface feature heights and widths, yet the surface with the highest R_a, the 29.8 at.% silver coating, retained the most bacteria of both microorganism species. However, the trend of increased cell retention did not follow

the trend of R_a for the other surfaces. It is possible that the roughness on a nanotopographical scale could potentially be affecting the retention of the bacteria since the surface features differ in size as seen in the AFM micrographs when deposited onto the silicon wafer (2.3.5; Page 75). The nanotopography of the coatings is investigated in more detail in future work (5.3.4; Page 157). Puckett *et al.* (2010) studied the relationship of nanostructured titanium orthopaedic implant surfaces and bacterial attachment and found that certain nanometre sized topographies display potential for reducing bacteria adhesion and also promoting the attachment and growth of bone tissues. This demonstrates that nanotopographies are important in orthopaedic implant technology, however although the properties of macro and micro scale topography are well known the nanoscale topographies are not as comprehensively documented. Also the bacteria-substrate interactions and eukaryotic cell-surface interactions are mediated by the proteins that are adsorbed onto the substrate from the biological environment, which are affected by the nanotopography (Anselme *et al.*, 2010). The potential effect of surface nanotopography on cell retention was more apparent on the total cell counts obtained from the LiveDead staining.

LiveDead retention assays displayed a significant kill ($p<0.05$) of both *S. aureus* and *S. epidermidis* as the silver concentration increased. *S. epidermidis* had one-log fewer total cells present on the surface than *S. aureus*. Work by others has suggested that *S. epidermidis* tends to colonise polymer biomaterials more whilst *S. aureus* prefers metal substrates (Vuong and Otto, 2002, Harris and Richards, 2006, Ziebuhr *et al.*, 2006, Montanaro *et al.*, 2007). The total amount of cells on each surface matched the trend for the roughness values (2.3.5; Page 75) and the average sizes of depths measured with the AFM and the width sizes measured with the WLP. Surface wettability between the coatings did not show a trend with bacterial retention. However, in future work, relating the hydrophobicity of the cells using MATH (microbial adhesion to hydrocarbons) assays to that of the substrate using a physicochemistry measurements

was investigated in order to determine if such parameters affect cell retention (Chapter 6) (van der Mei *et al.*, 1995, Starostina *et al.*, 1997, Bos *et al.*, 1999). The LiveDead™ staining results of total cell counts conflict with the acridine orange results, but tally with the SEM results, with the numbers of retained bacteria being similar throughout the four surfaces and 15.5 at.% silver retained the least bacteria. This trend was the case for both bacterial species although *S. epidermidis* retained a factor of ten less than *S. aureus*. For both microorganisms, the amount of dead cells in relation to viable cells significantly increased for the two coatings containing silver (Figure 32).

The contrasting SEM and LiveDead results when compared to staining with acridine orange may suggest that the use of SEM for the visualisation of the bacteria should be at higher magnification since at lower magnifications, although the pattern of distribution of clumped cells can be observed, it is possible that the total cell counts, including individual cells cannot be correctly assessed. It is also known that the cell size of the *S. aureus* and the *S. epidermidis* differ. *S. aureus* cells are said to be between 0.8-1.0 μm in diameter, whereas the *S. epidermidis* cells are between 0.5-1.5 μm in diameter (Baird-Parker, 1975). Therefore *S. epidermidis* have the ability to grow as smaller cells, which could be the case with the SEM images.

The conflict between the total cell retention when using different analysis techniques creates difficulties. Thus it may be suggested that in order to obtain an accurate representation of bacterial retention on the surfaces a number of methods need to be used. Further, in light of these results, in future work the physicochemistry of the surfaces was more thoroughly tested to determine if these factors influenced bacterial retention (*vide infra* 5.3.6; Page 173 and 6.3.9; Page 203). A novel mathematical method to determine the distribution and density of the cells was also developed in order to provide further discriptors and understanding of the bacteria-surface interactions (*vide infra* Chapter 8).

To determine whether the ZrN/Ag surfaces gave rise to contact kill, an adaption of the method developed by Barnes et al. (1996) was used. A redox dye, (Tetrazolium Violet) was used to indicate respiring cell colonies on a surface. The results obtained from the assay showed a decrease in the number of viable colonies as the silver content in the surface increased. However, it was difficult to keep cells viable on the bare stainless steel substrate, and this could be due to the surface behaviour. The cell suspension, when spread on the stainless steel surface, would not separate or spread across the surface area but just remained in a single droplet. This may have resulted in a reduced number of cells in contact with the substrate. Combined with the drying effects, the cells may have dried in a small area resulting in a reduction of viable colonies. The increase in silver content reduced the viable cell counts of both microorganisms tested. The ZrN/Ag with a silver content of 29.8 at.% displayed no viable colonies for the *S. epidermidis* and very low numbers of *S. aureus*, after initial deposition of around 5 x 10^4 cells onto the surfaces. It could be hypothesised that the formation of the silver in the coatings affected the contact kill of the two microorganisms. The 15.5 at.% Ag completely eradicated the *S. aureus*, but it was still viable on the 29.8 at.% Ag whereas the opposite occurred with the *S. epidermidis*, suggesting selective efficacy towards different microorganisms.

Zone of inhibition assays demonstrated that the surfaces did not leach silver ions into the surrounding area, inhibiting the growth of the microorganisms. From the results it can be seen that there were no clear zones surrounding the substrates. These results agree with a similar investigation by Kelly et al. (2010a) where it was found that no zones of inhibition were seen using *S. aureus*. Leaching of products into the surrounding area is not always considered desirable and can be problematic in some circumstances. Although no zones of inhibition were observed from leaching of Ag^+ ions it cannot be entirely ruled out that silver ions are not leaching out of the coatings. Leaching could be occurring so slowly that the leached concentration was sub-

inhibitory. The amount of silver ions being released into the surroundings can be determined by using inductively coupled plasma-atomic emission spectroscopy (ICP-AES), which was investigated in future work (Chapter 5; Page 178)(Lewen and Nugent, 2010).

3.6 Concluding Remarks

Following characterisation of the ZrN/Ag coatings in the previous chapter, the antimicrobial properties and bacterial retention characteristics of the surfaces were assessed using *S. aureus* and *S. epidermidis* as the test microorganisms. SEM images of the retention assays demonstrated differing distribution of the bacteria retained on the different coating compositions, with fewer bacteria retained on the silver containing coatings. *S. epidermidis* was retained in fewer numbers than *S. aureus* on all surfaces, however quantitative data could not be attained from this method, therefore future work did not include this assay. Epifluorescent microscopy using acridine orange staining demonstrated a rapid method to enumerate the retained bacteria on the surfaces, which also provided a quantitative bacterial percentage coverage value. The results demonstrated an increase in the retention of both microorganisms with an increase in silver concentration, however *S. epidermidis* was retained in fewer numbers (1 log). Following LiveDead staining it was demonstrated that with an increase in silver concentration *S. aureus* decreased in numbers of live cells and the number of dead cells increased, displaying antimicrobial efficacy. *S. epidermidis* only displayed a decrease in live cells with the increase in silver content and little change to dead coverage numbers were observed, demonstrating less of an antimicrobial effect or a different mode of action. NTV assays demonstrated that an effective contact kill was observed, the ZrN/15.5 at.% Ag coating was more effective towards *S. aureus* and the ZrN/29.8 at.% Ag coating towards *S. epidermidis*. No antimicrobial leaching was observed from the surface coatings for either microorganism; further investigation into quantifying the leaching of silver was undertaken in Chapter 5 using ICP-AES. The

successful kill of the ZrN/Ag coatings towards staphylococci demonstrated the potential of the coatings to combat pin tract infections. However, the coatings were found to be brittle and poorly adhered to the stainless steel, flaking away from the substrates during the stresses of antimicrobial testing. Therefore further developments to improve the coating adhesion properties were undertaken (Chapter 4).

4 Development of Coating Adhesion and Surface Properties using Graded ZrN and Ti Interlayers

4.1 Introduction

Following characterisation of the coatings produced previously (Chapter 2) and their testing against bacteria to replicate fixation pin infection, a number of issues arose. The main issues were:

1. The coatings were poorly adhered to the stainless steel, observed during use in the microbiological assays.
2. The concentrations of silver were produced in a higher concentration for 230 W and a lower concentration for 150 W than seen in previous work performed by the research group using the same conditions (Kelly *et al.*, 2010b, Kelly *et al.*, 2011).

To combat these issues experimental arrays were designed to investigate the effect of substrate bias, magnetron pulse frequency, and duty on the coatings adhesion and friction coefficients. The coatings were tested for silver content, adhesion to the underlying substrate, and resistance to wear in terms of coefficient of friction. Following the improvement to the tribological properties of the coatings a study into the silver content in relation to power application to the silver magnetron was undertaken to calculate what power set-points should be used to gain the desired amounts of silver.

Improving the adhesion of a thin film to a substrate can be achieved in many ways from the preparation of the substrate surface prior to coating *ex vacuo* or in the vacuum chamber, and the alteration of deposition parameters. A negative voltage bias to the substrate holder increases the argon ion flux and increases the energy at which the ions collide with the substrate and the growing film, potentially creating a more dense coating structure. However, increasing the bias voltage beyond a certain point results in disruption of growth and re-sputtering may occur at the substrate surface and start eroding or affecting the growth of the coating. The addition of a metallic interlayer or multiple layers can be used to increase the adhesion of the coating to the substrate.

When graded interlayers are deposited, adhesion to the substrate is improved greatly in comparison to immediate ZrN deposition (Li *et al.*, 2006). In this investigation the addition of metallic interlayers, the grading of the reactive gas to give a gradient from Zr to ZrN, the addition and alteration of deposition parameters and varying the power to the silver magnetron to produce different silver contents were all variables used to improve the coating properties in terms of tribology.

4.1.1 Taguchi L_9 Array

To improve thin film deposition and the resulting coating properties there are many parameters on a magnetron sputtering system that can act as variables to alter the behaviour of the deposition. For this investigation examples include; power, DC or pulsed DC power modes, duty (amount of time power is applied throughout the pulse waveform), pulse frequency, process gas pressure, reactive gas mixture in relation to the optical emission signal, substrate bias and substrate power delivery mode (DC or pulsed DC). Attempting individual coating runs of every parameter combination would be time consuming due to the duration required for the sputtering equipment to achieve the required minimum vacuum pressure so decisions on which parameters to alter are critical. In this investigation three variables were chosen due to their known effect towards tribology improvements: the magnetron DC pulse frequency, the duty and the substrate DC bias voltage. Due to the potential for large amounts of experimental parameter combinations (27 combinations) a method was used to cover a range of variables in fewer experiments, yet allow structure to the choice of variables for each individual experiment. For the investigation an adaption of a Taguchi L9 experimental array was used which employs an orthogonal pattern to the three levels (Roy, 1990). This is plotted out into a table which gives a spread of each variable of each parameter to give only 9 production runs, thus reducing the amount of experiments but obtaining relevant data from multiple variables (Table 8). The variables chosen for the three parameters were chosen from previous work and literature, since previous work stated

that the chosen parameters have the desired effects when changed (Valvoda, 1995, Kelly and Arnell, 2000, Lee *et al.*, 2008, Kelly and Bradley, 2009, Kong *et al.*, 2011, Wei and Gong, 2011, Yongqiang *et al.*, 2013).

Table 8: The nine coating runs that were undertaken to fulfil a Taguchi L_9 array, displaying the three parameters required.

Run Number	Frequency	Duty	Bias
1	100 kHz	50 %	0 V
2	100 kHz	70 %	15 V
3	100 kHz	90 %	30 V
4	200 kHz	50 %	15 V
5	200 kHz	70 %	30 V
6	200 kHz	90 %	0 V
7	300 kHz	50 %	30 V
8	300 kHz	70 %	0 V
9	300 kHz	90 %	15 V

4.1.2 Varying the Silver Content

From the first investigation in chapter two it was concluded that the percentage of silver in the coatings tested did not relate to the literature on which preliminary studies were undertaken. It was discussed that at low concentrations of silver, the power that needed to be applied to the magnetron was so low that the zirconium deposition tended to contaminate the silver target with zirconium nitride, reducing deposition rates. This was visible on the target after deposition; the area outside of the sputter erosion path was coated and the area was reduced.

Altering the amount of silver in a coating can have both beneficial and detrimental effects. In terms of mechanical properties and antimicrobial efficacy. Silver has the ability to act as a solid lubricant in situations where the surrounding interfaces are harder than the silver itself (Tyagi *et al.*, 2010, Papi *et al.*, 2012). This could be beneficial in areas where movement between two interfaces occur for example a moving interface on a prosthetic hip joint. However, high silver contents can be detrimental to the coating. Structurally, when a high content of silver is added to the zirconium nitride this decreases the desirable tribological/hardness properties of the nitride coating, decreasing both the wear resistance and hardness (Kelly *et al.*, 2011). A decreased hardness will also decrease the scratch resistance of the thin film, thus defeating one of the qualities of using a nitride co-sputtered nanocomposite instead of sputtering pure metallic silver onto the surfaces as other authors have performed (Wassall *et al.*, 1997, Massè *et al.*, 2000).

In terms of antimicrobial efficacy, more important to external fixation pins, it may be speculated that an increase in silver contents will increase antimicrobial efficacy (Schierholz *et al.*, 1998, Edwards-Jones, 2009, Kelly *et al.*, 2011). Medically, having surfaces containing a high amount of silver can give rise to potential toxicity issues towards local tissues and in some cases become a systemic problem throughout the whole body (Gosheger *et al.*, 2004). This is why it is important to test a range of silver

concentrations, because the surface with the highest amount of silver may not have the highest antimicrobial efficacy and the surface with the best structural properties may not possess the best antimicrobial properties, so a balance between sacrificing coating strength to benefit the antimicrobial properties needed to be established.

4.1.3 Interlayers

Throughout thin film technology the use of metallic interlayers is widespread (Rahman *et al.*, 2005, Zhang *et al.*, 2006, Polcar *et al.*, 2009, Fontalvo *et al.*, 2010, Lackner *et al.*, 2013). Zirconium has been shown to possess immiscibility towards iron and has been used in applications where deliberate segregation occurs (Polizzotti and Burton, 1977). Since 316L stainless steel typically contains around 62-69% iron, it may be that adhesion of zirconium nitride to the stainless steel surface is compromised. To ensure this did not occur it is possible to deposit an interlayer of titanium between the stainless steel and the ZrN and ZrN/Ag coatings. Titanium is more compatible with iron if deposited onto the stainless steel before the zirconium was deposited it may increase coating adhesion (Chien and Liou, 1985). Further, by introducing the reactive gas in incremental steps the initial coating is deposited in a gradient. This has demonstrated improved adhesion and wear properties of nitride coatings in tribology investigations (Monaghan *et al.*, 1993). An investigation by Deng et al (2008a) demonstrated that without an interlayer the zirconium nitride coatings displayed a higher hardness but the films with the initial interlayer had better substrate adhesion and wear resistance. This indicates that the addition of a titanium interlayer prior to nitride deposition and grading the zirconium in increments at the start of deposition would be beneficial towards the coatings in this investigation for use in external fixation pins.

4.2 Methodology

4.2.1 Magnetron Sputtering

The magnetron sputtering for this investigation was undertaken on the same Teer UDP 350 sputtering system in a closed field, unbalanced magnetic configuration (Chapter 1.3.2). Power was supplied to the magnetron using a Pinnacle Plus (Advanced Energy, USA). The duty of the pulse cycle was also altered on the power supply by altering the off time (the amount of time that power was not applied in the pulse waveform) in proportion to the pulse frequency, to give a percentage of time that the power was applied to the magnetron in total over an entire pulse wave form (Figure 9; Page 29). The bias applied to the substrates was a DC current from an MDX power supply (Advanced Energy, USA) at 15 V and 30 V. For 0 V the substrate was left isolated at the floating potential.

The metallic interlayers were deposited as follows; the sputtering system contained three targets: titanium, zirconium and silver. The substrates were sputter cleaned at 150 W at 100 kHz and a 1.2 µs off time for 20 minutes in 0.4 Pa argon. In contrast to previous experiments, the chamber contained a shutter to shield the silver target from contamination when not in use. This was used to cover the silver target throughout titanium and zirconium deposition until co-sputtering was to be used then it was moved across to the titanium target to shield it throughout the coating process. The titanium layer was deposited at 100 kHz and 90% duty at one kilowatt for four minutes with the substrate holder rotating at 16 rpm. Following titanium deposition and the zirconium interlayer and introduction of nitrogen via the plasma emissions monitoring system was undertaken. One kilowatt was applied to the zirconium magnetron and the pulse frequencies and duties were determined by the Taguchi array. Following deposition of the titanium interlayer a pure zirconium interlayer was deposited for three minutes until the reactive sputter controller was turned on at 80% of the full metal signal (light

wavelength of the zirconium plasma) of zirconium. The signal was always calibrated to ‘1000’ on the display prior to initiating reactive gas control. The reactive gas was graded from 80% down to 45% altering in 5% increments every 30 seconds (Figure 35). The silver target was cleaned prior to exposure to the substrates by applying power, to sputter the surface and covering the magnetron with the movable shield inside of the chamber. Once the zirconium was being sputtered in full reactive mode (45% FMS) the shutter was moved from the silver target to the titanium target area to expose the silver target and initiate the ZrN/Ag co-sputtering process. The entire coating run, not including the 4 minutes of titanium deposition totalled one hour to achieve a 1 μm thickness and was left for 45 minutes to cool following deposition to reduce stress from thermal expansion.

Figure 35: Theoretical diagram of a cross section of the coating layers (not to scale) illustrating each individual increment used. The ZrN layers are to illustrate the conditions used to produce a graded coating and not discrete layers.

4.2.2 EDX

Energy dispersive X-Ray spectroscopy was used to gather information on the coating compositions. The method was followed from the previous investigation (2.2.5; Page 65). EDX analysis was used to quantify the amounts of zirconium, nitrogen and silver in the Taguchi array coatings and also the amount of silver in the investigation involving varying the power to the silver magnetron.

4.2.3 Scratch Testing

Scratch testing was undertaken on the coatings to test the adhesion to the substrate. The substrates used were the same 1.5 mm, 316L stainless steel used in previous work but cut into 35 x 35 mm coupons. The scratch test parameters were matched to follow the BS EN 1071-3:2005 standard (Anonymous, 2005a). This was undertaken using a CSM ReveTest scratch tester (CSM Instruments, Switzerland). The scratch was performed using a Rockwell C diamond stylus (200 µm radius) and a progressive load scratch over 20 mm, with a loading rate of 100 N/min and speed of 10 mm/min starting at 1 N and finishing at 60 N. The scratch failures were determined by means of acoustic emissions monitoring, friction force and microscopic evaluation.

4.2.4 Pin on Disk

The pin on disk testing was undertaken using a TRIBOtester pin on disk instrument (Tribotechnic, France). The unlubricated wear test was performed as an oscillating movement with 1 N load on the static tungsten carbide ball (6,000 µm diameter) was used to perform an unlubricated wear test. The sliding speed was set at 60 mm/s and the length at 20,036 mm over a 10 mm eccenter path length with the temperature and humidity at room conditions measured on the day (24.9ºC and 38.5 % R.H.). The software captured data relating to the coefficient of friction, friction force and the maximum coefficient of friction value was recorded. Tests were undertaken in duplicate for each sample and an average calculated.

4.3 Results

4.3.1 Taguchi T9 Array results

4.3.1.1 EDX Analysis

The EDX results were obtained to show whether the application of different deposition parameters affected the silver content in the array coatings when keeping the power to the silver target the same throughout (90 W) (Figure 36). The zirconium and nitrogen contents remained similar throughout all of the coatings; 40 at.% for zirconium and between 50-55 at.% for nitrogen. The silver contents varied with the highest content being from ‘number 1’ (100 kHz, 50 5 Duty, 0 V Bias), at 10.3 at.% Ag and the lowest being ‘number 7’ (300 kHz, 50 % duty, 30 V bias) at 0 at.%. This suggests that the duty and frequency of the power delivery affected the deposition rate of the materials, therefore altering the silver contents observed. Both increasing the frequency and decreasing the duty decrease the deposition rate of the sputtered material, the duty because there is less time the power is applied to the target and the frequency because the pulsing affects the ion flux and causes a slight decrease in deposition rate/sputter yield.

4.3.1.2 Scratch Testing

The first Taguchi plot displayed the effect of frequency towards the scratch test critical loads, which are related to the adhesion of the coating to the substrate (Figure 37). At 200 kHz frequency the coatings demonstrated the lowest critical load (26.5 N), demonstrating the poorest adhesion. The lowest frequency (100 kHz) gave the second least adhered coating (29.9 N). At 300 kHz the best adhered coating was produced (42.4 N). Plotting the effect of duty in relation to coating adhesion demonstrated a similar trend to frequency (Figure 38). At 70% duty the poorest adhered coating was produced (26.4 N), followed by 50% (34.3 N) and the best performing was 90% duty (38.1 N). The coatings demonstrated that in relation to substrate bias an increase in

bias led to a linear increase in coating adhesion (Figure 39). The lowest value was observed when 0 V was applied to the substrate holder (24.1 N) followed by -15 V (33.95 N) and the best performing coating had -30 V applied to the substrate holder (40.8 N).

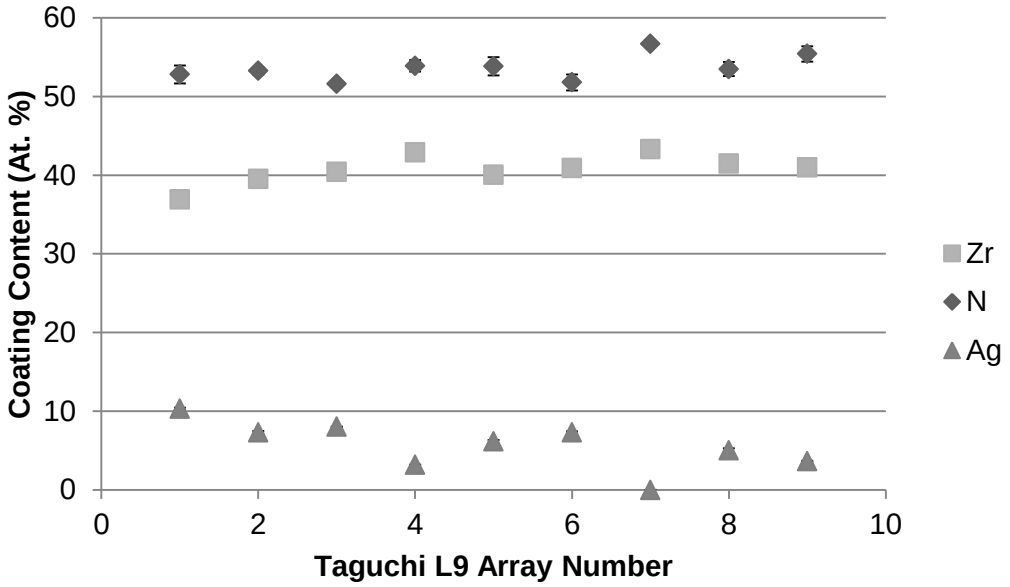

Figure 36: EDX analysis of the nine coating parameter combinations of the Taguchi L9 array, demonstrating that all coatings contained similar zirconium and silver contents; however, silver content varied even though it was set as a constant.

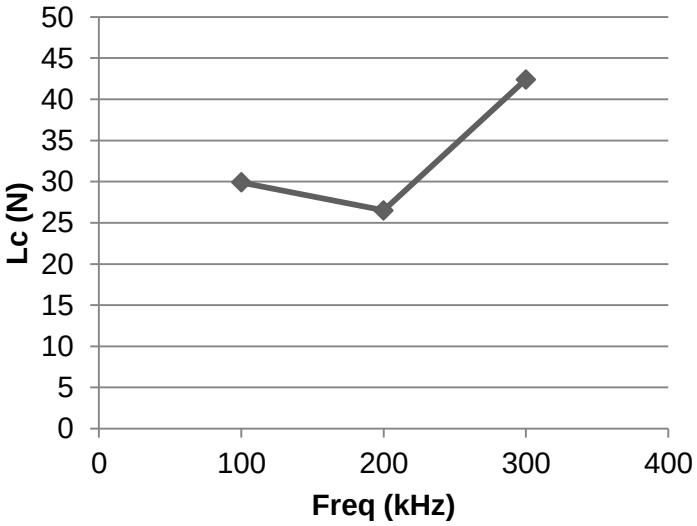

Figure 37: Scratch test critical loads of the Taguchi array in terms of frequency (kHz) demonstrating that at 200kHz the coating demonstrated the poorest adhesion properties, followed by 100 kHz and the best performing coating was deposited at the highest investigated frequency (300 kHz).

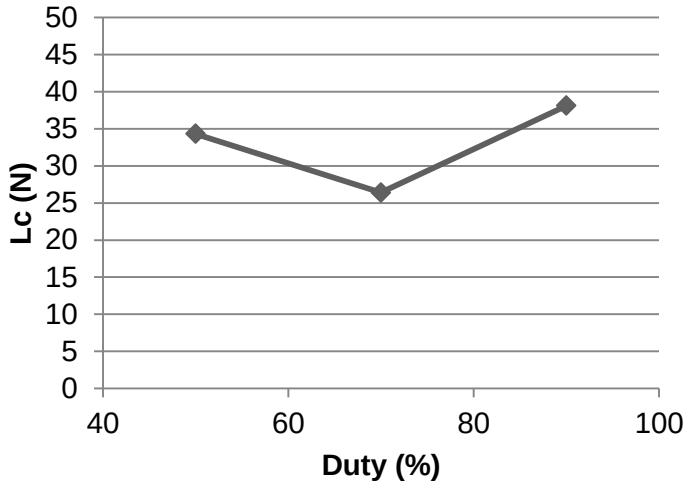

Figure 38: Scratch test critical loads against the effect of duty cycle, demonstrating the best performing coatings on the 50% and 90% duty cycles.

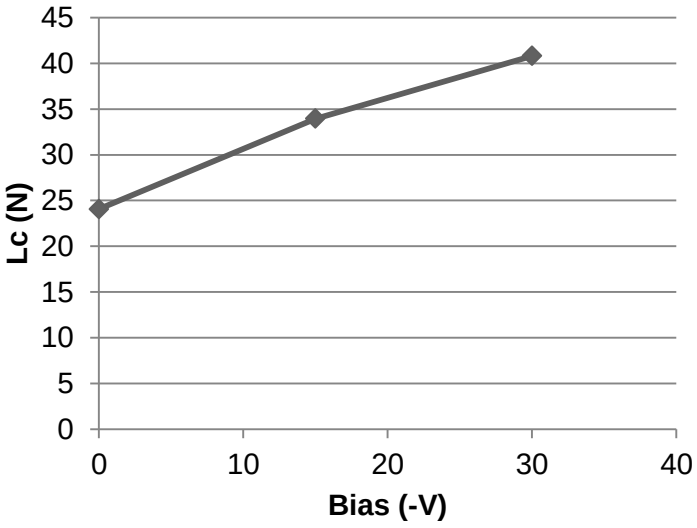

Figure 39: Scratch test critical loads of the Taguchi coatings in relation to substrate bias, demonstrating an increase in critical load (adhesion) with an increase in substrate bias

4.3.1.2.1 Scratch Testing Friction Forces

From the scratch tests the critical loads were calculated by means of a sharp alteration in the friction force and this area was then investigated with the optical microscope. The point was visualised at the marker point on the view finder and the software calculated the critical load. The results displayed that the point at which the critical load was defined all possessed a similar appearance. The results also demonstrated the friction forces observed when the coatings fail. When the coating fails the friction force tended to increase steeply, however, some coatings did not display this and had to be inspected for coating failure visually. The micrographs of the coating failure and the friction force graphs of the best performing (Taguchi 7: 300 kHz, 50 % duty, 30 V bias) (Figure 40) and the worst performing (Taguchi 1: 100 kHz, 50 % duty, 0 V bias) (Figure 41) coatings are presented to display examples of the failure observed by the scratch test hardware and software from the micrograph and friction force graph, respectively. The critical failures are marked with a red line on each figure (a). The graph obtained from the scratch tester contained multiple axes; the bottom *x* axis denotes the scratch length (mm), the top *x* axis denotes the load (N), the right *y* axis displays the coefficient of friction, the centre axis in purple displays the friction force (N) and the left *y* axis demonstrates the normal force of the stylus (N) (Figure 39a).

a)

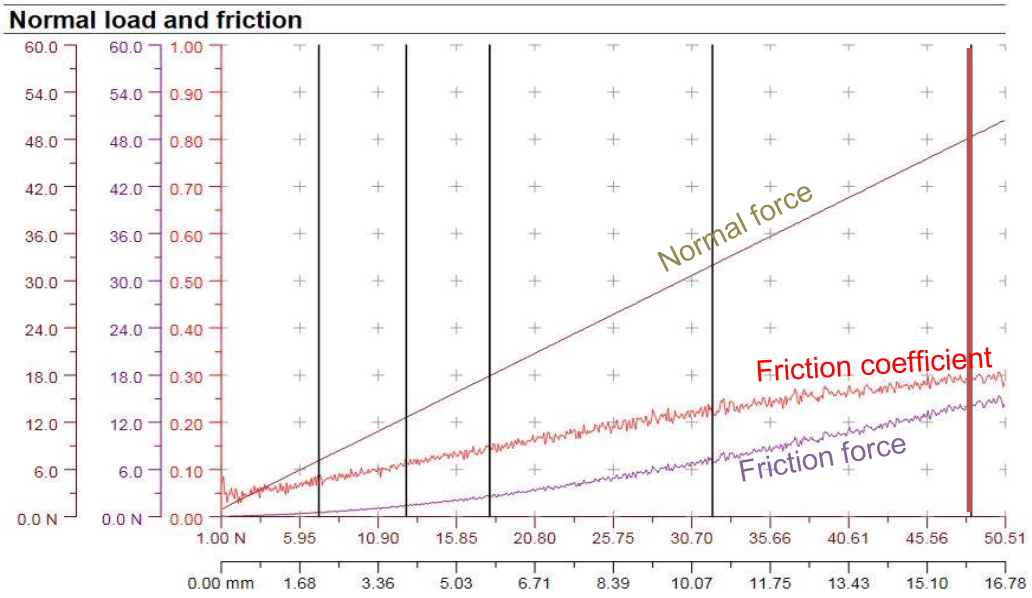

b)

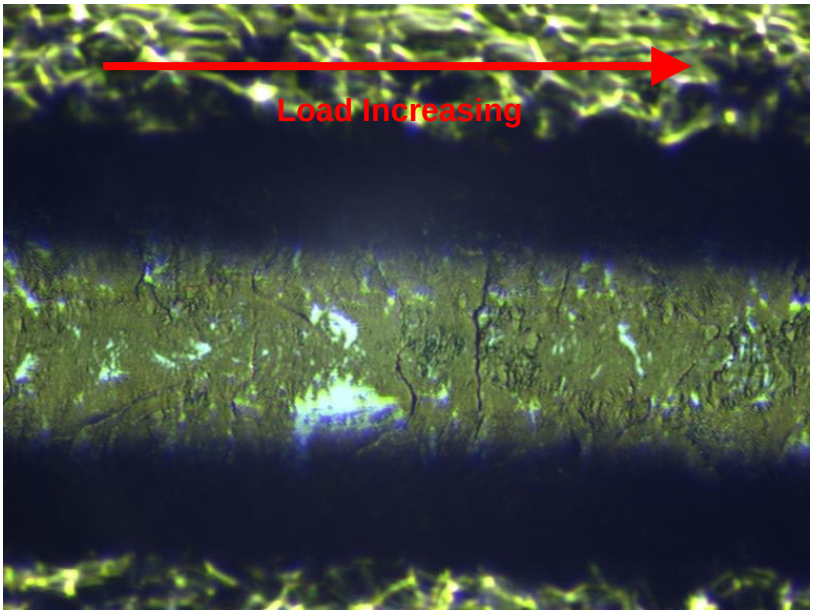

Figure 40: Taguchi Number 7 scratch test of a) friction force graph across the scratch length (critical failure indicated at the red line) and b) micrograph of the scratch critical failure point (X 100 magnification)

a)

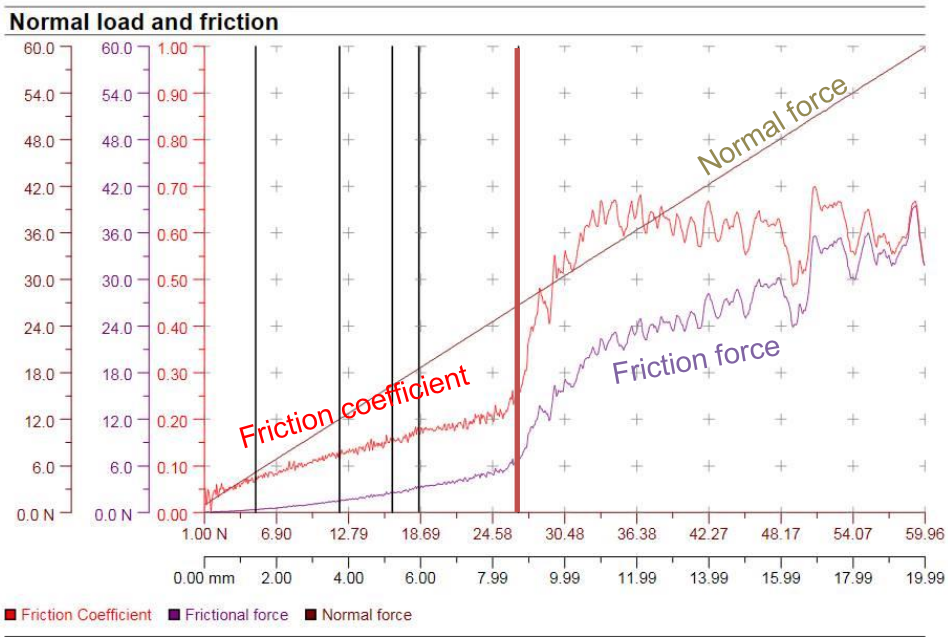

b)

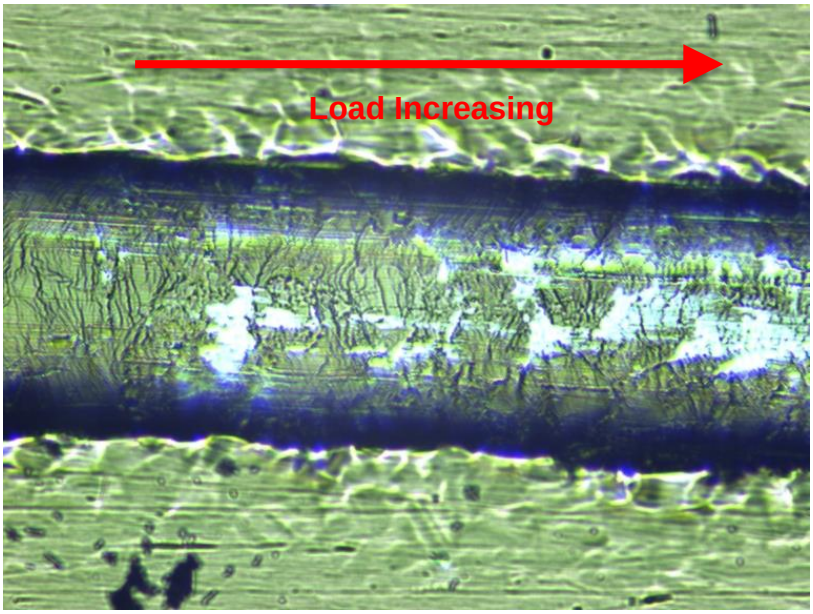

Figure 41: Taguchi Number 1 scratch test of a) friction force graph across the scratch length (critical failure indicated at the red line) and b) micrograph of the scratch critical failure point (X 100 magnification)

4.3.1.3 Pin on Disk (Coefficient of Friction)

The pin on disk wear tests displayed the average coefficient of friction of the Taguchi L9 array in relation to the altering parameters. The coefficient of friction in relation to pulse frequency and duty varied for the three different frequencies (Figure 42). The 100 kHz frequency displayed that as the frequency increased to 200 kHz the coefficient of friction decreased from 0.46 to 0.44 and then increased to 0.48 when the frequency was 300 kHz. The frequency related similarly to the results seen for the scratch critical loads (Figure 37) so at low and high frequencies the coefficients of friction were high, as were the critical loads/adhesion, whereas the middle frequency, 200 kHz displayed a lower value.

The Taguchi plot in relation to duty (Figure 43) demonstrated that the plot also followed the same trend to the scratch test plot (Figure 38). For 70 % duty, the friction coefficient was the lowest (0.44). A duty of 90 % produced the highest coefficient of friction (0.48) followed by 50 % duty (0.46). The coefficients of friction in relation to bias demonstrated that 0 V displayed a coefficient of friction 0.44 and increasing the bias linearly increased the coefficient of friction (Figure 44). At -15 V bias the coefficient of friction was 0.46 and increased slightly to 0.47 when -30 V bias was applied.

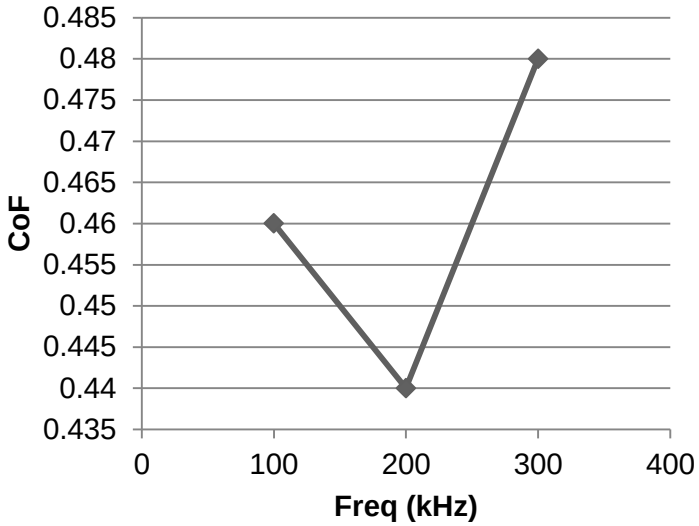

Figure 42: Taguchi Pin on disk coefficients of friction in relation to frequency, demonstrating that an increase in frequency to 200 kHz decreased the CoF value and increasing to 300 kHz produced the highest CoF.

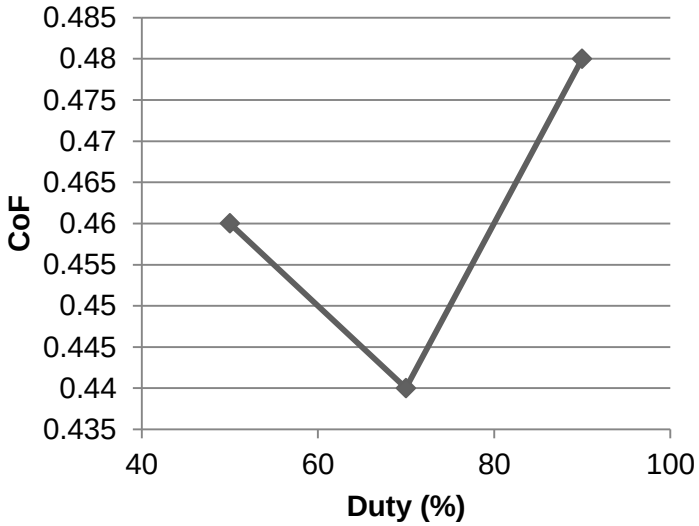

Figure 43: Taguchi Pin on disk average coefficient of friction in relation to duty, demonstrating a similar pattern to the frequency results. The lowest value was observed on the 15 V bias (0.44) and the highest on the 30 V bias (0.48)

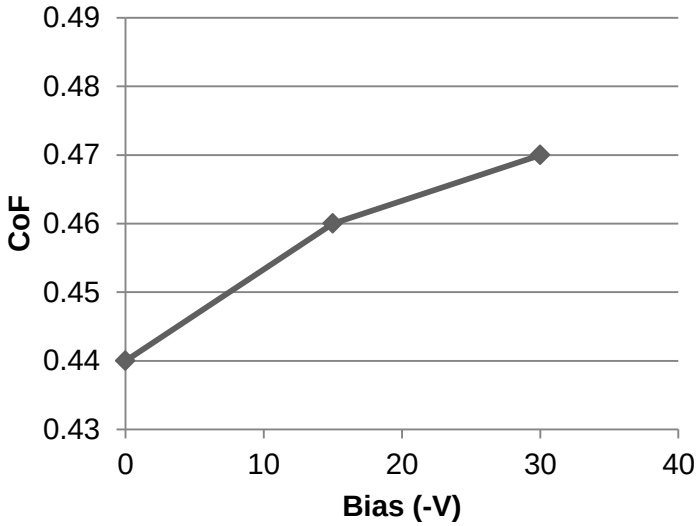

Figure 44: Taguchi Pin on disk average coefficient of friction results in relation to substrate bias. An increase in substrate bias led to an increase in coefficient of friction.

4.3.2 Silver concentration results

Following the Taguchi L_9 array the optimum coating conditions were chosen, which were 300 kHz pulse, 50% duty and 30 V substrate bias. Following this a range of experiments were undertaken to vary power to the silver magnetron to observe the difference in silver content in relation to power applied. This ranged from 90 W to 140 W increasing the power by 10 W increments.

4.3.2.1 EDX analysis

Following deposition of the coatings, energy dispersive X-ray analysis was used to quantify the silver content in the coatings, using pure ZrN as a control. As the power increased the silver content increased with a linear trend (Figure 45). An increase in 10W tended to display an increase of approximately two percent silver. The outlier is the 120W power, which contained only 7%.

4.3.2.2 Scratch Testing

Scratch testing of the surfaces allowed the quantification of coating adhesion to the underlying substrate and to demonstrate whether an increase in silver content affected adhesion. The results did not display any clear trends in critical load point as the silver content increased (Figure 46). However, excluding the coating containing 6.3 at.% silver, the trend observed that critical loads inversely matched the trend of the pin on disk coefficients of friction (Figure 47). Between 2.5-7.0 at.% Ag there appeared to be a lower adhesion and a higher coefficient of friction. Therefore the coatings with higher amounts of silver, also pure ZrN displayed better adhesion and a lower coefficient of friction. Excluding ZrN/6.3 at.% Ag, the trend of the critical load related to the coefficient of friction graph (Figure 47) and as adhesion decreased, so did the coefficient of friction. The higher silver content, pure ZrN and 6.3 at.% Ag coatings displayed the best adhesion.

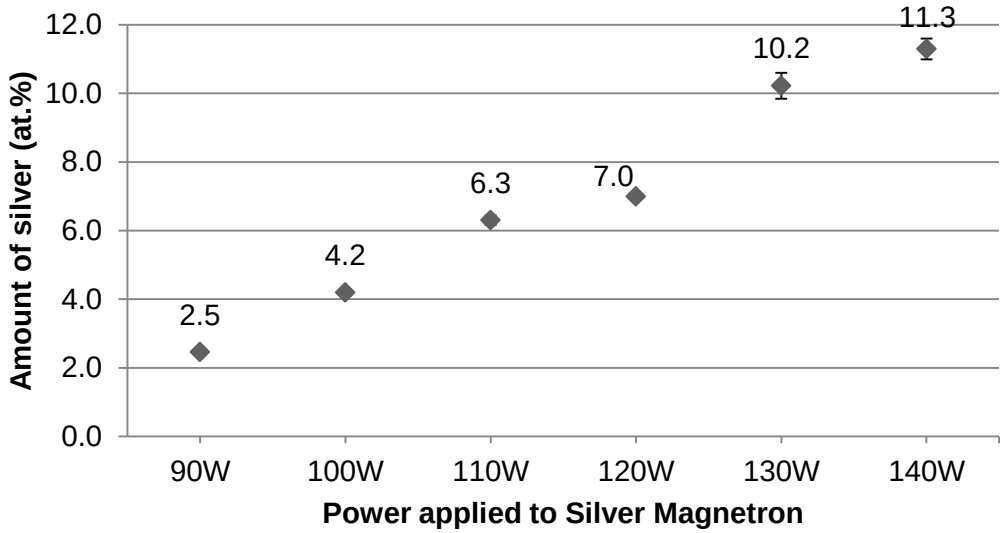

Figure 45: Silver content of coatings derived from EDX, in relation to increasing powers applied to the silver magnetron. The silver content increased with a linear trend as the power applied to the magnetron increased.

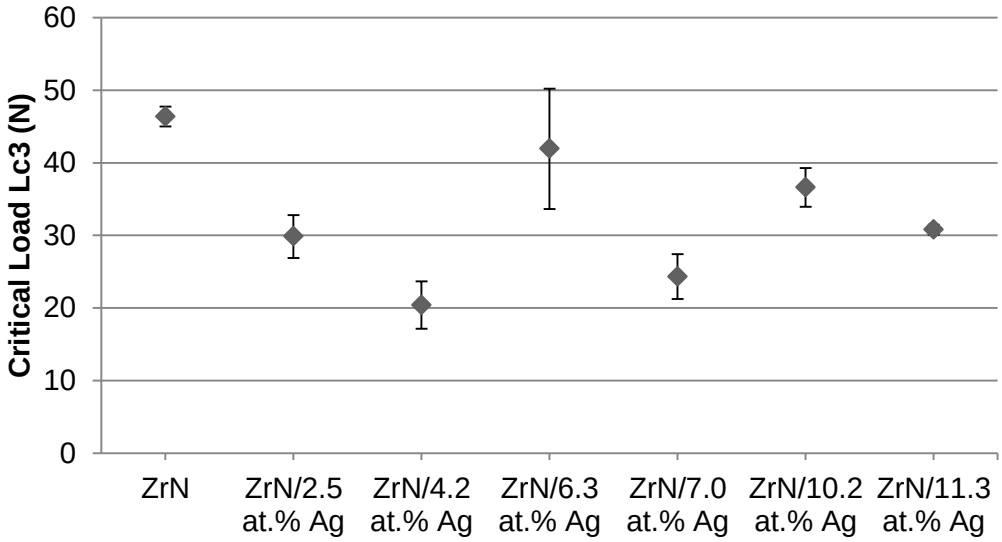

Figure 46: Critical loads of the coatings following scratch testing on the ZrN and ZrN/Ag coatings of varying silver contents demonstrating poorer adhesion from the coatings containing silver in comparison to the ZrN

4.3.2.3 Pin On Disk Testing

Pin on disk testing was used to obtain friction data on the coatings when sliding wear occurs. The results showed that as the silver content increased the coefficient of friction decreased (Figure 47). This suggests that the silver was acting as a solid lubricant beyond 6.5 at.% and decreasing the friction force. However, the error bars increased in size as the silver content increased, suggesting that the coatings could be starting to fail when the silver content is higher due to the coating being softer or less well adhered. Also, the pure ZrN displayed a similar coefficient of friction to the coating containing the highest amount of silver (11.3 at.% Ag).

Performing white light profilometry at low magnification (X 63 magnification) on the wear scars demonstrated that the test did not penetrate more than 600 nm on any of the surfaces. Examples of the WLP line profiles are displayed for pure ZrN and ZrN/11.3 at.% Ag coatings (Figure 48). The pin on disk test created a deeper wear scar in the pure ZrN (- 0.6 μm) than the 11.3 at.% Ag coating (- 0.4 μm).

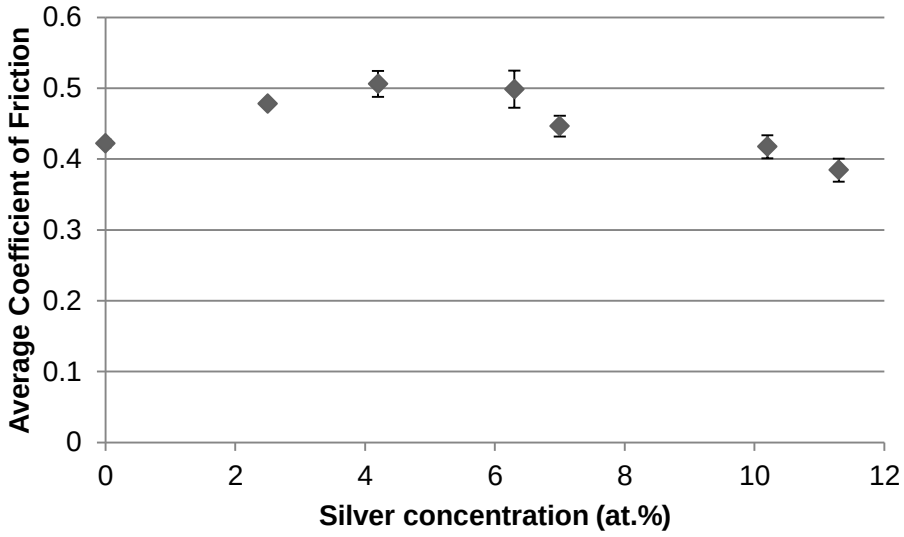

Figure 47: The average coefficients of friction taken from pin on disk testing demonstrated a similar trend to the scratch testing.Tthe higher silver concentrations (> 6.3 at.% Ag) possessed lower coefficients of friction (and higher adhesion) than the lower silver coatings.

a)

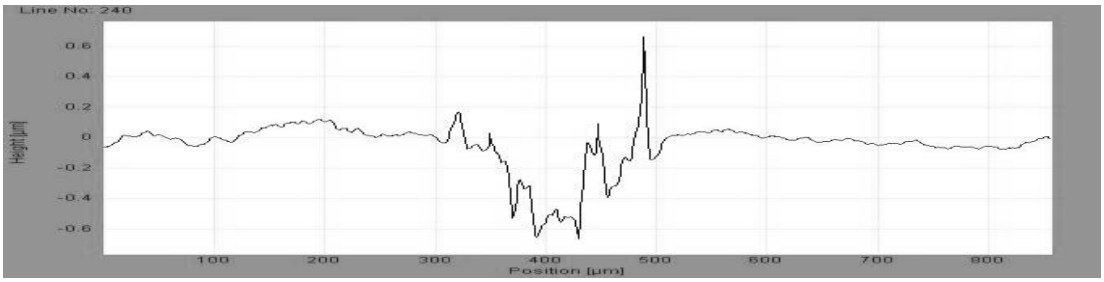

b)

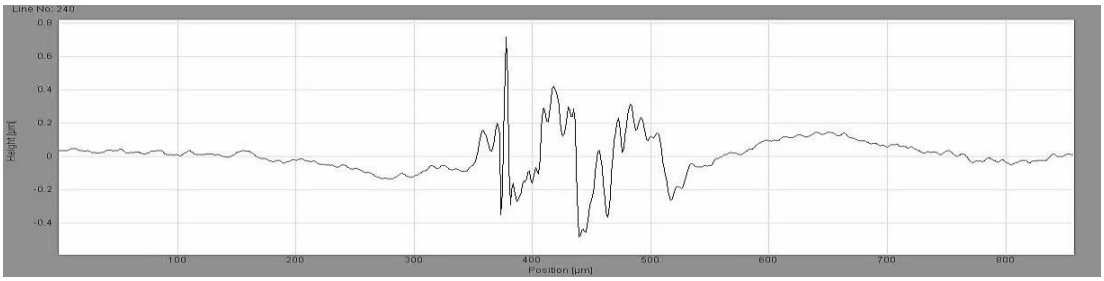

Figure 48: An example of white light profilometry line profiles of the pin on disk wear scars of a) ZrN, and b) ZrN/11.3 at.% Ag coating surfaces following a pin on disk test. The results demonstrated that the wear scars did not exceed 600 nm, therefore did not penetrate the 1 µm thick coatings.

4.4 Discussion

A Taguchi *L9* experimental array was used to improve the coating properties in terms of adhesion to the underlying substrate. Following improvement of the deposition technique using the experimental array an investigation was then carried out applying increasing powers to the silver magnetron to map out what powers needed to be used to achieve three coatings of the desired silver contents, these were to be tested further in terms of film properties and for antimicrobial efficacy in later chapters (Chapter 5 and Chapter 6, respectively).

The EDX analysis showed that all nine coatings contained very similar zirconium and nitrogen contents with the zirconium at 40 at.% and nitrogen between 50-55 at.% throughout. The silver concentration, varied due to only 90 W power being applied to the magnetron. The majority of the coatings contained around 5-10 at.% but No.4 and 9 were the lowest amounts of silver and No. 7 was determined as having no silver present in the coating. EDX was performed on these coatings for assurance of the chemical compositions, which should have theoretically being the same. Taguchi numbers 4 and 7 (No.4: 200 kHz 50 % duty and No.7: 300 kHz 50% duty) contained the lowest amounts of silver but this could be because of the pulse frequencies and duty applied. It has been hypothesised in the literature that an increased pulse frequency decreased deposition rates. A lower duty also means less “on time” throughout the pulse waveform which equates to lower deposition rates.

The scratch testing of the nine coatings revealed that the changing parameters affected the adhesion to the substrate and the best coatings occurred when the pulse frequency and the substrate bias was high. Number ‘7’ (300 kHz pulse frequency, 50% duty and 30 V bias) displayed the best adhesion, however as stated earlier the lack of silver in the coating may have increased the performance of the coating. Increasing the substrate bias increased the adhesion properties as numbers ‘3, 5 and 7’ were the best

performing, and excluding ‘7’, number ‘9’ performed best which had 15 V bias and 90% duty. This led to the conclusion that 300 kHz frequency and 30 V bias were essential and the duty either 50% or 90%. 50% duty was chosen due to the superior arc suppression.

The pin on disk results displayed all coatings with a maximum coefficient of friction within 0.4 - 0.5 throughout. The coatings that had the highest maximum coefficient of friction were ‘3, 7 and 9’, which corresponds to the surfaces with the least amounts of silver in. The lack of silver could lead to lack of solid lubrication in comparison to the other coatings which contained higher silver concentrations.

Following the results from EDX, scratch testing and pin on disk testing, the optimum conditions were chosen and a study on the content of silver in relation to magnetron power was investigated. In the previous chapter (Chapter 2; Page 59) it was found that 150 W power created a 15.5 at.% silver content and 230 W created a 29.8 at.% silver content. In this same study coatings of 70 W to the magnetron were produced but upon EDX analysis for chemical composition the result was a silver content of less than 1 at.% on average so these coatings were not included for characterisation. This investigation was carried out to clarify and stabilise silver concentrations for the coatings.

EDX demonstrated the content of silver in the coatings. With a constant increase in magnetron power (10 W increments) a near linear increase in atomic percentage content was observed. The coatings displayed decreased critical loads as soon as silver was added (excluding 6.3 at. % Ag). Further, as the silver concentration increased, the adhesion decreased, but further silver amounts caused increased adhesion again. This could be due to the silver being deposited as larger particles or more particles in the coating. Further work could include performing SEM on the surfaces to visualise surface morphology alterations and backscattered electron

detection would indicate the size, shape and frequency of the silver particles. This would act as a solid lubricant, allowing the stylus to slide more easily.

The pin on disk testing displayed a trend opposite to that from the scratch testing. As the silver content increased the average coefficient of friction increased. This increase stopped when the silver content reached around 5 at.% and from thereafter started to decrease in a bell shape trend. Performing white light profilometry on the wear scars of the coatings displayed the depth of penetration following the complete pin on disk test. The line profiles of the wear scars showed that following the test the maximum penetration depth was around 600 nm indicating that the coatings did not fail as they were around one micron thick. The profile of the wear track was raised at the edges due to a build-up of debris removed from the surface throughout the procedure.

In future work, more care was taken to prevent the silver target being contaminated with zirconium nitride using the movable shield arrangement discussed in the methods section of this chapter (4.2.1; Page 117). Prior to deposition the target was cleaned by applying 90 W to the magnetron while covered with a movable shield, which prevented contamination of the substrates from the silver magnetron and contamination of the silver target from the zirconium deposition.

4.5 Concluding Remarks

This work was designed to improve the tribology of the pre-existing coatings and design and fabricate new ZrN/Ag coatings by determining the optimum deposition parameters. A primary titanium interlayer was used to improve adhesion to the substrate and prevent potential insolubility between the zirconium and the iron in the stainless steel. The new coatings produced from the data obtained in this chapter comprised of a titanium interlayer, followed by a graded Zr-ZrN interlayer, followed by three different silver co-sputtering powers of 90W, 130W and 160W to produce silver contents with a range of 5 % to 25 %.

Following Taguchi arrays and testing the coatings using scratch testing it was found that a higher frequency and higher substrate bias produced better adhered coatings and the duty of the pulse did not provide conclusive evidence of changes in the surface characteristics. However, trends indicated lower duties produced improved coating adhesion to the underlying substrate. Producing multiple coatings and increasing the power to the silver magnetron each time in increments of 10 W demonstrated that the silver content increased in a linear trend when the power to the magnetron was increased. All of the silver containing coatings possessed decreased adhesion in comparison to pure ZrN, however an increase in silver concentration did not display a clear decreasing trend in adhesion. The friction characteristics of the surfaces were higher than the pure ZrN and started to decrease as the silver content increased, but stayed higher than pure zirconium nitride throughout. In the application of external fixation pins the coefficient of friction would not be of significant importance as much as other potential biomaterial applications with increased sliding movement, such as prosthetic joints.

5 Characterisation of Ti-ZrN/Ag

5.1 Introduction

5.1.1 Coating Improvements

Previous work in Chapter 2 (Page 59) demonstrated the production of ZrN/Ag coatings. It was found that following characterisation, the coatings were brittle and poorly adhered to the underlying substrate. An investigation into improving adhesion of the coatings to the underlying stainless steel and development of the coating properties, to meet the needs of the application, were applied in Chapter 4 (Page 111). New nanocomposite Ti-ZrN/Ag coatings were produced with improved adhesion and wear resistance. Surface properties that could potentially affect the retention of microorganisms and antimicrobial efficacy were also investigated. These surface properties included surface hydrophobicity, microtopography, nanotopography and determining the amount of zirconium and silver ions leached from the surfaces with increasing time periods.

5.1.1.1 Interlayers to Improve Tribology

The addition of metallic interlayers and using a gradient of reactive gas over time produces coatings with improved properties such as increased adhesion to the substrate, hardness and wear resistance. Kusano *et al*., (1998) found that applying multi-compositional layers of TiO_2/Ti/TiN, ZrO_2/Zr/ZrN and TiO_2/Ti/Zr/ZrN enhanced the adhesion of a hard coating (ZrN and TiN) to the underlying substrate, in comparison to single layer TiN or ZrN coatings. Multilayer coatings also had improved hardness since the metallic layer prior to the nitride improved the mixing of the two components. The authors found that slowly increasing the reactive gas into the sputtering chamber until fully reactive/stoichiometric created graded coatings, possessing improved hardness in comparison to single layer coatings of ZrN, TiN or CrN (Yao *et al.*, 2011).

The aim of the previous chapter was to improve the tribology of the deposited coatings. The aim of this chapter was to determine the surface properties that might affect microbial retention and subsequent antimicrobial efficacy.

5.1.2 Inductively Coupled Plasma – Atomic Emission Spectroscopy (ICP-AES): Quantifying Metallic Ion Leaching

Previously, the ZrN/Ag coatings were tested for inhibitory leaching of the antimicrobial silver by using a 'zones of inhibition' assay. The results concluded that no inhibitory leaching towards the bacterial strains investigated was observed. However, this may be due to the microbial assay not being sensitive enough to demonstrate an antimicrobial effect. Although the amounts of silver released towards the bacteria were not inhibitory there could still be a release of sub-inhibitory concentrations of silver into the surrounding area and this could have potential toxic or detrimental effects to the body if implanted (Lansdown, 2010). To quantify this release inductively coupled plasma-atomic emission spectroscopy (ICP-AES) was used.

Inductively coupled plasma – atomic emission spectroscopy (ICP-AES) is a method which evaluates the content of trace metals in a solution (1.4.2; Page 34). The flexibility of this technique means it can be used for many applications to quantify trace metal and ion release into an aqueous solution, such as; quantifying lithium in cleaning validation swabs (Lewen and Nugent, 2010) trace elements in edible oils (Cindric *et al.*, 2007), trace element detection in human serum (Al, Fe, Mn, Li and K). (Bianchi *et al.*, 2007) in drinking water (Atanassova *et al.*, 1998) and characterisation of soils in archaeology and meteorology (Knudson *et al.*, 2004).

In this investigation silver release was quantified over time when submerged into a solution that contained some of the components that might surround the pin in the body; thus the *in vitro* tests used brain heart infusion broth.

5.1.3 Surface Hydrophobicity

There are many different factors which affect bacterial adhesion, which relate to both the surface characteristics of the bacterium and the substrate (Table 9). Since many variables contribute towards the behaviour of bacterial retention, it is important to select and test the most relevant in terms of use for the final application and the most important in terms of how the bacteria interact with the surface *in vivo*.

Wettability is the amount water can spread across a surface and is 'wetted'. This is measured by calculating the outside contact angle of water on the surface. The lower the contact angle the more wettable the substrate. However, this is often defined as 'hydrophobicity' even though it can only be used as purely a descriptive term. It has been stated that defining surfaces as wetting or non-wetting by water is not a satisfactory criterion to claim "hydrophobicity" (Van Oss and Giese, 1995).

As discussed in the introductory chapter (1.4.6; Page 42), surface hydrophobicity plays an important role in the physicochemical reactions between the substratum surface and other molecules such as conditioning film components adsorbing on the surface and the strength and ability of a bacterial cell to attach to the surface. In chapter 2 (Page 59), only surface wettability was evaluated. In this work, the surface analysis has been expanded to examine the physicochemistry calculations including hydrophobicity, surface free energy, acid base interactions, Liftshitz van der Waals forces, electron accepting and donating capabilities. The definition of hydrophobicity is the calculation of "free energy of interfacial interaction between particles in an aqueous environment" (van Oss and Good, 1988, Good and van Oss, 1991, Van Oss and Giese, 1995). Further, other physicochemical factors such as surface charge, surface components and surface free energy can provide information which may determine surface properties that affect microbial retention. Since no relationship was observed for the wettability and bacterial retention on the ZrN/Ag coatings previously tested, this work investigated physicochemistry alongside other surface characteristics (Table 9).

Surface hydrophobicity was selected as an important value to investigate because of its importance in biomaterial and implant design and its effect towards bacterial biofilm formation.

Table 9: The variables that control bacterial adhesion adapted from Campoccia et al. (2013). Highlighted in red are the variables that have been included throughout this body of work.

Variables controlling bacterial adhesion	
Variables influencing bacterial adhesion and colonisation on biomaterial surfaces	
Surface morphometry	Macroporosity
	Microporosity
	Micro-roughness
	Nano-roughness
Physico-chemical properties	Surface energy
	Hydrophilicity
	Hydrophobicity
	Hydrophobic functional groups
	Polar functional groups
	Charged functional groups
	Functional groups with specific activities
	Degree of hydration
Environmental conditions	Electrolytes
	pH
	Temperature
	Host proteins/host adhesins
	Shear rate/fluid viscosity
	Fluid flow rate
Pathogen	Gram-positive/Gram-negative
	Genus/Species
	Bacterial shape
	Surface energy
	Strain type and specific set of expressed adhesins

Bacterial attachment, adhesion and retention in relation to substratum hydrophobicity have been thoroughly investigated throughout many disciplines. The biomaterial industry often investigates the role of hydrophobicity in relation to the behaviour of bacterial cells towards the surface, investigating many types of material. The effect of surface hydrophobicity has been extensively investigated in contact lens design to prevent microbial adhesion, in particular *Pseudomonas aeruginosa* (Bruinsma *et al.*, 2001, Bruinsma *et al.*, 2003). Surface hydrophobicity in relation to the hygienic status of metallic orthopaedic implants has also been investigated. It has been suggested that a low surface energy, hydrophobic surface, will help inhibit biofilm formation and it has also been found to improve the biocompatibility of a metal surface (Roosjen *et al.*, 2006, Pendyala *et al.*, 2009, Panjwani and Sinha, 2012). Thus the surfaces were investigated to see if these properties were found on the Ti-ZrN/Ag coatings.

This chapter investigated the characterisation on the new titanium-zirconium nitride silver coatings with graded metallic zirconium interlayers, and includes further surface characterisation, including hydrophobicity and ICP-AES.

5.2 Methodology

The methods used to analyse the Ti-ZrN/Ag surfaces included EDX, SEM, Backscattering, XRD, Scratch Testing, AFM and White Light Profilometry. New methods included in the surface analysis for the Ti-ZrN/Ag surfaces included surface hydrophobicity and metal leaching (ICP-AES).

5.2.1 Hydrophobicity Measurements:

The hydrophobicity was calculated by obtaining the surface contact angles of two polar liquids: HPLC grade water (Fisher Scientific; Loughbrough, UK) and Formamide (Sigma Aldrich; Dorset, UK) and one non-polar solvent: 1-bromonaphthelene (Sigma Aldrich; Dorset, UK). The contact angles were obtained using the sessile drop technique (Kruss MobileDrop II, Kruss, Germany). This instrument deposits 2 µl volume drops from a standard dropper. The drop contact angle on the surface is then measured using a camera and prism inside the device. The image was analysed using Kruss SW23 (DSA2) (Kruss, Germany) analysis software, using the Young-Laplace bubble fit method to obtain the angle between the 'bubble' and the surface interface. The contact angles of the three liquids were calculated as demonstrated in Chapter 1.4.6 (Page 42).

5.2.2 ICP-AES Analysis

ICP-AES was used to evaluate the release of silver ions into a liquid medium. The amount of zirconium ion release was also measured in the same solutions. The coupons were cleaned using ethanol and distilled water and then put inside a sealed beaker and autoclaved at 121 ºC for 15 minutes. Sterile brain heart infusion broths (100 ml) (Oxoid, UK) were used for the liquid medium to replicate a nutrient rich substance, and to keep a constant between the other assays, such as the zones of inhibition testing. The coated stainless steel coupons (n = 16) were added to the broth aseptically and sealed with a sterile foam bung and aluminium foil. The samples were

placed in an orbital incubator at 37 ºC at 150 RPM. At intervals of 24h, 1 week and 1 month 10 ml samples were extracted aseptically and diluted 1:1 in HPLC Grade Water (Fisher Scientific, UK) and filter sterilised with a 0.2 µm filter membrane (Acrodisk, UK) and a Luerlock™ syringe (Sigma Aldrich, Dorset, UK). Samples were stored at 4 ºC in the dark until analysis was to be undertaken.

ICP-AES was performed on Varian Vista XA (CCD simultaneous ICP-AES) with sample introductory system of glass spray chamber and glass nebuliser. Analysis was undertaken using blanks of the brain heart infusion broth as a negative control and liquid standards of silver and zirconium (Sigma Aldrich, Dorset, UK) were used in the ICP instrument to produce a calibration curve of 0.1, 0.5, 1.0 and 5.0 parts per million (ppm) concentrations.

5.3 Results

5.3.1 Chemical Composition

EDX analysis was undertaken on the four Ti-ZrN/Ag coatings deposited onto silicon wafers. The silver content demonstrated averages of 6.0 at.%, 15.6 at.% and 24.7 at.% for magnetron powers of 90 W, 130 W and 160 W respectively (Figure 49).

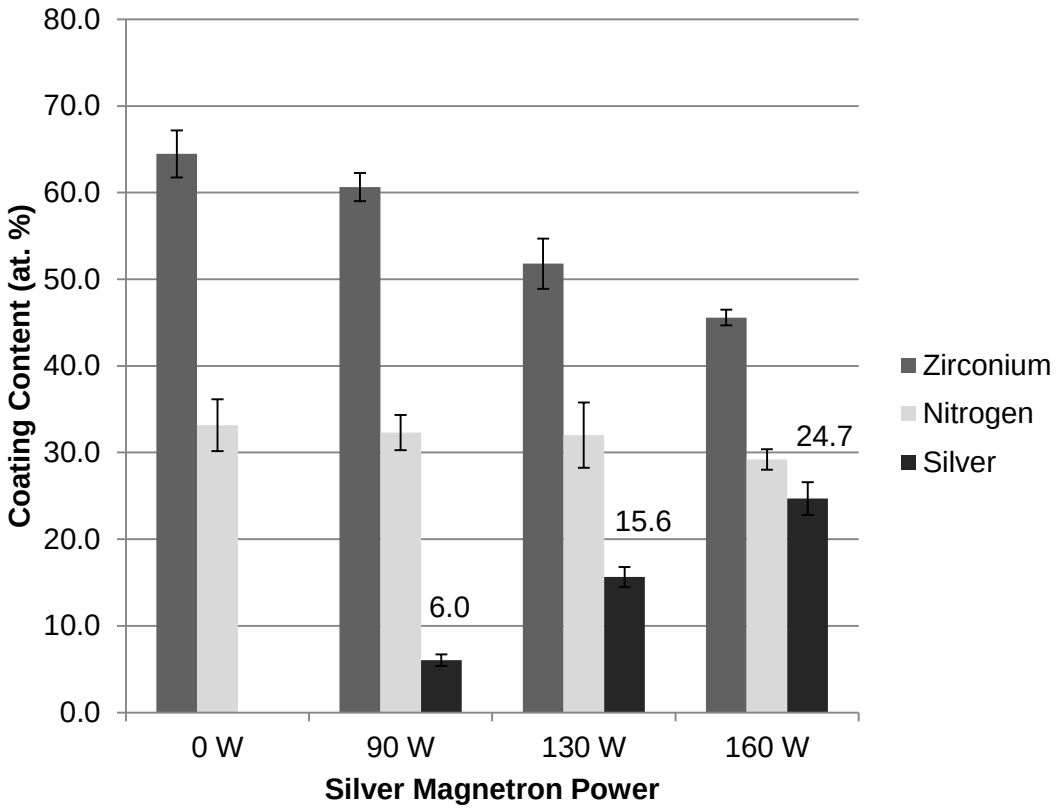

Figure 49: EDX analysis of the four coating compositions displaying the zirconium and nitrogen content as well as silver content in relation to magnetron power, with the numerical value of the average included.

5.3.2 SEM Results

5.3.2.1 SEM of Coating Surface Morphology on Silicon Wafer

High magnification SEM images were obtained of the four different titanium-zirconium nitride coatings deposited onto silicon wafer for means of surface morphology visualisation. The pure Ti-ZrN coating (Figure 50a) displayed a relatively porous columnar surface with small columns of similar sizes. As the silver content of the coatings increased, the size of the grains increased and the film became more dense. In addition, the silver particles became more visible, especially on the 24.7 at.% silver coating (Figure 50d).

5.3.2.2 SEM of Fracture Cross Sections of Ti-ZrN/Ag Coatings Deposited onto Silicon Wafers

Fracture cross sections give a view throughout the coating structure. The pure Ti-ZrN, like the previous image (Figure 50), displayed a columnar structure consisting of small pillar like grains (Figure 51a). The silver containing coatings had larger grain sizes but a more dense structure, with what appeared to be a smoother surface. The Ti-ZrN/15.6 at.% silver coating displayed the coating titanium interlayer and the grading of the zirconium from metallic into a stoichiometric nitride, just above the surface of the silicon wafer (bottom black/darker grey area) (Figure 51c). The Ti-ZrN/24.7 at.% silver coating demonstrated most clearly the silver nanoparticles within the coating as well as displaying one of the more dense film structures out of the four samples (Figure 51d).

a)

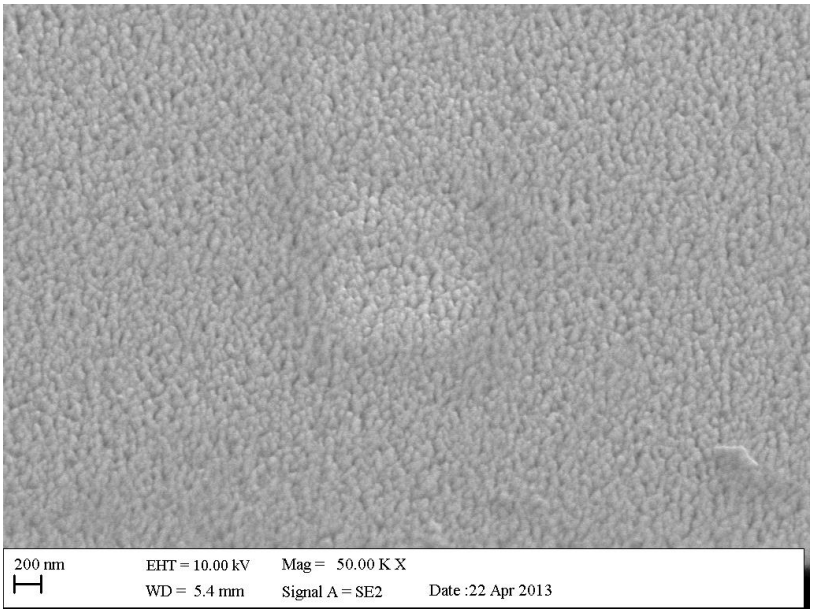
200 nm
EHT = 10.00 kV
Mag = 50.00 K X
WD = 5.4 mm
Signal A = SE2
Date :22 Apr 2013

b)

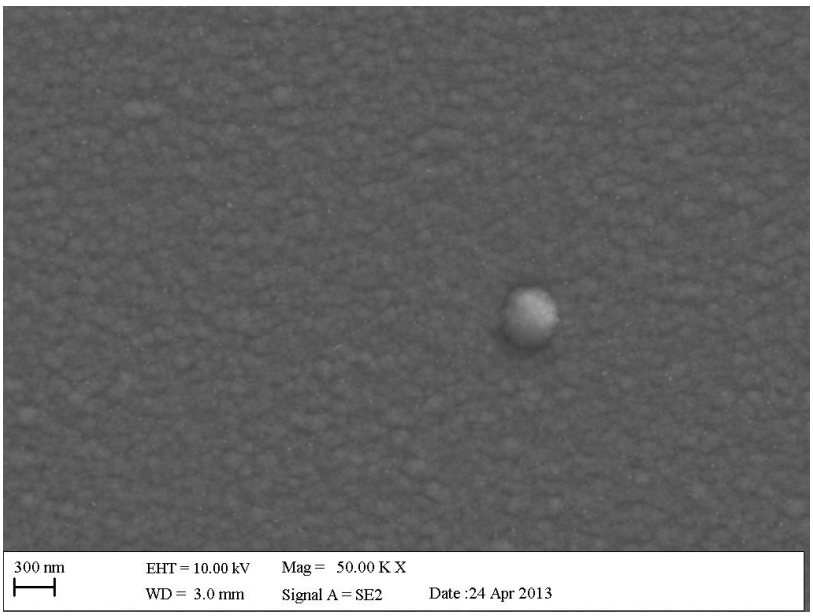
300 nm
EHT = 10.00 kV
Mag = 50.00 K X
WD = 3.0 mm
Signal A = SE2
Date :24 Apr 2013

c)

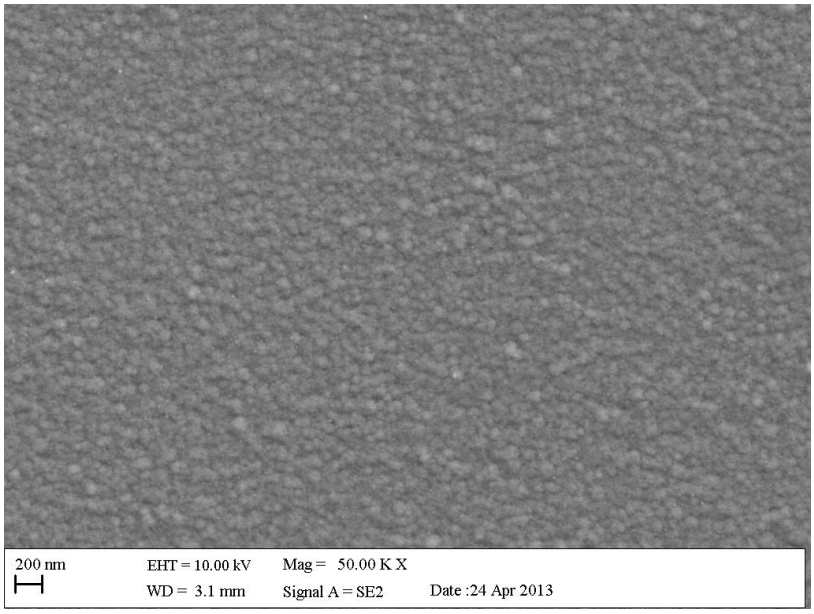

d)

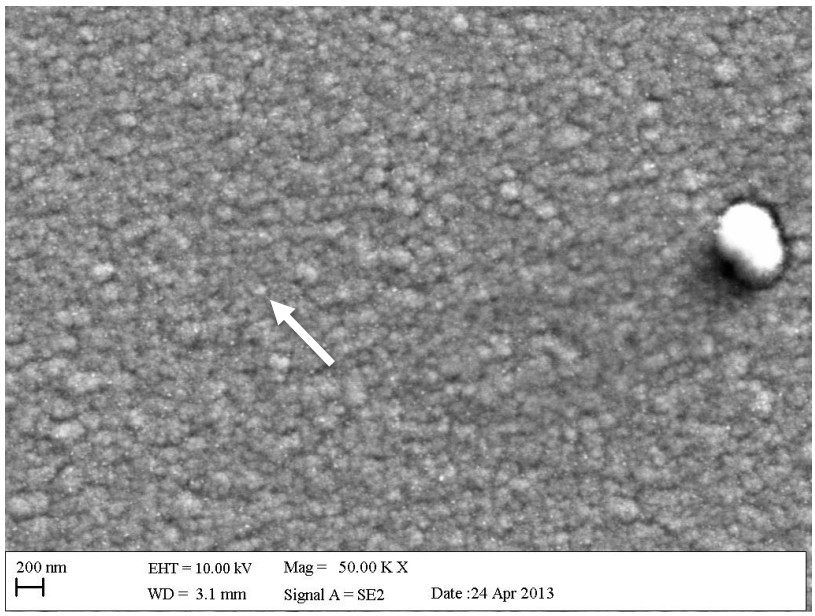

Figure 50: SEM images (X 50,000 mag) of the four coatings produced; a) Ti-ZrN, b) Ti-ZrN/ 6.0 at.% Ag, c) Ti-ZrN/ 15.6 at.% Ag and d) Ti-ZrN/ 24.7 at.% Ag, displaying the difference in surface morphology and density as the silver content increases. The silver particles can be seen clearly as white particles in d (indicated) but they are not as clear as in b and c.

a)

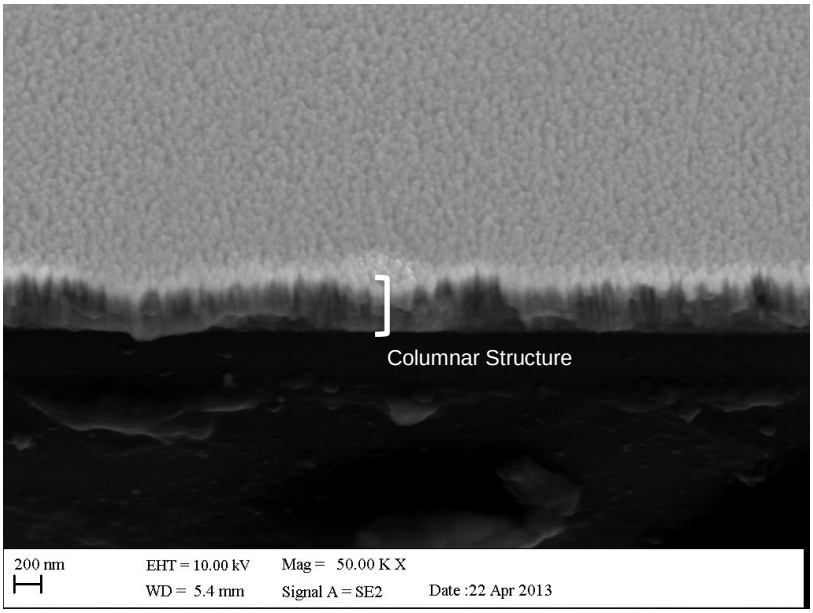
Columnar Structure
200 nm
EHT = 10.00 kV
WD = 5.4 mm
Mag = 50.00 K X
Signal A = SE2
Date :22 Apr 2013

b)

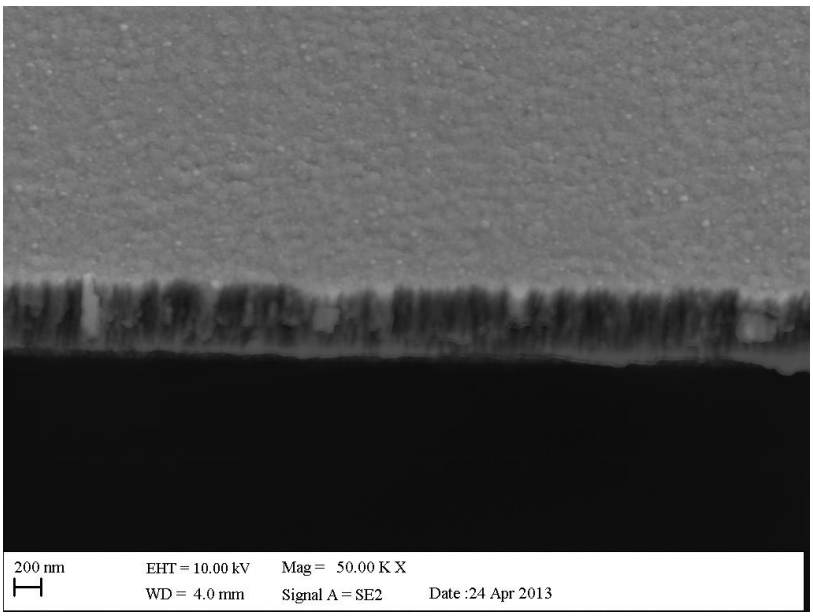
200 nm
EHT = 10.00 kV
WD = 4.0 mm
Mag = 50.00 K X
Signal A = SE2
Date :24 Apr 2013

c)

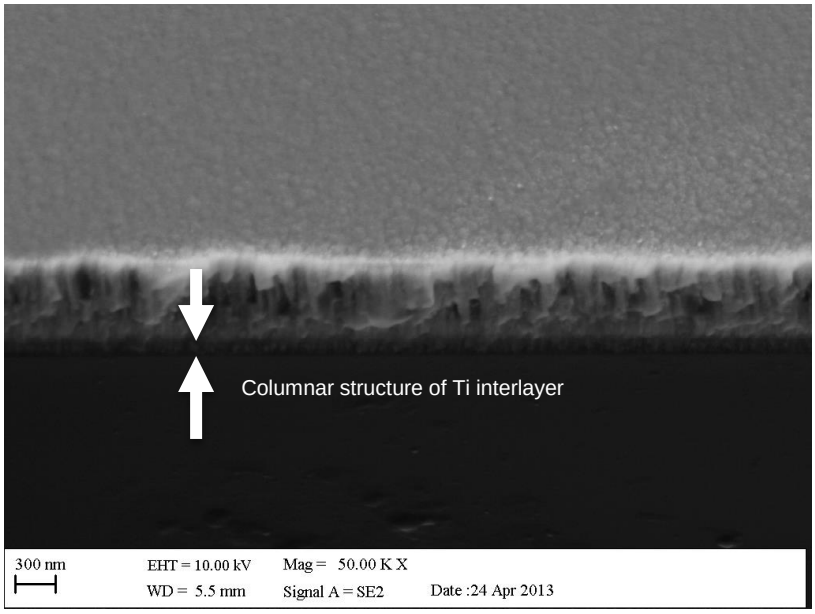

d)

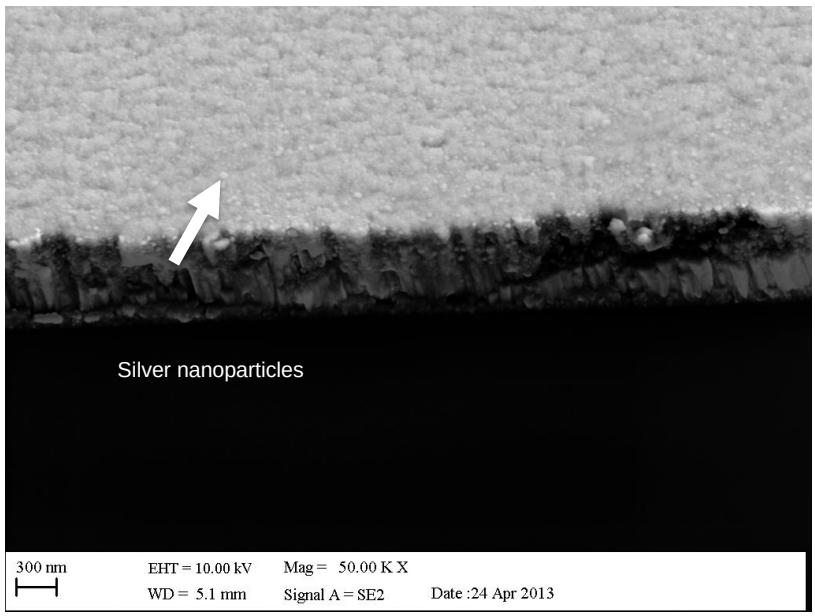

Figure 51: SEM of fracture cross sections of the nanocomposite thin films (X 50,000 mag); a) Ti-ZrN, b) Ti-ZrN/6 at.% Ag, c) ZrN/15.6 at.% Ag and d) ZrN/24.7 at.% Ag. All four coatings have similar structure morphology, but the silver coatings display more dense structure than the pure ZrN.

5.3.2.3 Electron Backscattered Imaging of the Coatings

Obtaining images of the surfaces using the backscattered electron detector allowed visualisation of the chemical elemental distribution on a sample surface. Due to heavier elements being able to backscatter electrons more freely, they are displayed on the image as a brighter phase. This allows visualisation of the silver particles, which are heavier than zirconium, and their distribution throughout the surfaces. The pure Ti-ZrN was examined as a negative control and displayed a relatively homogenous surface, demonstrated by a similar colour phase (Figure 52a). The 6.0 at.% silver coating possessed silver particles of various sizes around 8 nm, with many being larger than others and sparsely distributed (Figure 52b). The 15.6 at.% silver coating displayed a different morphology, with the silver particles being overall smaller, of a similar size (around 5 nm) and regularly distributed but more closely packed (Figure 52 c). The 24.7 at.% silver coating showed mixed sized silver particles (10-20 nm) which were closely spaced (Figure 52d).

5.3.3 Scratch Testing

Scratch testing of the coatings defines the strength of adhesion of the coatings to the substrate. The critical load is the load at which the stylus fully delaminated the coating, obtained by visual analysis. The results demonstrated a reduction in coating adhesion strength between the silver coatings and the pure ZrN. However, the increase in silver did not reduce the coating adhesion and no trends were observed between silver content and coating adhesion (Figure 53).

a)

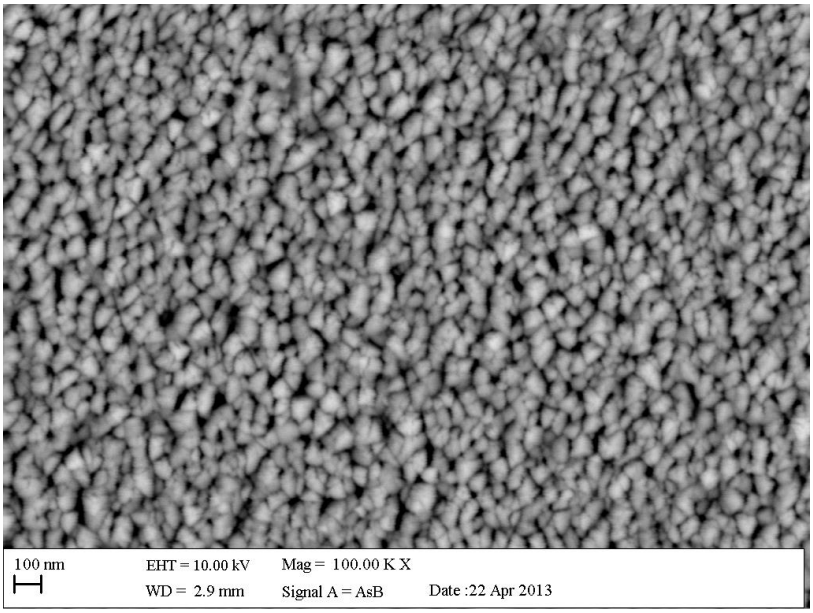
100 nm
EHT = 10.00 kV
WD = 2.9 mm
Mag = 100.00 K X
Signal A = AsB
Date :22 Apr 2013

b)

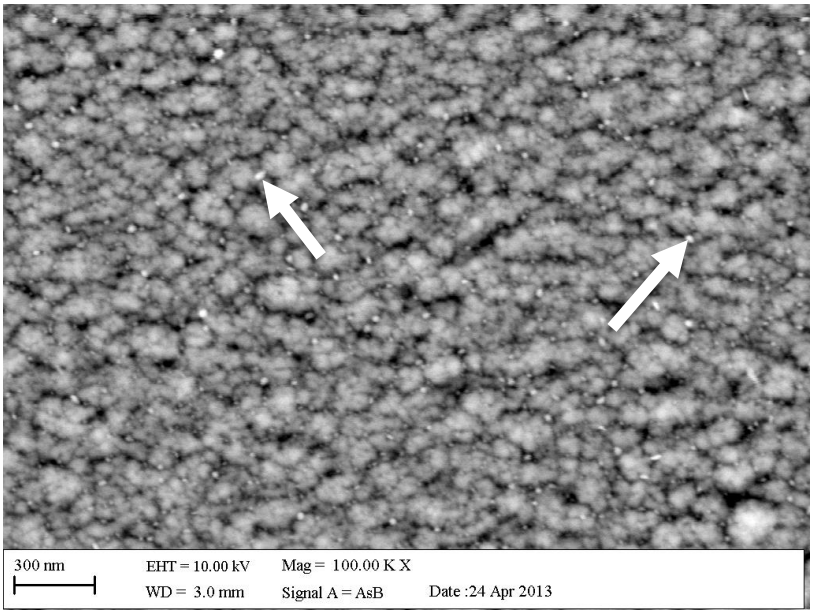
300 nm
EHT = 10.00 kV
WD = 3.0 mm
Mag = 100.00 K X
Signal A = AsB
Date :24 Apr 2013

c)

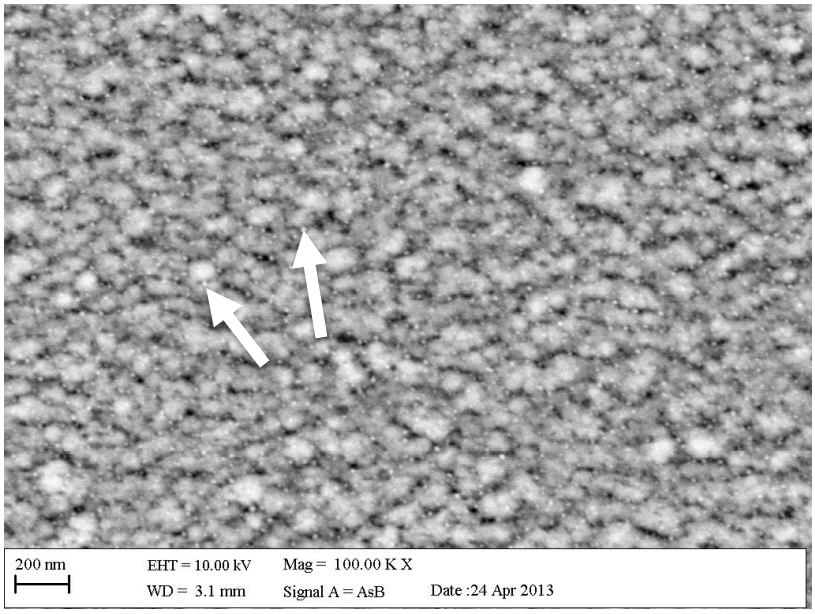

d)

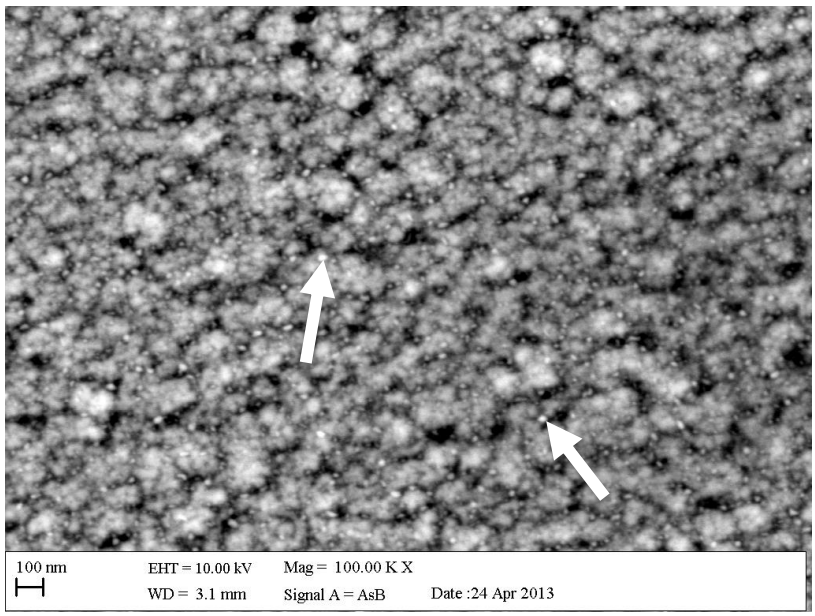

Figure 52: Electron backscatter detector images of the four coatings (X 100,000 magnification); a) Ti-ZrN, b) Ti-ZrN/6.0 at.% Ag, c) Ti-ZrN/15.6 at.% Ag and d) Ti-ZrN/24.7 at.% Ag. The white particles seen on b), c) and d) are silver nanoparticles. No particle appears to be any larger than 10 nm in b and c but few appear to be larger on d (silver indicated with white arrows).

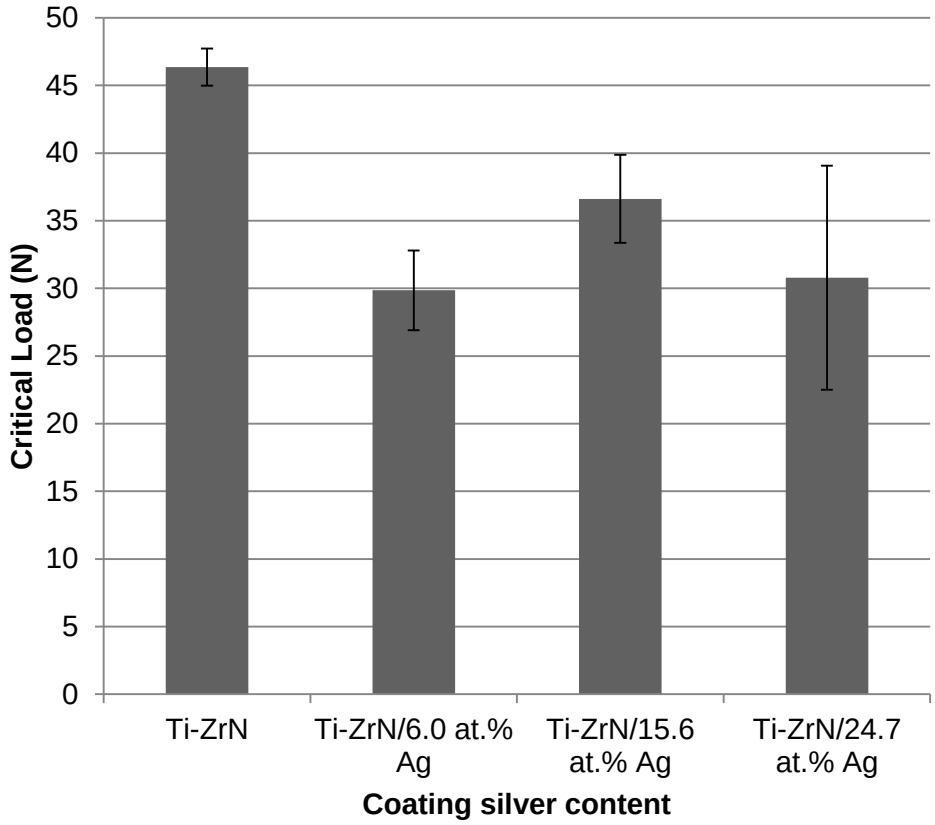

Figure 53: The critical load points obtained from scratch testing. This is the point where the coating fully delaminates from the underlying substrate, often known as the point of failure. The results demonstrated that the addition of silver reduced coating adhesion.

5.3.4 AFM Analysis

AFM scans of the coatings, deposited onto silicon wafer, were undertaken to display the surface topography of the coating, without topographical influence from the underlying medical grade 316L stainless steel on which the coatings would be deposited. Scans of one square micron allowed the grain boundaries of the coating structure and the effect of silver on the nanotopography of the coating to be visualised. The topography of the Ti-ZrN contained a consistent series of small peaks throughout the surface but overall the amplitude of the features remained low (maximum: 76.2 nm) (Figure 54a). The surface with the greatest nano topographical differences overall were demonstrated by the scans taken of the Ti-ZrN/6.0 at.% Ag (Figure 54b). The Ti-ZrN/15.6 at.% and Ti-ZrN/24.7 at.% coatings possessed similar appearances in nanotopography as each other, with regular high peaks throughout a matrix of grains with a hexagonal appearance and the increase in silver increased the frequency and amplitude of the peaks observed, due to the silver particles protruding from the surface (Figure 54c and d).

5.3.4.1 Roughness Values

Roughness values in terms of R_a, *RMS* and "Average Height" were obtained. The values were taken from one square micron scans of the surfaces of coatings deposited onto silicon wafers, thus the values represent alterations in surface topography at the nanoscale and also how the coating deposition morphology affected the surface nanotopography. It was seen that R_a, RMS and Average height values both increased for the coatings containing 15.6 at.% and 24.7 at.% silver (Figure 55). This was expected due to the particles of silver protruding from the surface. Further, the increase in silver denoted an increase in particles, as seen in the backscattered images (Figure 52d). The Ti-ZrN surface had higher overall roughness values than the 6.0 at.% silver coating but with no significant difference ($p < 0.05$). However, the increase in

roughness between the surfaces as the content of silver increased was significant ($p < 0.05$).

5.3.4.2 Line Profiles and feature sizes

Line profiles of the AFM scans were taken and the features were measured in terms of average valley width and depth. The surface area of the AFM scan was also obtained. The line profiles displayed the shape and size of the surface features and the individual topographies of the coatings. The average width and height measurements quantify the size of the peaks and valleys in terms of height and width measured individually. The Ti-ZrN/6.0 at.% Ag coating had the lowest Z height, (Figure 56b). The 15.6 at.% and 24.7 at.% coatings had similar nanotopographies but they were visually different because of the increased Z scale of the 24.7 at.% silver profile caused by single large peaks throughout the scan area (Figure 56c and d, respectively). However, the width scale was the same for all of the profiles. The 15.6 at.% Ag surface possessed widest average widths out of the three silver containing coatings (Figure 57). The Ti-ZrN/24.7 at.% silver demonstrated a lower width value over the other three surfaces (Figure 57) with an average of 66.6 nm and this is also represented visually on the line profile (Figure 56d). As the silver content increased the average depth tended to increase also showing that the silver particles are affecting the surface nanotopography. The 6.0 at.% Ag decreased to a value of 6.6 nm but increasing silver increased the depth sizes to 29.1 nm and 42.3 nm for 15.6 at.% Ag and 24.7 at.% Ag respectively (Figure 57).Thus an increase in silver led to an increase in surface feature depth but a decrease in feature widths. There was a strong trend towards the surface area increasing as the silver content increased (Figure 58). This value was averaged from the overall surface area minus the two dimensional (one μm^2) surface area.

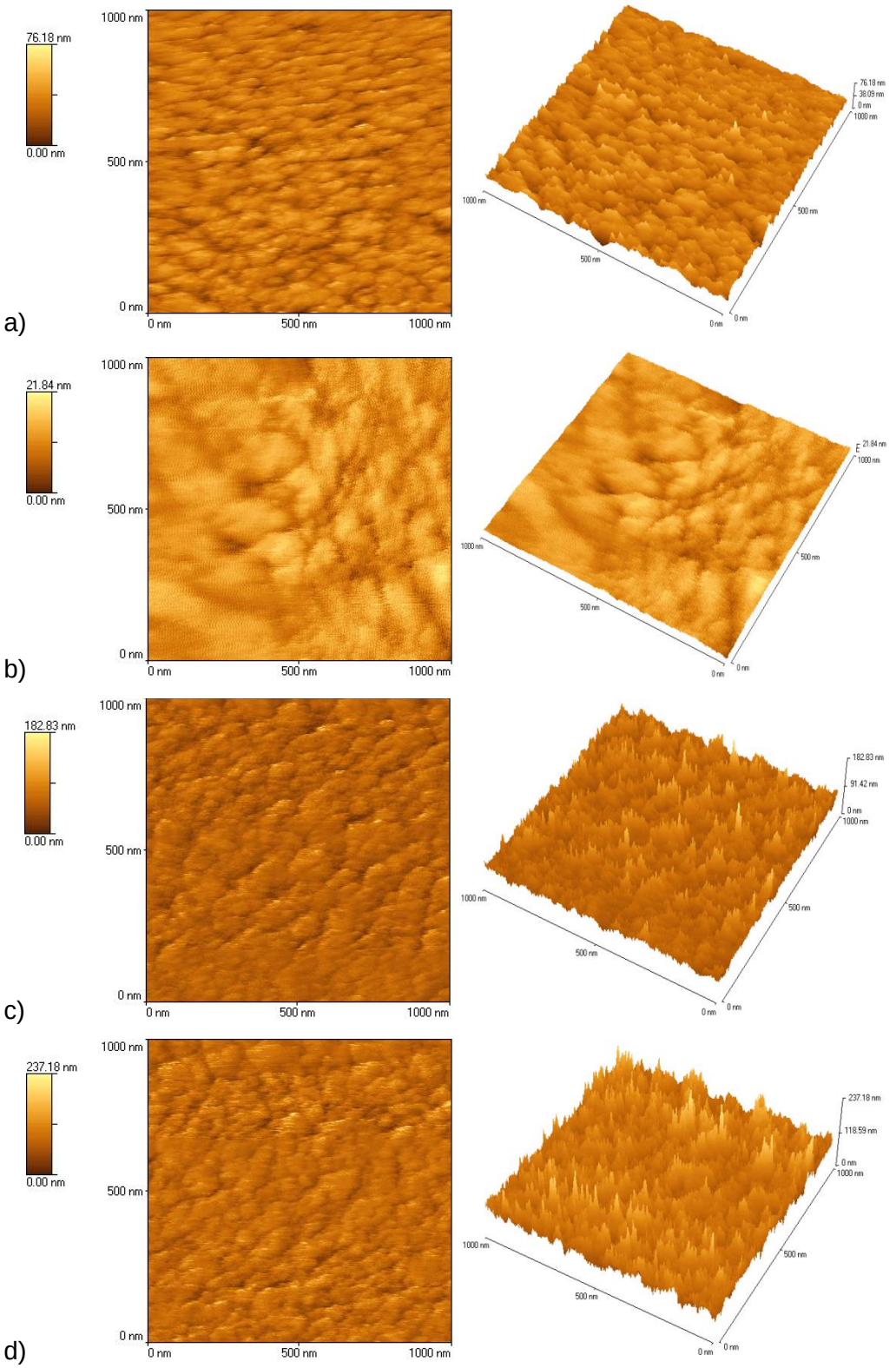

Figure 54: AFM Scan (one x one µm) two dimensional and three dimensional images of a) Ti-ZrN, b) Ti-ZrN/6.0 at.% Ag, c) Ti-ZrN/15.6 at.% Ag and d) Ti-ZrN/24.7 at.% Ag, deposited onto silicon wafer. The surfaces demonstrate the nanotopography of the four coatings.

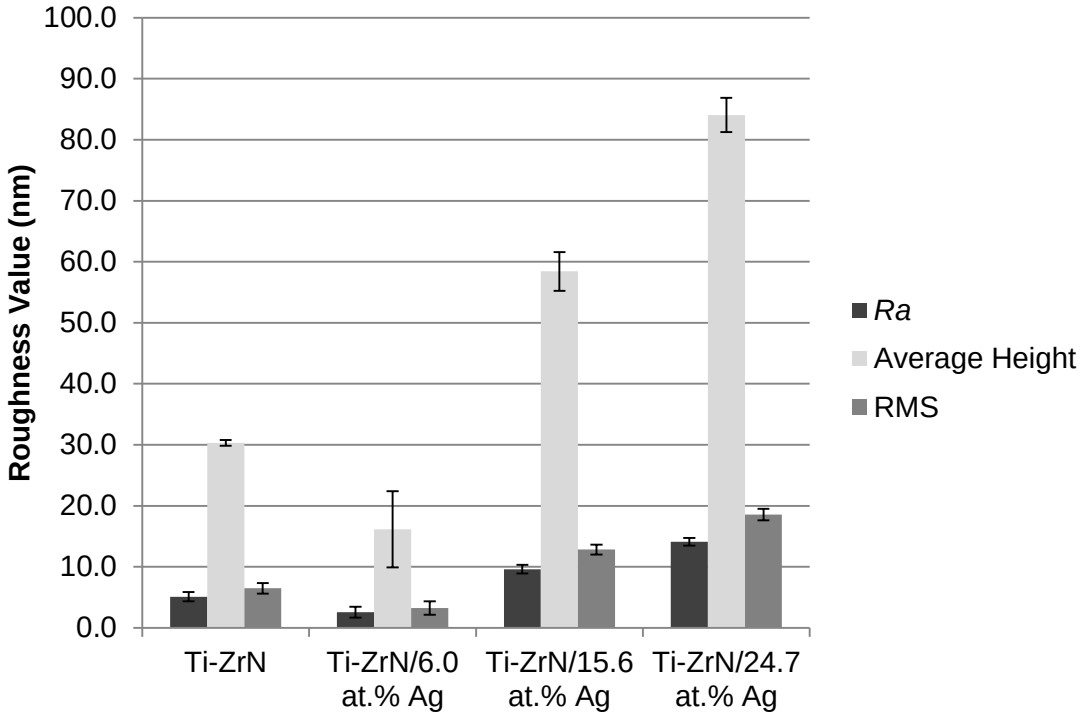

Figure 55: Roughness values for the four surfaces, deposited onto silicon wafer. The results show alterations of roughness in terms of nanotopography. Both R_a and average height display an increasing trend as the silver content increases suggesting that silver alters the nanotopoography.

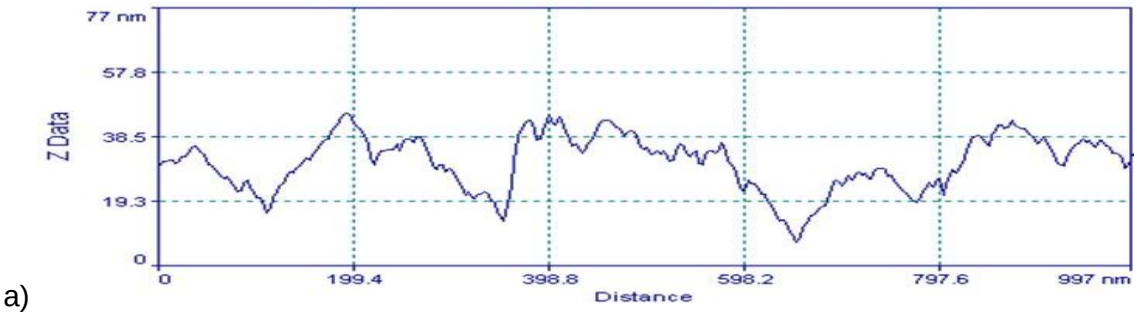

a)

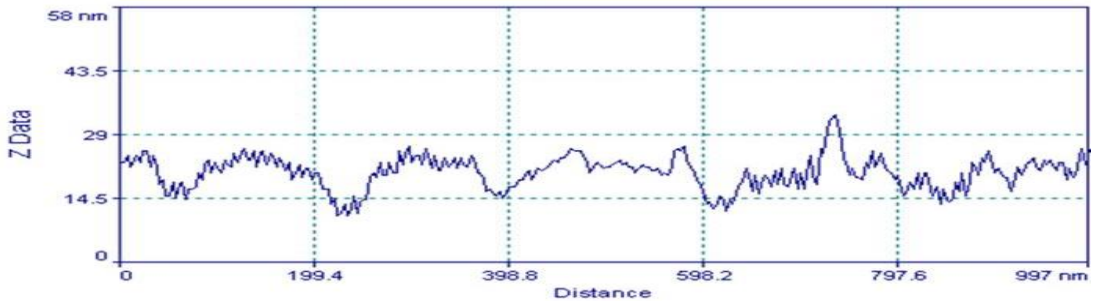

b)

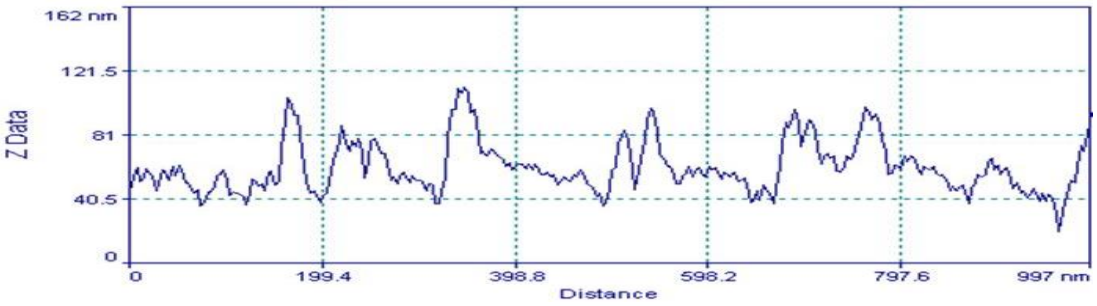

c)

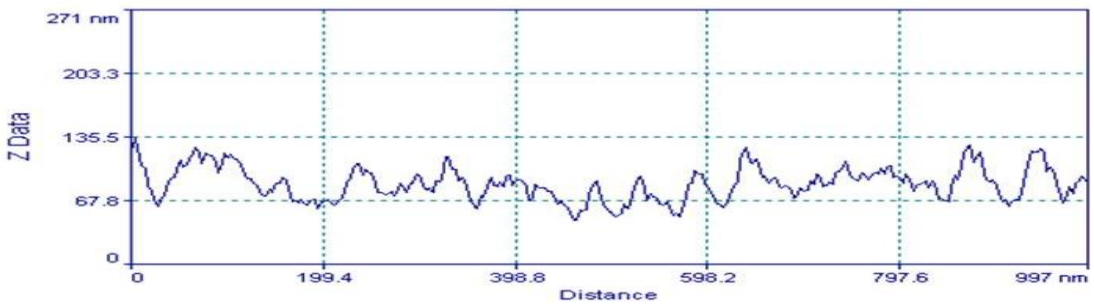

d)

Figure 56: AFM line profiles of the four coatings deposited on silicon wafer; a) Ti-ZrN, b) Ti-ZrN/6.0 at.% Ag, c) Ti-ZrN/15.6 at.% Ag and d) Ti-ZrN/24.7 at.% Ag, demonstrating the differing nanotopographies of the four surfaces. Note that the *Z* scales differ for all four profiles and 24.7 at.% Ag has the highest *Z* scale at 271 nm and 6.0 at.% Ag the lowest, at 58 nm.

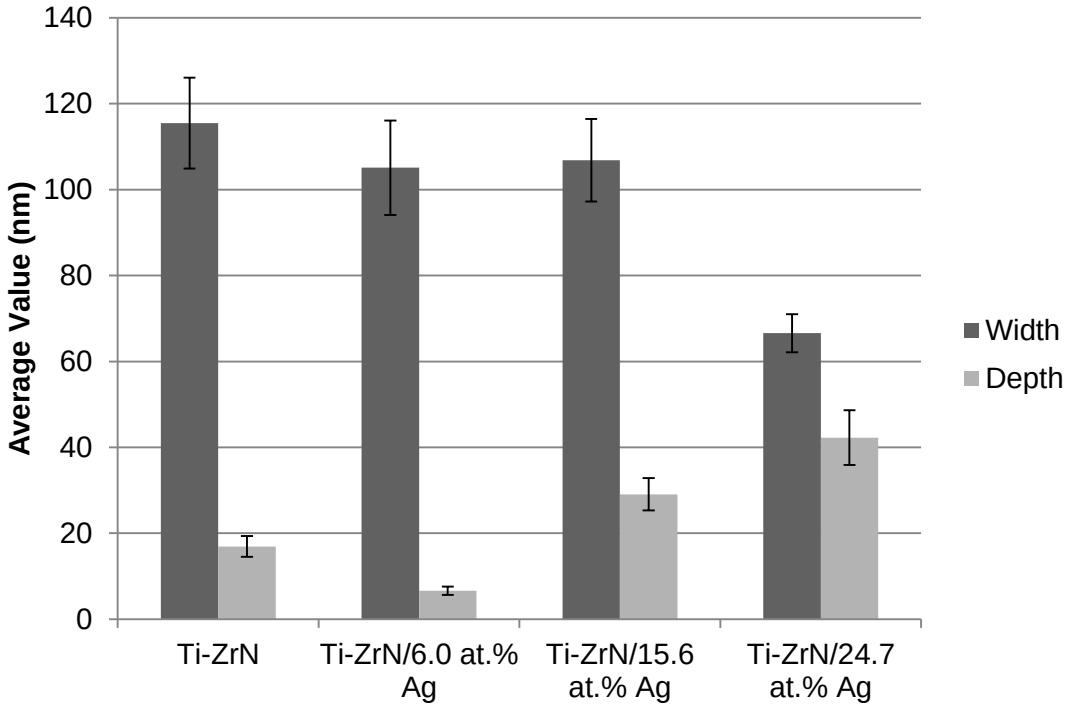

Figure 57: Average width and depths of features measured from AFM line profiles of the Ti-ZrN and Ti-ZrN/Ag coatings deposited onto silicon wafer. Feature sizes represent the nanotopographies of the surfaces.

5.3.4.3 AFM surface area (Silicon wafer)

AFM measurements calculated the surface area of the scans; a higher surface area denotes more surface features on the surface. The 6.0 at.% Ag surface had a lower surface area than the Ti-ZrN but as the silver content increased the surface area increased significantly ($p < 0.05$) (Figure 58).

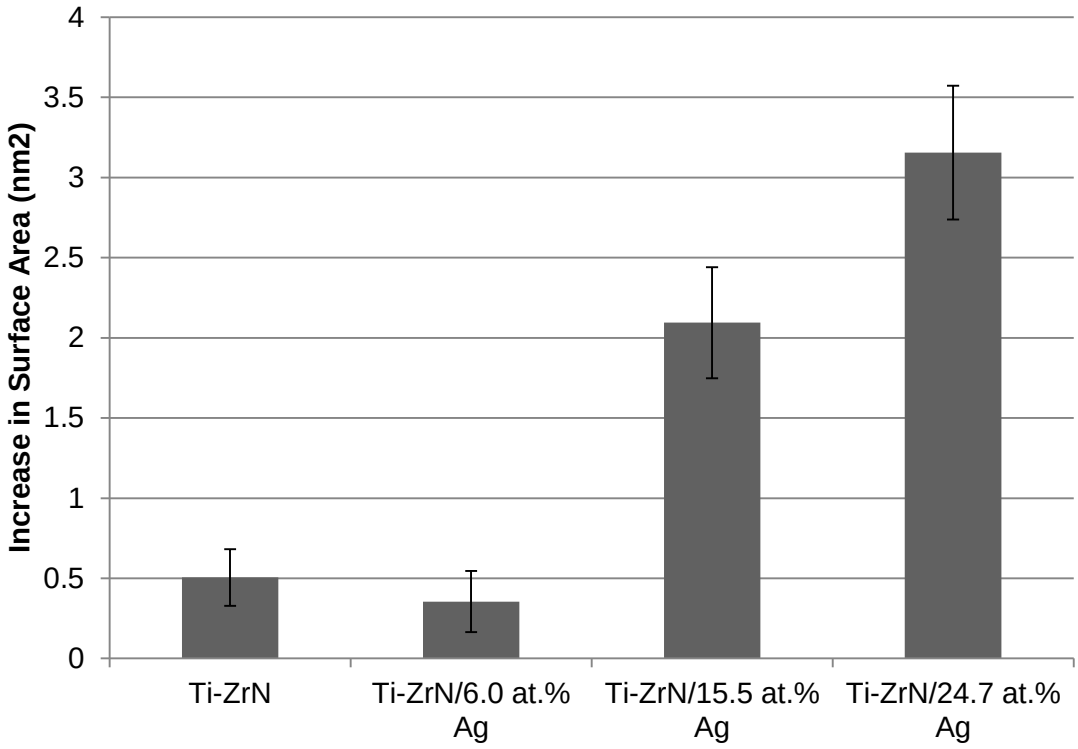

Figure 58: The increase in surface area of the Ti-ZrN and Ti-ZrN/Ag coatings on silicon. The increase in silver increased the surface area and thus an increased nanotopography.

5.3.4.4 AFM *R* values on Stainless Steel Substrates

AFM was undertaken on stainless steel substrates (10 x 10 µm scans) to determine the roughness values of the coatings in relation to the stainless steel in terms of nanotopography. The values obtained were the *Ra* and RMS; these are universal roughness parameters used throughout literature and international standards. The average height is a parameter calculated by the AFM software (1.4.3.6; Page 37) that has significance to the characterisation of the roughness. The results showed that the addition of silver increased the roughness of the coatings and that there was a trend of increasing roughness in relation to the increase in silver content (Figure 59). The average height values for the surfaces demonstrated an increase between stainless steel and the coated samples and as the silver content increased, the average height also increased, with exception of 24.7 at.% Ag (Figure 60). There was no significant difference ($p < 0.05$) between any of the roughness values taken and between any two surfaces. This suggests that in relation to the stainless steel, the addition of the coatings did not significantly alter the microtopography but did significantly alter the nanotopography.

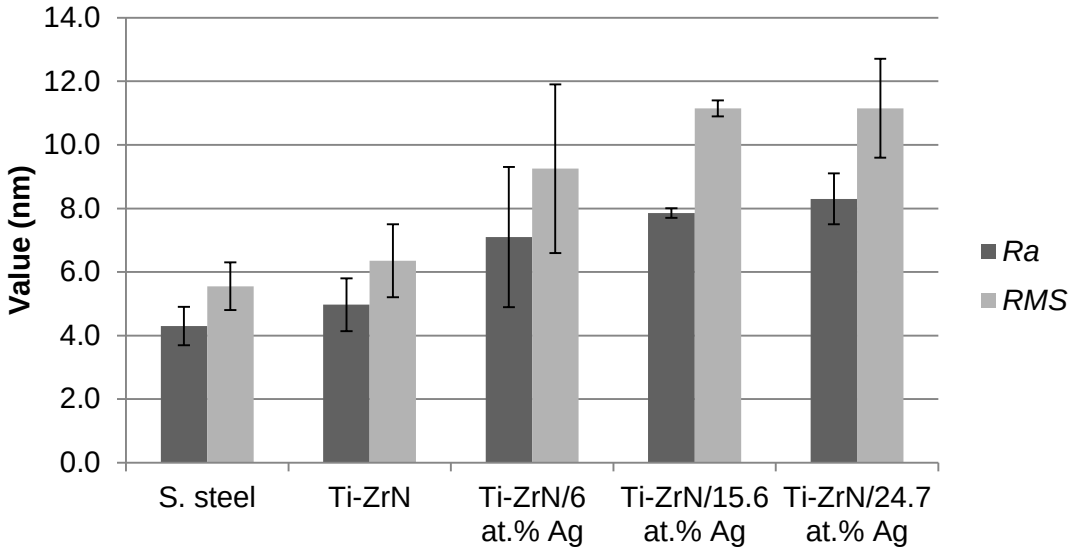

Figure 59: R_a and *RMS* values from the AFM (10 x 10 µm scans) of the stainless steel, Ti-ZrN and Ti-ZrN/Ag coatings on stainless steel. The roughness values increased between stainless steel and Ti-ZrN and Ti-ZrN/Ag surfaces.

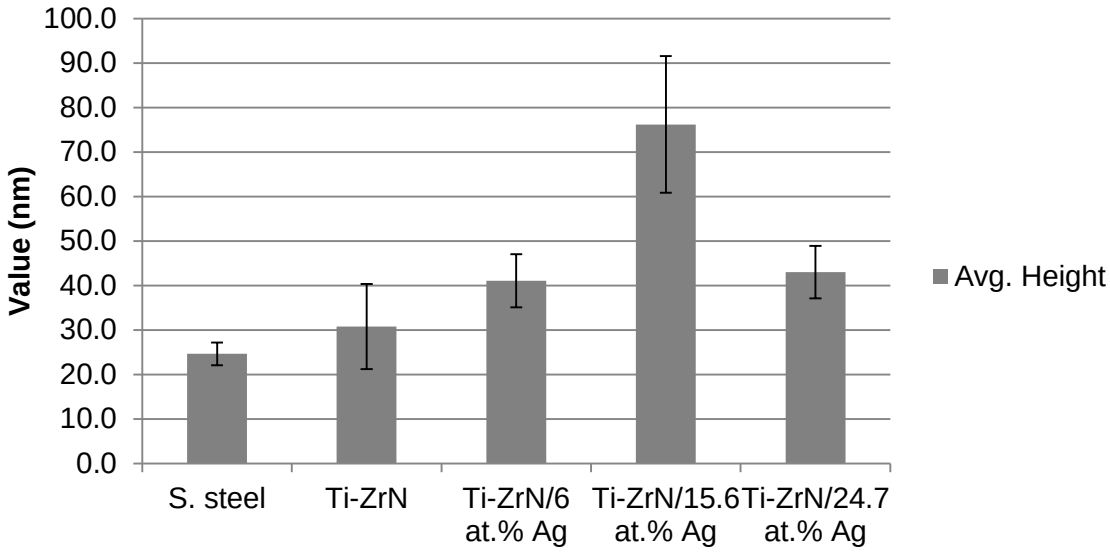

Figure 60: Average height roughness value obtained from the AFM (10 x 10 µm scan) demonstrating the 15.6 at.% silver coating had the highest average height, thus it contained the greatest amount of high amplitude peaks and valleys.

5.3.5 White Light Profilometry

White light profilometry was undertaken on the coatings deposited onto stainless steel substrates to demonstrate the microtopography of the surfaces. This method was particularly important since it demonstrated surface features that were of microbial dimensions. Line profiles allowed measurement of the cross sections of a specific line or feature of the scan profile. This was used for measuring individual valleys that could potentially be the size of a microbial cell and provide space for the cells to reside and be protected from cleaning stresses. The results demonstrated that the coatings did not alter the surface microtopography. The surface features of the stainless steel were visible on the coated samples (Figure 61). The differences were that the silver coatings tended to contain a small amount of large peaks on the surface, which may have been large silver particles. The white light profilometer also provided a three dimensional representation of the surface topography allowing the microtopography, and the nanotopography, to be visualised alongside the two dimensional/real-time images.

The line profiles taken from the white light profilometer scans displayed the topographical features of the coatings on a single cross section. The results demonstrated that no obvious alterations in the surface microtopography occurred when the silver content increased. To calculate the differences in feature sizes average measurement values were obtained (Figure 65).

5.3.5.1 Roughness values (WLP)

The white light profilometer was also used to obtain roughness values of the surfaces at a microtopography scale. The *S* values refer to the same definition as *R* values taken from the AFM but is different due to the roughness values being taken from non-contact, reflected light in contrast to the AFM's 'contact' method. The S_a remained similar throughout the five surfaces, with no significant difference ($p > 0.05$), at this scale. The highest value was obtained from the Ti-ZrN/15.6 at.% silver, at 0.03 µm and the other surfaces were all 0.02 µm and differ within a range of a few nanometres

(Figure 64). The S_p (peak height) was lowest for the stainless steel and the pure Ti-ZrN (0.08 and 0.10 µm, respectively) and the silver coatings decreased from the highest value- 0.21 µm for 6.0 at.% Ag, to 0.09 for 24.7 at.% Ag. This indicates that the increase in silver content starts to decrease the peak heights, suggesting that the larger silver particles were also not protruding as much as the particles from the low silver surfaces. The Ti-ZrN/6.0 at.% was the only surface to display a significantly different S_p value compared to the rest of the surfaces, the exception being 6.0 at.% and 15.6 at.% silver surfaces which did not display a significant difference. The S_v (Valley depths), with the exception of the Ti-ZrN/15.6 at.% silver surface, demonstrated a decreasing trend throughout the coatings, with the Ti-ZrN/24.7 at.% silver coating possessing the lowest value of 0.11 µm, however the Ti-ZrN/15.6 at.% silver coating had the highest average value but out-lies the trend pattern. There was no significance between any of the coatings but between 15.6 at.% Ag and 24.7 at.% Ag (p = 0.0535), demonstrating a near significant difference between the two surface roughness values.

The average width of the features from the line profiles fell between 2.9 µm (Ti-ZrN) and 2.0 µm (6.0 at.% Ag) (Figure 65). The addition of silver reduced the size of the widths in the topography but no trend was observed with increasing silver. The depths were smaller than the widths with the largest average depth value of 0.072 µm observed on the Ti-ZrN/ 15.6 at.% Ag, significantly higher than the other surfaces (Figure 66). The other depth values were of similar numbers, stainless steel displayed the lowest average of 0.037 µm, followed by Ti-ZrN (0.029µm), Ti-ZrN/6.0 at.% Ag (0.033 µm) and Ti-ZrN/24.7 at.% Ag showed a value of 0.032 µm. The depth values were not significant in relation to the size of a microbial cell (1-2 µm), however the width values were.

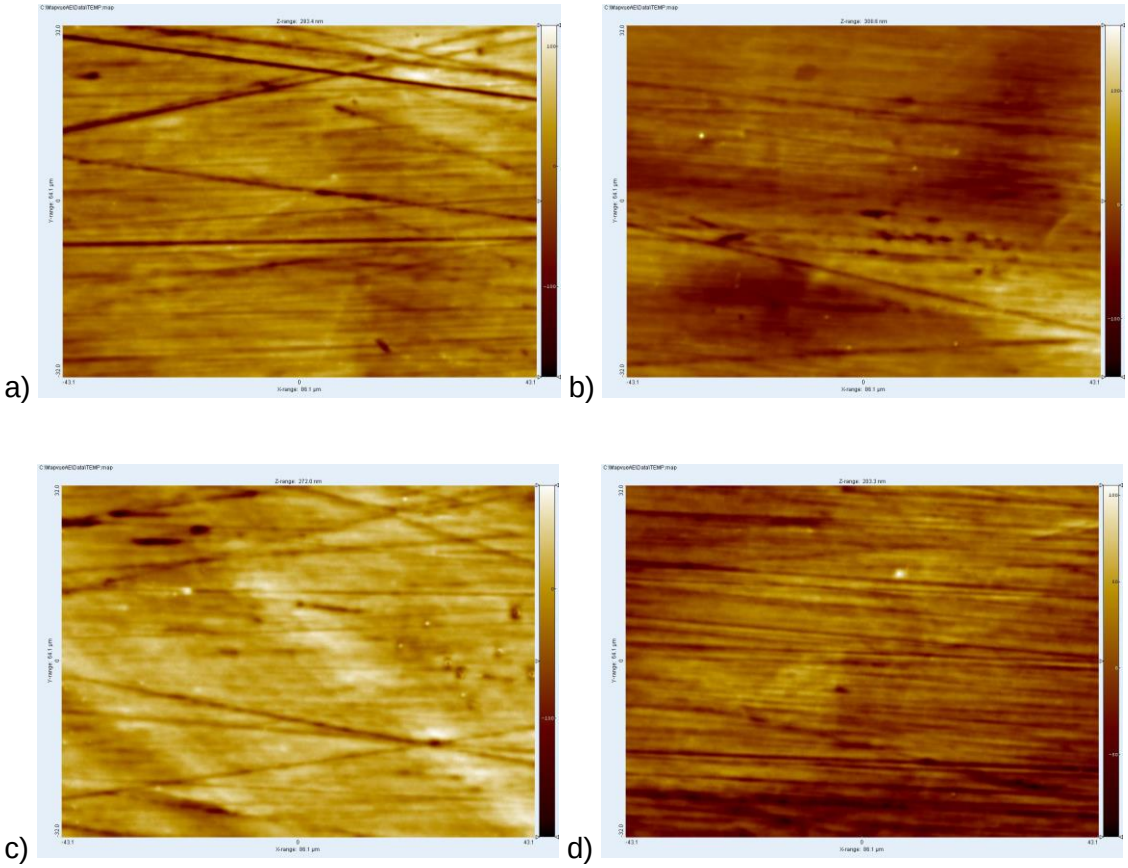

Figure 61: White light profilometry (X100 magnification/ 64 x 86 μm) of the four coatings: a) Ti-ZrN, b) Ti-ZrN/6.0 at.% Ag, c) Ti-ZrN/15.6 at.% Ag and d) Ti-ZrN/24.7 at.% Ag, displaying the mircrotopographies of the surfaces. The Z range (Max height) for the four surfaces were; a) 293.4 nm, b) 308.6 nm, c) 272.0 nm and d) 203.3 nm.

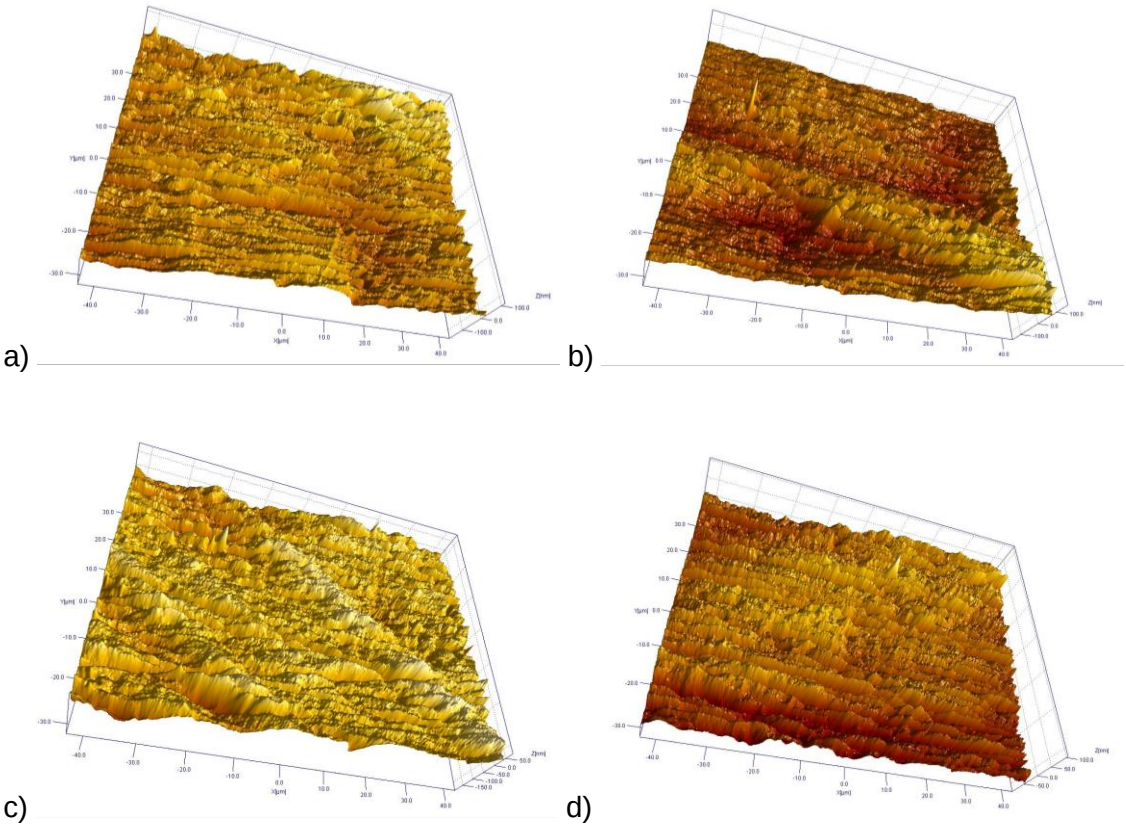

Figure 62: White light profilometry three dimensional representations of the coating surfaces displaying their surface topographies: a) Ti-ZrN, b) Ti-ZrN/6.0 at.% Ag, c) Ti-ZrN/ 15.6 at.% Ag and d) Ti-ZrN/24.7 at.% Ag. All coatings appeared to possess similar microtopographies, with the silver coatings demonstrating individual high peaks on the surfaces.

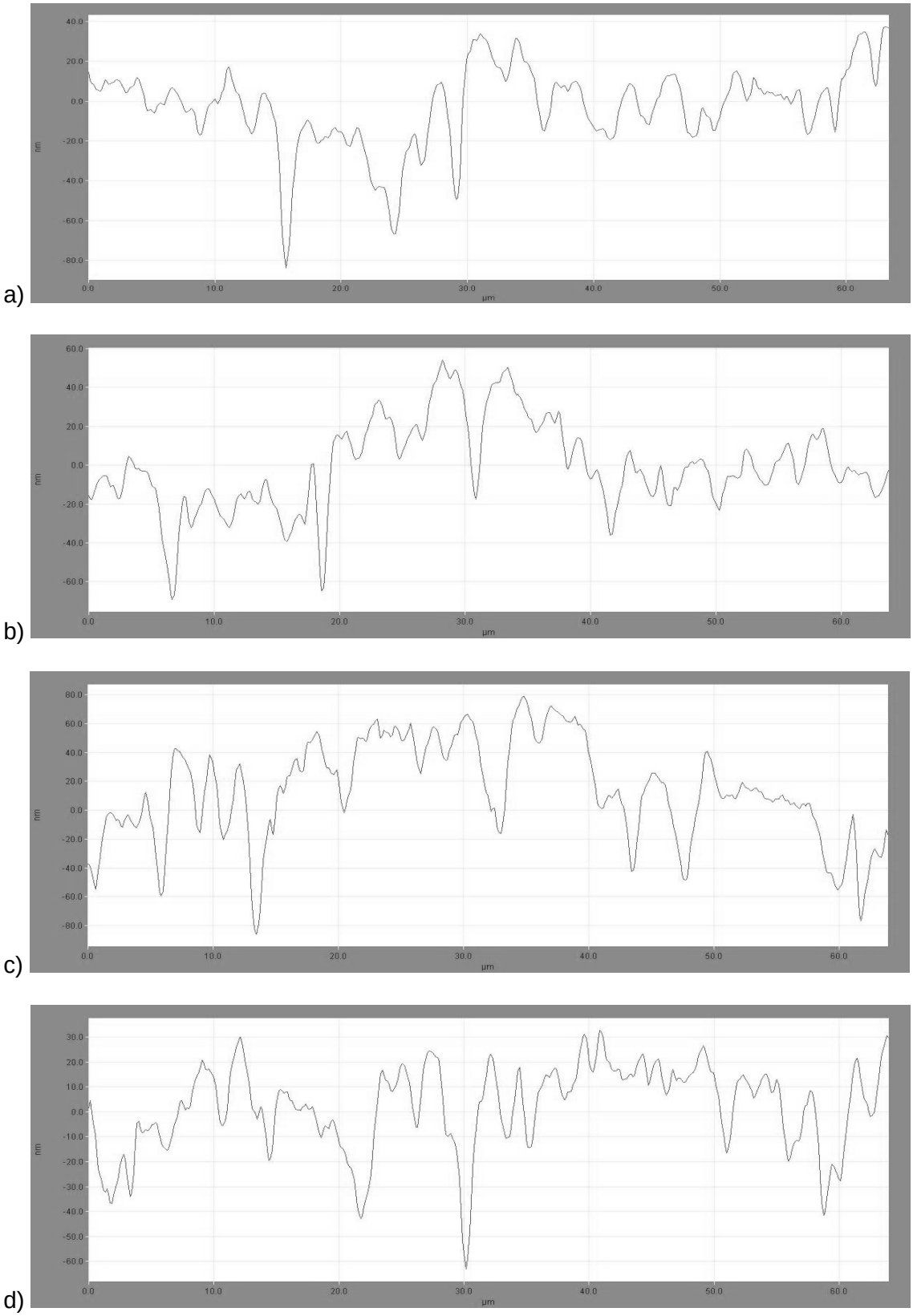

Figure 63: Line profiles taken from the WLP images of: a) Ti-ZrN, b) Ti-ZrN/6.0 at.% Ag, c) Ti-ZrN/15.6 at.% Ag and d) Ti-ZrN/24.7 at.% Ag, demonstrating the differences in microtopography of the four coatings. Note the Y axis scale differs for each image.

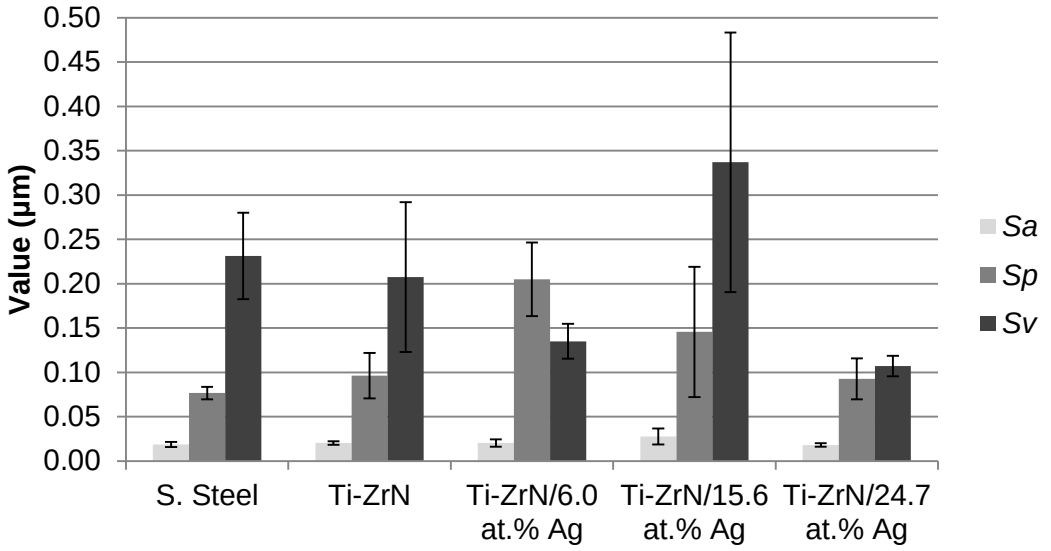

Figure 64: White light profilometry *S* values of the S_a (R_a) S_p (R_p) for the highest peak and S_v (R_v) for the lowest valley. Results showed that the S_a was not affected between the different surfaces but there was a decreasing trend in the size of the peaks (S_p) as the silver content increased.

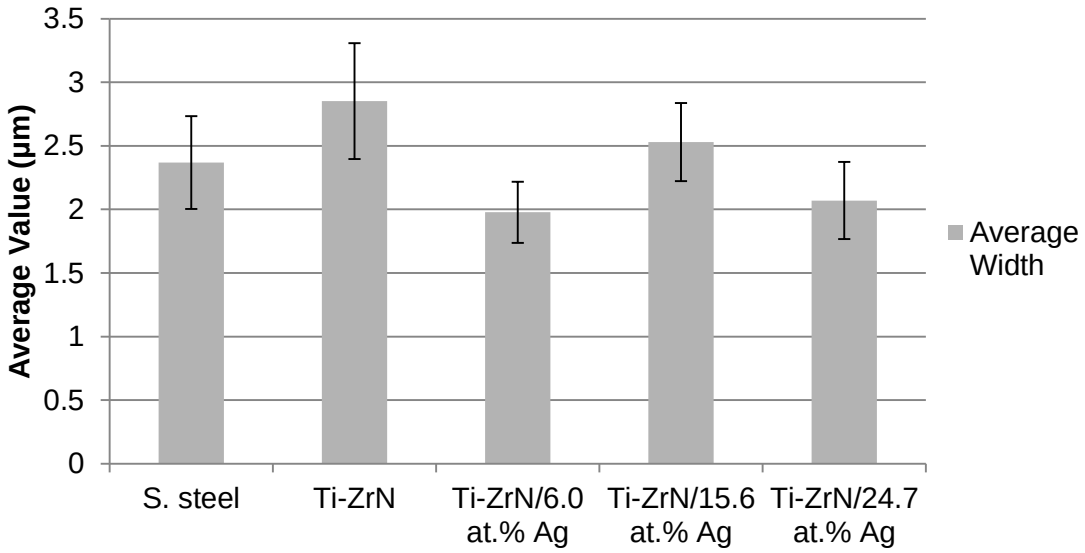

Figure 65: Average widths of the surface features of the coatings taken from the white light profilometry line profiles, demonstrating a decrease in width size when silver is added to the coatings. The average width value of the stainless steel was similar to that of the three silver containing coatings.

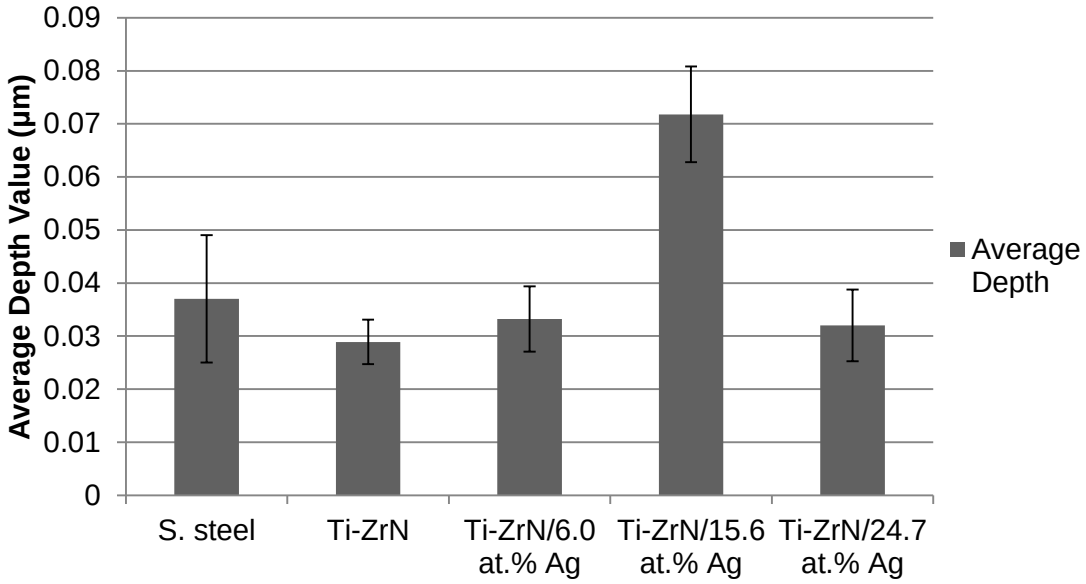

Figure 66: Average depth values of the coatings taken from the white light profilometry line profiles demonstrating that all surfaces, with the exception of Ti-ZrN/15.6 at.% Ag possessed similar values between 0.029 µm (Ti-ZrN) and 0.037 µm (stainless steel) but Ti-ZrN 15.6 at.% Ag demonstrated a value of 0.072 µm, significantly higher than the other values.

5.3.6 Hydrophobicity

The hydrophobicity of the coatings were calculated by obtaining the contact angles using two polar solvents (water and formamide) and one non-polar solvent (1-bromonaphthalene) to calculate the ΔG_{iwi}, the quantitative measure for hydrophobicity/hydrophilicity. The results showed that all of the five surfaces possessed negative ΔG_{iwi} values indicating that the surfaces were all hydrophobic with the pure Ti-ZrN being the least hydrophobic at ΔG_{iwi} -40 and the 15.6 at.% Ag being the most hydrophobic, at ΔG_{iwi} -77 (Figure 67). All surfaces were significantly different to one another with the exception of comparison between 6.0 at.% Ag and 15.6 at.% Ag.

The surface free energy (γ_s) of the coatings were calculated from the contact angles and demonstrate the overall surface energy. The results demonstrated no clear trend between the five surfaces with the γ_s being between 35 and 43 (Figure 68). All five of the surfaces displayed strong significant differences in the surface energies. Ti-ZrN/6.0 at.% Ag had a surface free energy of 35 and this increased with additional silver. The Liftshitz van der Waals forces (γ_s^{LW}) demonstrated lower values on the Ti-ZrN/6.0 at.% Ag (34) and Ti-ZrN/15.6 at.% Ag (38) coatings over the stainless steel (38) and Ti-ZrN (41) (Figure 69). The Ti-ZrN/24.7 at.% Ag coating possessed a higher value (39) to the Ti-ZrN/15.6 at.% Ag, however the Lifshitz van der Waals forces were significantly ($p < 0.05$) lower for the silver containing coatings than the Ti-ZrN. The Acid-Base interactions (γ_s^{AB}) of the five surfaces demonstrated that with the exception of Ti-ZrN/24.7 at.% Ag the coated samples begin with Ti-ZrN being significantly higher than the stainless steel and then as the silver content was increased the Acid Base value dropped significantly each time (Figure 70). However, the Ti-ZrN/24.7 at.%Ag surface has a much higher γ_s^{AB} value than the 15.6 at.% Ag, but this relates to other results where the 24.7% silver coating has performed differently in comparison to the other coatings and the trends observed, for example the S_v values were lower on 24.7% silver than the 15.6% silver (Figure 64), the average height value being lower and not

matching the trend (Figure 60), the average width measurements being significantly lower than the others (Figure 57) and the coating critical load being lower, although the trend was increasing for the other silver surfaces (Figure 53). This suggests that there reaches a point where the addition of silver becomes too great and begins to be detrimental towards the coating properties producing a less hydrophobic coating, with a smoother valley profile but a higher peak topography with wider feature widths being created within the topography, which then reduce the adhesion performance to the underlying substrate.

The γ_s^+ of the five surfaces found that the addition of a coating to the stainless steel increased the positive charge from 0.18 to 0.23 and then further increase as silver was added (Figure 71). The highest value was Ti-ZrN/24.7 at.% Ag at 2.29 and the trend suggested that either the addition of silver increased the electron accepting capabilities and the 15.6% silver surface is the outlier or the increase in silver decreases the electron accepting ability and the 24.7 at.% silver coating is the outlier. This could be investigated by performing hydrophobicity contact angles on the surfaces produced in the previous chapter (Chapter 4) and determine whether increasing the silver content in small increments causes the surface charge/hydrophobic properties to increase or decrease.

The Ti-ZrN possessed a significantly ($p < 0.05$) higher γ_s^- electron donor than the stainless steel and the 6.0 at.% silver surface had a significantly lower charge than the Ti-ZrN surface, suggesting that the addition of a silver decreases the electron donor ability (Figure 72). As the silver content increased the electron donor values were 1.85, 1,63 and 3.49 for 6.0 at.% Ag, 15.6 at.% Ag and 24.7 at.% Ag, respectively.

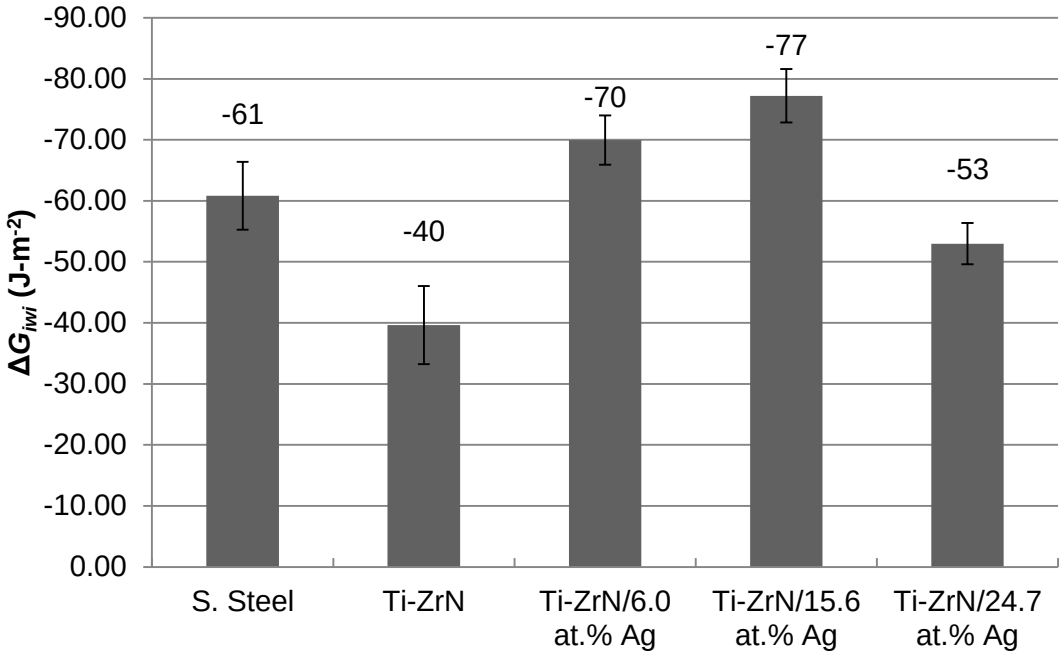

Figure 67: The ΔG_{iwi} of the five surfaces with stainless steel used as a control. All five values were in the negative scale implying that the surfaces were hydrophobic.

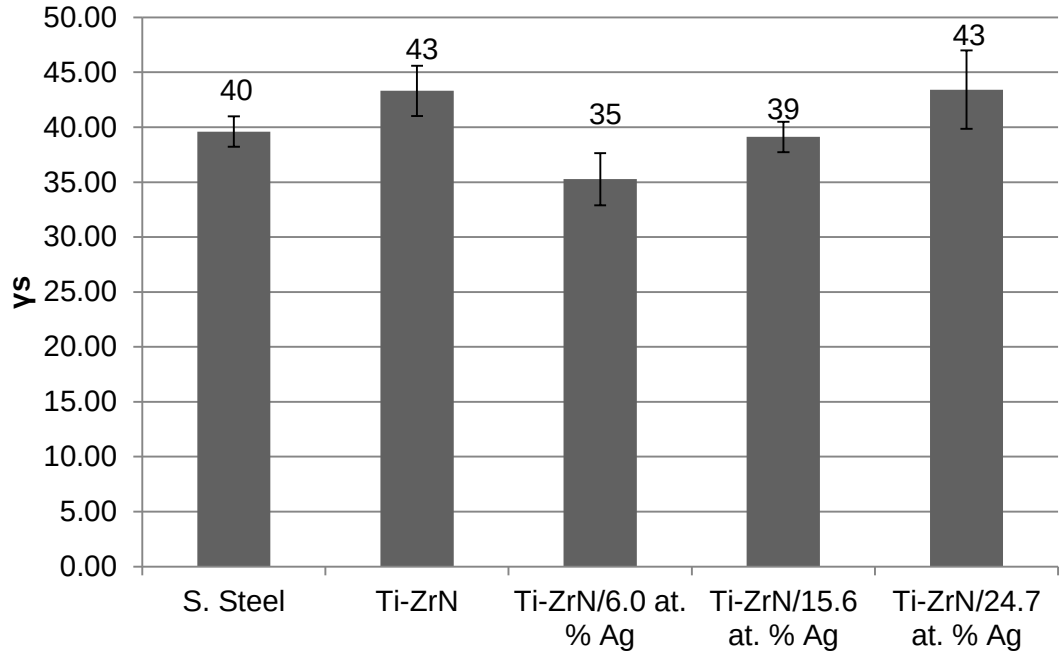

Figure 68: γ_s values of the surfaces demonstrating the surface free energy (SFE) of the coated surfaces. From the 6.0 at.% Ag coating, the addition of silver increased the surface free energy.

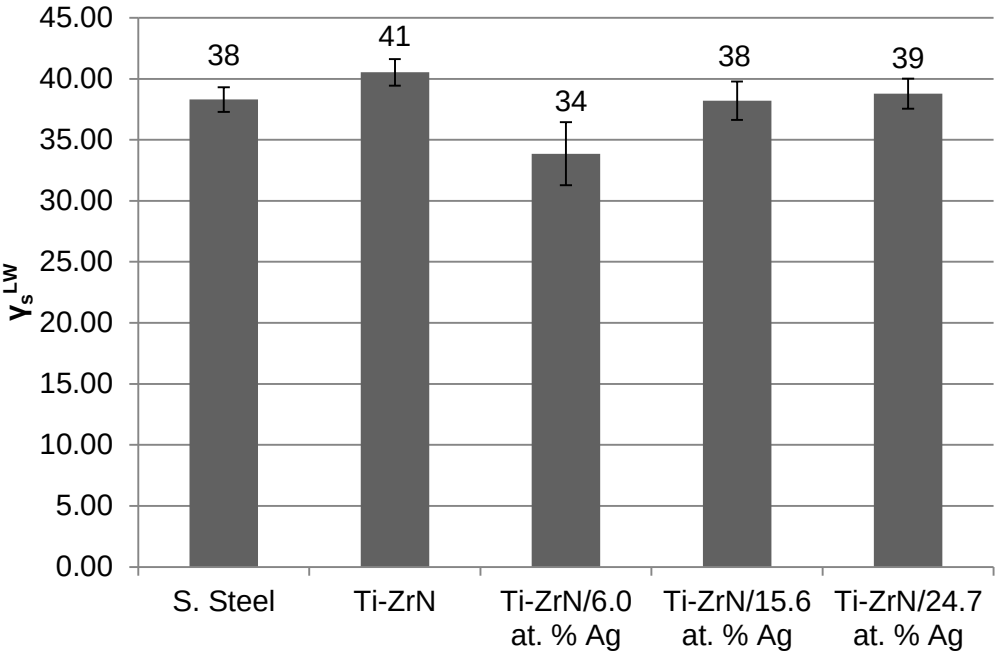

Figure 69: γ_s^{LW} of the surfaces, demonstrating the Lifshitz van der Waals forces acting upon the surfaces. The Lifshitz van der Waals forces again increased with the increase in silver concentration.

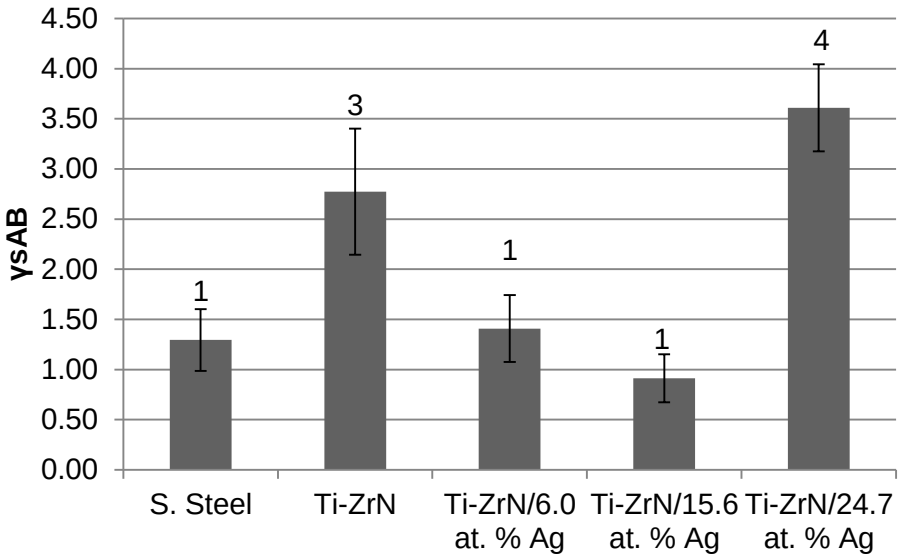

Figure 70: γ_s^{AB} of the surfaces demonstrating the Acid-Base interactions on the surfaces. The coated samples begin with a higher AB value but begin to decrease as the silver is added but the 24.7% silver coating possessed the highest AB value suggesting that the addition of silver, at a threshold, alters the surface charge characteristics.

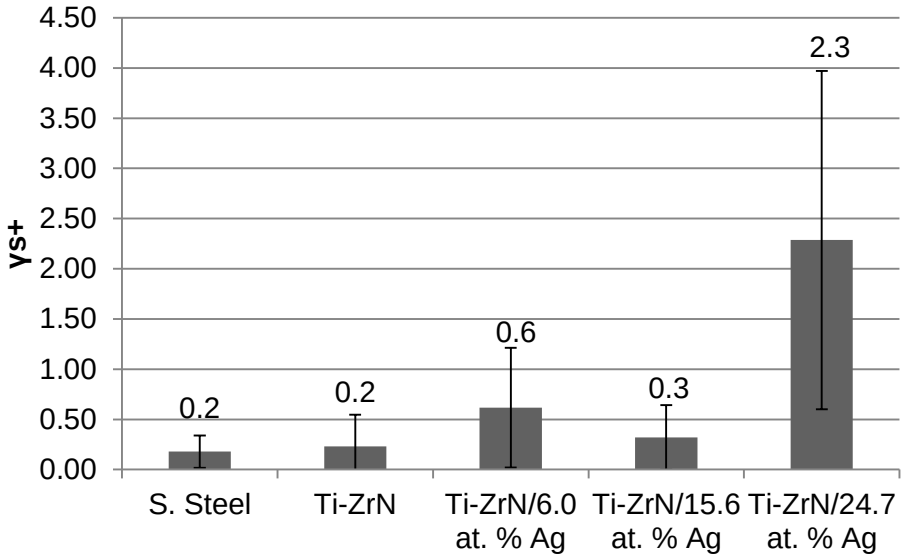

Figure 71: Average γ_s^+ of the five surfaces displaying the electron accepting value at the surface. The addition of a coating increased the electron accepting ability at the surface and the addition of silver also displayed more electron accepting but whether the trend suggests that increasing the silver content increases or decreases the γ_s^+ value would require further investigation.

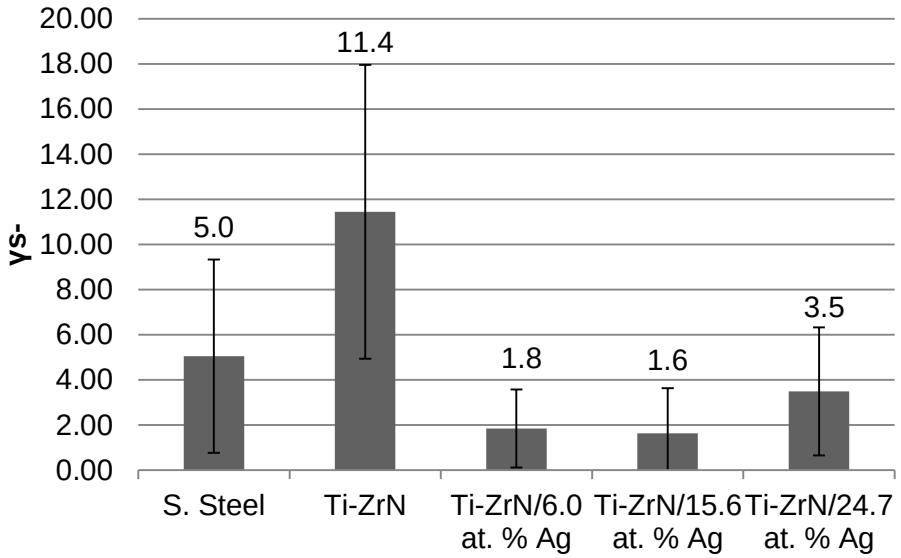

Figure 72:γ_s^- of the five surfaces displays the amount of electon donors at the surface. The Ti-ZrN displays significantly more electron donating than the stainless steel but drops significantly once silver was added. There was no significant increase in γ_s^- as it increased along with the silver content.

5.3.7 Ion Coupled Plasma – Atomic Emission Spectroscopy (ICP-AES)

ICP-AES was used to quantify the leaching of elements from the coatings, in this case to detect the leaching of silver and zirconium. The results demonstrated that the silver coatings leached silver into the surrounding broth, with 24.7 at.% silver coating leaching the most following one month (11.29 ppm) (Figure 73). The minimum inhibitory concentration (MIC) of silver towards Staphylococci has been stated to be around 10 ppm (Cho *et al.*, 2005) and Sandstrom (2011) found that silver demonstrated an MIC of 8 ppm towards S. aureus and a minimum bactericidal concentration (MBC) of 32 ppm.

All of the surfaces demonstrated extremely low zirconium leaching following one month exposure (Ti-ZrN: 0.09 ppm, 6.0 at.% Ag: 0.045 ppm, 24.7 at.% Ag: 0.069 ppm), with the exception of Ti-ZrN/15.6 at.% Ag, which seemed to display greater zirconium leaching (1.76 ppm) (Figure 74). The amount of zirconium leached would not be enough to present harm to human cells (toxic amount around 150 ppm)(Gough *et al.*, 1979), however it was statistically different in comparison to the other four surfaces ($p = 9.7 \times 10^{-6}$).

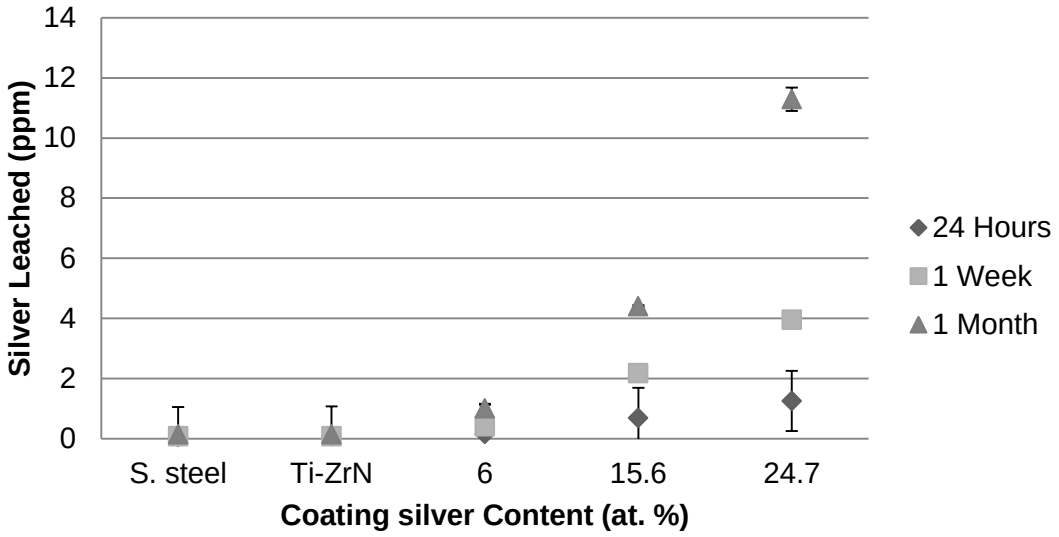

Figure 73: ICP-AES results of the silver release from the coatings following 24 h, one week and one month incubation at 37^0C, demonstrating a steady increase in silver detected in the broth over time. The amount of silver present was highest for the coating that contained the highest silver content.

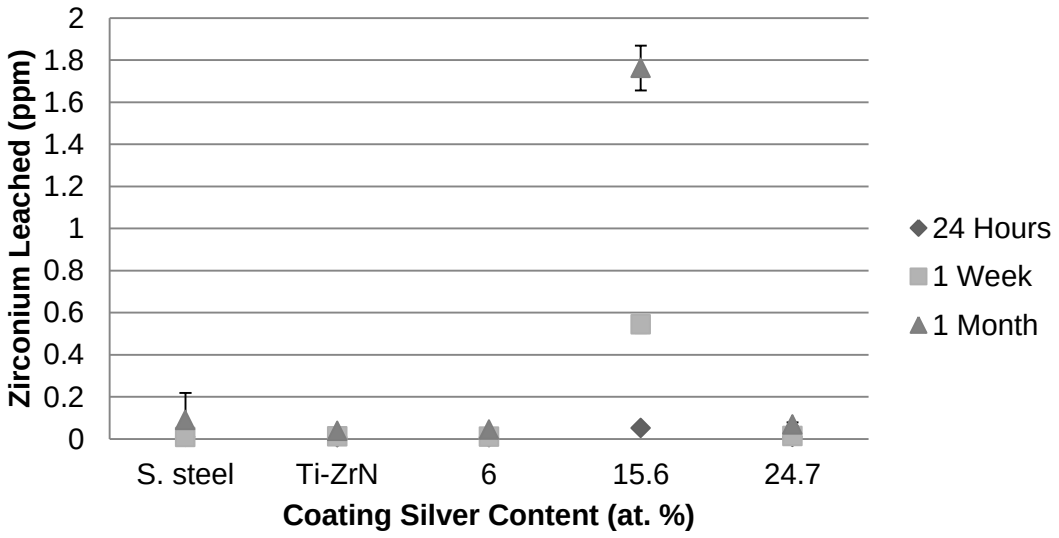

Figure 74: ICP-AES analysis of the release of zirconium leaching after incubation times of 24 h, one week and one month at 37ºC. Only the 15.6 at.% coating displayed significantly more ($p< 0.005$) than any of the other coatings.

5.4 Discussion

The EDX analysis showed that the silver contents of the coatings were 6.0 at.%, 15.6 at.% and 24.7 at.% silver for magnetron powers of 90 W, 130 W and 160 W, respectively. All of the coatings had a stoichiometric zirconium and nitrogen ratio. The nitrogen content appeared to be lower than expected but nitrogen has a tendency to be difficult to detect by EDX due to its low molecular weight.

The SEM images showed that the Ti-ZrN coating had a smaller but more porous columnar appearance out of the four coatings. As the power to the silver magnetron increased, so does the plasma density and ion flux, increasing the coating density (Miao *et al.*, 2003). The white particles observed were the silver within the coating and were seen as nanoparticles (< 100 nm) embedded within the ZrN matrix.

The SEM cross sections displayed the structure of the coatings. The titanium interlayer was around 100 nm thick and was visible in some of the images. The coatings containing silver displayed silver particles throughout the structure showing that the silver was deposited as embedded particles and did not become a homogenous solid solution. The benefits of an SEM cross section was that the layers on a multilayer thin film could be visualised, however the structure of the coating could not be quantified in terms of grain orientation. Further work would include XRD to investigate the coatings crystalline structure.

Backscattered electron detection of the surfaces allowed observation of the distribution of silver particles throughout the surface. The silver particles were situated close together so that if bacteria were to make contact with the surface they would come in contact with a silver particle. This indicated the method of bacterial kill of the surfaces may relate with contact with the silver particles. Thus, in Chapter 6 contact kill assays were improved and undertaken (NBT and JIS methods). The previous chapter on antimicrobial efficacy (Chapter 4, Page 88) showed that a contact kill occurred, so it

would be expected that these coatings would display similar effects. Previous studies into nitride/silver nanocomposites tested against microorganisms found that not all microorganisms were susceptible to leaching of silver, whereas all of the coatings demonstrated a contact kill efficacy (Kelly *et al.*, 2010a, Kelly *et al.*, 2011).

The scratch testing critical load was defined by measurements taken from the scratch tester instrument in both quantitative and qualitative format. From the results obtained there were no clear trends observed from the scratch testing. The best adhered coating was the pure Ti-ZrN and the addition of silver, a soft metal, decreased the coating adhesion and has been shown in previous studies to affect a coatings hardness (Kelly *et al.*, 2010a, Kelly *et al.*, 2011). For the coatings the critical loads were found to be between 30-40 N for the three Ti-ZrN/Ag coatings. No trend was observed between the pure Ti-ZrN and the silver containing coatings; as the silver concentration increased, coating adhesion did not linearly decrease. This could be due to the coatings having similar properties. The addition of silver acted as a solid lubricant and decreased the coefficient of friction on a sliding wear test. Silver has also been used as a solid lubricant in tribology applications where cutting tools were coated with $(Cr\text{-}Ag)_x$ multilayers to maintain lower friction forces to increase tool life (Yao *et al.*, 2011).

The roughness values from the AFM showed that the lowest R_a and average height came from the Ti-ZrN/6.0 at.% silver coating surface, and the highest, 24.7 at.% silver. The line profiles, displayed the different nanotopographies with the widths of the features being different for all four surfaces. The addition of silver decreased the size of surface nanotopography widths. The coatings containing 6.0 at.% Ag and 15.6 at.% Ag displayed similar width sizes, however, the width value decreased for 24.7 at.% Ag. This showed that in the nanotopography the feature widths were larger than the depths.

White light profilometry of the surfaces measures the surface topography over a much larger area than the AFM and measures the microtopography. The microtopography of a surface is important when the substrate, such as the stainless steel is used as it has surface features around the micron range, similar to the dimensions of a bacterium, in the case of Staphylococci. The images created demonstrated that, on a micro scale, the deposition of thin films (1 μm thick) onto the stainless steel using magnetron sputtering did not affect the micro topography. The S_a was also similar for all surfaces demonstrating that the coatings did not affect the micro-roughness of the surfaces. However it was found that there was a change in the sizes of the peaks and the valleys when other surface parameters were examined (S_v and S_p). With the exception of Ti-ZrN/15.6 at.% Ag coating, there was a decreasing trend of S_v values as the silver increases and S_p values were larger for the silver containing coatings than the Ti-ZrN or stainless steel, suggesting the protruding silver particles are increasing the peak heights.

This demonstrates the need to carry out more detailed topography analysis of the surface widths and depths. Results from the AFM, showed that the nanotopography was altered and obtaining width and depth values of the line profiles from the white light profilometer displayed the differences in microtopography. The results demonstrated that the addition of silver reduced the size of the feature widths in the microtopography from 2.85 μm (Ti-ZrN) to 1.98 μm, the lowest value, obtained from the 6.0 at.% Ag coating. The average depth of the topographical features were much smaller, between 0.029 and 0.072 μm with the lowest value being for Ti-ZrN and the highest value for the 15.6 at.% Ag coating. No significant difference between the coating depth microtopography was observed and the size of the features suggests that even with the feature widths being suitable microbial dimensions, the depth of the features being tens of nanometres may reduce the ability of the bacteria to reside in the surface scratches.

The hydrophobicity varied throughout the surfaces but no trend in relation to surface composition was observed. All the surfaces were hydrophobic, but the Ti-ZrN/15.6 at.% Ag was the most hydrophobic (ΔG_{iwi} -77.22) and pure Ti-ZrN the least (ΔG_{iwi} -39.63). The stainless steel displayed a ΔGiwi of -61 mJ-m^{-2}, differing from other literature suggesting a value of 11.5 mJ-m^{-2}, however the water contact angle in their results was lower (62) than the value seen from the surface used in this investigation of 88.8° (Figure 26; Page 82) (Hamadi *et al.*, 2014). The 15.6 at.% silver coating being the most hydrophobic ties in with other results seen where it was seen as an outlier. On stainless steel substrates the 15.6 at.% silver coating displayed the highest S_v, the largest average height and the RMS was the equal highest along with the 24.7 at.% silver coating. This trend was not observed when the nanotopography was investigated on the silicon wafer substrates, suggesting that the nanotopography did not affect the hydrophobicity of the surface but the microtopography did; as the roughness increased so did the hydrophobicity. This could be due to the liquid droplet having more surface area available on a rougher surface allowing more surface tension between the solid-liquid interfaces. The theory behind wetting of solid surfaces suggests that if the surface is hydrophilic a rougher topography has a greater net energy decrease to induce spreading, therefore the rougher surface tends to wet more rapidly. However in the case of a surface with hydrophobic tendencies, the dry interface has a lower surface energy and the liquid assumes a more spherical form therefore a rough surface will be more water repellent as there will be more surface involved at the solid-liquid interface (Wenzel, 1936).

For this investigation the ion release of zirconium and silver metal ions were analysed. The ion release was determined in brain heart infusion broth of the same concentration used in the *in vitro* bacterial testing to replicate the environment and simulate a nutrient rich environment that would be found surrounding an implant. ICP-AES was used because the amount of silver present in the coatings was not producing antimicrobial

leaching towards the test microorganisms but leaching into the surrounding test medium has been previously demonstrated (El-Kady *et al.*, 2012, Pasricha *et al.*, 2012, Campoccia *et al.*, 2013).

With the exception of the 15.6 at.% silver coating was an anomaly with the highest release of zirconium being 2 ppm in 10ml of solution. Zirconium release in all the surfaces was negligible. The disadvantage of this method in relation to the *in vivo* situation is that it is performed in a liquid solution. To keep it close to the conditions of the antimicrobial assays and relating it to the nutrient rich surroundings of a bodily implant, the brain heart infusion broth was used as the liquid medium. However, *in vivo*, the body will be a combination of solid bone structures, soft muscles and fat, with surrounding blood, plasma, proteins and varying amounts of moisture. This will affect the amount of release of metals from the surfaces as well as the conditioning films created from these molecules adsorbing to the surface, which could potentially reduce metal release.

5.5 Concluding Remarks

The new Ti-ZrN/Ag coatings produced were characterised for chemical composition, coating structure, surface nanotopography and microtopography, quantification of silver leaching and surface physicochemistry. The coatings demonstrated three distinct silver contents of 6.0 at.%, 15.6 at.% and 24.7 at.%. The Ti-ZrN had a columnar structure, differing to the cuboidal morphology the Ti-ZrN/Ag displayed as the silver increased. The silver was dispersed throughout the coatings as particles. There was no relationship between the coating adhesion and coefficient of friction and silver content. The nano-roughness of the coatings increased with increasing silver. The average widths of thenanotopographies decreased with increasing silver content but the feature depth size decreased with a silver increase. The surface area of the coatings increased with the increase in silver concentration. White light profilometry demonstrated similar S_a values and a decrease in S_p as silver content increased. Average widths of the microtopography were lower for the Ti-ZrN than the Ti-ZrN/Ag coatings but no trends were observed with increasing silver content. The average microtopographical depths remained similar for all of the surfaces with the exception of 15.6 at.% Ag. There were greater amounts of silver leached from the coatings with higher silver contents, no difference was observed with the amount of leached zirconium with the increase in silver. Surface free energy and Lifshitz van der Waals forces increased with the coating silver content. The most hydrophobic coating was the Ti-ZrN/15.5 at.% Ag and the least hydrophobic was Ti-ZrN, with no trend observed between coating composition and ΔG_{iwi} value. The results obtained in this chapter will be used to determine their effect on microbial retention and explain the antimicrobial efficacy of the coatings towards *S. aureus* and *S. epidermidis* (Chapter 6).

6 Antimicrobial Efficacy and Bacterial Retention of Ti-ZrN/Ag Coatings

6.1 Introduction

Following the previous investigation on the antimicrobial activity of zirconium nitride silver nanocomposite coatings (Chapter 3; Page 88) it was found that the antimicrobial action was primarily a contact kill. Therefore, following production of the Ti-ZrN/Ag coatings, further investigation into the efficacy of the contact kill was undertaken. The Japanese standard JIS Z2801 (JIS assay), was used to quantify contact kill efficacy of the surfaces over a longer period of time. This method also reduced the likelihood of cell death from drying on the substrata by producing the assay in humid conditions. The NTV assay relied on the bacterial suspension to be dried on to the surface, otherwise when the agar overlay was added the microorganisms were washed away, whereas the JIS assay relied on the agitation of the sample coupons in broth to release the bacteria to enumerate them.

6.1.1 JIS Z2801: Japanese Industrial Standard for Antimicrobial Efficacy (Contact Kill)

The Japanese industrial standard JIS Z2801 was designed as a standardised platform to evaluate the antimicrobial efficacy of antimicrobial products, in particular the efficacy towards bacteria on the surface of an antimicrobial product (Anonymous, 2010b). This standard has been practised throughout many applications such as the antimicrobial properties of; ZnO/Ag coated food packaging against *E. coli*, (Panea *et al.*, 2014), electron beam deposition of silver nanoparticles onto TiO_2 nanotubes for bio-implants against *S. aureus* (Uhm *et al.*, 2013) and the photocatalytic activity of titanium dioxide and the prevention of bacterial colonisation (Oka *et al.*, 2008). It has also been used to develop standards for specific antibacterial products such as the ISO 22196 standard to evaluate antibacterial activity in plastics and non-porous materials (Anonymous, 2011). This assay was chosen to test for antimicrobial efficacy in the surfaces of this study because it can be altered to replicate similar environmental properties found in

the body, such as being able to keep the sample wet, performing the assay at body temperature whilst keeping constant bacterial contact with the surface. This assay has been used in other studies investigating the antimicrobial properties of metals. Kawakami *et al.,* (2008) investigated 21 metallic elements following the JIS 2801 method to evaluate antimicrobial efficacy. The JIS 2801 assay had also been used to test the antimicrobial activity of a TiO_2-Cu composite thin films on *Staphylococcus aureus.* These coatings have similarities to the coatings produced in this study (Mungkalasiri *et al.*, 2013). Mungkalasiri *et al.* (2013) used TiO_2-Cu coatings with copper contents of 1.3 and 3.5 at.% and following testing using the JIS 2801 found that with an increase in the antimicrobial component (copper) there was a relative increase in antimicrobial efficacy towards the *S. aureus* test organism and following 24 hours incubation both surfaces achieved 100 % kill rate. This result relates to what was found in the following work, however the contents of silver were much higher, but at 6.0 % there was shown to be a 100% kill rate.

6.1.2 CTC-DAPI

To complement bacterial colony respiration experiments using the nitro tetrazolium violet stain in the NTV assay, an epifluorescent staining method was used to evaluate individual cell respiration, indicating cells which could be both viable and viable but non-culturable (VNC). The CTC-DAPI method utilises 5-cyano-2.3-ditolyl tetrazolium chloride (CTC), a tetrazolium salt that is reduced by the microorganism's electron transport chain into fluorescent insoluble formazan, which then accumulates in the active cells (Federighi *et al.*, 1998). The most frequently used tetrazolium salts are 2-(p-iodophenyl) -3- (p-nitrophenyl)-5-phenyltetrazolium chloride (INT) and CTC (Zimmermann *et al.*, 1978, Severin *et al.*, 1985, Schaule *et al.*, 1993, Bovill *et al.*, 1994), however, CTC has been proven superior to INT to quantify viable respiring bacterial cells (Coallier *et al.*, 1994, Federighi *et al.*, 1998). The formazan is visualised

under a microscope and either the cell numbers counted or the percentage coverage be calculated using the microscope software.

The aim of this work was to determine the antimicrobial efficacy of the Ti-ZrN/Ag thin films against *S. aureus* and *S. epidermidis*, focussing on the contact kill mode of action and the respiration status of the microorganisms and to determine the effect of the surface properties on microbial retention.

6.2 Methodology

6.2.1 CTC DAPI

5-cyano-2,3-ditolyl tetrazolium chloride (CTC) is a redox dye, which reduces into formazan which fluoresces red in the presence of UV radiation. Coupons were subjected to a standardised retention assay (3.2.3; Page 91) before staining. CTC (Sigma Aldrich, Dorset, UK) was prepared from powder and dissolved to a 5 mM concentration in sterile membrane filtered water (Millipore Elix, Darmstadt, Germany) and filter sterilising (0.2 µm Acrodisk, UK) before use. Direct staining of the coupons was performed by pipetting 500 µl of CTC onto the substrata/retained bacteria and incubated in a sealed container, without agitation, for 30 minutes at 37ºC. Following incubation, the surfaces were rinsed with sterile distilled water with a 3 mm nozzle at a 45º angle for five seconds and counter stained by pipetting 500 µl of 1 µg/ml DAPI (Sigma Aldrich, Dorset, UK), prepared from the powder dissolved in sterile membrane filtered water. This was applied to the surface and left to incubate at room temperature in the dark in a class II microbiological flow cabinet for 15 minutes. The coupons were rinsed again with sterile distilled water and then left to dry in the class II cabinet for 45 minutes until the coupon surface was completely dry. Stained samples were stored at 4ºC, in the dark and the substrata plus retained cells were visualised using epifluorescent microscopy (Nikon Eclipse E600 epifluorescence microscope, Tokyo, Japan), and Cell-F image visualisation software (Olympus, UK) was used for image

capture and analysis. The two stains were differentiated by using filters of 590/650 nm for red excitation and emission spectra (CTC/Formazan) and 350/470 nm for the blue (DAPI) excitation and emission spectra, respectively.

6.2.2 JIS Method

This method was adapted from the Japanese industrial standard (JIS) for testing of antimicrobial surfaces, the JIS Z-2801:2010 (Anonymous, 2010b). Bacterial suspensions were prepared in accordance to the previous chapter (3.2.1 & 3.2.2; Page91). Sixteen microliters of cell suspension was applied to each 10 x 10 mm coupons and a piece of Parafilm® M (1 x 1 cm) (Sigma Aldrich, Dorset, UK) previously sterilised with 70% ethanol and left to dry, was placed using sterile forceps on top of the surface to reduce evaporation and create contact across the whole surface. Bacterial suspensions were prepared at 1.0 OD at 540 nm (3.2.2; Page 91) and dilutions of 10^{-1} and 10^{-2} dilutions were tested for *S. aureus* and *S. epidermidis*, respectively. The numbers of bacterial cells applied to the surfaces were 9.2 x 10^4 CFU and 1.36 x 10^4 CFU for *S. aureus* and *S. epidermidis,* respectively. Samples were tested immediately at T0 and after T24 hours in both dry (room humidity) and humid conditions (>80% humidity), created by saturating paper towels in sterile distilled water. After incubation samples at T0 and T24 were placed into 10ml of brain heart infusion broth by removing the Parafilm™ with sterile forceps and placing the film and coupon into the broth. The coupon and suspension were vortexed for 30 seconds to remove the bacteria from the surfaces and then serially diluted down to 10^{-2} before 100 µl of all dilutions were plated out in duplicate on brain heart infusion agar plates. The plates were incubated overnight at 37 ºC and the colonies counted to calculate the CFU/ml recovered from each sample. All coupons were tested in triplicate and the investigation was repeated in duplicate.

6.2.3 Microbial Adhesion to Hydrocarbons (MATH) Assay

The microbial affinity to hydrocarbons (MATH) assay was followed according to an adapted method described by Bellon-Fontaine *et al*., (1996). Bacterial suspensions were washed 3 times in PUM Buffer pH 7.1 (PUM Buffer; $K_2HPO_4.3H_2O$ (BDH, Basingstoke, Hampshire, UK) 22.2; KH_2PO_4 (BDH, Basingstoke, Hampshire, UK) 7.26; Urea (Sigma, Dorset Poole, UK) 1.8; $MgSO_4.7H_2O$ (BDH, Basingstoke, Hampshire, UK) 0.2 g L^{-1}) and re-suspended to an OD 1.0 at 400 nm. Washed bacterial cells suspended in PUM buffer (1.2 ml) were added to round bottom 15 mm diameter glass test tubes cleaned with 70% ethanol, rinsed with sterile distilled water (10 ml) and dried in a Class II microbiological cabinet. The solvents used were chloroform, ethyl acetate, decane and hexadecane (Sigma Aldrich, Dorset, UK). Two hundred microliters of the solvent under investigation was added to the test suspension. Suspensions were all equilibrated to room temperature prior to use. The samples were mixed for 2 min by vortexing, and allowed to stand for 15 minutes to ensure complete separation of the two phases. The lower aqueous phase (1 ml) was transferred a clean cuvette, and the OD determined at 400 nm. The calculation used to determine spore affinity to hydrocarbons was as that of Rosenberg et al. (1980);

$$\%\ adherence = \left(1 - \frac{A}{A_0}\right) \times 100$$

Where A_0 is the original optical density measured at 400 nm prior to mixing and A is the absorbance of the aqueous phase after mixing.

6.3 Results

6.3.1 Acridine Orange Staining Retention in Relation to Hydrophobicity and Topography

The percentage coverage of the *S. aureus* and *S. epidermidis* were plotted against the ΔG_{iwi} hydrophobicity values. It was seen that as the coverage of *S. aureus* cells increased and decreased along with the ΔG_{iwi} value (Figure 75). The *S. epidermidis* displayed a preference to the less hydrophobic surfaces, such as Ti-ZrN where the percentage coverage was the highest (1.21 %) and the ΔG_{iwi} value was the lowest (-39.63 mJ m^{-2}). This demonstrated that *S. aureus* (hydrophobic) displayed a preference for hydrophobic surfaces and *S. epidermidis* (Hydrophilic) displayed a preference for less hydrophobic/hydrophilic surfaces.

The total percentage coverage of both microorganisms were compared to S_a roughness values. The results demonstrated that with a increase in S_a on the coating surfaces, the *S. aureus* retention numbers followed the trend (Figure 76). On stainless steel the S_a value was low and the percentage coverage high, however the hydrophobicity was high and followed the same trend as the *S. aureus* retention coverage. This demonstrates that *S. aureus* was affected by both roughness and hydrophobicity. The *S. epidermidis* did not display any relation towards retention numbers and S_a roughness values, but was affected by the alterations in ΔG_{iwi} values (Figure 75).

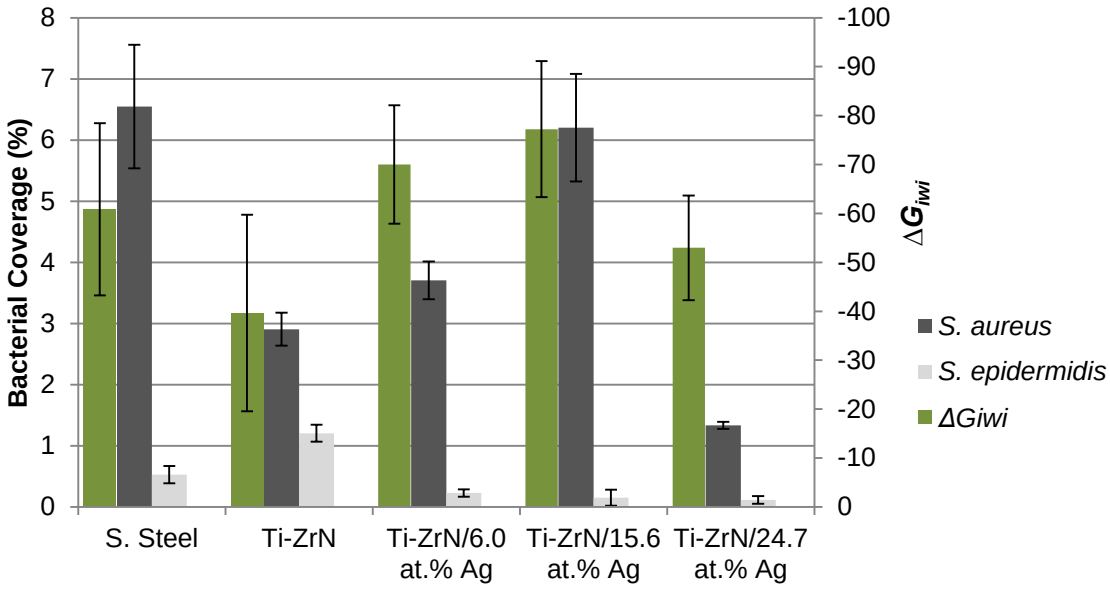

Figure 75: The total percentage coverage of *S. aureus* and *S. epidermidis* retained on stainless steel, Ti-ZrN and Ti-ZrN/Ag coatings, demonstrating an increase in retention of *S. aureus* when hydrophobicity increases and a decrease in retention for *S. epidermidis*.

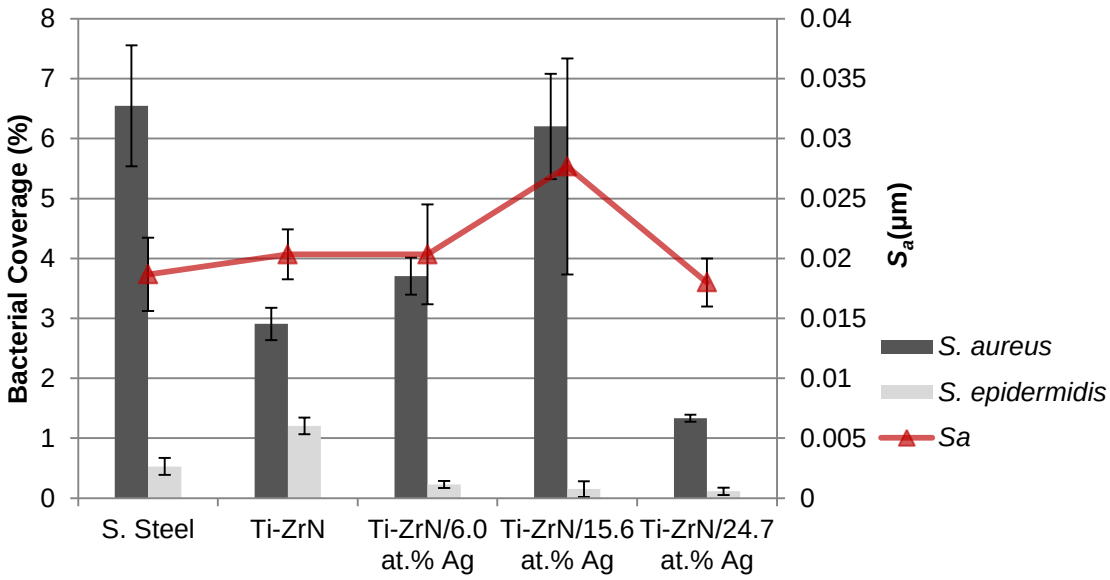

Figure 76: The total percentage coverage of S. aureus and S. epidermidis in relation to the S_a roughness values, demonstrating a similar trend between S_a and *S. aureus* coverage but no trend was observed towards the *S. epidermidis* coverage.

6.3.2 LiveDead™ Staining

LiveDead™ staining of the microorganisms retained on the coatings was used to determine the viability of the bacteria in terms of cell membrane integrity. The results demonstrated that Ti-ZrN contained less viable *S. aureus* and *S. epidermidis* cells on the surface than stainless steel and there was a decreasing trend in viable bacterial coverage as the silver content increased (Figure 77). *S. epidermidis* cells were retained in fewer numbers than *S. aureus* and only low coverage of viable *S. epidermidis* cells (green) were observed on all of the surfaces; Stainless steel: displayed 0.04 % coverage, Ti-ZrN: 0.07 % coverage, 6.0 at.% Ag displayed 0.04 % coverage, 15.6 at. % Ag displayed 0.01 % coverage and no cells were observed on the 24.7 at.% Ag coating (Figure 77). The results from the detection of the dead cells (Figure 78) demonstrated that for *S. aureus* the stainless steel had the highest number of detected dead cells and the amount was significantly less ($p < 0.05$) for both Ti-ZrN and 6.0 at.% silver coatings (Figure 78). The 15.6 at.% and 24.7 at.% silver surfaces demonstrated a significant increase in dead *S. aureus* cells compared to the ZrN and 6.0 at.% Ag coatings, however there was no significant increase in dead cells between the 15.6 at.% and the 24.7 at.% surfaces. The *S. epidermidis* was detected in lower numbers than the *S. aureus* but a trend of increasing dead cells occurred with increasing silver content. The increase in dead *S. aureus* cells was not significant between the surfaces. Although the stainless steel displayed the highest coverage of dead cells out of the five surfaces this does not denote antimicrobial efficacy as it can be seen on Figure 77 that the stainless steel also had the highest coverage of ‘Live’ cells.

6.3.3 CTC-DAPI Staining (Cell Respiration/ Viability)

The CTC-DAPI staining was used to quantify the respiration of the bacterial cells at a microscopic level. The results demonstrated that initially the silver present in the surfaces (6.0 at.% Ag) reduced the coverage of respiring *S. aureus* cells on the surfaces but the increase in silver content increased the amount of respiring bacteria

(Figure 79). The results obtained from the *S. epidermidis* showed similar percentage coverage on each surface, with the exception of 24.7 at.% Ag, where no viable bacteria were displayed (Figure 79).

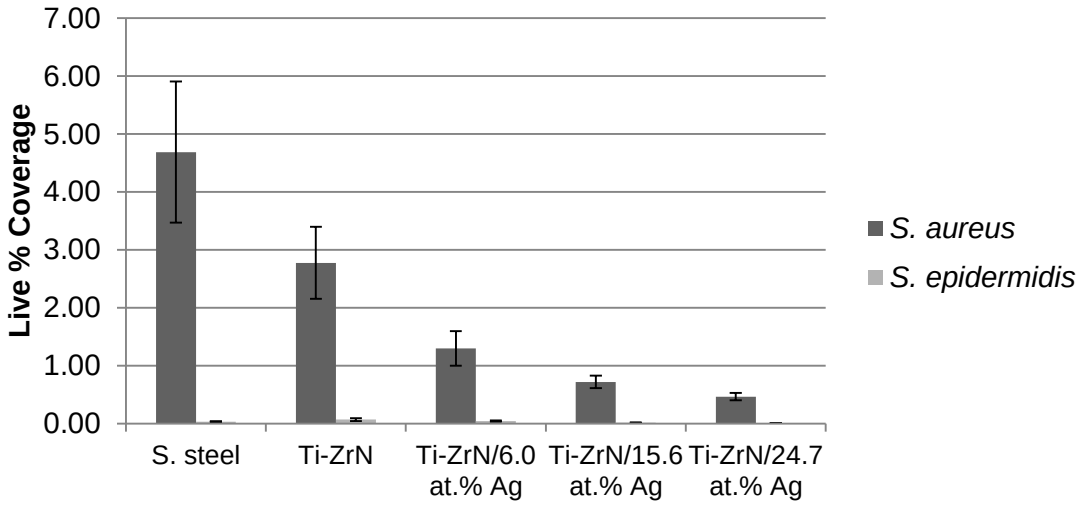

Figure 77: LiveDead "Live" percentage coverage of both *S. aureus* and *S. epidermidis* retention demonstrating a decreasing trend in 'Live' cells as the silver content increased. There was a significant difference ($p < 0.05$) in live cells between the stainless steel and Ti-ZrN/24.7 at.% silver coating for the *S. aureus*.

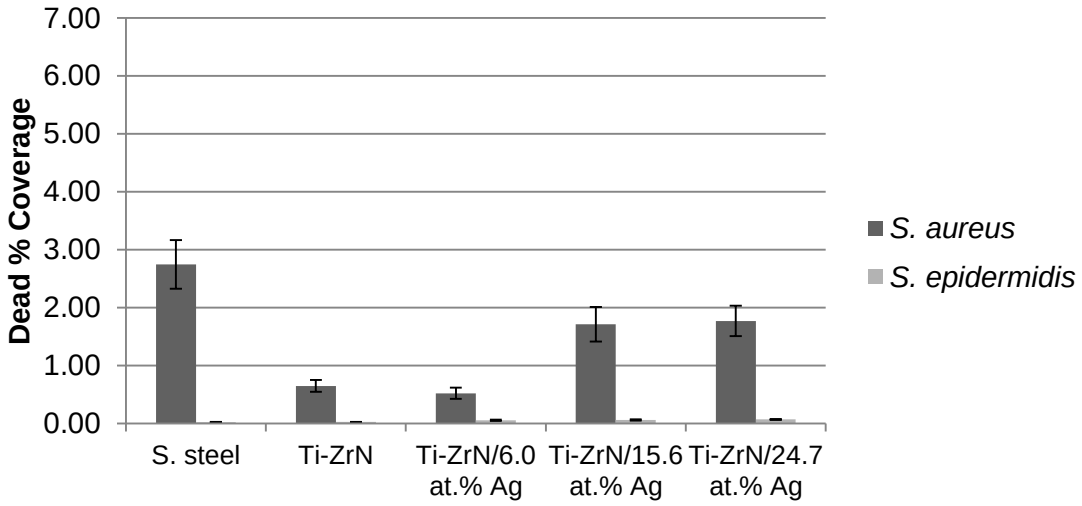

Figure 78: LiveDead "Dead" percentage coverage demonstrating the increase in percentage coverage of *S. epidermidis* cells as the silver content increased and an increase in dead *S. aureus* cells for the surfaces containing over 6.0 at.% silver coating.

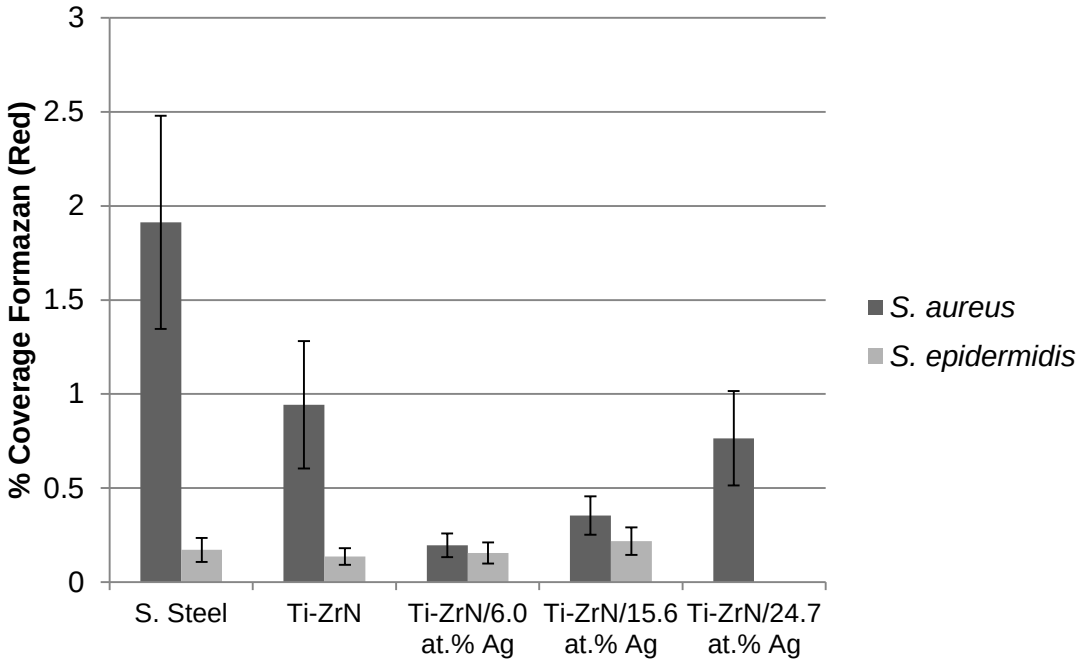

Figure 79: CTC-DAPI staining of the retained bacteria on the surfaces, displaying the percentage coverage of the red stain corresponding to respiring, viable cells. Ti-ZrN/6.0 at.% Ag decreased the respiring *S. aureus* cells but respiration started to increase as the silver concentration increased. The percentage coverage of the *S. epidermidis* was not significantly different with increased silver concentration, except on the 24.7 at.% Ag coating.

6.3.4 NTV Assay

As seen in previous investigations (3.4.2; Page 103) nitro tetrazolium violet testing of bacterial colonies *in situ* on the zirconium nitride silver coatings was a viable method to determine the contact kill efficacy of the antimicrobial surface(s). The results demonstrated that the surfaces of all three silver containing coatings successfully inhibited the bacteria (Figure 80). The results demonstrated that the silver coatings produced an effective antimicrobial contact kill and all significantly ($p < 0.05$) reduced the survival of both microorganisms, however an increase in silver did not significantly increase the efficacy as the silver increased. The two microorganisms displayed differing survival patterns on the surfaces with the most efficacious for the *S. aureus* on the Ti-ZrN/6.0 at.% Ag coating and the *S. epidermidis* on the Ti-ZrN/24.7 at.% Ag surface.

6.3.5 Zones of Inhibition

Following the zones of inhibition assay there was no visible inhibition or clear zones observed from all of the surfaces (Results not shown). The amount of silver leaching from each surface was quantified using ICP-AES in the previous chapter (5.3.7; Page 178). Although it had been demonstrated that silver was leaching from the surfaces, in the presence of the agar the amount of leaching did not cause antimicrobial effects to occur.

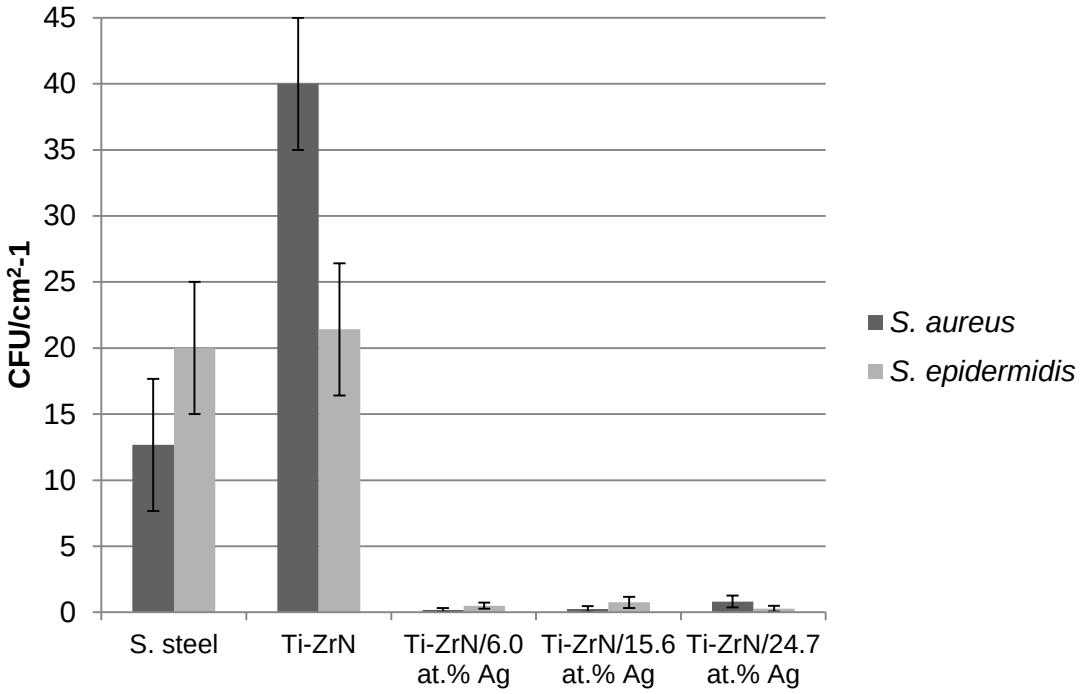

Figure 80: Nitro-tetrazolium violet staining of bacterial colonies on the surfaces following 1h drying and 24h agar incubation, indicating the amount of colonies per cm^2 which decreased with increasing silver in the coatings. Both of the bacterial species survived more on the pure Ti-ZrN than the stainless steel.

6.3.6 JIS antimicrobial testing

The JIS antimicrobial testing method was used to quantify antimicrobial contact kill following two different incubation times and humidity conditions. The test was undertaken in room temperature and room humidity conditions (≈35% R.H.) to replicate bacterial contact with an external fixation pin outside the body and in a humidity chamber (>85 % R.H) at 37ºC to replicate conditions on a fixation pin inside the body.

6.3.7 JIS Standard in Dry/Room Conditions

The results following the JIS standard method in room conditions found that following immediate recovery at T0 the silver containing coatings had an immediate effect on the bacteria (Figure 81). At T0, 1.63% and 2.02% of the total *S. epidermidis* bacteria were recovered from the stainless steel and Ti-ZrN, respectively. The addition of silver reduced the amount of *S. epidermidis* cells recovered, with 6.0 at.% Ag being the most efficacious with 0.37% recovery, followed by 24.7 at.% Ag with 0.76% recovery and 15.5 at.% Ag recovered 0.77% bacteria. *S. aureus* at T0 was recovered in highest numbers from the Ti-ZrN coating (0.87%) followed by 6.0 at.% Ag (0.39%) and stainless steel (0.24%). The coating containing a 24.7 at.% silver possessed the most effective antimicrobial properties towards *S. aureus* with significant reductions ($p < 0.005$). The 24.7 at.% Ag coating recovered 0.1% bacteria and 15.5 at.% Ag was most effective recovered no viable bacteria.

Following 24 hours of contact in dry conditions significant reduction ($p < 0.05$) of bacteria occurred on all the surfaces. No cells were recovered from any of the silver containing surfaces demonstrating an effective contact kill over time (Figure 82). On the stainless steel 0.02% of the *S. epidermidis* cells were recovered and no viable *S. aureus* were recovered. *S. aureus* displayed a preference for Ti-ZrN and 0.03% recovery was observed whereas no viable *S. epidermidis* cells were recovered.

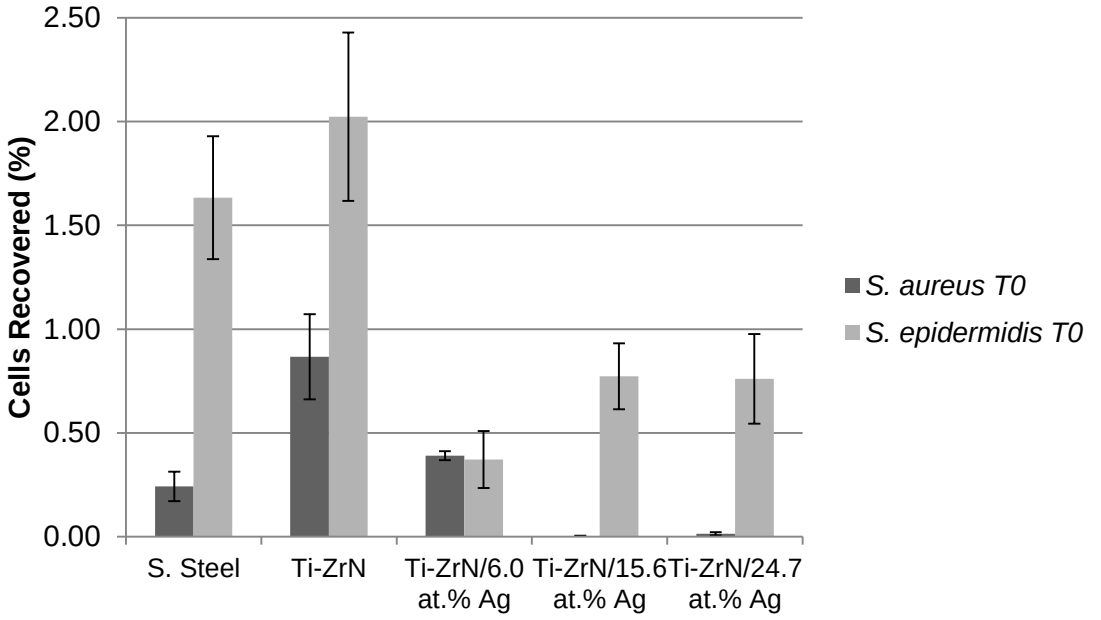

Figure 81: JIS method in dry/room conditions. Samples recovered at T0 immediately after inoculation, demonstrating amounts of contact kill of immediate effect from the silver coatings

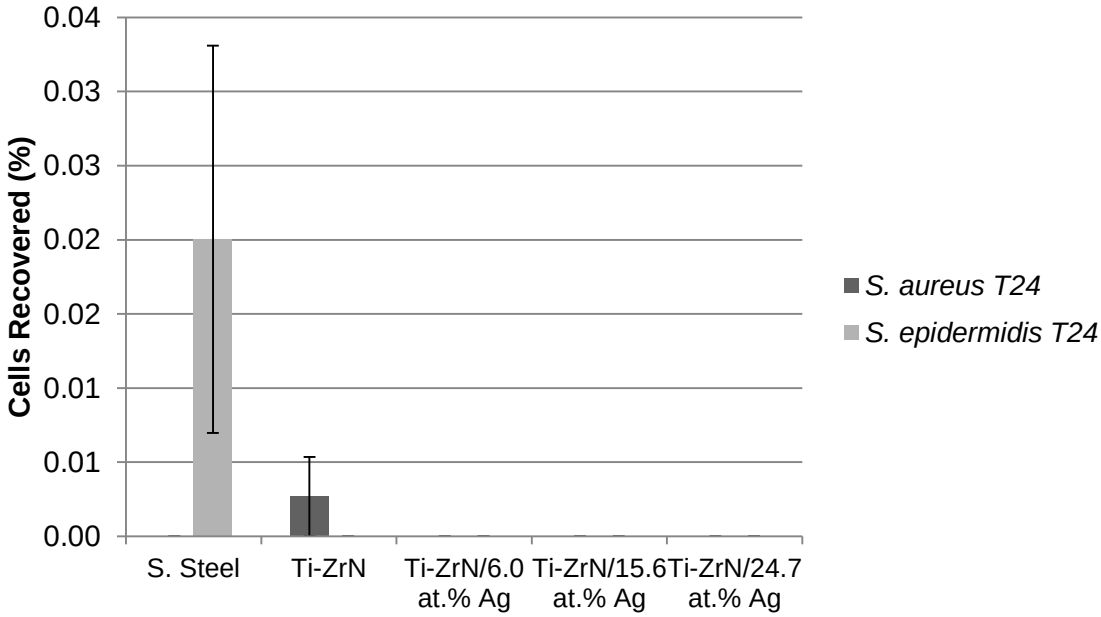

Figure 82: JIS recovery after 24 hours incubation at room temperature conditions. The *S. epidermidis* survived on the stainless steel and the *S. aureus* survived on the ZrN. All other surfaces cultured negative.

6.3.8 JIS Standard in Humid Conditions

The JIS method was also undertaken in humid conditions to prevent drying of the bacterial suspension, removing the drying effect towards the bacteria from the factors contributing to cell death. The bacteria were recovered at a higher percentage than the dry condition assay and the 24.7 at.% Ag coating recovered the most *S. epidermidis* bacteria out of all the surfaces (Figure 83). The 6.0 at.% and 15.6 at.% silver containing surfaces demonstrated a kill of *S. epidermidis* and all three surfaces reduced the bacterial viability but no significant difference was observed. The *S. aureus* at the T0 time point, however no significant reduction was observed ($p > 0.05$) for the 6.0 at.% Ag but a significant decrease was observed for the 15.6 and 24.7at.% Ag coatings. Following 24 hours incubation in humid conditions the recovery of bacteria was only seen on the stainless steel (*S. aureus*: 0.01%; *S. epidermidis*: 3.24%) and the zirconium nitride (*S. aureus*: 0.09%; *S. epidermidis*: 1.03%). The coatings containing silver did not recover any viable bacteria, demonstrating a successful contact kill (Figure 84).

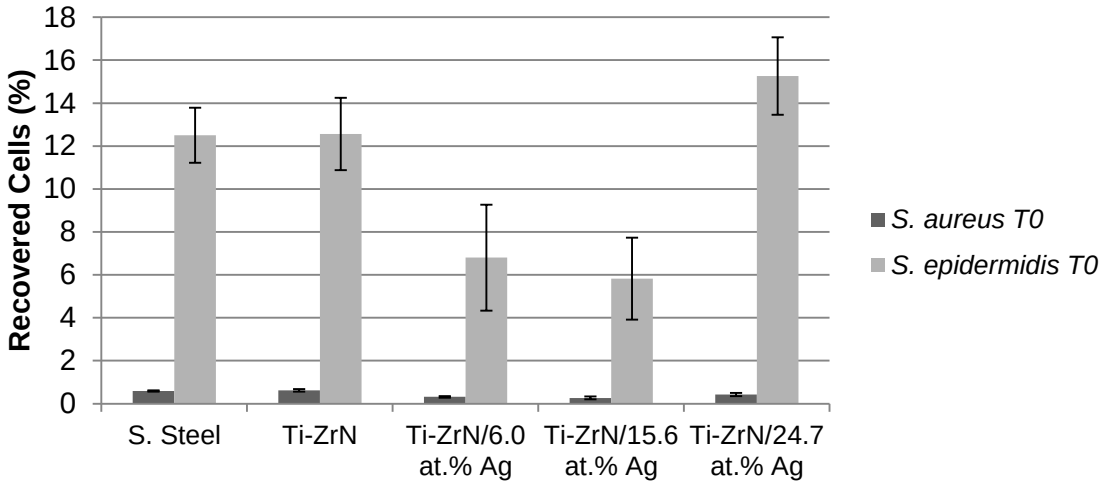

Figure 83: JIS method in humid conditions demonstrating a higher T0 recovery percentage than the previous assay in dry conditions. The silver coatings recovered fewer bacteria apart from 24.7 at. % silver, which displayed less of an antimicrobial effect.

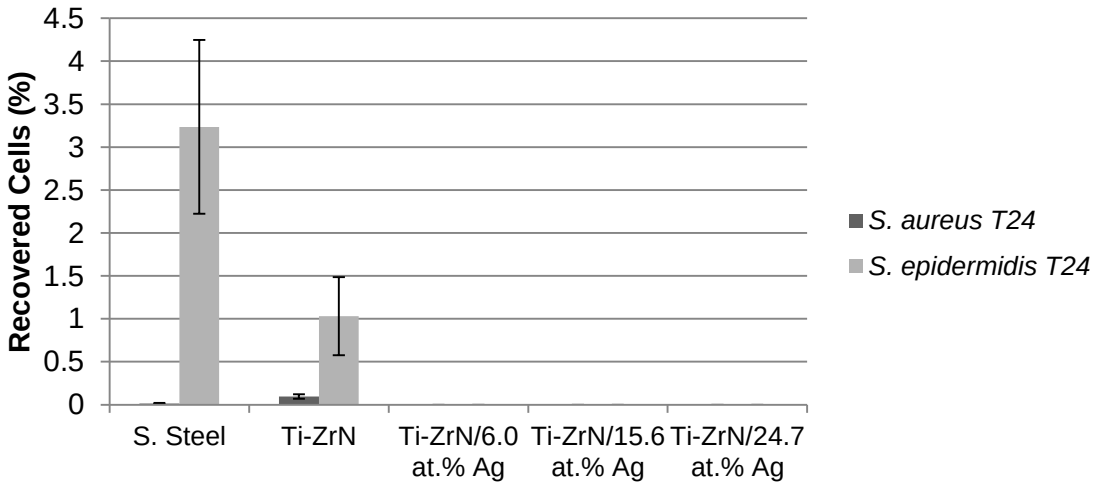

Figure 84: JIS method in humid conditions at T24 displaying the recovered cells after 24 h contact with the surfaces. The non-silver coatings retained viable bacteria but the silver containing coatings demonstrated a complete inhibition of all the bacteria with no bacteria recovered.

6.3.9 MATH Assay

The microbial adhesion to hydrocarbons (MATH) assay determines the hydrophobic properties of bacterial cells in a liquid suspension by calculating the percentage of bacteria adhered to hydrocarbon solvents. A high affinity to apolar hydrocarbons (hexadecane and decane) denotes a high cell surface hydrophobicity and a low affinity to the polar hydrocarbons (chloroform and ethyl acetate) indicates hydrophilicity. The comparison of the solvent pairs chloroform (polar) and hexadecane (apolar) demonstrates the ability of the bacterial surface to donate electrons, when there is higher affinity for chloroform over hexadecane. Comparing the solvent pair ethyl acetate (polar) and decane (apolar) demonstrates the ability to accept electrons when there is a stronger affinity towards ethyl acetate.

The results showed that *S. aureus* displayed a high affinity for chloroform (99.1%) and 100% affinity for hexadecane (Figure 85). This demonstrated that the *S. aureus* possessed strong electron donor and hydrophobic properties. *S. aureus* displayed a lower affinity for the solvent pair ethyl acetate (78.5%) and decane (93%) along with a higher affinity for ethyl acetate over decane, suggesting that the cell surface was polar. The *S. epidermidis* displayed lower affinities towards all four solvents than *S. aureus*. This suggested that the cell surfaces of the *S. epidermidis* cells were less electron donating and less polar. The affinity towards chloroform (82.4%) was higher than that of hexadecane (74.8) suggesting less electron donating and more hydrophilic properties. The increased affinity towards decane, the non-polar solvent (40.1%) over ethyl acetate (18%) suggested less polar properties and more electron accepting properties, than *S. aureus*. A high bacterial affinity towards hexadecane and decane indicates a high hydrophobicity. *S. aureus* displayed a high affinity for both solvents, demonstrating a hydrophobic cell surface. *S. epidermidis* displayed a lower affinity for the two solvents demonstrating that it was less hydrophobic than *S. aureus*.

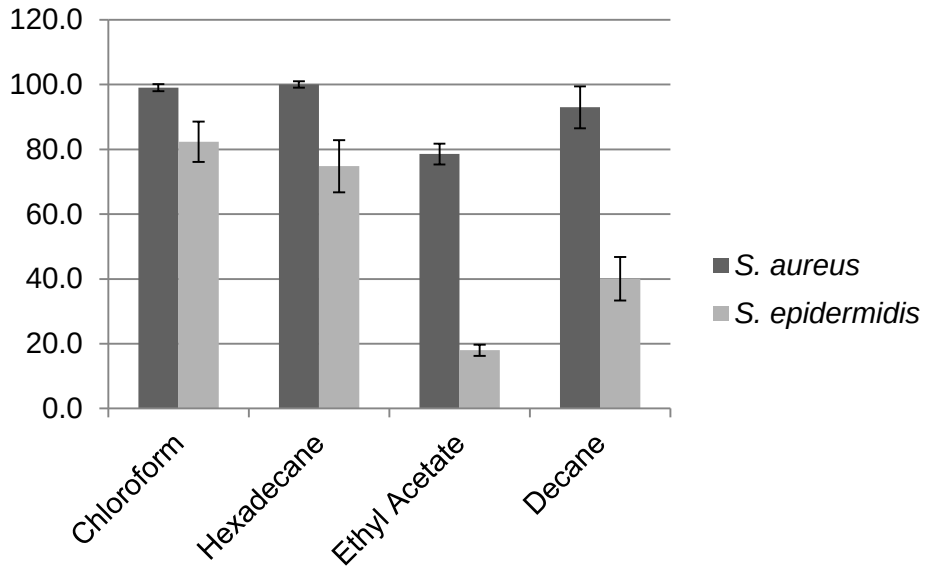

Figure 85: MATH assay percentage affinity of the microorganisms and the solvents. *S. aureus* displayed an extremely high affinity for hexadecane and chloroform but less of an affinity for ethyl acetate and decane. *S. epidermidis* displayed a reduced affinity for hexadecane over chloroform, suggesting that it is more electron accepting than *S. aureus*, which had more affinity for chloroform.

6.4 Discussion

When the hydrophobicity values were plotted against percentage coverage of retained bacterial cells on the Ti-ZrN and Ti-ZrN/Ag coatings it was demonstrated that an increase in hydrophobicity led to an increase in *S. aureus* retention and a decrease in *S. epidermidis* retention. The MATH assay (6.3.9; Page 203) demonstrated that *S. aureus* possessed hydrophobic cell surface properties and *S. epidermidis* displayed more hydrophilic surface properties. This shows that hydrophobic bacteria were attracted to hydrophobic surfaces and hydrophilic bacteria to hydrophilic surfaces. This also supports the theory that the more hydrophilic the surface the more repulsive it is towards bacterial cells (Bos *et al.*, 1999).

Following comparisons of the S_a roughness parameters with the retention numbers of *S. aureus* and *S. epidermidis*, the effect of microtopography in relation to bacterial retention was displayed. The *S. aureus* was affected by an increase in S_a on the coated samples, however the stainless steel retained a high percentage coverage with a low S_a value. Previously discussed, the hydrophobicity of the stainless steel was high, demonstrating that the hydrophobic properties of the surfaces played a role in *S. aureus* retention as well as surface microtopography. *S. epidermidis* displayed no trends towards bacterial retention and S_a values, demonstrating the retention of *S. epidermidis* was not affected with alterations in roughness at the amounts observed.

LiveDead staining evaluated the viability of bacterial cells by indicating the integrity of the cell membrane of the microorganisms by the means of two fluorescent markers. The results displayed a decrease in live *S. aureus* cells on the coated samples and the efficacy of the coatings increased with the silver content. The *S. epidermidis* was detected in extremely low numbers and no trend was observed. The coverage of dead cells was high for *S. aureus* on stainless steel suggesting that the surface had a high coverage of microorganisms and the amount of dead coverage decreased for Ti-ZrN

and 6.0 at.% Ag to increase for both the 15.6 and 24.7 at.% Ag, suggesting that the 24.7 at.% Ag was most efficacious but retained less total bacteria than the 15.6 at.% Ag surface. The *S. epidermidis* displayed an increase in dead cells as the silver content increased, suggesting that the silver was also compromising the membrane of the microorganisms, agreeing with the theory in literature that the antimicrobial action of silver is multi-action affecting many areas of the cell physiology. The LiveDead staining kit stains all of the bacterial cells green using SYTO-9 (green), and then propidium iodide (red) dominantly over-stains any cells in the population with a compromised cell membrane and these are classed as dead (Williams *et al.*, 1998). However, cells may still be viable with a compromised membrane or non-viable with an intact membrane, therefore this method may not be absolutely reliable. This is particularly true if there is potential for silver ions to enter the cell via channels, such as protein channels, and affecting the DNA, thus rendering the cell unable to respire and replicate (Radzig *et al.*, 2013). Noyce *et al.,* (2006) demonstrated a method involving a fluorescent redox dye, (5-cyano-2, 3-ditolyl tetrazolium (CTC)), which is reduced in metabolically active cells, staining them red/orange. CTC staining was used alongside LiveDead™ staining in order to provide further insight into the action of the silver within the coatings.

Following the CTC assays it was found that the increase in silver content of the coatings did not decrease cell respiration as would be expected. There was a significant decrease in viable coverage on the 6.0 at.% Ag (p = 0.008) and 15.6 at.% Ag (p = 0.02) coatings in comparison to stainless steel. The viable *S. aureus* coverage was highest on the stainless steel, followed by Ti-ZrN, 24.7 at.% Ag, 15.6 at.% Ag and the most efficacious was the 6.0 at.% Ag coating. The effect of the coatings on the *S. epidermidis* showed that no significant difference in the viable coverage was observed on all surfaces. The coating with the most viable cells was the 15.6 at.% Ag, followed by stainless steel, 6.0 at.% Ag, Ti-ZrN and the 24.7 at.% Ag displayed the best

antimicrobial effect towards *S. epidermidis*, with no viable coverage observed. The CTC-DAPI staining assay displayed the respiration of individual microorganisms by reducing the tetrazolium of the stain in the electron transport chain of the microorganism to produce insoluble, fluorescent formazan. The epifluorescent microscope uses software to allow the percentage coverage of the red formazan to be quantified. The results demonstrated that *S. aureus* displayed more respiring cell coverage than *S. epidermidis*. The silver containing coatings produced an antimicrobial effect towards *S. aureus*, reducing the cell respiration, however the best performing surface was Ti-ZrN/6.0 at.% Ag and the respiration of the cells increased when the silver content increased. The *S. epidermidis* displayed lower respiration on the non-silver surfaces but proved more resistant on the 6.0 at.% silver and 15.6 at.% silver. However, the respiration was higher for 15.6 at.% silver than 6.0 at.%, sharing a similar trend to *S. aureus*. These results suggest that the mode of action of the silver is a combination of bacteriostatic and bactericidal, allowing some respiration from some of the microorganisms but not allowing them to reproduce and also arresting respiration of the other microorganisms that may be more susceptible. The CTC-DAPI method is used in situations where rapid detection and enumeration of viable bacteria are required. It has been suggested that using this method of detection does not detect dead bacteria or ones with low levels of activity, such as dormant cells or spores, but it is also not clear in the method whether or not viable bacteria that are injured or viable but non-culturable will continue to reduce the CTC and contribute towards the number of viable and culturable cells detected (Schaule *et al.*, 1993). Therefore, testing the bacterial respiration alongside the NTV assay helps further characterise the respiration occurring and the NTV assay allows enumeration of respiring culturable colony forming units.

The NTV assay demonstrated a successful decrease in cell numbers for the test microorganisms following one hour contact in room temperature conditions. The

organisms survived better on the pure Ti-ZrN than the stainless steel. This could have been due to the greater hydrophobicity of the stainless steel surface forcing the cell suspension to sit on the surface as 'beads' thus reducing cell contact with the surface. When the bacterial suspension dried on the stainless steel it dried over a small area, potentially killing the bacterial cells faster as little have contact with the surface to attach to, to then proliferate. The Ti-ZrN demonstrated the cells had the highest survival on this coating and the *S. aureus* tended to survive in higher numbers than the *S. epidermidis*. This reinforces previous hypotheses that *S. aureus* tends to prefer metallic biomaterials (Harris and Richards, 2006). The silver containing coatings displayed significant ($p < 0.05$) reduction in cell survival. The increase in silver content did not display an increase the antimicrobial effect. The three silver surfaces, however, demonstrated a similar number of colony forming units on the surface, regardless of the silver content. This could suggest that in an environment where the bacteria are exposed to a dry surface of the biomaterial the effect of drying reduces the viability of the bacteria on the surface. These results could suggest that the silver contents used did not actively stop the respiration of the cells but other assays such as the NTV showed that the bacteria were not multiplying into colonies so this would suggest it is damaging the cell membrane, as seen from the LiveDead assay, and causing a contact kill (NTV) but not fully arresting the respiration of all of the bacteria.

Following the zones of inhibition assay the results concluded that the zirconium nitride silver coatings did not demonstrate inhibitory leaching towards the test microorganisms. This was also observed with the earlier coatings. Further investigation into the silver release had been undertaken and ICP-AES analysis was used to calculate the release of silver into the surroundings. These results were displayed in section 5.3.7 (Page 178). The result for the highest silver content release from the 24.7 at.% Ag coating, over 24 hours was calculated out:

1.249 ppm release over 24 h (n=16) in 100ml solution

(10 ml sample diluted in 10 ml water)

$$\frac{1.249}{1000} = 0.001249 \frac{ppm}{ml} (n = 16)$$

$$\frac{0.001249}{16} = \mathbf{0.078\ ppb}/ml/coupon/day$$

The minimum inhibitory concentration for silver towards staphylococci was between 0.5-10 mg/L (≈ 500 - 10,000 ppb), which was several orders of magnitude higher than the amount the coatings released over a 24 hour period (Schierholz *et al.*, 1998). Further, it has been shown that silver is more effective towards gram negative cells due to the much thinner 'murein'/peptidoglycan wall (2-3 nm) in comparison to gram positive (10 nm) cells. It has also been found that the peptidoglycan adsorbs the silver reducing the bactericidal effects towards the cells (Modak and Fox, 1973, Schierholz *et al.*, 1998).

The JIS standard assay demonstrated the effectiveness of a surface contact kill after immediate application and following 24 hours contact time, by means of cell recovery; removing the cells from the surface using agitation and counting viable cells from serial dilutions. In dry conditions, at room temperature and room relative humidity, both strains of bacteria were completely killed and no viable bacteria were recovered from the coatings. At T0 *S. epidermidis* was not viably recovered from the 15.6 and 24.7 at.% silver surfaces. The *S. aureus* was also recovered in lower numbers from the silver surfaces than the non-silver surfaces, suggesting that an immediate antimicrobial effect was occurring as well as efficacy over a 24 hour exposure. Following 24 hours exposure in both dry and humid conditions all three silver containing surfaces recovered no viable bacteria of both *S. aureus* and *S. epidermidis*. The Ti-ZrN and stainless steel surfaces recovered significantly less microorganisms ($p < 0.05$) following 24 hours incubation, however in the environment of an external fixation pin it would take very few bacterial cells to trigger an infection.

The Japanese industrial standard method was reproduced in humid conditions at 37ºC to replicate body conditions and to exclude surface drying stress towards the microorganisms that were tested. The cell recovery at T0 showed that the *S. aureus* was initially recovered in lower numbers (0.6% on stainless steel) in comparison to *S. epidermidis* (12.5% on stainless steel), but following 24 hours contact time a significant reduction in recovered bacteria was apparent for all five of the test surfaces. Following 24 hours incubation time all three of the silver containing surfaces recovered no bacteria, demonstrating a successful kill over the non-silver containing surfaces. Stainless steel recovered 0.01% of *S. aureus* cells and 3.24% of *S. epidermidis* and Ti-ZrN recovered 0.09% of *S. aureus* and 1.03% of *S. epidermidis*.

The bacterial cell hydrophobicity and electron donating/accepting properties were addressed using the microbial affinity for hydrocarbons method (MATH). A high affinity towards non-polar hydrocarbons (decane and hexadecane) indicated a high surface hydrophobicity. The electron donating and accepting characteristics of the bacterial surfaces is based on comparing the affinities of the solvents grouped into polar and non-polar hydrocarbons. High affinity to the non-polar solvents (hexadecane and decane) denotes a high cell surface hydrophobicity. Comparing the bacterial cells towards the polar (chloroform) and non-polar (hexadecane) pair will indicate the electron donation capabilities of the cell surface and comparing the solvent pair, including ethyl acetate (polar) and decane (non-polar), will display the cell surface electron accepting abilities (Bellon-Fontaine *et al.*, 1996, Skovager *et al.*, 2012). Although testing for cell surface hydrophobicity using the MATH method is a universal way to test microorganisms, the affinity of the microorganisms to the hydrocarbons may be affected by alterations in ion content and pH of the liquid the cells are suspended in and influence the microorganism-hydrocarbon interactions (Busscher and Van Der Mei, 1995, van der Mei *et al.*, 1995). To ensure the results were comparable, all of the bacterial suspensions were produced in the same batch of buffer throughout. The *S.*

aureus cells displayed a high affinity for hexadecane and decane, demonstrating a hydrophobic cell surface. The *S. epidermidis* possessed a higher affinity for chloroform than hexadecane and an increased affinity for decane (than ethyl acetate. This demonstrated less hydrophobic *S. epidermidis cell* surfaces than the *S. aureus*. *S. aureus* displayed a stronger affinity towards chloroform and hexadecane over ethyl acetate and decane, demonstrating that the cell surfaces are more electron donating. *S. epidermidis* also displayed higher affinity over chloroform and hexadecane over ethyl acetate and decane, but displayed a significantly lower affinity for ethyl acetate and decane over *S. aureus*, suggesting that *S. epidermidis* could be more electron accepting and less electron donating than *S. aureus*. *S. aureus* was more hydrophobic and was retained on the surfaces that were more hydrophobic. The *S. epidermidis* was less hydrophobic and less cells overall were retained suggesting that an increase in hydrophobicity of the bacterial cell surface corresponds to an increase in bacteria retained.

6.5 Concluding Remarks

The Ti-ZrN/Ag coatings were assessed for retention characteristics using acridine orange staining in comparison to surface chemistry, hydrophobicity and topography. The addition of silver to the coatings decreased the number of *S. epidermidis* retained and a decreasing trend was observed with an increase in silver concentration. This suggests that surface chemistry affected the retention characteristics of the *S. epidermidis* cells. The *S. aureus* demonstrated different characteristics, increasing in bacterial retention as the silver increased but reducing for the coating containing 29.8 at.% Ag. This suggests that other properties are affecting the retention of *S. aureus*. *S. aureus* displayed a retention trend matching that of the ΔG_{iwi} hydrophobicity values demonstrating that physicochemical properties were affecting the adhesion of *S. aureus*, an increase in hydrophobicity led to the increase in retained bacteria. *S. epidermidis* displayed increased retention on the surfaces that were less hydrophobic demonstrating that hydrophobic bacteria (*S. aureus*) were attracted to more hydrophobic surfaces and hydrophilic bacteria (*S. epidermidis*) to hydrophilic surfaces. *S. aureus* also displayed a trend of increased retention when the microtopography increased on the coatings, however the *S. epidermidis* did not. Neither microorganism displayed any difference in retention pattern in comparison to nanotopography. Thus it may be speculated that the effect of surface properties on microbial retention is species dependent.

Following LiveDead assays it was demonstrated that *S. aureus* was retained in higher total numbers than *S. epidermidis*. The live *S. aureus* decreased with increasing silver content and Ti-ZrN displayed less live bacteria than stainless steel. The highest numbers of dead cells were from stainless steel, Ti-ZrN/15.6 and 24.7 at.% Ag, however 6.0 at.% Ag displayed fewer dead *S. aureus*. *S. epidermidis* displayed similar numbers of live cells throughout and the dead cells increased as the silver content increased. CTC-DAPI demonstrated the Ti-ZrN/6.0% Ag to be the most efficacious

towards *S. aureus*, but not from the LiveDead assay, suggesting the bacterial kill arrested respiration but the cell membrane was not compromised. An increase in silver led to an increase in viability of *S. aureus*. The *S. epidermidis* displayed 6.0 at.% Ag and 15.6 at.% Ag had similar numbers to the stainless steel and Ti-ZrN and the 24.7 at.% Ag displayed no visible respiring cells, therefore the Ti-ZrN/24.7 at.% Ag coating was the most antimicrobial. The NTV assay found that both microorganisms were killed significantly on all of the silver containing coatings in comparison to the stainless steel and Ti-ZrN demonstrating a successful contact kill. The NTV assay demonstrated that an increase in silver content did not increase antimicrobial efficacy. The JIS method in room/dry conditions found that an antimicrobial effect was observed from the silver containing coatings at T0. Following 24 hours incubation no microorganisms were recovered from the silver containing coatings demonstrating a successful kill of both *S. aureus* and *S. epidermidis*. The JIS assay was performed in humid conditions demonstrating less kill from the silver containing coatings towards both staphylococci species at T0. Following 24 hours incubation in humid conditions all of the microorganisms were reduced to 0 on the silver containing coatings but viable colonies of both *S. aureus* and *S. epidermidis* were recovered from the stainless steel and Ti-ZrN. This result is significant because in external fixation pin hygiene as little as a few tens of microorganisms surviving on the surface could initiate an infection, therefore an effective kill following 24 hours exposure would be beneficial in external fixation pin infection control. Therefore the best performing coatings was the Ti-ZrN/15.6 at.% Ag for the antimicrobial efficacy.

7 The Effect of a Blood Conditioning Film on the Antimicrobial and Surface Properties of Ti-ZrN and Ti-ZrN/Ag

7.1 Introduction

The prerequisite for colonisation of microorganisms on a substratum is initial bacterial attachment. If this initial attachment phase can be prevented, complications with bacterial colonisation and biofilms/biofouling could potentially be avoided (Verran and Whitehead, 2005). It has been demonstrated that bacterial cells do not attach to a bare substratum, but to an interface that has been exposed to the surrounding environment and has been 'conditioned' (Busscher and Van der Mei, 2000, Sauer *et al.*, 2002). The conditioning film occurs when a layer of organic molecules are adsorbed onto the surface from the surrounding environment (Bos *et al.*, 1999, Whitehead *et al.*, 2005a). The structure of the conditioning film depends upon the composition of the surrounding liquids and products and the surface properties of the biomaterial. In the case of external fixation pins the environment will include blood, plasma, lymph, and various proteins from muscle and bone cells and inflammatory cells surrounding the site. This will produce a surface interface on the biomaterial with various proteins, adhesins and receptors for surrounding cells, both bacterial and eukaryotic, to interact.

The organic soiling of a biomaterial with a conditioning film has the potential to alter the surface topography by masking surface features, which will affect the cell - surface interface and create cell – soil and soil – substratum interfaces, increasing the factors contributing towards microbial retention (Pringle and Fletcher, 1986, Frank and Chmielewski, 1997, Verran and Jones, 2000, Verran and Whitehead, 2006). Unconditioned surfaces, classed as 'clean' will rapidly accumulate a conditioning film and will never return to possessing the same surface properties observed prior to fouling (Mettler and Carpentier, 1998). Therefore, it has been suggested that *in vitro* it may be beneficial to re-use test surfaces and subject them to a standardised cleaning regimen, rather than use new samples, to replicate an *in vivo* situation, giving a more 'real life' challenge to the surfaces (Verran *et al.*, 2002). Thus, testing the antimicrobial

efficacy and the surface properties of biomaterial surfaces in the presence of a conditioning film will provide a greater insight into the behaviour of the biomaterial surface in a similar environment *in vivo*.

The aim of this work was to investigate the surface properties once coated with a relevant conditioning film and the antimicrobial efficacy of the Ti-ZrN/Ag coatings in the presence of a conditioning film. Blood was used as the conditioning film as it is relevant in the external fixation pins environment. In the MATH assay, where optical density of the liquid was important, blood plasma was used as the conditioning film to keep alterations to the optical density measurements to a minimum.

7.2 Methodology

7.2.1 White Light Profilometry

Sterile defibrinated sheep's blood (Oxoid, UK) (5 ml) was diluted 50:50 using 5 ml of sterile distilled and mixed using a vortex for 20 seconds. Twenty microliters were pipetted onto the surfaces and spread using the side of the pipette tip then placed in a class II microbiological flow cabinet for one hour to dry. The surfaces were visualised on the white light profilometer using the same method as section 2.2.7 (Page 66) at 101.6 X magnification. A two dimensional map and three dimensional image were obtained as well as a line profile. Results were obtained in triplicate for each sample.

7.2.2 Surface Hydrophobicity (Contact Angles)

The Ti-ZrN and Ti-ZrN/Ag coatings were deposited onto 35 x 35 mm coupons of the 316L stainless steel and 100 µl of 50% sheep's blood (50 % blood : 50 % sterile distilled water) was added and spread as described above. Samples were left to dry in a class II microbiological flow cabinet for at least two hours to ensure the conditioning film had completely dried prior to testing. The contact angles were obtained using the same method described in section 5.2.1 (Page 145).

7.2.3 Microbial Adhesion to Hydrocarbons (MATH) Assay: in the presence of a blood plasma conditioning film

The microbial adhesion to hydrocarbons assay was followed the same as the method in section 6.3.9 (Page 203). Prior to testing, 20 ml of standardised bacterial suspension and 10 ml of sterile human blood plasma (Oxoid, UK) was vortexed for one minute. The liquid was centrifuged at 604 *g* for 10 minutes and rinsed once with 10 ml PUM buffer and diluted to an OD of 1.0 at 400 nm in PUM buffer. All hydrocarbons were repeated in triplicate and the experiment was duplicated.

7.2.4 Nitro Tetrazolium Violet (NTV) respiratory staining assay with a blood plasma conditioning film

The NTV assay was performed to the same specifications as chapter 3.2.7 (Page 94) but prior to starting the assay 20µl of 50% defibrinated sheeps blood, diluted in sterile distilled water, was added to the surfaces and spread using a sterile spreader. The blood was left to dry for one hour in a class II microbiological flow cabinet.

7.2.5 Japanese Industrial Standard (JIS) assay in the presence of a blood conditioning film

The method was adapted from the previous method in chapter 6.2.2 (Page 190). The bacterial strains were washed and diluted to an optical density of 1.0 at 540 nm in sterile distilled water, and then 10ml of the bacterial suspension was mixed with 5 ml of 50 % defibrinated sheeps blood and vortexed for 20 seconds. The bacterial suspension including the blood was then added to the surface.

7.3 Results

7.3.1 White Light Profilometry

White light profilometry of the surfaces following the addition of a blood conditioning film demonstrated the microtopography of the blood coated surfaces. The blood layer changed the surface topography and the surface features of the stainless steel were no longer visible (Figure 86). From the two dimensional map it appeared that the shape of the red blood cells may be visible on the surface topography; this was more apparent on the Ti-ZrN and Ti-ZrN/Ag coatings (Figure 86b-e). The topography scale bars of the five line profiles all differ due to surface alterations such as deep pits included in the line profile (Figure 87). Taking into consideration the scale bar differences for the line profiles once conditioned with blood the surface topographies remained similar throughout, with the exception of stainless steel which possessed rougher peaks and valleys but in no larger amplitudes. The holes in the conditioning film displayed in the two dimensional images indicated that the conditioning film could be up to and over three microns thick, therefore the features of the surfaces were covered as the topography rarely exceeded one micron in height.

The average height values were obtained from measuring the individual peaks and valleys of the white light profilometer cross sections. The lowest average height was observed on the stainless steel (64.8 nm) and the coated samples displayed a significantly rougher surface topography in the presence of the blood conditioning film (Figure 88). The highest average height was shown on the Ti-ZrN coating (579 nm), which was significantly more than the other values. However, comparing this value with the line profile, the large valleys observed have increased the average, but the other topographical features remain a similar size to the ones observed for the other topographies of the coated samples. The silver containing coatings displayed significantly higher average feature heights than the stainless steel but between the

values of the three coatings no significant difference was observed; Ti-ZrN/6.0 at.% Ag was 155 nm, Ti-ZrN/15.6 at.% Ag was 119.4nm and Ti-ZrN/24.7 at.% Ag was 165 nm. However, the depths of the features were not as large as the dimensions of a microbial cell (1 μm). The values obtained did not match the trend seen on the surfaces without a conditioning film (Figure 66; Page 172) and the surface features in the presence of the conditioning film were ten times the size.

The largest average feature widths were observed on the stainless steel surface (5.2 μm) and the average widths of the coated samples were smaller, with the Ti-ZrN being the only surface to be significantly smaller than the stainless steel (Ti-ZrN = 2.76 μm) (p = 0.0009) (Figure 89). The sizes of the average width values increased with increasing silver; from Ti-ZrN (2.76 μm), Ti-ZrN/6.0 at.% Ag (3.4 μm) and Ti-ZrN/15.6 at.% Ag (4.28 μm), but decreases for the Ti-ZrN/24.7 at.% Ag coating (3.6 μm). These values, with the exception of Ti-ZrN followed the same trend as the values obtained from the surfaces without a conditioning film present (Figure 65; Page 171).

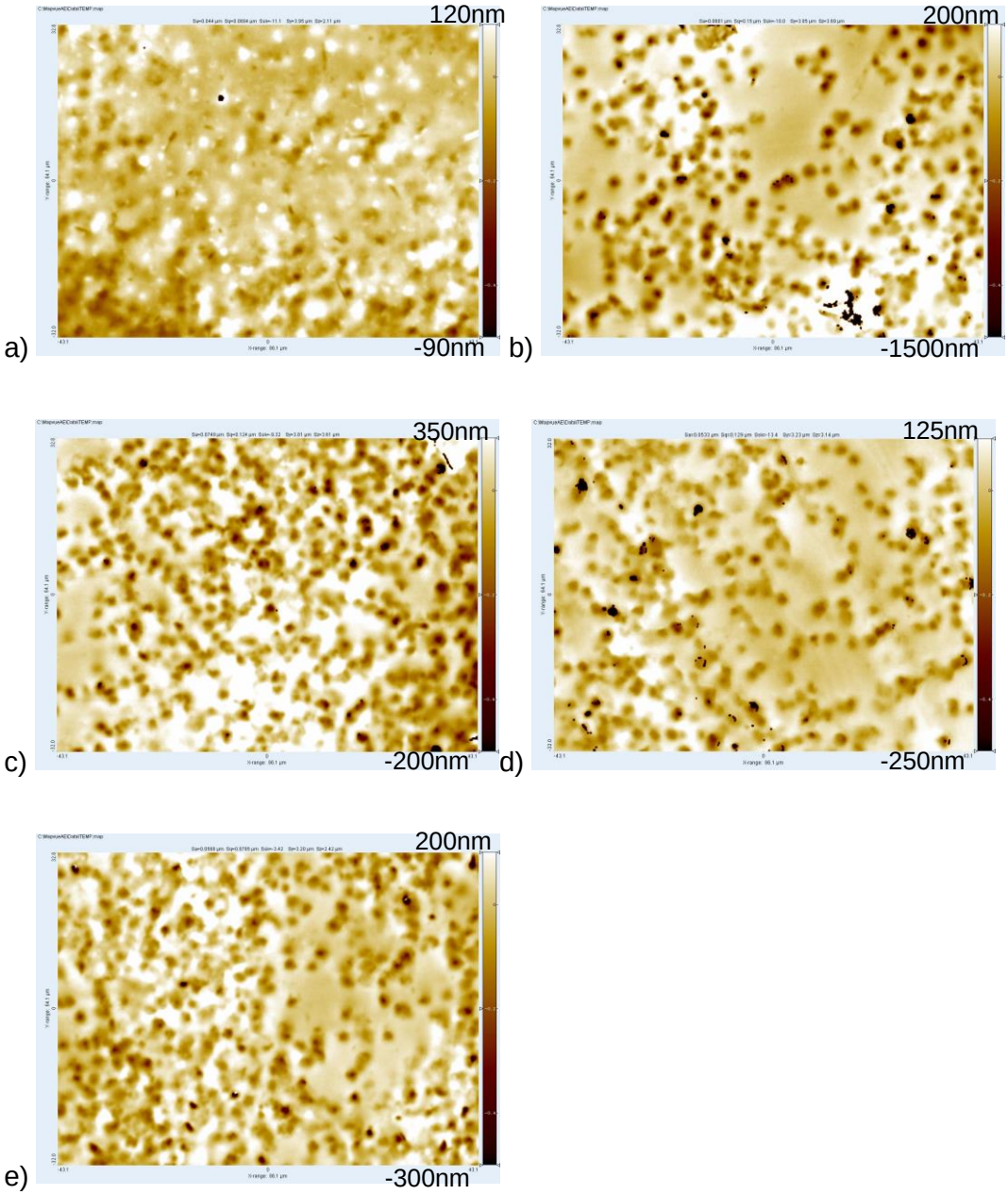

Figure 86: White light profilometry images of a blood conditioning film on a) stainless steel, b) Ti-ZrN, c) Ti-ZrN/6.0at.% Ag, d) Ti-ZrN/15.6 at.% Ag and e) Ti-ZrN/24.7 at.% Ag, demonstrating different surface microtopographies of the blood dried on the surfaces.

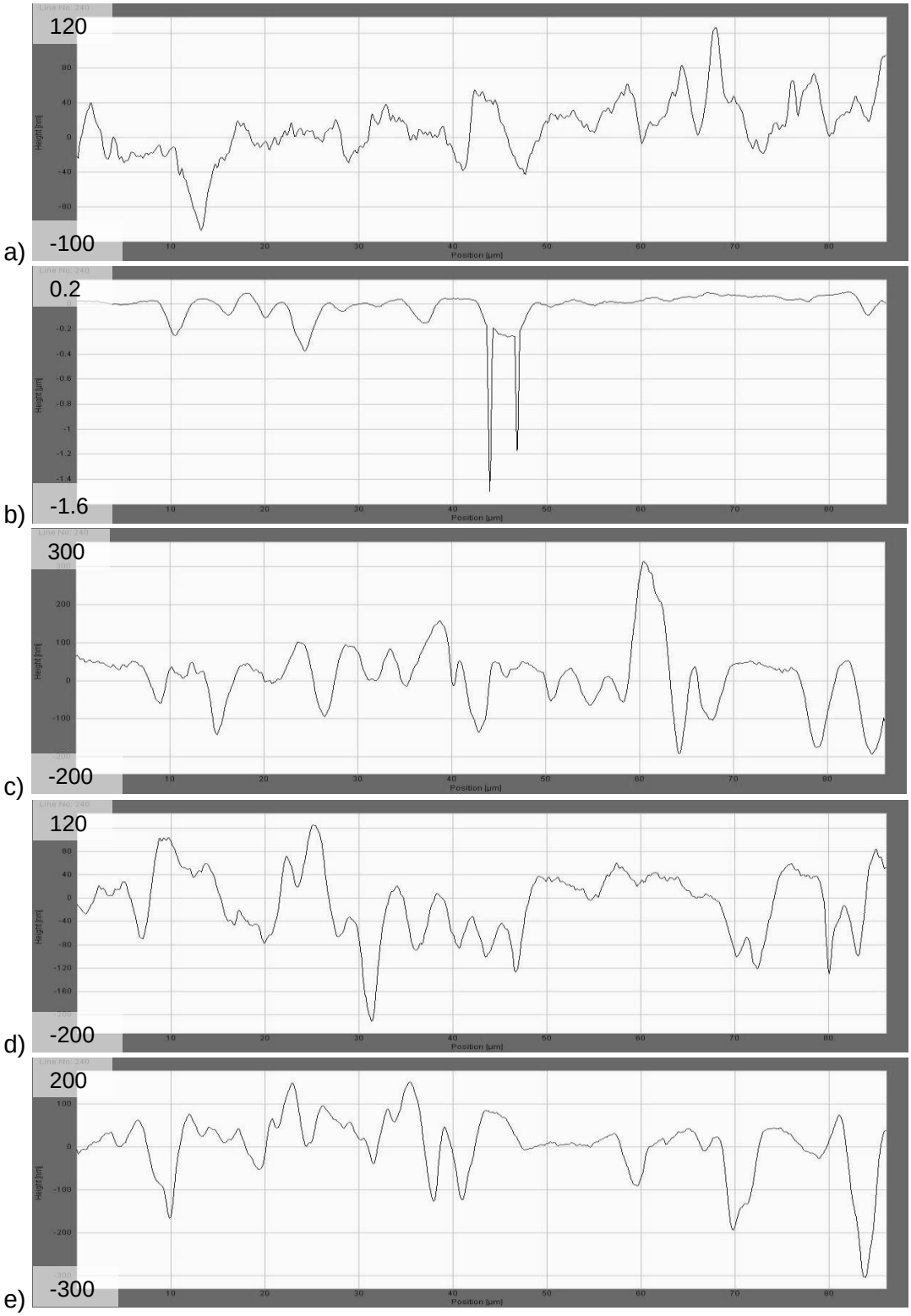

Figure 87: White light profilometry line profiles of blood conditioning film on a) stainless steel, b) Ti-ZrN, c) Ti-ZrN/6.0 at.% Ag, d) Ti-ZrN/15.6 at.% Ag and e) Ti-ZrN/24.7 at.% Ag, demonstrating the difference in microtopography features through a cross section.

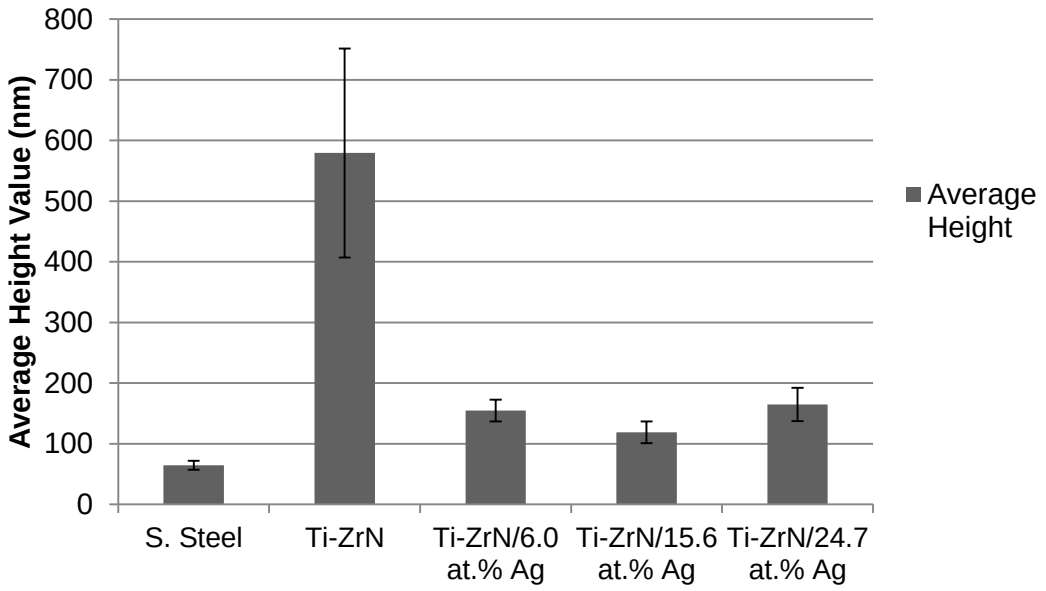

Figure 88: Average height values of the surface features on a cross section taken from the white light profilometer demonstrating differing microtopographical features. Stainless steel possessed a significantly lower average height value than the coated samples and Ti-ZrN displayed a significantly higher value than the coatings containing silver.

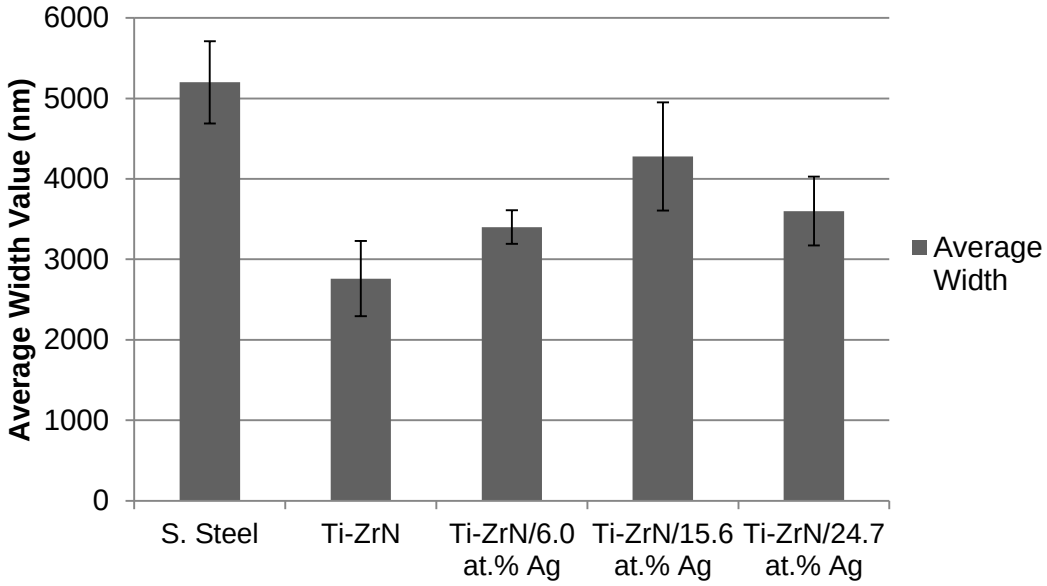

Figure 89: The average width values of the surfaces from a line profile, taken from the white light profilometer, in the presence of a blood conditioning film.

7.3.2 Surface Hydrophobicity and Surface Free Energies

Following contact angle measurements the hydrophobicity and surface charges of the conditioning film on the different surfaces were obtained. The ΔG_{iwi} demonstrates the surface hydrophobicity/ hydrophilicity of a surface as a numerical value (mJ m^{-2}). Positive results indicate a hydrophilic surface and negative results a hydrophobic surface. All of the test surfaces with a blood conditioning film were hydrophilic, with the stainless steel being the most hydrophilic with a decreasing trend throughout the coatings and Ti-ZrN/24.7 at.% silver being the least hydrophilic at ΔG_{iwi} 2.29, differing from the hydrophobic values observed on the unconditioned surfaces (Figure 90). The average γ_s demonstrated that Ti-ZrN had the highest γ_s at 44.23, however the other four surfaces possessed similar γ_s values, all around 39.5 ± 0.5 (Figure 91) demonstrating no significant difference (p = 0.13) between all of the surfaces. Although the differing surfaces affected the ΔG_{iwi} (hydrophilicity) it did not alter the surface free energy in the same way. The $\gamma_s LW$ Lifshitz van der Waals forces displayed no significant difference between any of the surfaces, the highest values were for Ti-ZrN and Ti-ZrN/15.6 at.% silver surfaces with a $\gamma_s LW$ value of 36.8, followed by stainless steel and Ti-ZrN/24.7 at.% silver with a value of 36.0 and the lowest value was from Ti-ZrN/6.0 at.% silver at 35.71 (Figure 92). The values of the γ_sAB acid base and the γ+ values both followed the same trend, with Ti-ZrN being the highest value, and decreasing with the Ti-ZrN/6.0 at.% Ag and the Ti-ZrN/15.6 at.% Ag having the lowest value, to increase for the Ti-ZrN/24.7 at.% Ag surface. The $\gamma_s AB$ Acid base displayed the highest value of 7.34 for the pure Ti-ZrN and the lowest of 2.44 for the Ti-ZrN/15.6 at.% Ag (Figure 93). There was no significant difference between the surfaces in terms of $\gamma_s AB$ properties. The γ^+ electron accepting capability values were also highest for the Ti-ZrN, at 0.54 and lowest for the Ti-ZrN/15.6 at.% Ag, at 0.1 (Figure 94). The Ti-ZrN possessed a significantly higher γ_s+ value than the stainless steel, Ti-ZrN/6.0 at.% Ag

and Ti-ZrN/15.6 at.% Ag but no significant difference was observed between the Ti-ZrN and the Ti-ZrN/24.7 at.% Ag coatings. The γ^- electron donating capability of the surfaces followed a similar trend to the ΔG_{iwi} with the stainless steel possessing the highest value at 58.32 for stainless steel, demonstrating a decreasing trend down to the lowest value of 28.9 for the 24.7 at.% Ag surface (Figure 95). No significant difference was observed between stainless steel and Ti-ZrN, however a significant decrease in electron donating γ- value was demonstrated on Ti-ZrN/6.0 at.% Ag, Ti-ZrN/15.6 at.% Ag and Ti-ZrN/24.7 at.% Ag coatings.

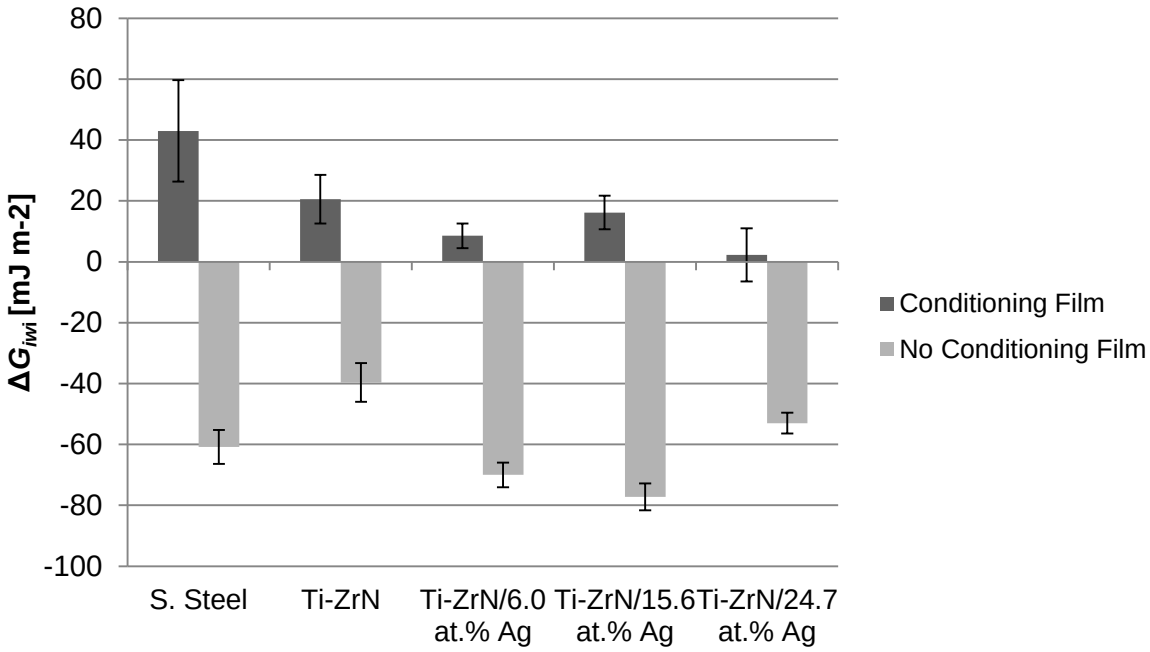

Figure 90: Average ΔG_{iwi} hydrophobicity values of the surfaces with a blood conditioning film, also displaying the ΔG_{iwi} of the surfaces without a conditioning film. Stainless steel was the most hydrophilic surface at ΔG_{iwi} 43.02, displaying a decreasing trend throughout the coatings with the least hydrophilic being the Ti-ZrN/24.7 at.% Ag coating at ΔG_{iwi} 2.29.

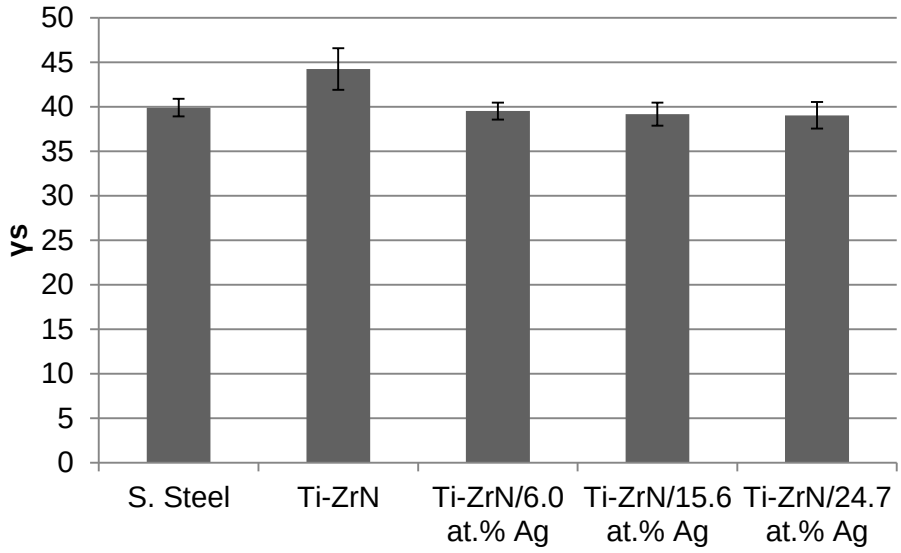

Figure 91: The average γ_s surface free energy values of the surfaces with a blood conditioning film added displaying no significant difference between the surfaces.

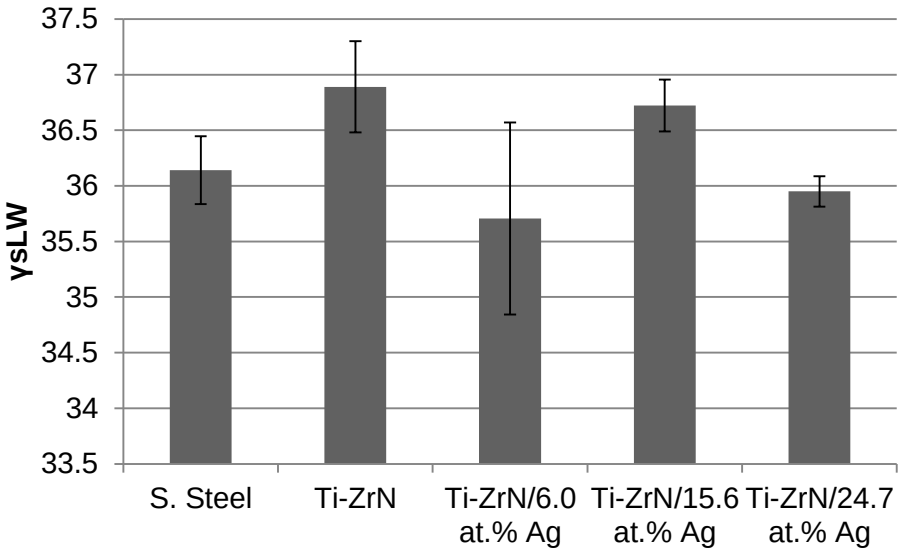

Figure 92: The average γ_s^{LW} Lifshitz van der Waals values of the surfaces with a blood conditioning film. The Ti-ZrN and 15.6 at.% Ag possessed similar highest values, followed by stainless steel and 24.7 at.% Ag and the 6.0 at.% Ag displayed the lowest value.

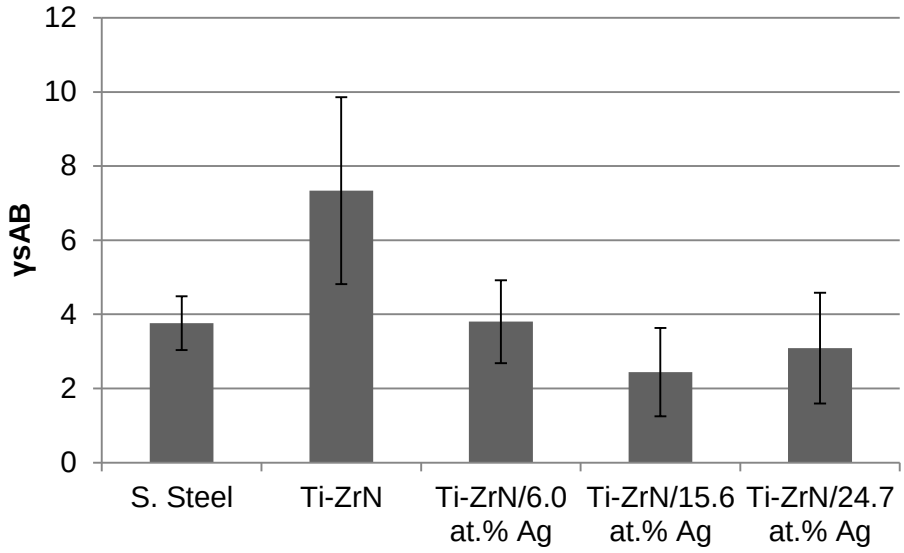

Figure 93: Average γ_s^{AB} Lewis Acid Base values of the surfaces with a blood conditioning film. The values increased from 3.76 from stainless steel to 7.34 for Ti-ZrN and then decreased for the silver coatings with the 15.6 at.% Ag displaying the lowest value at 2.44. The Ti-ZrN coating possessed a significantly higher value than the other surfaces. No significant difference was observed between the stainless steel, Ti-ZrN/6.0 at.% Ag, Ti-ZrN/15.6 at.% Ag and Ti-ZrN/24.7 at.% Ag.

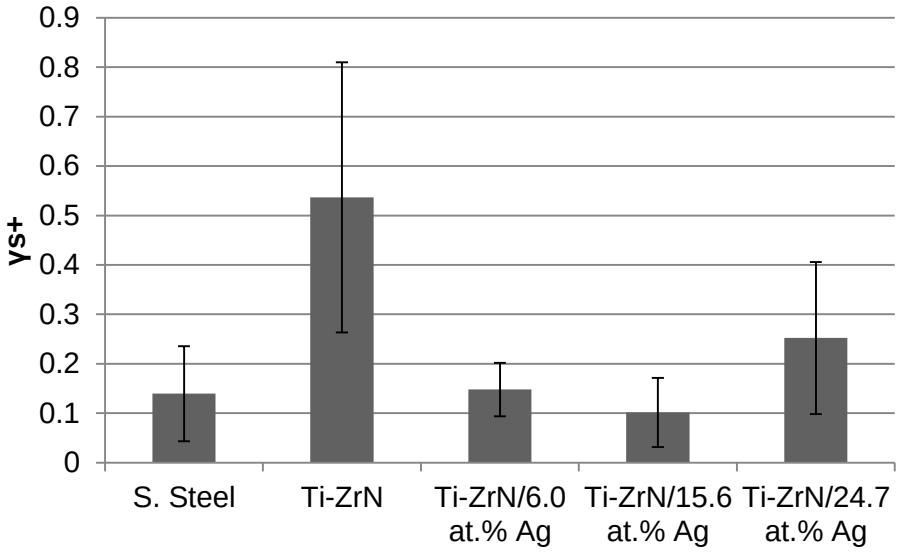

Figure 94: Average γ_s^+ positive charge values of the five investigated surfaces with a blood conditioning film. The values increased from 0.14 from stainless steel to 0.54 for Ti-ZrN and then decreased for the silver containing coatings with the 15.6 at.% Ag displaying the lowest value at 0.10.

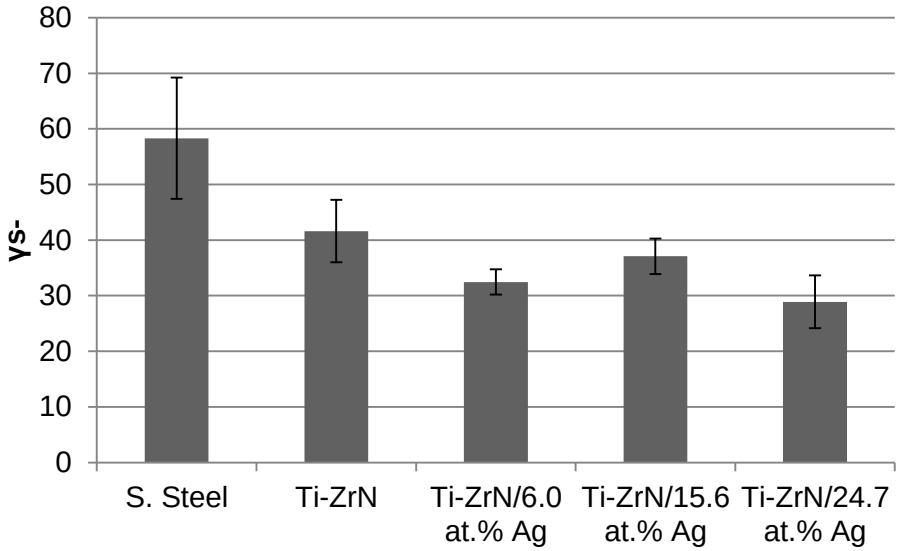

Figure 95: Average γ_s^- negative charge values of the five investigated surfaces with a blood conditioning film. The values decreased from 58.32 displayed by stainless steel and a decreasing trend, similar to the ΔG_{iwi}, was observed, with the 24.7 at.% Ag displaying the lowest value of 28.9. The stainless steel possessed a significantly higher value than the coated samples and no significant difference was observed between the coated samples.

7.3.3 Microbial Adhesion to Hydrocarbons (MATH) Blood Plasma Conditioning Film

Microbial adhesion to hydrocarbons (MATH) was undertaken on the bacterial cells following exposure to human blood plasma. Both *S. aureus* and *S. epidermidis* displayed the highest affinity for chloroform, followed by hexadecane (Figure 96), however, a lower value was demonstrated than was seen in the MATH assay without blood plasma present (Figure 85; Page 204). The results showed that the *S. aureus* was still more hydrophobic than *S. epidermidis*, which tended to display hydrophilic properties. Both *S. aureus* and *S. epidermidis* demonstrated electron donating properties.

7.3.4 Nitro Tetrazolium Violet Assay: Blood Conditioning Film

Following the nitro tetrazolium violet assay in the presence of a blood conditioning film it was demonstrated that the presence of blood reduced the contact kill efficacy of the Ti-ZrN/Ag nanocomposites. For *S. aureus* the least efficacious surface was the Ti-ZrN/24.7 at.% Ag at 20 (19.5) respiring colonies per cm^2 and the most was 15 at.% Ag with 13 respiring colonies per cm^2 (Figure 97). *S. epidermidis* also displayed a reduced antimicrobial effect in the presence of a conditioning film. The highest number of respiring colonies was calculated for both stainless steel and Ti-ZrN/6.0 at.% Ag and the most efficacious surface was Ti-ZrN/24.7 at.% Ag, with three respiring colonies per cm^2.

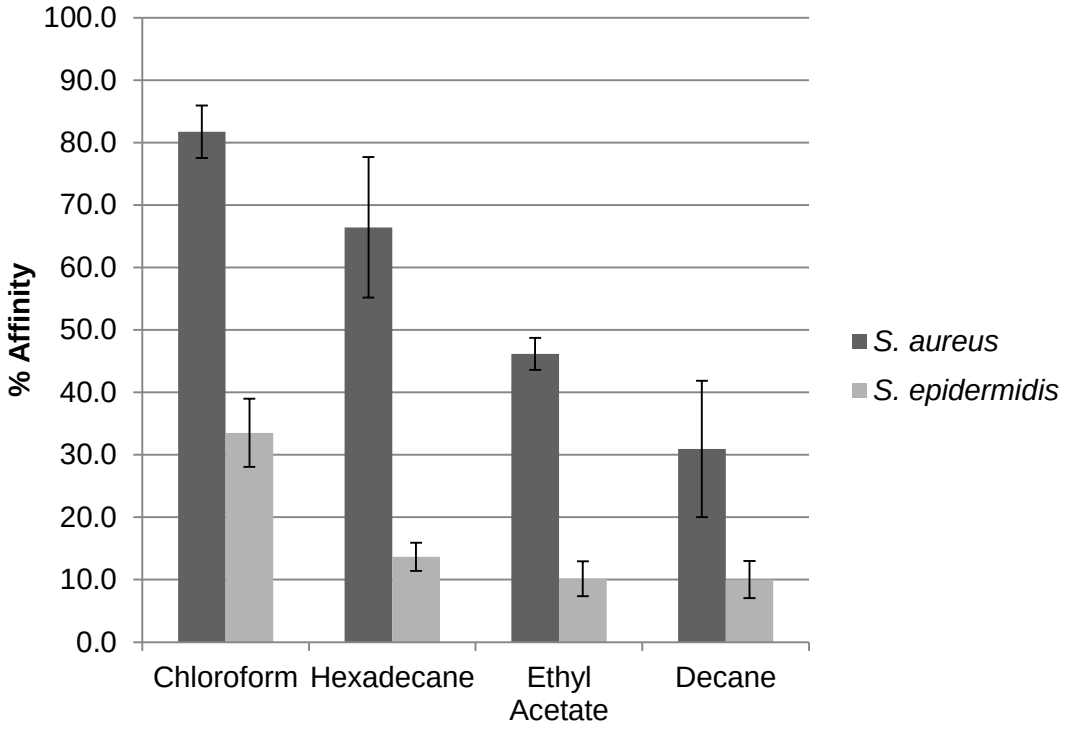

Figure 96: MATH assay percentage affinity of bacterial cells to the hydrocarbons following a human blood plasma rinse to subject the bacterial cell surfaces to a conditioning film demonstrating that *S aureus* was more hydrophobic than *S. epidermidis* and *S. aureus* was more of an electron donor than *S. epidermidis*. *S. epidermidis* was also an electron donor and displayed more hydrophilic properties.

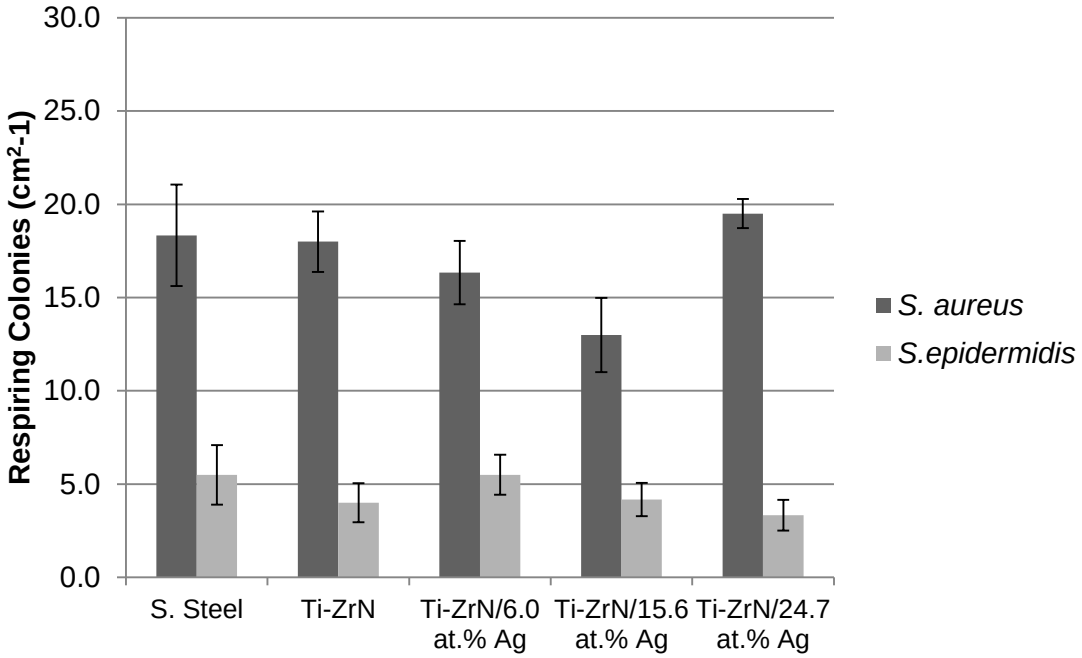

Figure 97: NTV assay in the presence of a blood conditioning following one hour contact time prior to agar overlay and incubation displaying the numbers of respiring colonies were higher than that of the unconditioned surfaces (Figure 80; Page 198). This demonstrates that the presence of a blood conditioning film reduced the antimicrobial effect of the silver.

7.3.5 JIS Antimicrobial Efficacy Assay: Blood Conditioning Film

Following testing of antimicrobial contact kill efficacy of the surfaces using the JIS standard at T0 the microorganisms demonstrated no significant difference ($p > 0.05$) between the surfaces. This suggested that no immediate antimicrobial action was observed and the blood conditioning film was inhibiting this effect. The Ti-ZrN/15.6 at.% Ag recovered the least microorganisms for *S. aureus* and the second least for *S. epidermidis* over pure Ti-ZrN (Figure 98). Following 24h exposure to the surfaces, at 37ºC in humid conditions there was a decreasing trend throughout the surfaces in terms of recovered microorganisms. The *S. aureus*, in contrast to T0, were recovered in lower numbers than the *S. epidermidis* and the Ti-ZrN recovered less cells than the stainless steel and decreased for the 6.0 at.% Ag and consequently the 15.6 at.% Ag (Figure 99). However, the Ti-ZrN/24.7 at.% Ag was not the most efficacious out of the silver coatings, but this coating had demonstrated different surface properties in comparison to the other two silver coatings. The *S. epidermidis* displayed a similar trend to the *S. aureus*, decreasing in recovered viable cells as the silver content increased, decreasing in antimicrobial efficacy on the 24.7 at.% Ag coatings. The *S. epidermidis* displayed more resilience surviving on surfaces over time in the presence of a conditioning film in comparison to the coating surfaces in absence of a conditioning film (Figure 84; Page 202). Ti-ZrN/24.7 at.% Ag did not display the best antimicrobial effects, suggesting that the amount of silver did not solely contribute to the efficacy of the surfaces.

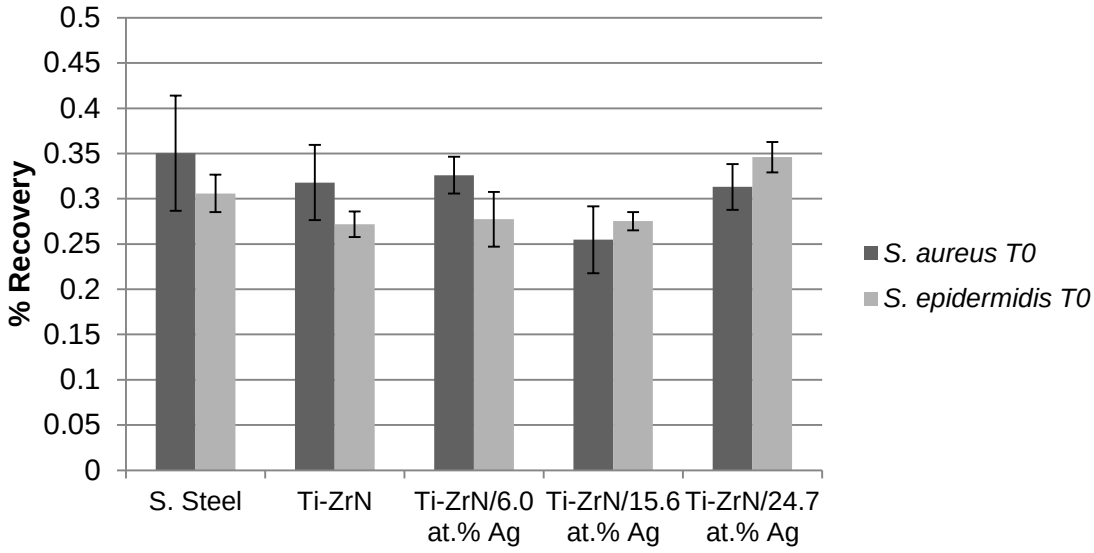

Figure 98: JIS method with a blood conditioning film displaying the percentage recovery of *S. aureus* and *S. epidermidis* at T0. Both microorganisms displayed no significant (p >0.05) decrease in viability throughout the five surfaces, suggesting that no antimicrobial action was observed.

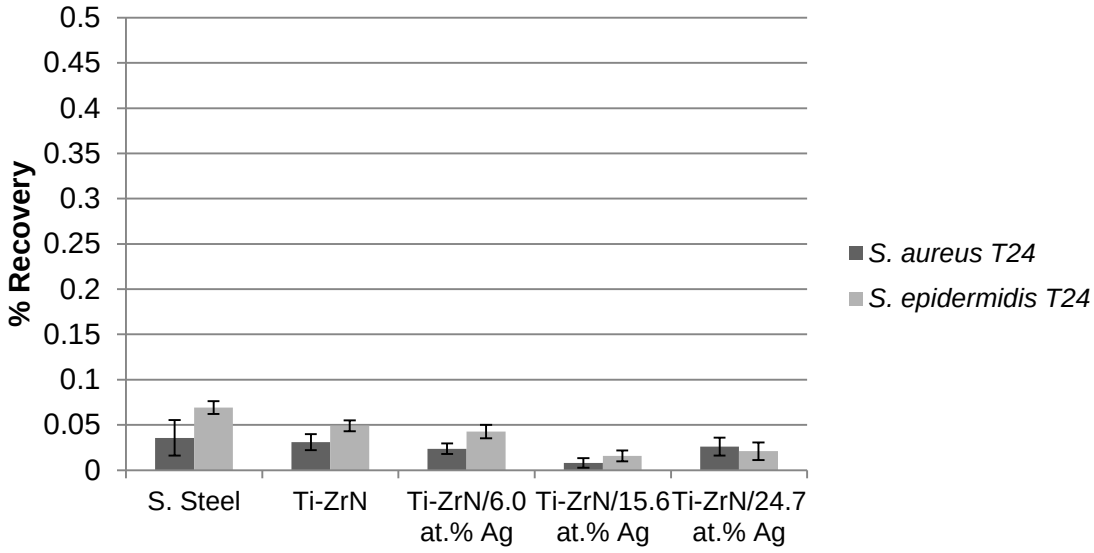

Figure 99: JIS method with a blood conditioning film displaying the percentage recovery of *S. aureus* and *S. epidermidis* at T24, demonstrating an antimicrobial effect on the silver containing coatings over the surfaces containing no silver.

7.4 Discussion

Characterising the coatings in the presence of a conditioning film was beneficial towards understanding how the biomaterial would perform *in vivo*. Replicating bodily fluids and temperature along with a high humidity during the JIS assay gave a replication of the fixation pin inside the body, whereas the NTV assay with blood already dried to the surface in room temperature conditions, replicated the outside of the body where the pin exits the wound.

The microtopography of the surfaces was assessed in the presence of a blood conditioning film. It was demonstrated that the surfaces had lost the topography characteristics of the 316L stainless steel and displayed topographies possessing circular pits across the surfaces. These pits were observed on the coated samples, but not on the stainless steel, suggesting that the stainless steel surface properties altered the drying characteristics of the blood. The pits observed resembled what could potentially be the outline of red blood cells on the surfaces; deep pits were also observed which suggested that when the blood dried on the surfaces the blood had created the pits (air pockets) during drying. Thus, it may be suggested that this alteration in topography could have the potential to retain more microorganisms on the surface. Further investigation into this could be undertaken by performing retention assays on the conditioned surfaces in comparison to the unconditioned surfaces.

The surface chemistry altered the characteristics of the conditioning film. This could be related to the type of bonding the conditioning film and substratum possess when adsorption occurs. The type of bond could vary between the different surface chemistries; ceramic bonds between the stainless steel or ZrN and blood, due to the oxide layers, however the Ti-ZrN/Ag surfaces presents metallic silver particles on the surface thus it may be that more metallic bonding at the surface resulted in the difference observed in the difference observed in the conditioning film adsorption.

The average height values of the blood conditioning film on the surfaces demonstrated that the Ti-ZrN possessed the highest value (579.4 nm), due to the large valleys in the profile, however the silver containing coatings and stainless steel displayed similar height values in terms of microtopography, (between 64.8 nm and 164.9 nm). In terms of microbial dimensions the depth of the features on the surface would not solely be responsible for creating increased bacterial efficacy. However, the physical size of the surface features of the blood conditioning film alone would not be the only component responsible for bacterial retention. The components of the blood as a conditioning film, for example proteins such as albumins, globulins and fibrinogen may act as organic components for the microorganisms to attach to, potentially increasing bacterial retention (Schultze and Heremans, 1969).

Comparing the roughness values of the surfaces with the physicochemical properties displayed the effect of topography on surface physicochemistry and the properties of a conditioning film adsorbed onto the substratum. An increase in average depth of the microtopographical features of an unconditioned surface led to the surface being more hydrophobic, demonstrated on stainless steel and Ti-ZrN/15.6 at.% Ag. Larger average widths in the surface microtopography caused the conditioning film to display hydrophilic tendencies and an increase in average depth values led to more hydrophobic surface properties on the conditioning film surface. No relationship between the surface topography and the γ_s surface free energy was observed. However, the Liftshitz van der Waals values demonstrated an inversely proportional trend to the average height and a proportional trend towards the width size for the Ti-ZrN/Ag coatings. In contrast to the γ_{LW}, the γ_{AB} Acid-Base values demonstrated a proportional trend with the average height values of the Ti-ZrN/Ag surfaces. However, in agreement with the γ_{LW} values, an inversely proportional trend between the average width values and the acid base values of the surfaces was seen, that suggested an increase in feature width size lead to a decrease in acid base value. The electron

accepting properties of the surfaces were all proportional to the trend of the average height values and the electron donating properties also displayed a proportional trend but towards the average width values. These results demonstrated that the width and height of the unconditioned surface features altered the physicochemical properties of the adsorbed conditioning film surface. A trend was observed between stainless steel and Ti-ZrN and then a separate trend was seen throughout the Ti-ZrN/Ag coatings. These were either proportional or inversely proportional to the surface feature heights and widths of the surfaces. The importance of this is that the ability to alter the surface properties of a conditioning film could be achieved by altering the substratum topography characteristics, therefore may lead to a more hydrophilic surface, with anti-adhesive properties. This would provide desirable surface properties in external fixation pins, potentially helping reduce the retention of bacteria on the surface as well as the antimicrobial efficacy of the Ti-ZrN/Ag for when the bacteria did become attached to the surface.

There were no linear increasing or decreasing trends observed in the surface topography between the coatings before and after addition of the conditioning film. The nanotopography and microtopography disappeared and the average peak height value was 10X higher with the addition of the conditioning film, the average width value however did not alter significantly. In future work a differentially stained retention assay could be undertaken to calculate the retention characteristics of the bacteria to the surfaces in the presence of a blood conditioning film.

In the previous chapters the surfaces were shown to display an antimicrobial effect, therefore the efficacy of the surfaces in the presence of a blood conditioning film was investigated for the NTV assay and JIS assay. The NTV assay replicated a situation where an external fixation pin would have been conditioned and the adsorbed material would have potentially affected the hygienic status of the pin outside of the body, where the blood would have dried onto the surface. When performing the NTV assay,

prior to adding the bacterial suspension, the blood was applied to the surface and dried. This may replicate conditions when the pin had been inserted in a sterile operating theatre, where the pin adsorbs blood and bodily fluid from the procedure. Following the procedure the pins will then be exposed to microorganisms in the environment. Following the NTV assay, in the presence of a dried blood conditioning film, the results demonstrated that the antimicrobial properties were decreased by the blood and reduced the antimicrobial surface efficacy. The Ti-ZrN and stainless steel acted similarly and the Ti-ZrN/Ag surfaces acted in a similar antimicrobial trend as the physicochemical properties. The decrease in antimicrobial efficacy suggested that the dry blood was protecting the bacterial cells. Marginally, the Ti-ZrN/15.6 at.% Ag was the most effective against the *S. aureus* and the Ti-ZrN/24.7 at.% Ag against *S. epidermidis*.

The JIS standard assay displayed different results. The samples taken at T0, under wet conditions, straight after inoculation, were found to have an enhanced effect (1 log difference) in the presence of the conditioning film (6.3.8; Page 201). Following 24 hours incubation in humid conditions (wet blood conditioning film) at 37 ºC, there was a significant reduction in recovered viable bacteria; a factor of 10 less *S. epidermidis* and a factor of 10 less *S. aureus*, in the presence of the conditioning film. Throughout the five surfaces a reduced recovery rate was seen for both the *S. aureus* and *S. epidermidis* on the 15.6 at.% Ag and 24.7 at.% Ag coatings, suggesting that an antimicrobial effect was observed for these two surfaces. The 24.7 at.% silver coating, however, did not give the greatest efficacy, suggesting that the content of silver added to the coatings is not the sole contributor to the antimicrobial efficacy of the silver and that perhaps the size and shape of the silver particles affect it. The benefits of using the JIS method to evaluate antimicrobial efficacy of the surfaces in the presence of a conditioning film was that the humid environment, temperature and blood for the conditioning film replicated similar environments of an external fixation pin inside of the

body. The length of bacterial contact time with the surfaces was also longer than that of the NTV assay, and therefore gave an insight into what antimicrobial activity occurs over a 24 hour time span. The JIS results suggested that the presence of a wet blood conditioning film enhanced the antimicrobial activity of the surface in comparison to a dried blood conditioning film. This related to the statements in literature that silver has to be in the presence of moisture to ionise and display antimicrobial properties (Klasen, 2000, Dunn and Edwards-Jones, 2004, Edwards-Jones, 2009, Sandstrom, 2011) Further work could include performing a series of investigations involving repeated fouling and cleaning of the same test coupons to replicate cleaning of a fixation pin *in vivo*. However, the dry blood on the surface of the Ti-ZrN/Ag surfaces protected the bacterial cells, therefore within a pin tract the pin interface would require regular cleaning to prevent infection or keep the surrounding area moist so that the silver is ionised and produce an antimicrobial kill. This result would require further investigation into the antimicrobial efficacy enhancement of the Ti-ZrN/Ag surfaces in the presence of a wet conditioning film.

Human blood plasma was used to replicate some of the components the bacteria would be expected to encounter inside the body such as albumin, fibrinogen, polysaccharides and lipids. Using the MATH assay in this way demonstrated how the presence of blood plasma altered the surface properties of the bacterial membrane. It was found that the *S. aureus* displayed a lower hydrophobicity than when the test was performed in the absence of the blood plasma conditioning film and the *S. epidermidis* displayed a higher hydrophilicity. There are a number of different theories regarding which of the surface physicochemical properties of substrata affect cell-substratum retention. It is generally agreed that when the ΔG_{iwi} was negative (< 0) the surface favoured microbial adhesion whereas when the ΔG_{iwi} was more than 0 adhesion to a surface was largely unfavourable (Bos *et al.*, 1999). It has also been stated by Katsikogianni et al. (2004) and Morra and Cassinelli (1998) that a higher

hydrophobicity of either the bacterial surface or the substratum surface resulted in an increase in bacterial attachment to the surface, due to the surrounding water being more easily displaced between the interface, allowing molecular interactions to occur more freely. This work is in agreement with Bos *et al.* (1999), Morra and Cassinelli (1998) and Katsikogianni and Missirlis (2004) in that *S. aureus*, possessing a more hydrophobic cell surface than *S. epidermidis*, displayed a preference for hydrophobic surfaces, whilst the more hydrophilic *S. epidermidis* preferred the more hydrophilic surfaces.

When bacterial strains are tested *in vitro* there are not any alterations in environmental dynamics that would be present *in vivo*. Accurate surface free energies of bacterial cells are difficult to obtain due to the complex surface chemistries and differing conditions that the cells will undergo *in vivo*. Thus, organic material encountered, such as surrounding polysaccharides, conditioning films, cell surface proteins, co-adhesion and bacterial physical change within the bacteria have the potential to affect the adhesion to an extent that prediction is almost impossible by calculating physicochemical models. However, Katsikogianni and Missirlis (2004) stated that prediction of 'well defined colloidal particles' upon the surfaces when investigating bacterial adhesion is important to create a base to which other biological factors can be added.

7.5 Concluding Remarks

Following the addition of a blood conditioning film to the surfaces of the Ti-ZrN and Ti-ZrN/Ag coatings it was demonstrated that the surface properties and antimicrobial properties were both affected. The blood conditioning film altered the microtopography of the surfaces from the regular polishing scratches of the 316L stainless steel to irregular pits of what appeared to be the outline of the red blood cells on the surface. The addition of a conditioning film altered the microtopographical features. The depth

of the features remained relatively similar. The average widths were all lower than that of the stainless steel and the addition of silver increased the average width value. The conditioning film changed the coatings from hydrophobic surfaces (negative ΔG_{iwi} values) to hydrophilic/partially hydrophilic surfaces (positive ΔG_{iwi} values). Following the MATH assay, reduced affinity towards the hydrocarbons was observed for both of the microorganisms demonstrating *S. aureus* was less hydrophobic in the presence of a conditioning film and *S. epidermidis* became more hydrophilic. Both microoorganisms displayed electron donating properties.

The addition of a conditioning film to the Ti-ZrN/Ag coatings reduced the short term antimicrobial efficacy. No contact kill was observed in the NTV assay following one hour contact time. There was no kill observed towards the microorganisms on the JIS assay at T0 but following 24 hours incubation there was reduced recovery on the silver containing coatings than the Ti-ZrN and stainless steel results. No antimicrobial leaching was observed in the zones of inhibition assays.

The addition of a conditioning film was used to replicate organic constituents that would adsorb to a biomaterial surface *in vivo* and the effect that would have on the surface properties and antimicrobial efficacy of the Ti-ZrN/Ag coatings.

The underlying topography of the surfaces were found to have an effect on the physicochemical properties of the adsorbed conditioning film. The surface chemistry also affected the adsorption of the conditioning film, with differences in surface morphology between the stainless steel and ZrN in comparison to the ZrN/Ag coatings. The antimicrobial mechanisms of the surfaces would need to be further investigated over longer periods of time and potential further work could include incubation periods followed by standardised cleaning assays used for external fixation pin care and inoculation cycles to test long term efficacy of the surfaces.

8 Quantifying Bacterial Dispersion using Multifractal Analysis (MATLAB)

8.1 Introduction

This chapter investigates the proof of concept of mathematical analysis programmes previously designed and created by Dr Stephen Lynch. The following work displays its use in providing quantitative descriptors of the dispersion of retained bacteria on surfaces using multifractal analysis. I would like to thank Dr Lynch for his time and patience throughout our collaboration and for providing the means and access to the software and programmes for such work to be performed.

Many engineered surfaces used in both medical and industrial situations present, either by design or due to wear, topographical surface features of different sizes and shapes that may be of regular or irregular dispersion across the surface. The topography of a surface is known to be one of the factors that contribute towards increased microbial contamination and fouling (Whitehead and Verran, 2007). The topography of any surface will take the form of a series of peaks and troughs which may vary in profile and dispersion, described to some extent in this investigation by R_a, *RMS, Average height* and *Max Range* (Z_{max}) parameters. As discussed in earlier chapters surface roughness may enhance microbial retention because of the increased surface area available for colonisation by increasing the microorganism-material interface and, in some cases, protect from shear stress (Timperley *et al.*, 1992, Quirynen and Bollen, 1995, Cooper *et al.*, 2011). It has been shown that the area of contact between a microorganism and the surface influences the rate and pattern of cell retention (Edwards and Rutenberg, 2001, Whitehead *et al.*, 2005b, Whitehead *et al.*, 2008). There has also been speculations that surfaces with features of microbial dimensions may retain microorganisms in higher numbers than smoother or rougher surfaces, and the cells tend to reside in these surface features (Tebbs *et al.*, 1994, Flint *et al.*, 2000, Verran *et al.*, 2010) Bacterial cells possess a hard peptidoglycan wall and having a characteristic shape impedes the interaction at a bacterium - surface interface

when the topographical features are less than the bacterial dimensions. Therefore the premise is that bacteria will be unable to interact with nano scale surface topography and would 'sit' on top of the peaks with less surface contact than usual. However, if the bacteria possess cell membrane appendages such as fimbriae, flagellae and pili, which usually have diameters of less than 10 nm and varying lengths of up to multiple microns, these can play an important role in bacterial attachment to surfaces with nanotopographical features (Anselme *et al.*, 2010).

Bacterial adhesion at a nanoscale is not yet fully understood, however bacteria, in contrast to eukaryotic cells have been shown to have the ability to adhere to an abiotic surface from the physicochemical interactions of both the bacterial cell wall and the surface interface (Anselme *et al.*, 2010). The results obtained from previous chapters (Chapters 5 and 6) demonstrated that *S. aureus* was affected by the microtopography of the surfaces; the largest S_a and S_v values retained the highest number of microorganisms. The *S. epidermidis* did not appear to be affected by the microtopography but displayed trends towards hydrophobicity and retention. The *S. epidermidis* cells displayed less hydrophobic properties than *S. aureus* and retained the most bacteria on the least hydrophobic surface (Ti-ZrN) and retained less microorganisms on the hydrophobic surfaces. The S. aureus cells display more hydrophobic cell surface properties and were also affected by differences in hydrophobicity (ΔG_{iwi}), the more hydrophobic the substratum surface, the more *S. aureus* cells were retained.

8.1.1 Calculating Bacterial Retention

Using microbiological retention assays (3.2.3; Page 91), the number of microorganisms or the percentage coverage of microorganisms retained on a surface can be assessed. This assay involves staining or fixing of the organisms, and visualization using a light, epifluorescent or scanning electron microscope in order to determine the number of cells per unit area, or the percentage of a surface covered by the cells (Pereni *et al.*,

2006, Huang *et al.*, 2010, Whitehead *et al.*, 2010, Whitehead *et al.*, 2011). Although the coverage of cells retained can be determined quantitatively, the density and dispersion of cells across the surfaces tends to be described qualitatively. Some descriptors of size of cell aggregates can be employed (Verran *et al.*, 1981), but a measure of the effect of the underlying surface morphology on the arrangement of cells has yet to be defined numerically.

Quantitatively describing the distribution of bacterial cells on a surface is beneficial for many reasons. The distribution of bacterial retention to a surface may specifically relate to surface hydrophobicity or roughness (Faille *et al.*, 2002). With a lack of methods to gather quantifiable data on bacterial density and dispersion, a direct comparison of the effect of such surface parameters on cell retention is difficult. The use of such quantitative methods has the potential to further predict the effect of surface parameters on cell distribution and may enable further understanding of the influence between surface features and microorganisms.

8.1.2 Multifractal Analysis

Multifractal analysis has the potential to be an approach to gain numerical data on cell dispersion. A fractal is defined as an object that displays self-similarity under magnification and can be constructed using a simple motif (an image repeated on ever-reduced scales). Multifractals are a generalization of a fractal, where a single dimension is not enough to describe it. Instead, a continuous spectrum of dimensions is required. Although fractals are idealized images that cannot exist, multifractal objects can be attained in the real world. The concept of multifractals was first introduced for turbulence (Mandelbrot, 1974) and then for the onset of chaos in a forced Rayleigh-Bénard system (Jensen *et al.*, 1985) and was then followed by the work of Halsey et al., (1986), on fractal measures.

There is an ongoing surge of interest in multifractal analysis for describing both artificial and physical objects and concepts have been increasingly applied across a wide range of scientific disciplines. Examples from the literature include; characterisation and elemental dispersion of sedimentary rocks (Block *et al.*, 1991), the dispersion of stars and galaxies in the universe (Coles and Jones, 1991), the theory and observation of rain and clouds (Tessier *et al.*, 1993), human heartbeat dynamics (Ivanov *et al.*, 1999), ageing and disease relations in physiology (Goldberger *et al.*, 2002), predicting the physical characteristics of plastics (Mills *et al.*, 2002, Mills *et al.*, 2005) and the detection of breast cancer (Li *et al.*, 2007). Kropp et al. (1997) carried out a restricted multifractal analysis of microbially induced magnesium calcite formation in recent tidal sediments using binary elemental dot maps. The abundance of multifractal analysis use in research shows that the potential for use in microbiological applications is viable.

8.1.3 Aim of the Investigation

The aim of the investigation was to prove the concept of using MATLAB as a tool to gain a quantitative value to describe the density and dispersion of retained bacterial cells on stainless steel, titanium-zirconium nitride (Ti-ZrN) and titanium-zirconium nitride/silver (Ti-ZrN/Ag) surfaces. Further, the MATLAB data was used to determine if the differences in surface topography and feature size had an effect on microbial density and dispersion.

8.2 Methods and Materials

Surfaces and coatings were produced following the method from Chapter 5 (Page139), as well as surface characterisation techniques (Chapter 5.3.4.4; Page 164, Chapter 5.3.5, Page 166, Chapter 5.3.6; Page 173) and the microbiological retention assay (Chapter 3.2.3; Page 91).

8.2.1 Multifractal analysis

To illustrate the properties of typical multifractal spectra, multifractal datasets were computed for each image using MATLAB®. Using the program, matrices (datasets) of size 512 x 512 pixels were computed by overlaying the given motifs (size of boxes that are used to analyse the image) one on top of another, so that upon the first iteration the image was split into a 4 x 4 pixel grid matrix, upon the second iteration a 8 x 8 pixel matrix was formed, until completion (256 x 256 pixels). Prior to analysis using the MathWorks® Image Processing Toolbox®, the datasets were converted into grayscale images (a value of zero would give black on this scale and a value of one would give white). The numerical $f(\alpha)$ spectra were computed and boxes of sizes: 4, 8, 16, 32, 64, 128 and 256 pixels, were used to fully cover the datasets in the image. Low magnification images (x 400) were taken of the retained bacteria on the Stainless steel, Ti-ZrN, Ti-ZrN/6.0 at.% Ag, Ti-ZrN/15.6 at.% and Ti-ZrN/24.7 at.% Ag, because higher magnification images did not display enough bacteria to establish a number for dispersion patterns. The $f(\alpha)$ curve is a way to demonstrate a multifractal spectrum, from the computed data a curve is produced utilising the values f against the (α) values (Figure 103). From the $f(\alpha)$ curves, values were obtained that denoted numerical values of the bacterial density and dispersion (Appendix 1; Page **Error! Bookmark not defined.**).

A resulting $f(\alpha)$ curve was generated. From this the Δαas was calculated (Appendix 1; Page **Error! Bookmark not defined.**). The $f(\alpha)$ curve may be either;

- Symmetric if the value generated is (= 1)
- Left skewed if the value generated is (> 1):more homogenous dispersion
- Right skewed if the value generated is (< 1): more heterogeneous dispersion

The maximum Y value of the $f(\alpha)$ curve (α = 0), gave a numerical value for the density of the cells on the surface.

8.3 Results

8.3.1 AFM analysis (nanotopography)

AFM images revealed that an increase in silver concentration led to an increase in the frequency of larger peaks. Following SEM backscattered electron detection (Results in Chapter 5; Page 153) it was determined that these outlying particles were particles of embedded silver protruding from the surface. The pure Ti-ZrN and stainless steel surfaces presented different surface morphologies. The addition of silver increased the depth of the features, but decreased the width. The valleys did not exceed 1µm in width, the approximate diameter of a *Staphylococcus* cell. This is reflected visually in the epifluorescent micrographs as none of the bacterial cells follow a linear pattern typically seen when the cells have resided in surface scratches (Figure 100 and Figure 101). None of the surface features exceeded heights of more than 150nm on the line profiles (Figure 56; Page 161) and the average max range only exceeded 150nm on the 24.7 at.% silver surface (Figure 56d; Page 161).

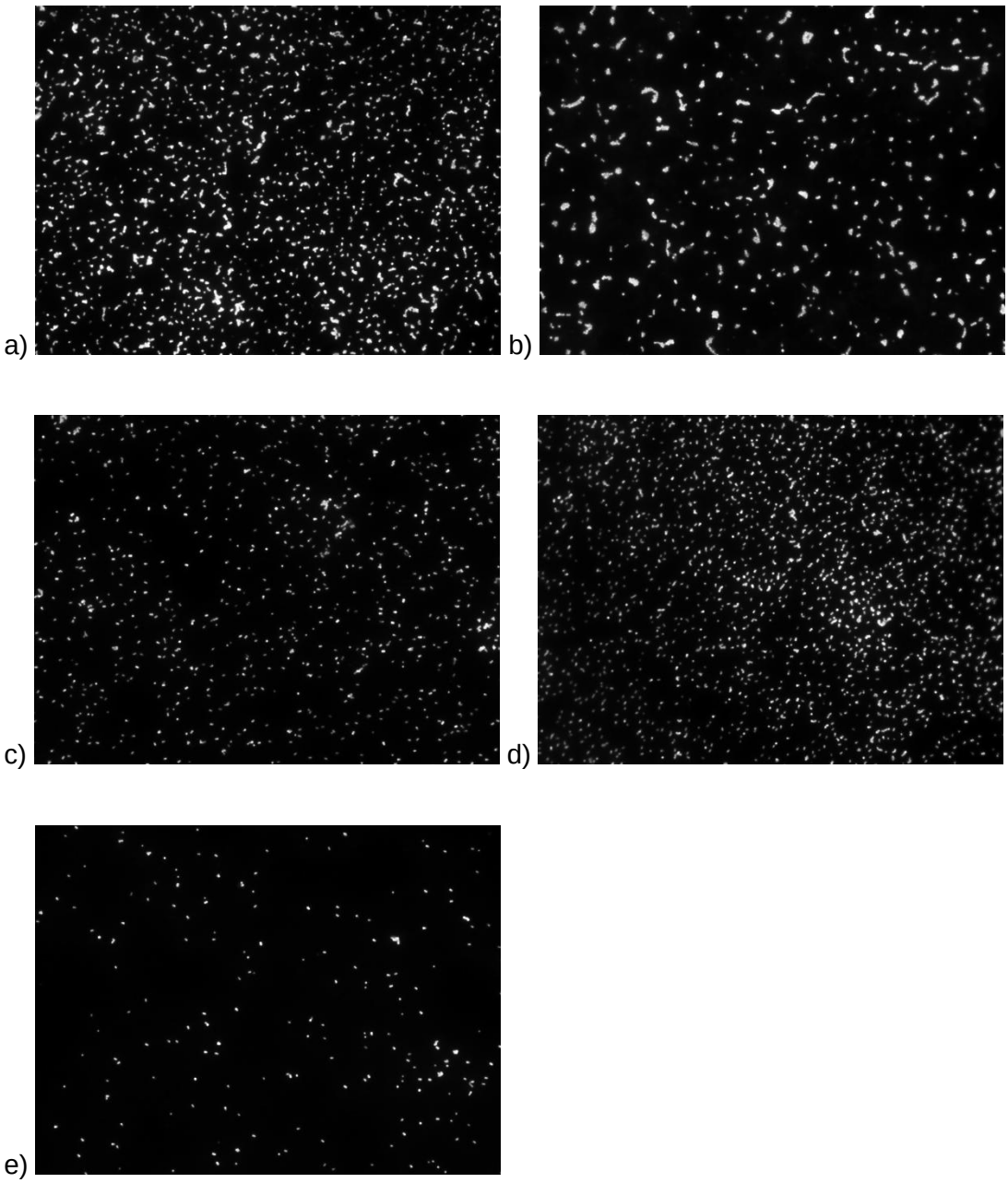

Figure 100: Epifluorescence images of retained *S. aureus* on a) Stainless steel, b) Ti-ZrN, c) Ti-ZrN/6.0 at.% Ag, d) Ti-ZrN/15.7 at.% Ag and e) Ti-ZrN/24.7 at.% Ag, demonstrating a visible difference in the densities and dispersion of the cells on the different surfaces.

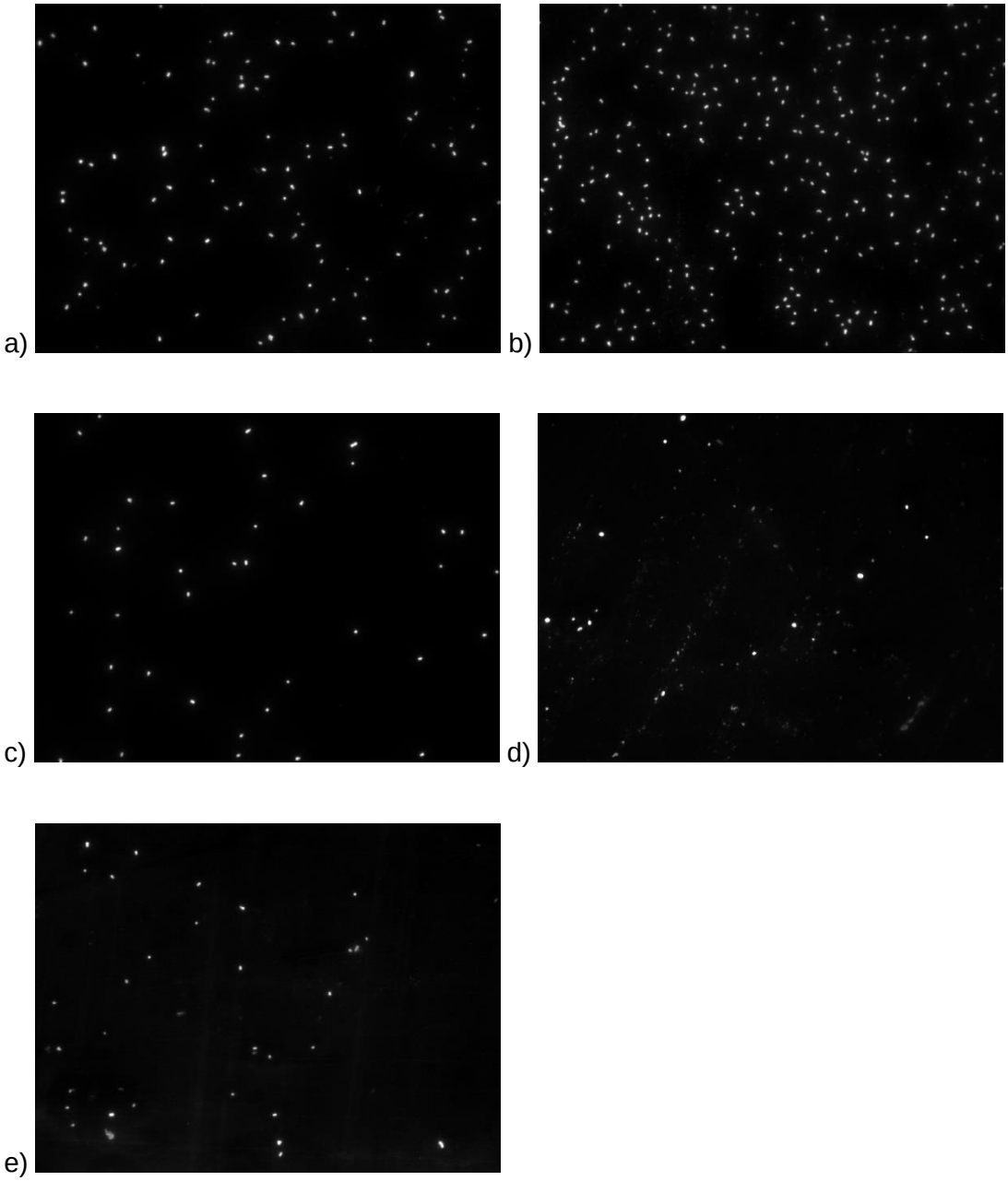

Figure 101: Epifluorescence images of retained *S. epidermidis* on a) Stainless steel, b) Ti-ZrN, c) Ti-ZrN/6.0 at.% Ag, d) Ti-ZrN/15.7 at.% Ag and e) Ti-ZrN/24.7 at.% Ag, demonstrating a higher density of cells retained on stainless steel and Ti-ZrN and similar dispersion patterns from the silver containing coatings.

8.3.2 Multifractal Analysis

8.3.2.1 Theory Results

Following multifractal analysis it was found that it was essential that the 'box sizes', covered the whole image and no pixels were excluded, otherwise the multifractal analysis would not function. Thus the images needed to be cropped to the required 512 x 512 pixels if they were of another dimension. In order to demonstrate how different data affected the motifs and the $f(\alpha)$ spectra, examples of modal data were demonstrated. These examples include data for motifs of; one value smaller than the other three quarters (Figure 102a), one value greater than the other three quarters (Figure 102b) and roughly equal values for all four quarters (Figure 102c). This data results in a right skewed $f(\alpha)$ multifractal (Figure 103a), a left skewed $f(\alpha)$ multifractal (Figure 103b) and a homogeneous $f(\alpha)$ multifractal, respectively (Figure 103c). In terms of cell distribution, this would denote a left skew, due to the majority of the image being densely covered with bacteria but with small areas of space (Figure 102a). The right skew would describe the cells being sparsely distributed but with a small, densely grouped area on the image (Figure 102b). The symmetrical curve denotes a sparsely distributed cell pattern with little to no grouping or very few, widely, regularly spaced cells on the surface meaning all values were approximately equal (Figure 102c). This leads to a narrow $f(\alpha)$ spectrum showing that the multifractal object is almost homogeneous; the object has almost the same dimension on all scales (Figure 103c). The theoretical (solid curves) and corresponding numerically computed ('+') multifractal $f(\alpha)$ spectra are displayed (Figure 103a-c) for the motifs shown (Figure 102 a-c). The f-alpha curve gives a measure of cell density.

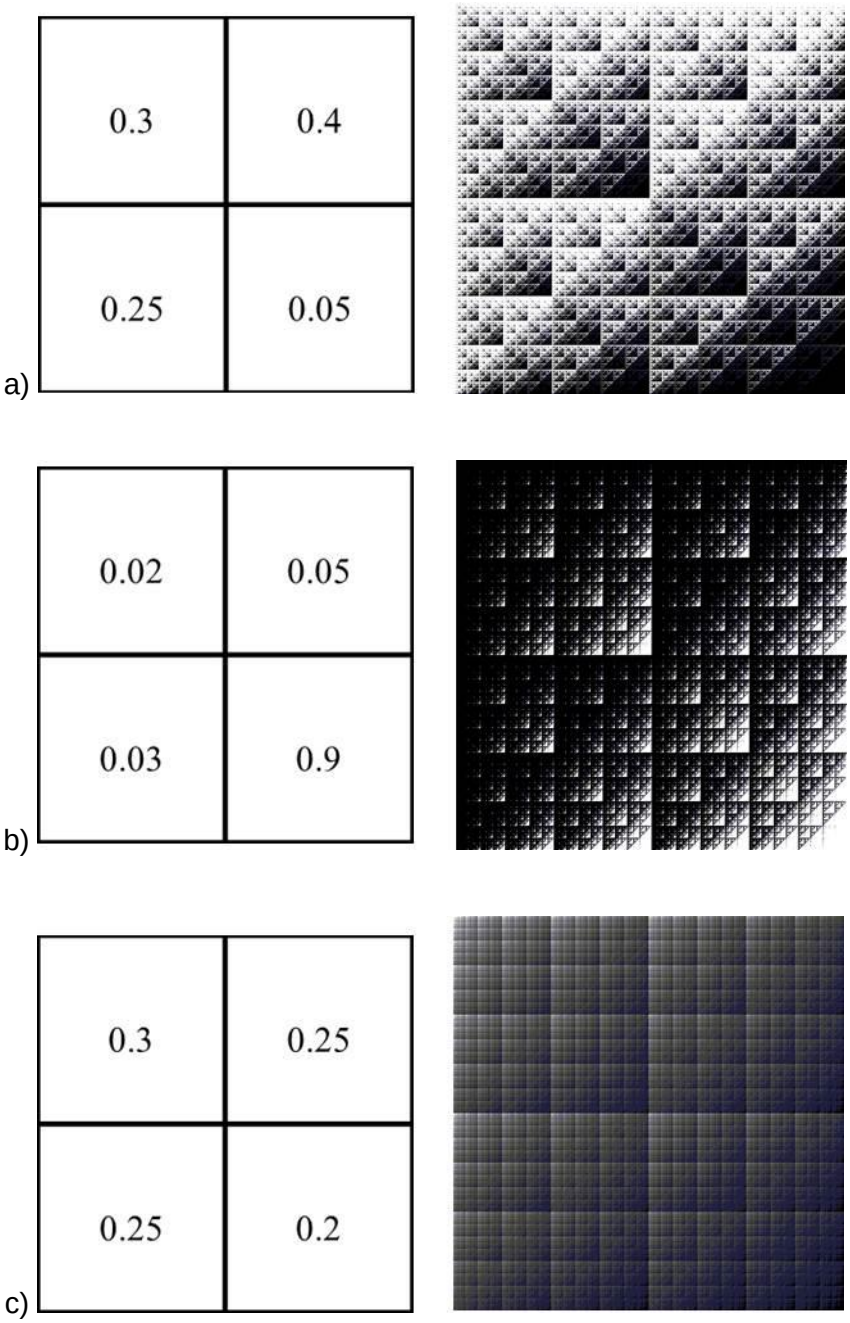

Figure 102: Multifractal motif examples. Theoretical and numerical singularity spectra for the multifractal generated with a) the motif with one value much smaller than the other three quarters, heterogeneous arrangement. b) The motif with one value much greater than the other three quarters, the most heterogeneous and c) The motif with similar values for all four quarters, the most homogeneous result.

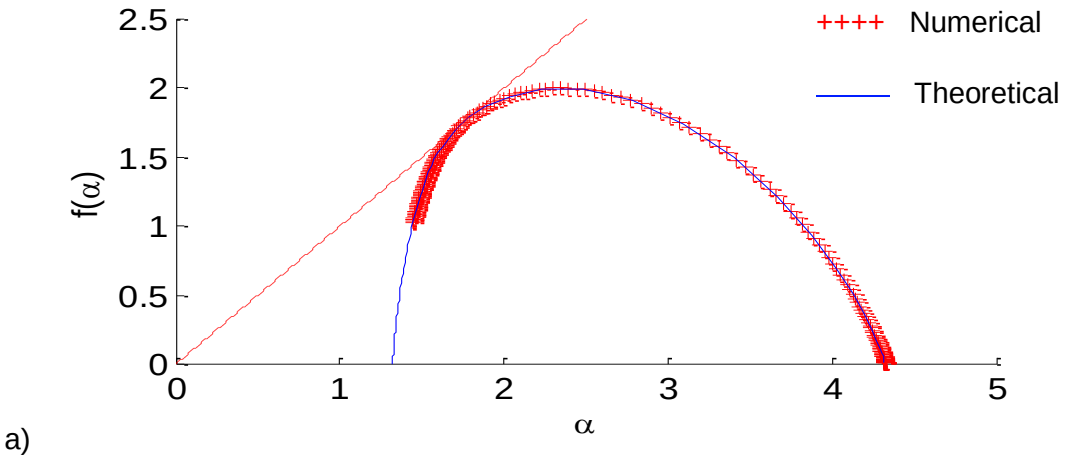

a)

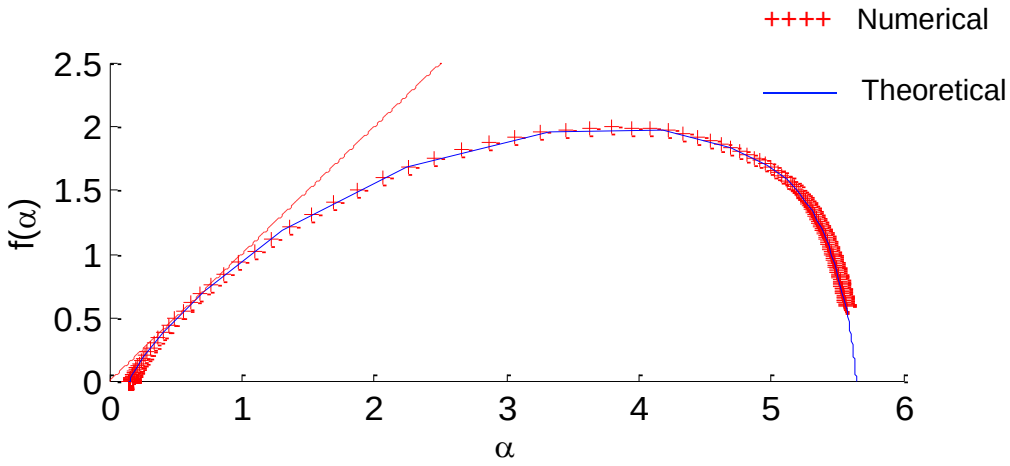

b)

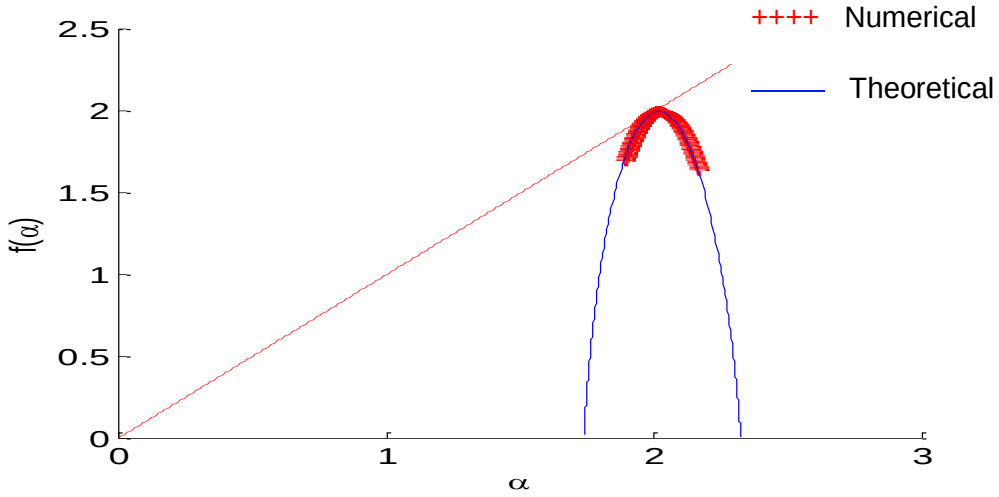

c)

Figure 103: $f(\alpha)$ curves displaying, a) right sided skewness, b) left sided skewness and c) symmetrical/homogeneous distributions.

Therefore the widths of the $f(\alpha)$ spectra indicate the heterogeneity or dispersion of the multifractal object. If the widths of the spectra are widespread this illustrates that these multifractal objects are more heterogeneous (Figure 103a and b). In fact, the multifractal generated by the motif (Figure 102b) is the most heterogeneous (value of approximately 5.5). The value in 'Figure 103b' is approximately 3 and the value in 'Figure 103c' is approximately 0.5.

8.3.2.2 Multifractal Analysis of Bacterial Dispersion

Following multifractal analysis on the bacterial retention images, numbers extracted from the $f(\alpha)$ curves created were calculated and given in the results as an average of dispersion from 10 readings ± the standard deviation (Figure 104). The dispersion of *S. aureus* and *S. epidermidis* on all of the surfaces remained similar on all images. The results obtained from the $f(\alpha)$ curves demonstrated for Ti-ZrN/15.6 at.% silver displayed the lowest dispersion for both microorganisms, however this was not significantly different to the dispersion of microorganisms seen on the other surfaces.

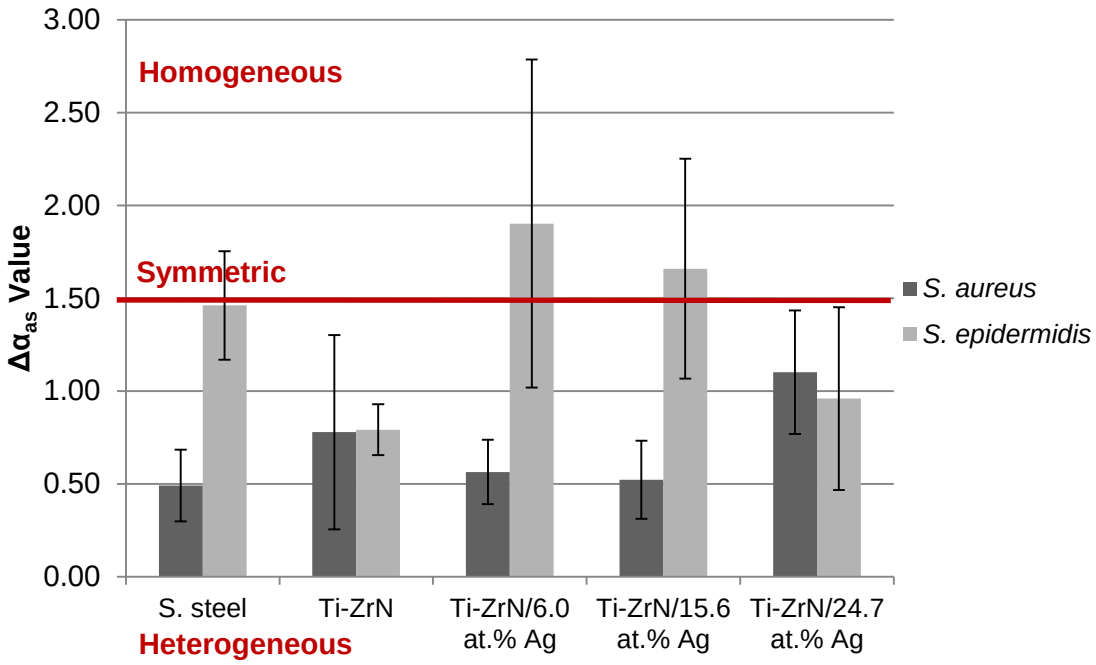

Figure 104: Δαas values of *S. aureus* and *S. epidermidis* on the surfaces demonstrating the difference in homogeneity and heterogeneity between the two microorganisms on the different surfaces. The *S. aureus* was primarily of heterogeneous spread with the exception of 24.7 at.% silver. The *S. epidermidis* was more homogeneous for the majority with the 6.0 at.% silver surface being the most homogeneous and became more symmetric as the silver content increased.

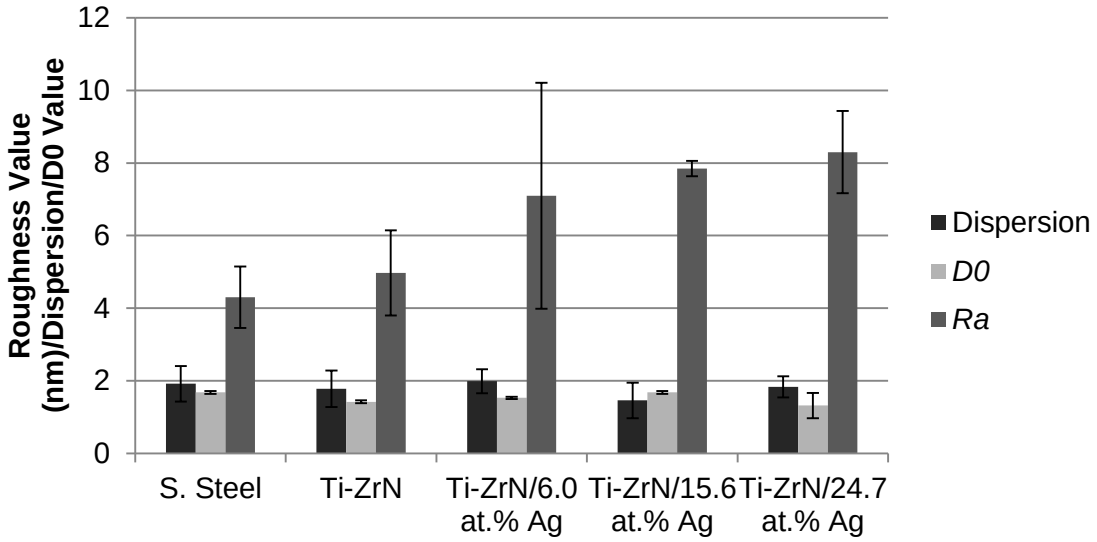

Figure 105: A plot of dispersion and density of *S. aureus* in comparison with the R_a of the five surfaces, demonstrating an increase of R_a throughout the coatings but no increase in dispersion or density (D0).

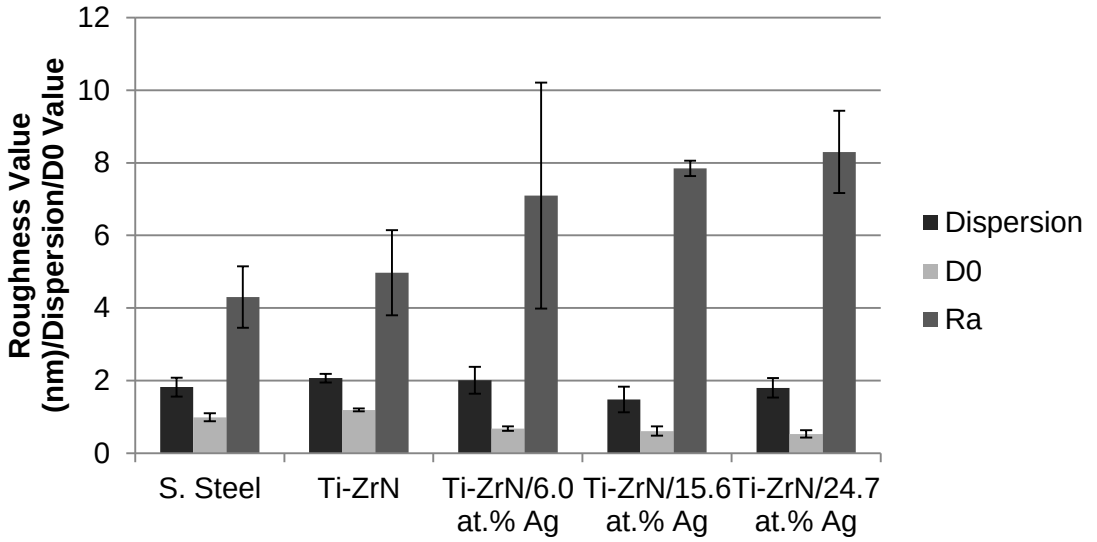

Figure 106: A plot of dispersion and density of *S. epidermidis* in comparison with the R_a of the five surfaces, demonstrating an increase of R_a throughout the coatings but no increase in dispersion or density (D0).

8.3.3 Percentage Coverage MATLAB vs Cell-F

The results taken from the multifractal analysis proved to be successful in quantitatively describing the dispersion of the retained bacterial cells on the five different surfaces. A comparison between the percentage coverage from the microscope program (Cell-F) and MATLAB was also made. The methods for calculating the cell coverage was different for the two programmes due to differing cell detection techniques (Figure 107). The MATLAB program picked up more cells and in turn calculated a higher surface coverage. The binary and original images were also compared side by side to check for consistency. This is not available on the microscope software analysis and works through a user defined threshold of the brightness phase. This may be the reason why the percentage coverage was calculated significantly lower ($p<0.05$) than the MATLAB interpretation. MATLAB can omit certain sized particles, or areas of a certain greyscale, out of the binary image, of which all of the measurements are taken from, in comparison to Cell-F, which works straight from the original greyscale image. The differences between the number of cells on the surfaces for *S. aureus* and *S. epidermidis,* to compare the results of MATLAB and Cell- F were demonstrated (Figure 107a). *Staphylococcus aureus* showed a difference in retention based on surface chemistry and not roughness. This can be determined because the ZrN and Stainless steel had similar roughness parameters, however the ZrN retained significantly less ($p < 0.05$) bacteria. Further, the ZrN/25at.% Ag was the roughest, yet it displayed the lowest coverage out of the five surfaces for the MATLAB detection.

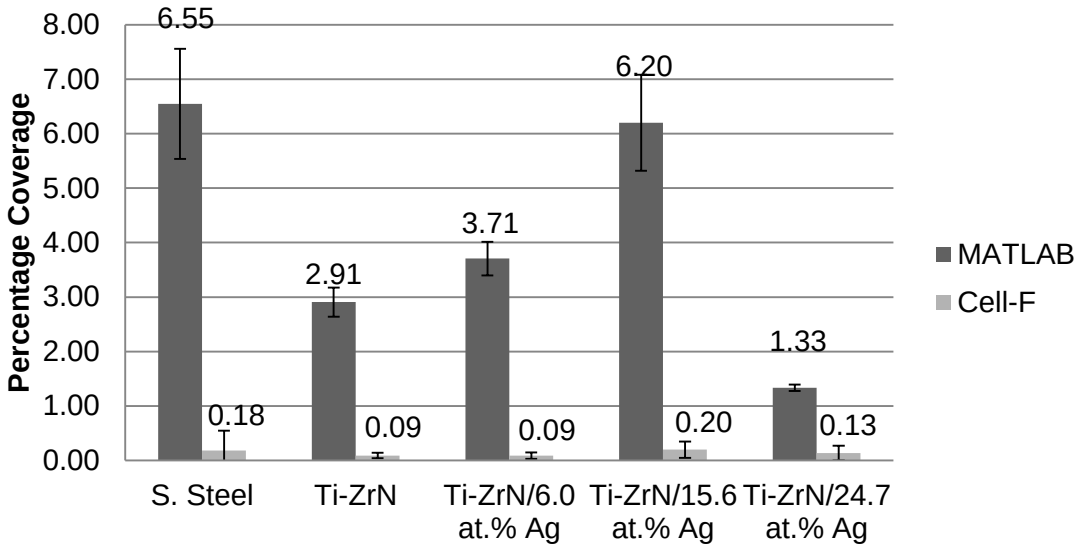

a)

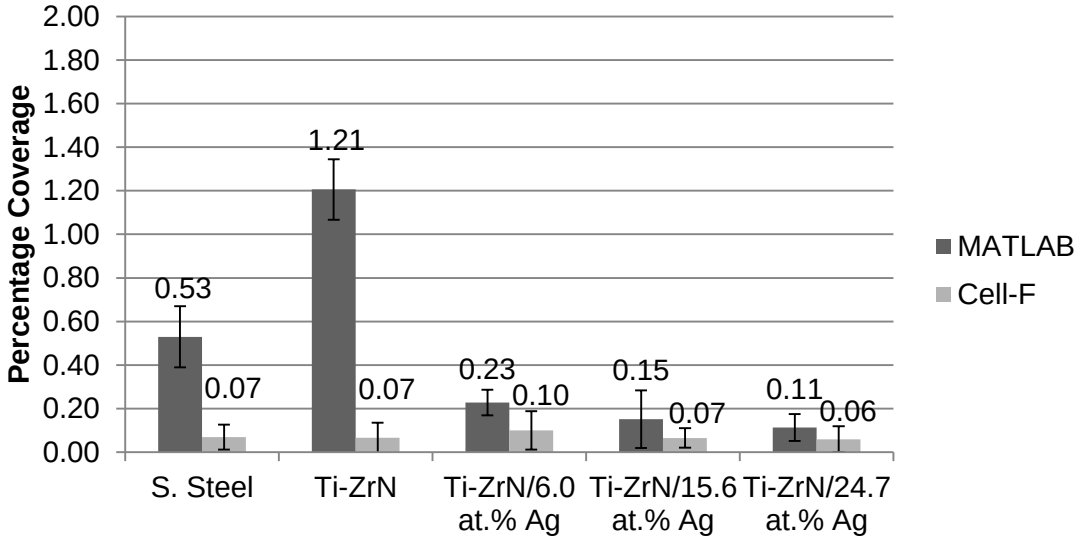

b)

Figure 107: Comparison of percentage coverage calculations of: a) *S. aureus* and b) *S. epidermidis,* between MATLAB and Cell-F programmes demonstrating although on different scales the trends were relatively similar between the two calculation methods. *S. epidermidis* displayed highest retention on ZrN, whereas *S. aureus* retained in highest numbers on the stainless steel. Note the differences in the Y axis scale for both graphs.

8.4 Discussion

The application of multifractal analysis was used to examine the density and dispersion and clumping/homogeneity of the microorganisms by using a monochrome image. The images were taken using epifluorescent microscopy to demonstrate the pattern of retention of *S. aureus* and *S. epidermidis* microorganisms on the test surfaces. This was carried out to test a proof of concept to determine if MATLAB could provide a quantitative value to demonstrate the differences in cell density, dispersion and clumping across a range of antimicrobial surfaces. It was hypothesised that if this was successful, such a tool may be used in order to quantify how differences in surface parameters such as nanotopography, microtopography, chemistry or physicochemistry affect such bacterial parameters.

The surface features for all five surfaces did not exceed 200 nm. It has been suggested that such nanotopography would not allow the bacteria to reside in the features physically (Anselme *et al.*, 2010). Further, an R_a value of less than 0.8 µm has been ascribed to a hygienic stainless steel surface (Flint *et al.*, 1997, Anonymous, 2008). The R_a values were 4.3 ± 0.8 nm, 5.0 ± 1.2 nm, 7.1 ± 3.1 nm, 7.9 ± 0.2 nm and 8.3 ± 1.4 nm, for stainless steel, Ti-ZrN, Ti-ZrN/6.0 at.%, Ti-ZrN/15.6 at.% and Ti-ZrN/24.7 at.% silver respectively (Figure 59; Page 165), showing that these measurements lie below the threshold for a hygienic surface. This might suggest that the interactions between the bacterial cells and the surfaces were due to the surface chemistry and physicochemistry of both the bacterial cell surface and the substrate to which it was retained rather than to topographical protection from shear forces.

Stainless steel samples with previously defined and characterised surface features were used as the underlying substrate for sputter coating the Ti-ZrN and Ti-ZrN/Ag nanocomposites. This material was used as it would be the underlying substrate to replicate a commercial external bone fixation pin. Although we aimed to maintain the

underlying surface topography following coating this was not always possible due to the deposition of the silver, resulting in raised silver islands, altering the nanotopography. In some studies, using surfaces with irregular features resulted in *R* values to become altered due to an unusually deep or high surface feature (Whitehead and Verran, 2006). This was the case in some instances with the coatings deposited here, however this can be qualitatively assessed using AFM images. It has been argued that parameters such as other *R* values (Korber *et al.*, 1997, Mettler and Carpentier, 1997) surface features (Mettler and Carpentier, 1998, Whitehead and Verran, 2006) and three-dimensional surface images (Whitehead *et al.*, 2005b) should also be used in order to fully describe and relate surface topography to cell retention.

There has been some debate, as to whether surface topography is important in cell retention. It has been shown that an increase in surface topography does increase cell retention (Jullien *et al.*, 2003, Medilanski *et al.*, 2002). However, Boulange-Petermann et al. (2004) found no clear relationship between the number of adhering cells and the average roughness of stainless steel in the range of 0.015–1.04 μm and other authors have reported similar findings in this R_a range between 0.01 and 1.04 μm (Barnes *et al.*, 1999, Tide *et al.*, 1999). Since it seems that it is an important factor that influences cell retention, it would seem likely that surface topography is also an important factor in maintaining the hygienic status of a surface, or in the prevention of cross contamination. Therefore advances that allow quantification of cellular density and dispersion across substrata are invaluable to the understanding of such cell-surface interface interactions.

Work using epifluorescence microscopy with the appropriate software enables the percentage coverage of cells on surfaces to be quantitatively measured (Holah *et al.*, 1989, Wirtanen *et al.*, 2001, Whitehead and Verran, 2007). Although multifractal analysis has been previously used to measure dispersion quality in polymer composites (Mills *et al.*, 2002, Mills *et al.*, 2004), and to predict the mechanical

properties of polymer surfaces (Mills *et al.*, 2005), it has not been used to attempt to quantify the pattern of cell distribution across a surface. This measureable parameter may have potential in terms of predicting the ability of a given surface to retain microorganisms. For this analysis, features do not need to be of a similar size and the analysis can be applied to images with connected (or linear) features.

For obtaining the images of the retained bacteria on the surfaces a magnification of X400 was chosen because it displayed enough bacteria across the surface for the MATLAB program to calculate the dispersion. The higher magnification (X1000) showed too few cells and the sizes were too large and the smaller magnification (X100) the camera on the microscope was too low resolution to be able to devise each individual cell due to the size in comparison to a single pixel on the image. For microbiologists, this is an important point since most cellular images are taken at higher magnifications to enable visualization of cellular features. However, for quantification of cell distribution and density of the surfaces, it is important to note that the images need to be obtained at lower magnifications.

However, a drawback of this method is that, analysis of cells in deep surface features is not possible, since the cells are not visible at such a low magnification because the depth of field of the microscope lens does not allow a clear view. However, in terms of how surface morphology affects microorganisms on surfaces with features of a microbial scale, this method is both novel and unique. Further, work in our laboratories and by others (Whitehead *et al.*, 2005b, Anselme *et al.*, 2010, Truong *et al.*, 2010) demonstrate that features of nanoscale topography may affect cell retention. This method also has the potential to be used to further analyse the criteria that influence microbial retention to surfaces.

Multifractal analysis therefore shows potential to be a novel technique that can be applied to describe the dispersion of features across a surface and the cell density and

pattern of dispersion across those surfaces. In this case, stainless steel and zirconium nitride silver thin films have been characterised and analysed for bacterial surface retention by using numerical indicators derived from the height and width of the multifractal spectrum, respectively. This work demonstrates a novel application of multifractal analysis to measure these parameters of bacterial cell density and dispersion on various surfaces.

8.5 Concluding Remarks

The aim of the investigation was to utilise MATLAB to demonstrate if microorganism differences could be related to quantitative values of density and dispersion of the *S. aureus* and *S. epidermidis* retention behaviour on stainless steel, Ti-ZrN and Ti-ZrN/Ag surfaces. Results demonstrated that the densities of *S. aureus* remained similar throughout the five surfaces. *S. epidermidis* displayed a decreasing trend as the silver content increased, suggesting the silver had an anti-adhesive effect towards this bacterial strain. The dispersion results did not demonstrate any patterns for both microorganisms but both displayed similar numbers for each surface individually. *S. aureus* displayed a more heterogeneous cell spread ($\Delta\alpha_{as} < 1$) and *S. epidermidis* was more symmetric and homogeneous ($\Delta\alpha_{as} \geq 1$).

The results that were extracted from $f(\alpha)$ curves implied that multifractal analysis is a method that can be used to quantitatively analyse the dispersion of retained microorganisms on a surface. Giving quantitative descriptors has the potential to aid the medical implant industry and determine the behaviour of bacterial cell retention on biomaterial surfaces.

9 Conclusions

External bone fixation is a method of rehabilitating severely broken bones with the aid of threaded pins which pierce the skin and are drilled into the bone, and are attached to an external support frame. This method of fixation is invaluable towards rehabilitation of the limb. However, since the pins penetrate through the skin they present an 'open wound' which presents an interface prone to infection. If the pin becomes infected, this will result in an increase in healthcare costs and staff time as well as increased physiological and psychological stress and discomfort to the patient. Further, the overuse of antibiotics is of serious concern with regards to the development of antimicrobial resistant microorganisms. Developing an antimicrobial coating with desirable properties for use in external fixation pins may help to eliminate some of these issues. In order to do this the coating has to be hard wearing, biocompatible and inert towards environments within and outside the body.

Using magnetron sputtering, zirconium nitride and zirconium nitride silver coatings were developed with silver concentrations of 15.5 at.% Ag and 29.8 at.% Ag. These were deposited onto 316L medical grade stainless steel for characterisation and antimicrobial testing. These coatings were columnar in formation, becoming denser with the addition of silver. The increase of silver displayed an increase of surface roughness; similar surface wettabilities were observed throughout. The nanotopography differed for all of the surfaces however this did not appear to affect the retention of bacteria.

The antimicrobial properties and bacterial retention characteristics of the ZrN and ZrN/Ag surfaces were tested using *S. aureus* and *S. epidermidis*. All of the surfaces retained fewer numbers of *S. epidermidis* cells than *S. aureus* and with an increase in silver concentration an increase in retention of both microorganisms was observed. LiveDead staining demonstrated that with an increase in silver concentration a decrease in viable bacteria was observed. A contact kill from the ZrN/Ag coatings was observed towards both microorganisms but no antimicrobial leaching occurred towards

either bacterial strain. The ZrN/Ag coatings displayed a brittle stressed structure causing delamination following use in the antimicrobial assays.

Due to the tribiological issues of the coatings, experiments were used to improve the coating properties. Optimum parameters were used alongside a titanium interlayer to produce Ti-ZrN/Ag nanocomposites, with improved adhesion and structural properties. Following a Taguchi experimental array and testing the adhesion of the coatings it was found that a higher frequency and higher substrate bias produced better adhered coatings. An increase in magnetron power to the silver target resulted in a linear trend with the silver content of the surfaces. All of the silver containing coatings possessed decreased adhesion in comparison to pure Ti-ZrN, however an increase in silver concentration did not display a clear decreasing trend in adhesion. The friction characteristics of the surfaces were higher than the pure Ti-ZrN and started to decrease as the silver content increased, but stayed higher than pure zirconium nitride throughout. The duty of the pulse did not provide conclusive evidence of improved characteristics. However, trends indicated that lower duties of the pulse waveform may result in improved surface properties. Thus well adhered coatings were produced on a series of interlayers (titanium, graded Zr-ZrN, ZrN/Ag) with a final surface coatings of Ti-ZrN/Ag.

The Ti-ZrN/Ag coatings were characterised for chemical composition, coating structure, coating chemical distribution, surface nanotopography and microtopography. The Ti-ZrN/Ag coatings demonstrated three distinct silver contents of 6.0 at.%, 15.6 at.% and 24.7 at.%. The Ti-ZrN possessed a columnar structure, differing to the cuboidal morphology the Ti-ZrN/Ag displayed with increasing silver. The silver was dispersed throughout the coatings as particles. There was no relationship between the coating adhesion and coefficient of friction and silver content. The nano-roughness (R_a) and surface area of the coatings increased with increasing silver. Microtopography profiles demonstrated similar S_a values and a decrease in S_p values as the silver content

increased. There were greater amounts of silver leached from the coatings with higher silver contents; no difference was observed with the amount of leached zirconium with the increase in silver. Surface free energy and Lifshitz van der Waals forces increased with the coating silver content. The most hydrophobic coating was the Ti-ZrN/15.5 at.% Ag and the least hydrophobic was Ti-ZrN, with no trend observed between coating composition and ΔG_{iwi} value. Thus the surfaces demonstrated increases in nanotopography, silver leaching, surface free energy and Lifshitz-van der Waals forces with greater silver concentration.

The Ti-ZrN/Ag coatings were assessed for retention characteristics in relation to surface chemistry, hydrophobicity and topography. The addition of silver to the coatings decreased the number of *S. epidermidis*. The *S. aureus* demonstrated different characteristics, increasing in bacterial retention as the silver increased but reducing in numbers for the coating containing 29.8 at.% Ag. For *S. aureus*, an increase in hydrophobicity led to the increase in retained bacteria. *S. epidermidis* displayed increased retention on the surfaces that were less hydrophobic. Thus the hydrophobic bacteria (*S. aureus*) displayed attraction to more hydrophobic surfaces and hydrophilic bacteria (*S. epidermidis*) to hydrophilic surfaces. *S. aureus* also displayed a trend of increased retention when the microtopography increased on the coatings, however the *S. epidermidis* did not. Neither microorganism displayed any difference in retention pattern in comparison to nanotopography. Thus the retention of both microorganisms was affected by the surface chemistry and hydrophobicity. However, only *S. aureus* was affected by microtopography. On the ZrN coatings only surface chemistry was shown to have an effect on microbial retention, however analysis of the surface properties was much less rigorous. This exemplifies the need for a thorough investigation of the surface properties if one is to fully elucidate their effect on microbial retention.

Following LiveDead assays it was demonstrated that *S. aureus* was retained in higher total numbers than *S. epidermidis*. The live *S. aureus* decreased with increasing silver content. *S. epidermidis* displayed similar numbers of live cells throughout and the dead cells increased as the silver content increased. CTC-DAPI demonstrated the Ti-ZrN/6.0% Ag to be the most efficacious towards *S. aureus*, and the 24.7 at.% Ag against *S. epidermidis*. The NTV assay found that both microorganisms were killed significantly on all of the silver containing coatings in comparison to the stainless steel and Ti-ZrN demonstrated a successful contact kill. The amount of silver did not affect the amount of efficacy displayed. The JIS method in room/dry conditions found that an antimicrobial effect was observed from the silver containing coatings at T0. Following 24 hours incubation no microorganisms were recovered from the silver containing coatings demonstrating a successful kill of both *S. aureus* and *S. epidermidis*. The JIS assay was performed in humid conditions demonstrating less kill from the silver containing coatings towards both staphylococci species at T0. Following 24 hours incubation in humid conditions all of the microorganisms were reduced to 0 on the silver containing coatings but viable colonies of both *S. aureus* and *S. epidermidis* were recovered from the stainless steel and Ti-ZrN. This result is significant because in external fixation pin hygiene as little as a few tens of microorganisms surviving on the surface could initiate an infection, therefore an effective kill following 24 hours exposure would be beneficial in external fixation pin infection control.

This further demonstrates the importance of testing the antimicrobial efficacy using a range of environmental conditions. Thus it was found that retention was species specific and an increase in silver content displayed an enhanced antimicrobial effect. Care needs to be taken when using methodologies because a drying effect may be misconstrued as antimicrobial action. The best performing coatings were the Ti-ZrN/15.6 at.% Ag for the antimicrobial efficacy and the Ti-ZrN/24.7 at.% Ag for the surface properties that control bacterial retention.

Following the addition of a blood conditioning film to the surfaces of the Ti-ZrN and Ti-ZrN/Ag coatings it was demonstrated that the surface properties and antimicrobial properties were both affected. The blood conditioning film altered the microtopography of the surfaces from the regular polishing scratches of the 316L stainless steel to irregular pits of what appeared to be the outline of the red blood cells on the surface. The conditioning film changed the coatings from hydrophobic surfaces (negative ΔG_{iwi} values) to hydrophilic/partially hydrophilic surfaces (positive ΔG_{iwi} values). In the presence of a blood plasma conditioning film rinse. The underlying topography of the surfaces were found to have an effect on the physicochemical properties of the adsorbed conditioning film. The surface chemistry also affected the adsorption of the conditioning film, with differences in surface morphology between the stainless steel and ZrN in comparison to the ZrN/Ag coatings. Reduced bacterial affinity towards the hydrocarbons was observed for both of the microorganisms demonstrating *S. aureus* was less hydrophobic in the presence of a conditioning film and *S. epidermidis* became more hydrophilic. Both microoorganisms displayed electron donating properties.

The conditioning film reduced the short term antimicrobial efficacy. No significant contact kill was observed in the NTV assay following one hour contact time. There was no kill observed towards the microorganisms on the JIS assay at T0 but following 24 hours incubation there was reduced recovery on the silver containing coatings than the Ti-ZrN and stainless steel results. No antimicrobial leaching was observed in the zones of inhibition assays. Thus the addition of the blood conditioning film altered the substrate surface topographies and physicochemistry, as well as the physicochemistry of the cells. The conditioning film reduced the short term but not the longer term antimicrobial efficacy of the surfaces.

Differences in the retention patterns of the microorganisms were observed in previous work but were not quantifiable. Using multifractal analysis and MATLAB the differences in retention behaviour of *S. aureus* and *S. epidermidis* in terms of density and

dispersion were quantified. Results demonstrated that the densities of *S. aureus* remained similar throughout the five surfaces (Stainless steel, Ti-ZrN, Ti-ZrN/Ag 6.0 at.% Ag, 15.6 at.% Ag and 24.7 at.% Ag). *S. epidermidis* displayed a decreasing trend in density as the silver content increased, suggesting the silver may have demonstrated an anti-adhesive effect towards this bacterial strain. There were no trends observed for both microorganisms in terms of dispersion, but both displayed similar numbers for each surface individually. *S. aureus* displayed a more heterogeneous cell spread ($\Delta\alpha_{as} < 1$) and *S. epidermidis* was more symmetric and homogeneous ($\Delta\alpha_{as} \geq 1$).

The results implied that multifractal analysis has the potential to be used in quantitative analysis of the dispersion of retained microorganisms on a surface. Giving quantitative descriptors has the potential to aid the medical implant industry and determine the behaviour of bacterial cell retention on biomaterial surfaces. This characterisation would further improve the design of medical device surfaces to improve the antiadhesive hygienic status of the surface.

To conclude, the application of titanitum-zirconium nitride/silver coatings were developed and the properties that were relevant to pin tract infections were characterised. The best performing antimicrobial coating was the Ti-ZrN/15.6 at.% Ag, displaying an effective kill towards both microorganisms. However, the 24.7 at.% Ag coating decreased the number of retained bacteria. It may be that the optimum coating to address both the antimicrobial efficacy and reduce microbial retention lies between these two Ag concentrations. Addition of a conditioning film is essential in this type of work if the surfaces are to be tested for an applied situation. A method was developed that could help describe the effects of changes in surface properties on microbial retention.

9.1 Further Work

Further work would include further characterisation of the Ti-ZrN/Ag using surface analysis such as XRD, as well as further investigation into the effect of conditioning films and introduction of pin tract models. Depositing the Ti-ZrN/Ag coatings onto external fixation pins and attempting infection models involving either agar or pig skin as the simulated skin interface could provide an *in vitro* visualisation of the effects of the coatings if taken to the stage of *in vivo* testing.

Further work involving conditioning films could involve characterising the durability and longevity of the silver in the coating over repeated cleaning and soiling cycles and testing the surfaces for antimicrobial efficacy and bacterial retention in comparison to new surfaces. In the presence of a conditioning film staining the retained bacteria following a retention assay and then follow with a full differential staining of both the surface soil and the bacterial cells would characterise the retention behaviour of the bacteria and analysing the images using MATLAB would provide dispersion and density data to be compared with the data obtained on the clean surfaces. Testing the Ti-ZrN/Ag surfaces for histocompatibility and investigating the effect towards human inflammatory cells would provide essential information that could contribute towards the Ti-ZrN/Ag coating material advancing as a solution towards the external fixation pin application. The antimicrobial mechanisms of the surfaces would need to be further investigated over longer periods of time and potential further work could include incubation periods followed by standardised cleaning assays used for external fixation pin care and inoculation cycles to test long term efficacy of the surfaces.

Creating a series of coatings with silver concentrations between 15.6 and 24.7% may provide a greater insight into whether the optimum silver concentration falls between these values, as stated in the conclusion. Alongside this development it may also be beneficial to compare the antimicrobial efficacy of the Ti-ZrN/Ag coatings to pure silver

coatings deposited onto identical medical grade stainless steel and characterise the surfaces and see if the silver produces any anti-adhesive effect or enhanced antimicrobial efficacy.

Testing the Ti-ZrN/Ag coatings for hardness and abrasion would help characterise the coating tribology. Designing and performing an abrasion in a standardised method, either by an existing machine or by designing the equipment relevant to eternal fixation pin movement would provide an insight into what the coatings could withstand throughout the life *in situ*.

This work has provided data on a scale hitherto unexplored by others. The body of work developed magnetron sputtering deposition of ZrN/Ag and Ti-ZrN/Ag coatings on medical grade stainless steel wherein the surfaces were characterised on how the effect of topography, physicochemistry and surface chemistry affected the retention of bacteria, the antimicrobial efficacy of the coatings and the adsorption characteristics of a medically relevant conditioning film. An increase in silver concentration in the coatings led to an increase in antimicrobial efficacy. The best performing coatings were the Ti-ZrN/15.6 at.% Ag for the antimicrobial efficacy and the Ti-ZrN/24.7 at.% Ag for the surface properties that control bacterial retention. Surface topography and physicochemistry of the underlying substrata affected the adsorption of the conditioning film. Testing antimicrobial biomaterials in the presence of a conditioning film is important because it replicates the conditioning of the biomaterial surface when *in vivo*.

10 Appendix 1: MATLAB

10.1.1 Mathematical method of multifractal analysis box counting.

The generalized (box-counting) fractal dimensions D_q, where $q \in \Re$, (where q is a real number) were defined by;

$$D_q = \lim_{\varepsilon \to 0} \frac{1}{1-q} \frac{\ln \sum_{i=1}^{N} p_i^q(\varepsilon)}{-\ln \varepsilon} \quad , \qquad [1]$$

where the index i labels the individual boxes of size ε and $p_i(\varepsilon)$ denotes the relative weight of the *i*'th box or the probability of the object lying in the box. The probability $p_s(\varepsilon)$ of segments of type *s* scales with the size ε of a box was calculated as follows:

$$p_s(\varepsilon) \propto (\varepsilon)^{\alpha_s} \quad , \qquad [2]$$

where α_s is the so-called coarse Hölder exponent defined by;

$$\alpha_s = \frac{\ln p_s(\varepsilon)}{\ln \varepsilon} \quad . \qquad [3]$$

The number of segments N_s of type *s* scales with the size ε of a box are calculated according to**:**

$$N_s(\varepsilon) \propto (\varepsilon)^{-f_s} \quad . \qquad [4]$$

The exponents α_s and f_s were then used to determine $f(\alpha)$. In many cases, $f(\alpha)$ is related to the Hausdorff-Besicovich dimension (Falconer, 2003).

The image to be analysed was covered with boxes of size ε and the corresponding box-measures $\mu_i(\varepsilon) = p_i(\varepsilon)$ were calculated. The Hausdorff dimension of the measure-theoretic support of $\mu(q)$ was given by;

$$f(q) = \lim_{\varepsilon \to 0} \frac{\sum_{i=1}^{N} \mu_i(q,\varepsilon) \ln \mu_i(q,\varepsilon)}{\ln \varepsilon} \qquad [5]$$

and

$$\alpha(q) = \lim_{\varepsilon \to 0} \frac{\sum_{i=1}^{N} \mu_i(q,\varepsilon) \ln p_i(\varepsilon)}{\ln \varepsilon} \ , \qquad [6]$$

where $\mu_i(q,\varepsilon)$ are the normalized probabilities

$$\mu_i(q,\varepsilon) = \frac{p_i^q(\varepsilon)}{\sum_{j=1}^{N} p_j^q(\varepsilon)} \quad . \qquad [7]$$

A crucial step in multifractal analysis is in determining the range of box sizes ($l \le \varepsilon \le L$) and the range of order *q* over which the analysis is to be applied. One possible solution was suggested by Aharony (1990). In the mathematical equations (1) and (2) there are limits as the box sizes $\varepsilon \to 0$, which are not physically realizable, but In practice, one constructs lines of best fit using linear regression for

$$\sum_{i=1}^{N} \mu_i(q,\varepsilon) \ln \mu_i(q,\varepsilon) \text{ versus } \ln \varepsilon \qquad [1]$$

and

$$\sum_{i=1}^{N} \mu_i(q,\varepsilon) \ln p_i(\varepsilon) \text{ versus } \ln \varepsilon \qquad [2]$$

in order to approximate $f(q)$ and $\alpha(q)$, respectively. The number and scale of box sizes is vitally important in the analysis and care needs to be taken as a consequence.

Following acquisition of the *f*(α) spectra the following quantitative outputs can be calculated. The minimum value of α is denoted by "α_{min}", ($q = +\infty$). The "α_{max}", is the point at which the curve intersects with the X axis at $q = -\infty$. The "α(0)" is the value *q*α at the maximum of the *f*(α) when *q* = 0. The three following points can be calculated in the following equations to give the dispersion (Δ∞)

$$\Delta\infty = \alpha Max - \alpha Min$$

and the measurement of asymmetry ($\Delta\alpha_{AS}$)

$$\Delta\alpha_{AS} = \frac{(\alpha 0 - \alpha Min)}{(\alpha Max - \alpha 0)}.$$

The ($\Delta\alpha_{AS}$) values correspond to whether the *f*(α) curve is skewed left or right, where curves are:

In most physical applications a problem arises with negative values of q (values from the left side of the *f*α curve); boxes with very low measure may contribute disproportionately. Several papers have been published addressing this so-called clipping problem (Veneziano, 2009, Pastén *et al.*, 2011).

11 References

AHARONY, A. 1990. MULTIFRACTALS IN PHYSICS - SUCCESSES, DANGERS AND CHALLENGES. *Physica A,* 168**,** 479-489.

AHLBORG, H. G., JOSEFSSON. PER OLOF 1999. Pin-tract complications in external fixation of fractures of the distal radius. *Acta Orthopaedica,* 70**,** 116-118.

ALFONSO, E., OLAYA, J. & CUBILLOS, G. 2011. Thin Film Growth Through Sputtering Technique and Its Applications. *Crystallization - Science and Technology***,** 397 - 432.

ALLAKER, R. P. 2010. The Use of Nanoparticles to Control Oral Biofilm Formation. *Journal of Dental Research,* 89**,** 1175-1186.

ANONYMOUS 1972. Method for the assessment of surface texture. Method and instrumentation. *BS 1134-1:1972.* British Standards.

ANONYMOUS 1988. BS 1134-1:1988. *Assessment of surface texture. Methods and instrumentation.* British Standards.

ANONYMOUS 1997. BS ISO 4287:1997. *Geometric product specifications (GPS). Surface texture: profile method. Terms, definitions and surface texture parameters.* British Standards.

ANONYMOUS 1998. BS EN ISO 13565-2:1998. *Geometric product specifications (GPS). Surface texture: Profile method. Surfaces having stratified functional properties. Height characterization using the linear material ration curve.* British Standards.

ANONYMOUS 2004. LIVE/DEAD BacLight Bacterial Viability Kits. Molecular Probes.

ANONYMOUS 2005a. BS EN 1071-3:2005. *Advanced technical ceramics. Methods of test for ceramic coatings. Determination of adhesion and other mechanical failure modes by a scratch test.* British Standards.

ANONYMOUS. 2005b. *Pinnacle® Plus+ Pulsed-DC Power Supplies* [Online]. Fort Collins, Colorado, USA: Advanced Energy. Available: http://www.advanced-energy.com/upload/File/DC/ENG-PNCLPLUS-210-05.pdf [Accessed 17/10/2013 2013].

ANONYMOUS 2008. ISO 14159:2008, Safety of machinery - Hygiene requirements for the design of machinery. Brussels: European Committee for Standardization.

ANONYMOUS 2009. BS EN ISO 4287:1998+A1:2009. *Geometrical product specification (GPS). Surface texture: Profile method. Terms, definitions and surface texture parameters.* British Standard.

ANONYMOUS 2010a. BS 1134:2010. *Assessment of surface texture. Guidance and general information.* British Standards.

ANONYMOUS 2010b. JIS Z 2801:2010: Antibacterial products -Test for antibacterial activity and efficacy. Japanese Standards Association.

ANONYMOUS 2011. BS ISO 22196:2011. *Measurement of antibacterial activity on plastics and other non-porous surfaces.* British Standards.

ANONYMOUS 2012. BS EN ISO 25178-2:2012 Geometrical product specifications (GPS) — Surface texture: Areal. British Standards.

ANONYMOUS. 2013. *Spectral characteristics of Molecular Probes dyes—Table 23.1* [Online]. Life Technologies. Available: http://www.lifetechnologies.com/uk/en/home/references/molecular-probes-the-handbook/tables/spectral-characteristics-and-recommended-bandpass-filter-sets-for-molecular-probes-dyes.html [Accessed 29/09/2013.

ANSELME, K., DAVIDSON, P., POPA, A. M., GIAZZON, M., LILEY, M. & PLOUX, L. 2010. The interaction of cells and bacteria with surfaces structured at the nanometre scale. *Acta Biomaterialia,* 6**,** 3824-3846.

ANTOCI, V., ONO, C. M., ANTOCI, V., JR. & RANEY, E. M. 2008. Pin-tract infection during limb lengthening using external fixation. *Am J Orthop (Belle Mead NJ),* 37**,** E150-4.

AOUADI, S. M., BOHNHOFF, A., SODERGREN, M., MIHUT, D., ROHDE, S. L., XU, J. & MISHRA, S. R. 2006. Tribological investigation of zirconium nitride/silver nanocomposite structures. *Surface & Coatings Technology,* 201**,** 418-422.

AOUADI, S. M., DEBESSAI, M. & FILIP, P. 2004. Zirconium nitride/silver nanocomposite structures for biomedical applications. *Journal of Vacuum Science & Technology B,* 22**,** 1134-1140.

ARCIOLA, C. R., CAMPOCCIA, D., SPEZIALE, P., MONTANARO, L. & COSTERTON, J. W. 2012. Biofilm formation in Staphylococcus implant infections. A review of molecular mechanisms and implications for biofilm-resistant materials. *Biomaterials,* 33**,** 5967-5982.

ARENS, S., SCHLEGEL, U., PRINTZEN, G., ZIEGLER, W. J., PERREN, S. M. & HANSIS, M. 1996. INFLUENCE OF MATERIALS FOR FIXATION IMPLANTS ON LOCAL INFECTION: AN EXPERIMENTAL STUDY OF STEEL VERSUS TITANIUM DCP IN RABBITS. *Journal of Bone & Joint Surgery, British Volume,* 78-B**,** 647-651.

ASAMI, K. & HASHIMOTO, K. 2003. Importance of initial surface film in the degradation of stainless steels by atmospheric exposure. *Corrosion Science,* 45**,** 2263-2283.

ASCHE, G., BURGESS, A., BURNY, F., COURT-BROWN, C. M., O. KARAHARJU, E., LATTA, L., SELIGSON, D. & ZYCH, G. 2006. Hoffmann® II Compact™ External Fixation System. *In:* AG, S. T. (ed.). Selzach, Switzerland: Stryker.

ATANASSOVA, D., STEFANOVA, V. & RUSSEVA, E. 1998. Co-precipitative pre-concentration with sodium diethyldithiocarbamate and ICP-AES determination of Se, Cu, Pb, Zn, Fe, Co, Ni, Mn, Cr and Cd in water. *Talanta,* 47**,** 1237-1243.

ATTAR, F. & JOHANNESSON, T. 1996. Adhesion evaluation of thin ceramic coatings on tool steel using the scratch testing technique. *Surface and Coatings Technology,* 78**,** 87-102.

AYDIN, G., KARAKURT, I. & AYDINER, K. 2013. Investigation of the surface roughness of rocks sawn by diamond sawblades. *International Journal of Rock Mechanics and Mining Sciences,* 61**,** 171-182.

BAGHRICHE, O., RUALES, C., SANJINES, R., PULGARIN, C., ZERTAL, A., STOLITCHNOV, I. & KIWI, J. 2012. Ag-surfaces sputtered by DC and pulsed DC-magnetron sputtering effective in bacterial inactivation: Testing and characterization. *Surface and Coatings Technology,* 206**,** 2410-2416.

BAIRD-PARKER, A. C. 1975. Gram Positive Cocci. *In:* BUCHANAN, R. E., GIBBONS, N. E. & COWEN, S. T. (eds.) *Bergeys Manual of Determinative Bacteriology.* 8th ed. Baltimore, USA: Williams and Wilkins.

BALACEANU, M., PETREUS, T., BRAIC, V., ZOITA, C. N., VLADESCU, A., COTRUTZ, C. E. & BRAIC, M. 2010. Characterization of Zr-based hard coatings for medical implant applications. *Surface and Coatings Technology,* 204**,** 2046-2050.

BALLA, V. K., XUE, W., BOSE, S. & BANDYOPADHYAY, A. 2009. Laser-assisted Zr/ZrO2 coating on Ti for load-bearing implants. *Acta Biomaterialia,* 5**,** 2800-2809.

BARNES, B. I., CASSAR, C. A., HALABLAB, M. A., PARKINSON, N. H. & MILES, R. J. 1996. An in situ method for determining bacterial survival on food preparation surfaces using a redox dye. *Letters in Applied Microbiology,* 23**,** 325-328.

BARNES, L. M., LO, M. F., ADAMS, M. R. & CHAMBERLAIN, A. H. L. 1999. Effect of milk proteins on adhesion of bacteria to stainless steel surfaces. *Applied and Environmental Microbiology,* 65**,** 4543-4548.

BELLON-FONTAINE, M. N., RAULT, J. & VAN OSS, C. J. 1996. Microbial adhesion to solvents: a novel method to determine the electron-donor/electron-acceptor or Lewis acid-base properties of microbial cells. *Colloids and Surfaces B: Biointerfaces,* 7**,** 47-53.

BERG, J. M., ERIKSSON, L. G. T., CLAESSON, P. M. & BORVE, K. G. N. 1994. Three-Component Langmuir-Blodgett Films with a Controllable Degree of Polarity. *Langmuir,* 10**,** 1225-1234.

BIANCHI, F., MAFFINI, M., MANGIA, A., MARENGO, E. & MUCCHINO, C. 2007. Experimental design optimization for the ICP-AES determination of Li, Na, K, Al, Fe, Mn and Zn in human serum. *Journal of Pharmaceutical and Biomedical Analysis,* 43**,** 659-665.

BLOCK, A., VONBLOH, W., KLENKE, T. & SCHELLNHUBER, H. J. 1991. Multifractal Analysis Of The Microdistribution Of Elements In Sedimentary Structures Using Images From Scanning Electron-Microscopy And Energy Dispersive-X-Ray Spectrometry. *Journal of Geophysical Research-Solid Earth,* 96**,** 16223-16230.

BLUNT, R. T. White Light Interferometry–a production worthy technique for measuring surface roughness on semiconductor wafers. CS MANTECH, 2006 Vancouver, British Columbia.

BOS, R., VAN DER MEI, H. C. & BUSSCHER, H. J. 1999. Physico-chemistry of initial microbial adhesive interactions – its mechanisms and methods for study. *Fems Microbiology Reviews,* 23**,** 179-230.

BOULANGE-PETERMANN, L., JULLIEN, C., DUBOIS, P. E., BENEZECH, T. & FAILLE, C. 2004. Influence of surface chemistry on the hygienic status of industrial stainless steel. *Biofouling,* 20**,** 25-33.

BOULANGEPETERMANN, L., RAULT, J. & BELLONFONTAINE, M. N. 1997. Adhesion of Streptococcus thermophilus to stainless steel with different surface topography and roughness. *Biofouling,* 11**,** 201-&.

BOVILL, R. A., SHALLCROSS, J. A. & MACKEY, B. M. 1994. Comparison of the fluorescent redox dye 5-cyano-2,3-ditolyltetrazolium chloride with p-iodonitrotetrazolium violet to detect metabolic activity in heat-stressed Listeria monocytogenes cells. *Journal of Applied Bacteriology,* 77**,** 353-358.

BRÄUER, G., BANDORF, R., BEWILOGUA, K., DIEHL, W., SZYSZKA, B. & VERGÖHL, M. Magnetron Sputtering and its Applications - Milestones and Future Challenges. Society of Vacuum Coaters 54th Annual Technical Conference Proceedings, April 16 - 21 2011 Chicago, IL.

BRUGNONI, C., LANZA, F., MACCHI, G., MÃ¼LLER, R., PARNISARI, E., STROOSNIJDER, M. F. & VINHAS, J. 1998. Evaluation of the wear resistance of ZrN coatings using thin layer activation. *Surface and Coatings Technology,* 100-101**,** 23-26.

BRUINSMA, G. M., RUSTEMA-ABBING, M., DE VRIES, J., BUSSCHER, H. J., VAN DER LINDEN, M. L., HOOYMANS, J. M. M. & VAN DER MEI, H. C. 2003. Multiple surface properties of worn RGP lenses and adhesion of Pseudomonas aeruginosa. *Biomaterials,* 24**,** 1663-1670.

BRUINSMA, G. M., VAN DER MEI, H. C. & BUSSCHER, H. J. 2001. Bacterial adhesion to surface hydrophilic and hydrophobic contact lenses. *Biomaterials,* 22**,** 3217-3224.

BUSSCHER, H. J. & VAN DER MEI, H. C. Initial microbial adhesion events: mechanisms and implications. *In:* ALLISON, D. G., GILBERT, P., LAPPIN-SCOTT, H. M. & WILSON, M., eds. SGM Symposium 59, 2000. Cambridge University Press, 25 - 34.

BUSSCHER, H. J. & VAN DER MEI, R. B. H. C. 1995. Initial microbial adhesion is a determinant for the strength of biofilm adhesion. *FEMS Microbiology Letters,* 128**,** 229-234.

CAMARGO, G. M. P. A., PIZZOLITTO, A. C. & PIZZOLITTO, E. L. 2005. Biofilm formation on catheters used after cesarean section as observed by scanning electron microscopy. *International Journal of Gynecology & Obstetrics,* 90**,** 148-149.

CAMATHIAS, C., VALDERRABANO, V. & OBERLI, H. 2012. Routine pin tract care in external fixation is unnecessary: A randomised, prospective, blinded controlled study. *Injury,* 43**,** 1969-1973.

CAMPOCCIA, D., MONTANARO, L. & ARCIOLA, C. R. 2006. The significance of infection related to orthopedic devices and issues of antibiotic resistance. *Biomaterials,* 27**,** 2331-2339.

CAMPOCCIA, D., MONTANARO, L. & ARCIOLA, C. R. 2013. A review of the biomaterials technologies for infection-resistant surfaces. *Biomaterials,* 34**,** 8533-8554.

CHECKETTS, R., OTTERBURN, M. & MACEACHERN, A. 1993. Pin Track Infection: definition, incidence and prevention. *International Journal of Orthopaedic and Trauma Nursing,* 3**,** 16-18.

CHECKETTS, R. G., MACEACHEM, A. G. & OTTERBUM, M. 2001. Pin Track Infection and the Principles of Pin Site Care. *In:* BASTIANI, G., APLEY, A. G. & GOLDBERG, A. (eds.) *Orthofix External Fixation in Trauma and Orthopaedics.* Springer London.

CHEN, W., LIU, Y., COURTNEY, H. S., BETTENGA, M., AGRAWAL, C. M., BUMGARDNER, J. D. & ONG, J. L. 2006. In vitro anti-bacterial and biological properties of magnetron co-sputtered silver-containing hydroxyapatite coating. *Biomaterials,* 27**,** 5512-5517.

CHIEN, C. L. & LIOU, S. H. 1985. Crystalline and amorphous FeTi and Fe2Ti. *Physical Review B,* 31**,** 8238-8241.

CHO, K.-H., PARK, J.-E., OSAKA, T. & PARK, S.-G. 2005. The study of antimicrobial activity and preservative effects of nanosilver ingredient. *Electrochimica Acta,* 51**,** 956-960.

CHOI, Y. S., PIEHLER, H. R. & ROLLETT, A. D. 2007. Introduction and application of modified surface roughness parameters based on the topographical distributions of peaks and valleys. *Materials Characterization,* 58**,** 901-908.

CINDRIC, I. J., ZEINER, M. & STEFFAN, I. 2007. Trace elemental characterization of edible oils by ICP–AES and GFAAS. *Microchemical Journal,* 85**,** 136-139.

COALLIER, J., PRÉVOST, M., ROMPRÉ, A. & DUCHESNE, D. 1994. The optimization and application of two direct viable count methods for bacteria in distributed drinking water. *Canadian Journal of Microbiology,* 40**,** 830-836.

COESTER, L. M., NEPOLA, J. V., ALLEN, J. & MARSH, J. L. 2006. The Effects of Silver Coated External Fixation Pins. *The Iowa Orthopaedic Journal,* 26**,** 48-53.

COHEN, A., LIU-SYNDER, P., STOREY, D. & WEBSTER, T. J. 2007. Decreased fibroblast and increased osteoblast functions on ionic plasma deposited nanostructured Ti coatings. *Nanoscale Research Letters,* 2**,** 385-390.

COLES, P. & JONES, B. 1991. A lognormal model for the cosmological mass-distribution. *Monthly Notices of the Royal Astronomical Society,* 248**,** 1-13.

COLON, G., WARD, B. C. & WEBSTER, T. J. 2006. Increased osteoblast and decreased Staphylococcus epidermidis functions on nanophase ZnO and TiO2. *Journal of Biomedical Materials Research - Part A,* 78**,** 595-604.

COOPER, S. P., FINLAY, J. A., CONE, G., CALLOW, M. E., CALLOW, J. A. & BRENNAN, A. B. 2011. Engineered antifouling microtopographies: kinetic analysis of the attachment of zoospores of the green alga Ulva to silicone elastomers. *Biofouling,* 27**,** 881-891.

CROOKES, W. 1891. On Electrical Evaporation. *Proceedings of the Royal Society of London,* 50**,** 88-105.

CURIEL, G. J. 1993. *Hygienic Design for Equipment* Chipping Campden, UK, EHEDC, Campden & Chorleywood Food Research Association.

D ANTONIO, P., LASALVIA, M., PERNA, G. & CAPOZZI, V. 2012. Scale-independent roughness value of cell membranes studied by means of AFM technique. *Biochimica et Biophysica Acta (BBA) - Biomembranes,* 1818**,** 3141-3148.

DANISMAN, K., DANISMAN, S., SAVAS, S. & DALKIRAN, I. 2009. Modelling of the hysteresis effect of target voltage in reactive magnetron sputtering process by using neural networks. *Surface and Coatings Technology,* 204**,** 610-614.

DAROUICHE, R. O. 1999. Anti-Infective Efficacy of Silver-Coated Medical Prostheses. *Clinical Infectious Diseases,* 29**,** 1371-1377.

DAVIES, R., HOLT, N. & NAYAGAM, S. 2005. The care of pin sites with external fixation. *J Bone Joint Surg Br,* 87**,** 716-9.

DEE, K. C., PULEO, D. A. & BIZIOS, R. 2003. *An Introduction to Tissue-Biomaterial Interactions*, Wiley.

DENG, J., LIU, J., DING, Z. & NIU, M. 2008a. Unlubricated friction and wear behaviors of ZrN coatings against hardened steel. *Materials & Design,* 29**,** 1828-1834.

DENG, J., LIU, J., ZHAO, J. & SONG, W. 2008b. Wear mechanisms of PVD ZrN coated tools in machining. *International Journal of Refractory Metals and Hard Materials,* 26**,** 164-172.

DESROUSSEAUX, C., SAUTOU, V., DESCAMPS, S. & TRAORÉ, O. 2013. Modification of the surfaces of medical devices to prevent microbial adhesion and biofilm formation. *Journal of Hospital Infection,* 85**,** 87-93.

DEVASCONCELLOS, P., BOSE, S., BEYENAL, H., BANDYOPADHYAY, A. & ZIRKLE, L. G. 2012. Antimicrobial particulate silver coatings on stainless steel implants for fracture management. *Materials Science and Engineering: C,* 32**,** 1112-1120.

DUDDRIDGE, J. E., KENT, C. A. & LAWS, J. F. 1982. Effect of surface shear stress on the attachment of Pseudomonas fluorescens to stainless steel under defined flow conditions. *Biotechnology and Bioengineering,* 24**,** 153-164.

DUNN, K. & EDWARDS-JONES, V. 2004. The role of Acticoat(TM) with nanocrystalline silver in the management of burns. *Burns,* 30**,** S1-S9.

EDWARDS-JONES, V. 2009. The benefits of silver in hygiene, personal care and healthcare. *Letters in Applied Microbiology,* 49**,** 147-152.

EDWARDS, K. J. & RUTENBERG, A. D. 2001. Microbial response to surface microtopography: the role of metabolism in localized mineral dissolution. *Chemical Geology,* 180**,** 19-32.

EL-KADY, A. M., RIZK, R. A., ABD EL-HADY, B. M., SHAFAA, M. W. & AHMED, M. M. 2012. Characterization, and antibacterial properties of novel silver releasing nanocomposite scaffolds fabricated by the gas foaming/salt-leaching technique. *Journal of Genetic Engineering and Biotechnology,* 10**,** 229-238.

EMSLEY, J. 2011. *Nature's building blocks: an A-Z guide to the elements,* Oxford, UK, Oxford University Press.

ERALP, L., KOCAOGLU, M., TOKER, B., BALCı, H. I. & AWAD, A. 2011. Comparison of fixator-assisted nailing versus circular external fixator for bone realignment of lower extremity angular deformities in rickets disease. *Arch Orthop Trauma Surg,* 131**,** 581-589.

FAILLE, C., JULLIEN, C., FONTAINE, F., BELLON-FONTAINE, M. N., SLOMIANNY, C. & BENEZECH, T. 2002. Adhesion of Bacillus spores and Escherichia coli cells to inert surfaces: role of surface hydrophobicity. *Canadian Journal of Microbiology,* 48**,** 728-738.

FAILLE, C., MEMBRE, J. M., TISSIER, J. P., BELLON-FONTAINE, M. N., CARPENTIER, B., LAROCHE, M. A. & BENEZECH, T. 2000. Influence of physicochemical properties on the hygienic status of stainless steel with various finishes. *Biofouling,* 15**,** 261-274.

FEDERIGHI, M., THOLOZAN, J. L., CAPPELIER, J. M., TISSIER, J. P. & JOUVE, J. L. 1998. Evidence of non-coccoid viable but non-culturableCampylobacter jejunicells in microcosm water by direct viable count, CTC-DAPI double staining, and scanning electron microscopy. *Food Microbiology,* 15**,** 539-550.

FERREIRA, N. & MARAIS, L. 2012. Prevention and management of external fixator pin track sepsis. *Strategies in Trauma and Limb Reconstruction,* 7**,** 67-72.

FLINT, S. H., BREMER, P. J. & BROOKS, J. D. 1997. Biofilms in dairy manufacturing plant description, current concerns and methods of control. *Biofouling,* 11**,** 81-97.

FLINT, S. H., BROOKS, J. D. & BREMER, P. J. 2000. Properties of the stainless steel substrate, influencing the adhesion of thermo-resistant streptococci. *Journal of Food Engineering,* 43**,** 235-242.

FONTALVO, G. A., DANIEL, R. & MITTERER, C. 2010. Interlayer thickness influence on the tribological response of bi-layer coatings. *Tribology International,* 43**,** 108-112.

FORSTER, H., MAROTTA, J. S., HESELTINE, K., MILNER, R. & JANI, S. 2004. Bactericidal activity of antimicrobial coated polyurethane sleeves for external fixation pins. *Journal of Orthopaedic Research,* 22**,** 671-677.

FRANK, J. F. & CHMIELEWSKI, R. A. N. 1997. Effectiveness of Sanitation with Quaternary Ammonium Compound or Chlorine on Stainless Steel and Other Domestic Food-Preparation Surfaces. *Journal of Food Protection,* 60**,** 43-47.

FRANSON, T. R., SHETH, N. K., ROSE, H. D. & SOHNLE, P. G. 1984. Scanning electron microscopy of bacteria adherent to intravascular catheters. *Journal of Clinical Microbiology,* 20**,** 500-505.

GADELMAWLA, E. S., KOURA, M. M., MAKSOUD, T. M. A., ELEWA, I. M. & SOLIMAN, H. H. 2002. Roughness parameters. *Journal of Materials Processing Technology,* 123**,** 133-145.

GARVEY, G. 1980. Endovascular and prosthetic implant infections. *Infections in theAbnorrmal Host, Yorke Med, New York***,** 693-745.

GERTH, J. & WIKLUND, U. 2008. The influence of metallic interlayers on the adhesion of PVD TiN coatings on high-speed steel. *Wear,* 264**,** 885-892.

GILBODY, J. & NAYAGAM, S. 2008. Lengthening of the First Metatarsal through an Arthrodesis Site for Treatment of Brachymetatarsia: A Case Report. *The Journal of Foot and Ankle Surgery,* 47**,** 559-564.

GOERING, R., DOCKRELL, H., ZUCKERMAN, M., WAKELIN, D., ROITT, I., MIMS, C. & CHIODINI, P. 2008. *Mim's Medical Microbiology*, Elsevier.

GOLDBERGER, A. L., AMARAL, L. A. N., HAUSDORFF, J. M., IVANOV, P. C., PENG, C. K. & STANLEY, E. H. Fractal dynamics in physiology: Alterations with disease and ageing. Colloquium of the National-Academy-of-Science on Self-Organised Complexity in the Physical, Biological, and Social Sciences, Mar 23-24 2001 2002 NAS Beckman CTR, Irvine CA. 2466-2472.

GOOD, R. J. & VAN OSS, C. J. 1991. Surface Enthalpy And Entropy And The Physico-Chemical Nature Of Hydrophobic and Hydrophilic Interactions. *Journal of Dispersion Science and Technology,* 12**,** 273-287.

GOODHEW, P. J., HUMPHREYS, J. & BEANLAND, R. 2001. *Electron Microscopy and Analysis,* London, Taylor & Francis.

GOODMAN, S. B., YAO, Z., KEENEY, M. & YANG, F. 2013. The future of biologic coatings for orthopaedic implants. *Biomaterials,* 34**,** 3174-3183.

GOSHEGER, G., HARDES, J., AHRENS, H., STREITBURGER, A., BUERGER, H., ERREN, M., GUNSEL, A., KEMPER, F. H., WINKELMANN, W. & VON EIFF, C. 2004. Silver-coated megaendoprostheses in a rabbit model--an analysis of the infection rate and toxicological side effects. *Biomaterials,* 25**,** 5547-5556.

GOUGH, L. P., SHACKLETTE, H. T. & CASE, A. A. 1979. *Element Concentrations Toxic to Plants, Animals, and Man,* Washington, UNITED STATES DEPARTMENT OF THE INTERIOR

GRANT, A. D., ATAR, D. & LEHMAN, W. B. 1992. Pin care using the Ilizarov apparatus: recommended treatment plan in Kurgan, Russia. *Bull Hosp Jt Dis,* 52**,** 18-20.

GREIF, D., WESNER, D., REGTMEIER, J. & ANSELMETTI, D. 2010. High resolution imaging of surface patterns of single bacterial cells. *Ultramicroscopy,* 110**,** 1290-1296.

GRISTINA, A. G. & COSTERTON, J. W. 1985. Bacterial adherence to biomaterials and tissue. The significance of its role in clinical sepsis. *The Journal of bone and joint surgery. American volume,* 67**,** 264-273.

GROVE, W. R. 1852. On the Electro-Chemical Polarity of Gases. *Philosophical Transactions of the Royal Society of London,* 142**,** 87-101.

GUGLIELMOTTI, M., GUERRERO, C. & CABRINI, R. 1997. Chronodynamic evaluation of the stages of osseointegration in zirconium laminar implants. *Acta odontológica latinoamericana: AOL,* 10**,** 11.

HALSEY, T. C., JENSEN, M. H., KADANOFF, L. P., PROCACCIA, I. & SHRAIMAN, B. I. 1986. Fractal measures and their singularities: The characterization of strange sets. *Physical Review A,* 33**,** 1141-1151.

HAMADI, F., ASSERNE, F., ELABED, S., BENSOUDA, S., MABROUKI, M. & LATRACHE, H. 2014. Adhesion of Staphylococcus aureus on stainless steel treated with three types of milk. *Food Control,* 38**,** 104-108.

HARDES, J., AHRENS, H., GEBERT, C., STREITBUERGER, A., BUERGER, H., ERREN, M., GUNSEL, A., WEDEMEYER, C., SAXLER, G., WINKELMANN, W. & GOSHEGER, G. 2007. Lack of toxicological side-effects in silver-coated megaprostheses in humans. *Biomaterials,* 28**,** 2869-2875.

HARRIS, L. G. & RICHARDS, R. G. 2006. Staphylococci and implant surfaces: a review. *Injury,* 37**,** S3-S14.

HARSHA, K. S. 2005. *Principles of Vapour Deposition of Thin Films,* New York, Alden Books.

HEINKE, W., LEYLAND, A., MATTHEWS, A., BERG, G., FRIEDRICH, C. & BROSZEIT, E. 1995. Evaluation of PVD nitride coatings, using impact, scratch and Rockwell-C adhesion tests. *Thin Solid Films,* 270**,** 431-438.

HOIBY, N., BJARNSHOLT, T., GIVSKOV, M., MOLIN, S. & CIOFU, O. 2010. Antibiotic resistance of bacterial biofilms. *International Journal of Antimicrobial Agents,* 35**,** 322-332.

HOLAH, J. T., BETTS, R. P. & THORPE, R. H. 1989. The Use Of Epifluorescence Microscopy To Determine Surface Hygiene. *International Biodeterioration,* 25**,** 147-153.

HSIEH, J. H., YEH, T. H., LI, C., CHIU, C. H. & HUANG, C. T. 2013. Antibacterial properties of TaN–(Ag,Cu) nanocomposite thin films. *Vacuum,* 87**,** 160-163.

HUANG, H.-L., CHANG, Y.-Y., LAI, M.-C., LIN, C.-R., LAI, C.-H. & SHIEH, T.-M. 2010. Antibacterial TaN-Ag coatings on titanium dental implants. *Surface and Coatings Technology,* 205**,** 1636-1641.

HUANG, J.-H., MA, C.-H. & CHEN, H. 2006. Effect of Ti interlayer on the residual stress and texture development of TiN thin films deposited by unbalanced magnetron sputtering. *Surface and Coatings Technology,* 201**,** 3199-3204.

IVANOV, P. C., AMARAL, L. A. N., GOLDBERGER, A. L., HAVLIN, S., ROSENBLUM, M. G., STRUZIK, Z. R. & STANLEY, H. E. 1999. Multifractality in human heartbeat dynamics. *Nature,* 399**,** 461-465.

JACOBS, R., MENEVE, J., DYSON, G., TEER, D. G., JENNETT, N. M., HARRIS, P., VON STEBUT, J., COMTE, C., FEUCHTER, P., CAVALEIRO, A., RONKAINEN, H., HOLMBERG, K., BECK, U., REINERS, G. & INGELBRECHT, C. D. 2003. A certified reference material for the scratch test. *Surface and Coatings Technology,* 174–175**,** 1008-1013.

JENSEN, M. H., KADANOFF, L. P., LIBCHABER, A., PROCACCIA, I. & STAVANS, J. 1985. Global Universality at the Onset of Chaos: Results of a Forced Rayleigh-Bénard Experiment. *Physical Review Letters,* 55**,** 2798-2801.

JULLIEN, C., BÉNÉZECH, T., CARPENTIER, B., LEBRET, V. & FAILLE, C. 2003. Identification of surface characteristics relevant to the hygienic status of stainless steel for the food industry. *Journal of Food Engineering,* 56**,** 77-87.

KATSIKOGIANNI, M. & MISSIRLIS, Y. F. 2004. Concise review of mechanisms of bacterial adhesion to biomaterials and of techniques used in estimating bacteria- material interactions. *European Cells and Materials,* 8**,** 37-57.

KAWAKAMI, H., YOSHIDA, K., NISHIDA, Y., KIKUCHI, Y. & SATO, Y. 2008. Antibacterial Properties of Metallic Elements for Alloying Evaluated with Application of JIS Z 2801:2000. *ISIJ International,* 48**,** 1299-1304.

KAZEMZADEH-NARBAT, M., KINDRACHUK, J., DUAN, K., JENSSEN, H. V., HANCOCK, R. E. W. & WANG, R. 2010. Antimicrobial peptides on calcium phosphate-coated titanium for the prevention of implant-associated infections. *Biomaterials,* 31**,** 9519-9526.

KAZEMZADEH-NARBAT, M., LAI, B. F. L., DING, C., KIZHAKKEDATHU, J. N., HANCOCK, R. E. W. & WANG, R. 2013. Multilayered coating on titanium for controlled release of antimicrobial peptides for the prevention of implant-associated infections. *Biomaterials,* 34**,** 5969-5977.

KELLY, P. J. & ARNELL, R. D. 2000. Magnetron sputtering: a review of recent developments and applications. *Vacuum,* 56**,** 159-172.

KELLY, P. J. & BRADLEY, J. W. 2009. Pulsed magnetron sputtering - process overview and applications. *Journal of Optoelectronics and Advanced Materials,* 11**,** 1101-1107.

KELLY, P. J., LI, H., BENSON, P. S., WHITEHEAD, K. A., VERRAN, J., ARNELL, R. D. & IORDANOVA, I. 2010a. Comparison of the tribological and antimicrobial properties of CrN/Ag, ZrN/Ag, TiN/Ag, and TiN/Cu nanocomposite coatings. *Surface and Coatings Technology,* In Press, Corrected Proof.

KELLY, P. J., LI, H., WHITEHEAD, K. A., BENSON, P. S. & VERRAN, J. Comparison of Tribological and Anti-microbial Properties of TiN/Ag and ZrN/Ag

Nanocomposite Coatings. Fouling and Cleaning in Food Processing, 22-24 March 2010b Cambridge. 16-23.

KELLY, P. J., LI, H., WHITEHEAD, K. A., VERRAN, J., ARNELL, R. D. & LORDANOVA, I. 2009a. A study of the antimicrobial and tribological properties of TiN/Ag nanocomposite coatings. *Surface & Coatings Technology,* 204**,** 1137-1140.

KELLY, P. J., WHITEHEAD, K. A., H LI, VERRAN, J. & ARNELL, R. 2011. The influence of silver content on the tribological and antimicrobial properties of ZrN/Ag nanocomposite coatings. *Journal of Nanoscience and Nanotechnology,* 11**,** 1-5.

KELLY, P. J. L., H., WHITEHEAD, K.A, VERRAN, J., ARNELL, R.D, IORDANOVA, I 2009b. A Study of the Anti-Microbial and Tribological Properties of TiN/Ag Nanocomposite Coatings. *Surface & Coatings Technology,* 204**,** 1137-1140.

KERTZMAN, Z., MARCHAL, J., SUAREZ, M., STAIA, M., FILIP, P., KOHLI, P. & AOUADI, S. 2008. Mechanical, tribological, and biocompatibility properties of ZrN-Ag nanocomposite films. *Journal of Biomedical Materials Research Part A,* 84A**,** 1061-1067.

KIM, J. S., KUK, E., YU, K. N., KIM, J.-H., PARK, S. J., LEE, H. J., KIM, S. H., PARK, Y. K., PARK, Y. H., HWANG, C.-Y., KIM, Y.-K., LEE, Y.-S., JEONG, D. H. & CHO, M.-H. 2007. Antimicrobial effects of silver nanoparticles. *Nanomedicine: Nanotechnology, Biology and Medicine,* 3**,** 95-101.

KLASEN, H. J. 2000. A historical review of the use of silver in the treatment of burns. II. Renewed interest for silver. *Burns,* 26**,** 131-138.

KNUDSON, K. J., FRINK, L., HOFFMAN, B. W. & PRICE, T. D. 2004. Chemical characterization of Arctic soils: activity area analysis in contemporary Yup'ik fish camps using ICP-AES. *Journal of Archaeological Science,* 31**,** 443-456.

KONG, Q., JI, L., LI, H., LIU, X., WANG, Y., CHEN, J. & ZHOU, H. 2011. Influence of substrate bias voltage on the microstructure and residual stress of CrN films deposited by medium frequency magnetron sputtering. *Materials Science and Engineering: B,* 176**,** 850-854.

KORBER, D. R., CHOI, A., WOLFAARDT, G. M., INGHAM, S. C. & CALDWELL, D. E. 1997. Substratum topography influences susceptibility of Salmonella enteritidis biofilms to trisodium phosphate. *Applied and Environmental Microbiology,* 63**,** 3352-3358.

KOYUNCU, I., BRANT, J., LÜTTGE, A. & WIESNER, M. R. 2006. A comparison of vertical scanning interferometry (VSI) and atomic force microscopy (AFM) for characterizing membrane surface topography. *Journal of Membrane Science,* 278**,** 410-417.

KROPP, J., BLOCK, A., VON BLOH, W., KLENKE, T. & SCHELLNHUBER, H. J. 1997. Multifractal characterization of microbially induced magnesian calcite formation in Recent tidal flat sediments. *Sedimentary Geology,* 109**,** 37-51.

KUO, Y.-C., LEE, J.-W., WANG, C.-J. & CHANG, Y.-J. 2007. The effect of Cu content on the microstructures, mechanical and antibacterial properties of Cr–Cu–N

nanocomposite coatings deposited by pulsed DC reactive magnetron sputtering. *Surface and Coatings Technology,* 202**,** 854-860.

KUSANO, E., KITAGAWA, M., KURODA, Y., NANTO, H. & KINBARA, A. 1998. Adhesion and hardness of compositionally gradient TiO2/Ti/TiN, ZrO2/Zr/ZrN, and TiO2/Ti/Zr/ZrN coatings. *Thin Solid Films,* 334**,** 151-155.

LACKNER, J. M., WALDHAUSER, W., HARTMANN, P., MAJOR, L. & KOT, M. 2013. Bio-inspired wear protection of soft materials by hard films: Mechanical and tribological properties of nacre and multilayer Ti–TiN films. *Archives of Civil and Mechanical Engineering,* In Press.

LAKES, R. S. & PARK, J. 2007. *Biomaterials: An Introduction,* New York, Springer Science + Business Medial LLC.

LANSDOWN, A. B. G. 2010. A Pharmacological and Toxicological Profile of Silver as an Antimicrobial Agent in Medical Devices. *Advances in Pharmacological Sciences,* 2010**,** 16.

LEE-SMITH, J. 1999. Can the orthopaedic team reduce the risk of infection? *Journal of Orthopaedic Nursing,* 3**,** 95-98.

LEE-SMITH, J., SANTY, J., DAVIS, P., JESTER, R. & KNEALE, J. 2001. Pin site management. Towards a consensus: part 1. *Journal of Orthopaedic Nursing,* 5**,** 37-42.

LEE, J.-W., KUO, Y.-C., WANG, C.-J., CHANG, L.-C. & LIU, K.-T. 2008. Effects of substrate bias frequencies on the characteristics of chromium nitride coatings deposited by pulsed DC reactive magnetron sputtering. *Surface and Coatings Technology,* 203**,** 721-725.

LEWEN, N. & NUGENT, D. 2010. The use of inductively coupled plasma-atomic emission spectroscopy (ICP-AES) in the determination of lithium in cleaning validation swabs. *Journal of Pharmaceutical and Biomedical Analysis,* 52**,** 652-655.

LI, D. J., LIU, F., WANG, M. X., ZHANG, J. J. & LIU, Q. X. 2006. Structural and mechanical properties of multilayered gradient CrN/ZrN coatings. *Thin Solid Films,* 506–507**,** 202-206.

LI, H., GIGER, M. L., OLOPADE, O. I. & LAN, L. 2007. Fractal Analysis of Mammographic Parenchymal Patterns in Breast Cancer Risk Assessment. *Academic Radiology,* 14**,** 513-521.

LI, J. 2013. Retro-fit Low Emissivity Window Films. *Technical Conference Proceedings, Coatings for Cleantech Energy Conversion and Related Processes.* Society of Vacuum Coaters.

LIN, J., MOORE, J. J., SPROUL, W. D., MISHRA, B., WU, Z. & WANG, J. 2010. The structure and properties of chromium nitride coatings deposited using dc, pulsed dc and modulated pulse power magnetron sputtering. *Surface and Coatings Technology,* 204**,** 2230-2239.

LINDSETH, I. & BARDAL, A. 1999. Quantitative topography measurements of rolled aluminium surfaces by atomic force microscopy and optical methods. *Surface and Coatings Technology,* 111**,** 276-286.

LIU, X., MOU, Y., WU, S. & MAN, H. C. 2013. Synthesis of silver-incorporated hydroxyapatite nanocomposites for antimicrobial implant coatings. *Applied Surface Science,* 273**,** 748-757.

MAHAN, J., SELIGSON, D., HENRY, S. L., HYNES, P. & DOBBINS, J. 1991. Factors in Pin Tract Infections. *Orthopedics,* 14**,** 305-308.

MANDELBROT, B. B. 1974. Intermittent turbulence in self-similar cascades-divergence of high movements and dimension of carrier. *Journal of Fluid Mechanics,* 62**,** 331-358.

MASSÈ, A., BRUNO, A., BOSETTI, M., BIASIBETTI, A., CANNAS, M. & GALLINARO, P. 2000. Prevention of pin track infection in external fixation with silver coated pins: Clinical and microbiological results. *Journal of Biomedical Materials Research,* 53**,** 600-604.

MEDILANSKI, E., KAUFMANN, K., WICK, L. Y., WANNER, O. & HARMS, H. 2002. Influence of the surface topography of stainless steel on bacterial adhesion. *Biofouling,* 18**,** 193-203.

MÉNDEZ-VILAS, A., DONOSO, M. G., GONZÁLEZ-CARRASCO, J. L. & GONZÁLEZ-MARTÍN, M. L. 2006. Looking at the micro-topography of polished and blasted Ti-based biomaterials using atomic force microscopy and contact angle goniometry. *Colloids and Surfaces B: Biointerfaces,* 52**,** 157-166.

METTLER, E. & CARPENTIER, B. 1997. Location, enumeration and identification of the microbial contamination after cleaning of EPDM gaskets introduced into a milk pasteurization line. *Lait,* 77**,** 489-503.

METTLER, E. & CARPENTIER, B. 1998. Variations over time of microbial load and physicochemical properties of floor materials after cleaning in food industry premises. *Journal of Food Protection,* 61**,** 57-65.

MIAO, L., JIN, P., KANEKO, K., TERAI, A., NABATOVA-GABAIN, N. & TANEMURA, S. 2003. Preparation and characterization of polycrystalline anatase and rutile TiO2 thin films by rf magnetron sputtering. *Applied Surface Science,* 212-213**,** 255-263.

MIENTUS, R. & ELLMER, K. 1999. Reactive DC magnetron sputtering of elemental targets in Ar/N2 mixtures: relation between the discharge characteristics and the heat of formation of the corresponding nitrides. *Surface and Coatings Technology,* 116–119**,** 1093-1101.

MILLER, D. C. V., R.J.; THAPA, A.; WEBSTER, T.J.; HABERSTROH, K.M. 2005. Comparison of fibroblast and vascular cell adhesion to nano-structured poly(lactic-co-glycolic acid) films. *Applied Bionics Biomechanics,* 2**,** 1-7.

MILLS, S. L., LEES, G. C., LIAUW, C. M. & LYNCH, S. 2002. Dispersion assessment of flame retardant filler/polymer systems using a combination of X-ray mapping and multifractal analysis. *Polymer Testing,* 21**,** 941-947.

MILLS, S. L., LEES, G. C., LIAUW, C. M. & LYNCH, S. 2004. An Improved Method for the Dispersion Assessment of Flame Retardant Filler/Polymer Systems Based on the Multifractal Analysis of SEM Images. *Macromolecular Materials and Engineering,* 289**,** 864-871.

MILLS, S. L., LEES, G. C., LIAUW, C. M., ROTHON, R. N. & LYNCH, S. 2005. Prediction of Mechanical Properties Following the Dispersion Assessment of Flame Retardant Filler/Polymer Composites Based on the Multifractal Analysis of SEM Images. *Journal of Macromolecular Science, Part B,* 44**,** 1137-1151.

MITTAL, K. L. 2001. *Adhesion Measurement of Films & Coatings: Volume 2*, Taylor & Francis.

MODAK, K. & FOX, C. 1973. Binding of Silver Sufadiazine in the cellular components of *Pseudomonas aeruginosa*. *Biochemical Pharmacology,* 22**,** 2392-2404.

MONAGHAN, D. P., TEER, D. G., LAING, K. C., EFEOGLU, I. & ARNELL, R. D. 1993. Deposition of graded alloy nitride films by closed field unbalanced magnetron sputtering. *Surface and Coatings Technology,* 59**,** 21-25.

MONTANARO, L., CAMPOCCIA, D. & ARCIOLA, C. R. 2007. Advancements in molecular epidemiology of implant infections and future perspectives. *Biomaterials,* 28**,** 5155-5168.

MØRETRØ, T., HØIBY-PETTERSEN, G. S., HALVORSEN, C. K. & LANGSRUD, S. 2012. Antibacterial activity of cutting boards containing silver. *Food Control,* 28**,** 118-121.

MORRA, M. & CASSINELLI, C. 1998. Bacterial adhesion to polymer surfaces: A critical review of surface thermodynamic approaches. *Journal of Biomaterials Science, Polymer Edition,* 9**,** 55-74.

MUELLER, C. K., SOLCHER, P., PEISKER, A., MTSARIASHVILLI, M., SCHLEGEL, K. A., HILDEBRAND, G., ROST, J., LIEFEITH, K., CHEN, J. & SCHULTZE-MOSGAU, S. 2013. Analysis of the influence of the macro- and microstructure of dental zirconium implants on osseointegration: a minipig study. *Oral Surgery, Oral Medicine, Oral Pathology and Oral Radiology,* 116**,** e1-e8.

MUNGKALASIRI, J., BEDEL, L., EMIEUX, F., CARA, A. V.-D., FRENEY, J., MAURY, F. & RENAUD, F. N. R. 2013. Antibacterial properties of TiO2–Cu composite thin films grown by a one step DLICVD process. *Surface and Coatings Technology,* In Press, Corrected Proof [26-10-2013].

MUSIL, J., BAROCH, P., VLČEK, J., NAM, K. H. & HAN, J. G. 2005. Reactive magnetron sputtering of thin films: present status and trends. *Thin Solid Films,* 475**,** 208-218.

MUSIL, J., BLAŽEK, J., FAJFRLÍK, K., ČERSTVÝ, R. & PROKŠOVÁ, Š. 2013. Antibacterial Cr–Cu–O films prepared by reactive magnetron sputtering. *Applied Surface Science,* 276**,** 660-666.

NAYAGAM, S. 2010. Femoral lengthening with a rail external fixator: tips and tricks. *Strategies in Trauma and Limb Reconstruction,* 5**,** 137-144.

NECULA, B., FRATILA-APACHITEI, L., BERKANI, A., APACHITEI, I. & DUSZCZYK, J. 2009a. Enrichment of anodic MgO layers with Ag nanoparticles for biomedical applications. *Journal of Materials Science: Materials in Medicine,* 20**,** 339-345.

NECULA, B. S., FRATILA-APACHITEI, L. E., ZAAT, S. A. J., APACHITEI, I. & DUSZCZYK, J. 2009b. In vitro antibacterial activity of porous TiO2–Ag composite layers against methicillin-resistant Staphylococcus aureus. *Acta Biomaterialia,* 5**,** 3573-3580.

NGUYEN, V. T., TURNER, M. S. & DYKES, G. A. 2011. Influence of cell surface hydrophobicity on attachment of Campylobacter to abiotic surfaces. *Food Microbiology,* 28**,** 942-950.

NICOLAUS, M. & SCHÄPERS, M. 2006. *Fundamentals of Thin-film Technology*, Wiley-VCH Verlag GmbH & Co. KGaA.

NIES, D. H. 1999. Microbial heavy-metal resistance. *Applied Microbiology and Biotechnology,* 51**,** 730-750.

NOYCE, J. O., MICHELS, H. & KEEVIL, C. W. 2006. Potential use of copper surfaces to reduce survival of epidemic meticillin-resistant Staphylococcus aureus in the healthcare environment. *Journal of Hospital Infection,* 63**,** 289-297.

OKA, Y., KIM, W.-C., YOSHIDA, T., HIRASHIMA, T., MOURI, H., URADE, H., ITOH, Y. & KUBO, T. 2008. Efficacy of titanium dioxide photocatalyst for inhibition of bacterial colonization on percutaneous implants. *Journal of Biomedical Materials Research Part B: Applied Biomaterials,* 86B**,** 530-540.

OKAZAKI, Y., ITO, Y., KYO, K. & TATEISHI, T. 1996. Corrosion resistance and corrosion fatigue strength of new titanium alloys for medical implants without V and Al. *Materials Science and Engineering: A,* 213**,** 138-147.

ORTIZ, A. J., FERNÁNDEZ, E., VICENTE, A., CALVO, J. L. & ORTIZ, C. 2011. Metallic ions released from stainless steel, nickel-free, and titanium orthodontic alloys: Toxicity and DNA damage. *American Journal of Orthodontics and Dentofacial Orthopedics,* 140**,** e115-e122.

OSORIO-VARGAS, P., SANJINES, R., RUALES, C., CASTRO, C., PULGARIN, C., RENGIFO-HERRERA, A. J., LAVANCHY, J. C. & KIWI, J. 2011. Antimicrobial Cu-functionalized surfaces prepared by bipolar asymmetric DC-pulsed magnetron sputtering (DCP). *Journal of Photochemistry and Photobiology A: Chemistry,* 220**,** 70-76.

PAL, S., TAK, Y. K. & SONG, J. M. 2007. Does the Antibacterial Activity of Silver Nanoparticles Depend on the Shape of the Nanoparticle? A Study of the Gram-Negative Bacterium Escherichia coli. *Appl. Environ. Microbiol.,* 73**,** 1712-1720.

PALEY, D. 1990. Problems, Obstacles, and Complications of Limb Lengthening by the Ilizarov Technique. *Clinical Orthopaedics and Related Research,* 250**,** 81-104.

PANEA, B., RIPOLL, G., GONZÁLEZ, J., FERNÁNDEZ-CUELLO, Á. & ALBERTÍ, P. 2014. Effect of nanocomposite packaging containing different proportions of ZnO and Ag on chicken breast meat quality. *Journal of Food Engineering,* 123**,** 104-112.

PANJWANI, B. & SINHA, S. K. 2012. Tribology and hydrophobicity of a biocompatible GPTMS/PFPE coating on Ti6Al4V surfaces. *Journal of the Mechanical Behavior of Biomedical Materials,* 15**,** 103-111.

PAPI, P. A., MULLIGAN, C. P. & GALL, D. 2012. CrN–Ag nanocomposite coatings: Control of lubricant transport by diffusion barriers. *Thin Solid Films,* 524**,** 211-217.

PARAMESWARAN, A. D., ROBERTS, C. S., SELIGSON, D. & VOOR, M. 2003. Pin Tract Infection With Contemporary External Fixation: How Much of a Problem? *Journal of Orthopaedic Trauma,* 17**,** 503-507.

PASHLEY, R. M. & KITCHENER, J. A. 1979. Surface forces in adsorbed multilayers of water on quartz. *Journal of Colloid and Interface Science,* 71**,** 491-500.

PASRICHA, A., JANGRA, S. L., SINGH, N., DILBAGHI, N., SOOD, K. N., ARORA, K. & PASRICHA, R. 2012. Comparative study of leaching of silver nanoparticles from fabric and effective effluent treatment. *Journal of Environmental Sciences,* 24**,** 852-859.

PASTÉN, D., MUÑOZ, V., CISTERNAS, A., ROGAN, J. & VALDIVIA, J. A. 2011. Monofractal and multifractal analysis of the spatial distribution of earthquakes in the central zone of Chile. *Physical Review E,* 84**,** 066123.

PENDYALA, L., JABARA, R., ROBINSON, K. & CHRONOS, N. 2009. Passive and active polymer coatings for intracoronary stents: Novel devices to promote arterial healing. *Journal of Interventional Cardiology,* 22**,** 37-48.

PERCIVAL, S. L., BOWLER, P. G. & RUSSELL, D. 2005. Bacterial resistance to silver in wound care. *Journal of Hospital Infection,* 60**,** 1-7.

PERENI, C. I., ZHAO, Q., LIU, Y. & ABEL, E. 2006. Surface free energy effect on bacterial retention. *Colloids and Surfaces B: Biointerfaces,* 48**,** 143-147.

PILLOUD, D., DEHLINGER, A. S., PIERSON, J. F., ROMAN, A. & PICHON, L. 2003. Reactively sputtered zirconium nitride coatings: structural, mechanical, optical and electrical characteristics. *Surface and Coatings Technology,* 174-175**,** 338-344.

POGORZELSKI, S. J., MAZUREK, A. Z. & SZCZEPANSKA, A. 2013. In-situ surface wettability parameters of submerged in brackish water surfaces derived from captive bubble contact angle studies as indicators of surface condition level. *Journal of Marine Systems,* 119–120**,** 50-60.

POLCAR, T., EVARISTO, M. & CAVALEIRO, A. 2009. Comparative study of the tribological behavior of self-lubricating W–S–C and Mo–Se–C sputtered coatings. *Wear,* 266**,** 388-392.

POLIZZOTTI, R. S. & BURTON, J. J. 1977. Surface segregation in alloys: dilute binary iron/zirconium solid solutions. *Journal of Vacuum Science & Technology,* 14**,** 347-350.

PRINGLE, J. H. & FLETCHER, M. 1986. Influence of substratum hydration and adsorbed macromolecules on bacterial attachment to surfaces. *Applied and Environmental Microbiology,* 51**,** 1321-1325.

PUCKETT, S. D., TAYLOR, E., RAIMONDO, T. & WEBSTER, T. J. 2010. The relationship between the nanostructure of titanium surfaces and bacterial attachment. *Biomaterials,* 31**,** 706-713.

QUIRYNEN, M. & BOLLEN, C. M. L. 1995. The Influence Of Surface-Roughness And Surface-Free Energy On Supragingival And Subgingival Plaque-Formation In Man - A Review Of The Literature

Journal of Clinical Periodontology, 22**,** 1-14.

RADZIG, M. A., NADTOCHENKO, V. A., KOKSHAROVA, O. A., KIWI, J., LIPASOVA, V. A. & KHMEL, I. A. 2013. Antibacterial effects of silver nanoparticles on gram-negative bacteria: Influence on the growth and biofilms formation, mechanisms of action. *Colloids and Surfaces B: Biointerfaces,* 102**,** 300-306.

RAHMAN, M., HAIDER, J., DOWLING, D. P., DUGGAN, P. & HASHMI, M. S. J. 2005. Deposition of magnetron sputtered TiN + MoSx coating with Ti–TiN graded interlayer. *Surface and Coatings Technology,* 200**,** 1071-1075.

RAI, M., YADAV, A. & GADE, A. 2009. Silver nanoparticles as a new generation of antimicrobials. *Biotechnology Advances,* 27**,** 76-83.

ROOSJEN, A., NORDE, W., VAN DER MEI, H. C. & BUSSCHER, H. J. 2006. The use of positively charged or low surface free energy coatings versus polymer brushes in controlling biofilm formation.

ROSENBERG, M., GUTNICK, D. & ROSENBERG, E. 1980. Adherence of bacteria to hydrocarbons: A simple method for measuring cell-surface hydrophobicity. *FEMS Microbiology Letters,* 9**,** 29-33.

ROY, R. 1990. *A Primer on the Taguchi Method,* Michigan, Society of Manufacturing Engineers.

SANDSTROM, S. 2011. *The antibacterial effect of silver with different release kinetics.* Master of Science, Chalmers University of Technology.

SANTY, J. 2010. A review of pin site wound infection assessment criteria. *International Journal of Orthopaedic and Trauma Nursing,* 14**,** 125-131.

SAUER, K., CAMPER, A. K., EHRLICH, G. D., COSTERTON, J. W. & DAVIES, D. G. 2002. Pseudomonas aeruginosa Displays Multiple Phenotypes during Development as a Biofilm. *Journal of Bacteriology,* 184**,** 1140-1154.

SAVVIDES, N. & WINDOW, B. 1986. Unbalanced magnetron ion-assisted deposition and property modification of thin films. *Journal of Vacuum Science & Technology A: Vacuum, Surfaces, and Films,* 4**,** 504-508.

SAWAN, S. P., SHALON, T., SUNDAR, S. & ALEXANDER, Y. 1998. *Contact-killing non-leaching antimicrobial materials*. US 08/736,823.

SAWAN, S. P., SUNDAR, S. & ALEXANDER, Y. 2000. *Contact-killing antimicrobial devices*. USA patent application US 09/151,495.

SCHAULE, G., FLEMMING, H. C. & RIDGWAY, H. F. 1993. Use of 5-cyano-2,3-ditolyl tetrazolium chloride for quantifying planktonic and sessile respiring bacteria in drinking water. *Applied and Environmental Microbiology,* 59**,** 3850-3857.

SCHEUERMAN, T. R., CAMPER, A. K. & HAMILTON, M. A. 1998. Effects of substratum topography on bacterial adhesion. *Journal of Colloid and Interface Science,* 208**,** 23-33.

SCHIERHOLZ, J. M., LUCAS, L. J., RUMP, A. & PULVERER, G. 1998. Efficacy of silver-coated medical devices. *Journal of Hospital Infection,* 40**,** 257-262.

SCHILLER, S., GOEDICKE, K., RESCHKE, J., KIRCHHOFF, V., SCHNEIDER, S. & MILDE, F. 1993. Pulsed magnetron sputter technology. *Surface and Coatings Technology,* 61**,** 331-337.

SCHULTZE, H. E. & HEREMANS, J. F. 1969. *Molecular biology of human proteins : with special reference to plasma proteins,* Amsterdam [etc.], [s.n.].

SCULCO, T. P. 1995. The economic impact of infected joint arthroplasty. *Orthopedics,* 18**,** 871-3.

SEDLAČEK, M., PODGORNIK, B. & VIŽINTIN, J. 2009. Influence of surface preparation on roughness parameters, friction and wear. *Wear,* 266**,** 482-487.

SEVERIN, E., STELLMACH, J. & NACHTIGAL, H.-M. 1985. Fluorimetric assay of redox activity in cells. *Analytica Chimica Acta,* 170**,** 341-346.

SHIRAI, T., TSUCHIYA, H., SHIMIZU, T., OHTANI, K., ZEN, Y. & TOMITA, K. 2009. Prevention of pin tract infection with titanium-copper alloys. *Journal of Biomedical Materials Research Part B: Applied Biomaterials,* 91B**,** 373-380.

SIMS, M. & SALEH, M. 2000. External fixation – the incidence of pin site infection: a prospective audit. *Journal of Orthopaedic Nursing,* 4**,** 59-63.

SKOVAGER, A., WHITEHEAD, K., SIEGUMFELDT, H., INGMER, H., VERRAN, J. & ARNEBORG, N. 2012. Influence of flow direction and flow rate on the initial adhesion of seven Listeria monocytogenes strains to fine polished stainless steel. *International Journal of Food Microbiology,* 157**,** 174-181.

SKOVAGER, A., WHITEHEAD, K., WICKENS, D., VERRAN, J., INGMER, H. & ARNEBORG, N. 2013. A comparative study of fine polished stainless steel, TiN and TiN/Ag surfaces: Adhesion and attachment strength of Listeria monocytogenes as well as anti-listerial effect. *Colloids and Surfaces B: Biointerfaces,* 109**,** 190-196.

SONDI, I. & SALOPEK-SONDI, B. 2004. Silver nanoparticles as antimicrobial agent: a case study on E. coli as a model for Gram-negative bacteria. *Journal of Colloid and Interface Science,* 275**,** 177-182.

SONG, D.-H., UHM, S.-H., KIM, S.-E., KWON, J.-S., HAN, J.-G. & KIM, K.-N. 2012. Synthesis of titanium oxide thin films containing antibacterial silver nanoparticles by a reactive magnetron co-sputtering system for application in biomedical implants. *Materials Research Bulletin,* 47**,** 2994-2998.

SPENCER, A., DOBRYDEN, I., ALMQVIST, N., ALMQVIST, A. & LARSSON, R. 2013. The influence of AFM and VSI techniques on the accurate calculation of tribological surface roughness parameters. *Tribology International,* 57**,** 242-250.

SPROUL, W. D., RUDNIK, P. J., GRAHAM, M. E. & ROHDE, S. L. 1990. High rate reactive sputtering in an opposed cathode closed-field unbalanced magnetron sputtering system. *Surface and Coatings Technology,* 43–44, Part 1**,** 270-278.

ŠROUBEK, Z. 1981. Theory of Charge States in Sputtering. *In:* TAGLAUER, E. & HEILAND, W. (eds.) *Inelastic Particle-Surface Collisions.* Springer Berlin Heidelberg.

STAROSTINA, N. G., KOSHCHAEV, A. G., RATNER, E. N. & TSIOMENKO, A. B. 1997. Assessment of cell-surface hydrophobicity in methanotrophic bacteria by their adherence to hydrocarbons. *Microbiology,* 66**,** 151-156.

STEWART, P. S. & COSTERTON, W. J. 2001. Antibiotic resistance of bacteria in biofilms. *The Lancet,* 358**,** 135-138.

STREINER, D. L., NORMAN, G.R., 2003. *Health Measurement Scales: A Practical Guide to their Development and Use,* Oxford, Oxford University Press.

SZLAVIK, J., PAIVA, D. S., MORK, N., VAN DEN BERG, F., VERRAN, J., WHITEHEAD, K., KNOCHEL, S. & NIELSEN, D. S. 2012. Initial adhesion of Listeria monocytogenes to solid surfaces under liquid flow. *International Journal of Food Microbiology,* 152**,** 181-188.

TAKAHASHI, H., SUDA, T., TANAKA, Y. & KIMURA, B. 2010. Cellular hydrophobicity of Listeria monocytogenes involves initial attachment and biofilm formation on the surface of polyvinyl chloride. *Letters in Applied Microbiology,* 50**,** 618-625.

TEBBS, S. E., SAWYER, A. & ELLIOT, T. S. J. 1994. Influence of surface morphology on in vitro bacterial adherence to central venous catheters. *British Journal of Anaesthesia,* 72**,** 587-591.

TEER, D. G. 1988. A magnetron sputter ion plating system. *Surface and Coatings Technology,* 36**,** 901-907.

TESSIER, Y., LOVEJOY, S. & SCHERTZER, D. 1993. Universal Multifractals: Theory and Observations for Rain and Clouds. *Journal of Applied Meteorology,* 32**,** 223-250.

TETERYCZ, D., FERRY, T., LEW, D., STERN, R., ASSAL, M., HOFFMEYER, P., BERNARD, L. & UÇKAY, I. 2010. Outcome of orthopedic implant infections due to different staphylococci. *International Journal of Infectious Diseases,* 14**,** e913-e918.

THORNTON, J. 1974. Influence of apparatus geometry and deposition conditions on the structure and topography of thick sputtered coatings. *J. Vac. Sci. Technol.,* 11**,** 666.

TIDE, C., HARKIN, S. R., GEESEY, G. G., BREMER, P. J. & SCHOLZ, W. 1999. The influence of welding procedures on bacterial colonization of stainless steel weldments. *Journal of Food Engineering,* 42**,** 85-96.

TIMMS, A., VINCENT, M., SANTY-TOMLINSON, J. & HERTZ, K. 2013. A fresh consensus for pin site care in the UK. *International Journal of Orthopaedic and Trauma Nursing,* 17**,** 19-28.

TIMPERLEY, D. A., THORPE, R. H. & HOLAH, J. T. 1992. IMPLICATIONS OF ENGINEERING DESIGN IN FOOD-INDUSTRY HYGIENE. *Biofilms - Science and Technology,* 223**,** 379-393.

TRAGANOS, F., DARZYNKIEWICZ, Z., SHARPLESS, T. & MELAMED, M. R. 1977. Simultaneous staining of ribonucleic and deoxyribonucleic acids in unfixed cells using acridine orange in a flow cytofluorometric system. *Journal of Histochemistry & Cytochemistry,* 25**,** 46-56.

TRAMPUZ, A. & ZIMMERLI, W. 2006. Diagnosis and treatment of infections associated with fracture-fixation devices. *Injury,* 37**,** S59-S66.

TRUONG, V. K., LAPOVOK, R., ESTRIN, Y. S., RUNDELL, S., WANG, J. Y., FLUKE, C. J., CRAWFORD, R. J. & IVANOVA, E. P. 2010. The influence of nano-scale surface roughness on bacterial adhesion to ultrafine-grained titanium. *Biomaterials,* 31**,** 3674-3683.

TYAGI, R., XIONG, D. S., LI, J. & DAI, J. 2010. Elevated temperature tribological behavior of Ni based composites containing nano-silver and hBN. *Wear,* 269**,** 884-890.

UHM, S.-H., SONG, D.-H., KWON, J.-S., LEE, S.-B., HAN, J.-G., KIM, K.-M. & KIM, K.-N. 2013. E-beam fabrication of antibacterial silver nanoparticles on diameter-controlled TiO2 nanotubes for bio-implants. *Surface and Coatings Technology,* 228, Supplement 1**,** S360-S366.

USGS. 2013. *ICP-AES Technique Description* [Online]. U.S. Department of the Interior. Available: http://minerals.cr.usgs.gov/gips/na/5process.html [Accessed 18/10/2013.

VALVODA, V. 1995. Structure of thin films of titanium nitride. *Journal of Alloys and Compounds,* 219**,** 83-87.

VAN DER MEI, H. C., VAN DE BELT-GRITTER, B. & BUSSCHER, H. J. 1995. Implications of microbial adhesion to hydrocarbons for evaluating cell surface hydrophobicity 2. Adhesion mechanisms. *Colloids and Surfaces B: Biointerfaces,* 5**,** 117-126.

VAN OSS, C. J. 1993. Acid—base interfacial interactions in aqueous media. *Colloids and Surfaces A: Physicochemical and Engineering Aspects,* 78**,** 1-49.

VAN OSS, C. J. 1994. *Interfacial Forces in Aqueous Media,* New York, Marcel Dekker.

VAN OSS, C. J. 1995. Hydrophobicity of biosurfaces — Origin, quantitative determination and interaction energies. *Colloids and Surfaces B: Biointerfaces,* 5**,** 91-110.

VAN OSS, C. J. & GIESE, R. F. 1995. The hydrophilicity and hydrophobicity of clay minerals. *Clays and Clay Minerals,* 43**,** 474-477.

VAN OSS, C. J. & GOOD, R. J. 1988. ON THE MECHANISM OF “HYDROPHOBIC” INTERACTIONS. *Journal of Dispersion Science and Technology,* 9**,** 355-362.

VENEZIANO, D. F. 2009. P Improved movement scaling estimation for multifractal signals. *Nonlinear Processes in Geophysics,* 16**,** 641-653.

VERRAN, J. & BOYD, R. D. 2001. The relationship between substratum surface roughness and microbiological and organic soiling: a review. *Biofouling,* 17**,** 59-+.

VERRAN, J., BOYD, R. D., HALL, K. E. & WEST, R. 2002. The detection of microorganisms and organic material on stainless steel food contact surfaces. *Biofouling,* 18**,** 167-176.

VERRAN, J., DRUCKER, D. B. & TAYLOR, C. J. 1981. Measurement Of Adherence To Glass Of Streptococcus-Mutans By Image-Analysis. *Journal of Dental Research,* 60**,** 1105-1105.

VERRAN, J. & JONES, M. V. 2000. Problems of biofilms in the food and beverage industry. Wiley.

VERRAN, J., PACKER, A., KELLY, P. & WHITEHEAD, K. A. 2010. The retention of bacteria on hygienic surfaces presenting scratches of microbial dimensions. *Letters in Applied Microbiology,* 50**,** 258-263.

VERRAN, J. & WHITEHEAD, K. 2005. Factors affecting microbial adhesion to stainless steel and other materials used in medical devices. *International Journal of Artificial Organs,* 28**,** 1138 - 1145.

VERRAN, J. & WHITEHEAD, K. A. 2006. Assessment of Organic Materials and Microbial Components on Hygienic Surfaces. *Food and Bioproducts Processing,* 84**,** 260-264.

VOGLER, E. A. 1998. Structure and reactivity of water at biomaterial surfaces. *Advances in Colloid and Interface Science,* 74**,** 69-117.

VON EIFF, C., JANSEN, B., KOHNEN, W. & BECKER, K. 2005. Infections associated with medical devices - Pathogenesis, management and prophylaxis. *Drugs,* 65**,** 179-214.

VUONG, C. & OTTO, M. 2002. Staphylococcus epidermidis infections. *Microbes and Infection,* 4**,** 481-489.

W-DAHL, A., SÖREN TOKSVIG-LARSENAND ANDERS LINDSTRAND 2003. No difference between daily and weekly pin site care A randomized study of 50 patients with external fixation. *Acta Orthopaedica,* 74**,** 704-708.

WANG, G., LIU, S.-J., UENG, S. W.-N. & CHAN, E.-C. 2004. The release of cefazolin and gentamicin from biodegradable PLA/PGA beads. *International Journal of Pharmaceutics,* 273**,** 203-212.

WARD, P. 1997. A one-hospital study to determine the reaction prevalence and infection risk indicators for skeletal pin sites. *Journal of Orthopaedic Nursing,* 1**,** 173-178.

WASSALL, M. A., SANTIN, M., ISALBERTI, C., CANNAS, M. & DENYER, S. P. 1997. Adhesion of bacteria to stainless steel and silver-coated orthopedic external fixation pins. *Journal of Biomedical Materials Research,* 36**,** 325-330.

WEAVER, L., MICHELS, H. T. & KEEVIL, C. W. 2008. Survival of Clostridium difficile on copper and steel: futuristic options for hospital hygiene. *Journal of Hospital Infection,* 68**,** 145-151.

WEI, Y. & GONG, C. 2011. Effects of pulsed bias duty ratio on microstructure and mechanical properties of TiN/TiAlN multilayer coatings. *Applied Surface Science,* 257**,** 7881-7886.

WENZEL, R. N. 1936. Resistance of solid surfaces to wetting by water. *Industrial & Engineering Chemistry,* 28**,** 988-994.

WETZEL, C., HOLLSTEIN, F., FUNK, R. H. W., OZKUCUR, N. & MONSEES, T. K. 2008. Investigation on zirconium-coated polyurethane surfaces with regard to biocompatibility. *Surface and Coatings Technology,* 202**,** 5728-5732.

WHITEHEAD, K., KELLY, P., LI, H. Q. & VERRAN, J. 2010. Surface topography and physicochemistry of silver containing titanium nitride nanocomposite coatings. *Journal of Vacuum Science & Technology B,* 28**,** 180-187.

WHITEHEAD, K. A., AIREY, P. J. & VERRAN, J. 2005a. Organic soil and hygienic surfaces: significance, consequences and measurement. *In:* MCBAIN, A., ALLISON, D., PRATTEN, J., SPRATT, D., UPTON, M. & VERRAN, J. (eds.) *Biofilms: Persistence and Ubiquity.* 1st ed. Manchester, UK: Biofilm Club.

WHITEHEAD, K. A., BENSON, P. & VERRAN, J. 2009. Differential fluorescent staining of Listeria monocytogenes and a whey food soil for quantitative analysis of surface hygiene. *International Journal of Food Microbiology,* 135**,** 75-80.

WHITEHEAD, K. A., COLLIGON, J. & VERRAN, J. 2005b. Retention of microbial cells in substratum surface features of micrometer and sub-micrometer dimensions. *Colloids and Surfaces B: Biointerfaces,* 41**,** 129-138.

WHITEHEAD, K. A., COLLIGON, J. S. & VERRAN, J. 2004. The production of surfaces of defined topography and chemistry for microbial retention studies, using ion beam sputtering technology. *International Biodeterioration & Biodegradation,* 54**,** 143-151.

WHITEHEAD, K. A., LI, H., KELLY, P. & VERRAN, J. 2011. The Antimicrobial Properties of Titanium Nitride/Silver Nanocomposite Coatings. *Journal of Adhesion Science and Technology,* 25**,** 2299-2315.

WHITEHEAD, K. A., SMITH, L. A. & VERRAN, J. 2008. The detection of food soils and cells on stainless steel using industrial methods: UV illumination and ATP bioluminescence. *International Journal of Food Microbiology,* 127**,** 121-128.

WHITEHEAD, K. A. & VERRAN, J. 2006. The effect of surface topography on the retention of microorganisms. *Food and Bioproducts Processing,* 84**,** 253-259.

WHITEHEAD, K. A. & VERRAN, J. 2007. The effect of surface properties and application method on the retention of Pseudomonas aeruginosa on uncoated and titanium-coated stainless steel. *International Biodeterioration & Biodegradation,* 60**,** 74-80.

WICKENS, D. J., WEST, G., KELLY, P. J., VERRAN, J., LYNCH, S. & WHITEHEAD, K. A. 2012. Antimicrobial activity of nanocomposite zirconium nitride/silver

coatings to combat external bone fixation pin infections. *International Journal of Artificial Organs,* 35**,** 817-825.

WILLIAMS, S. C., HONG, Y., DANAVALL, D. C. A., HOWARD-JONES, M. H., GIBSON, D., FRISCHER, M. E. & VERITY, P. G. 1998. Distinguishing between living and nonliving bacteria: Evaluation of the vital stain propidium iodide and its combined use with molecular probes in aquatic samples. *Journal of Microbiological Methods,* 32**,** 225-236.

WINDOW, B. & SAVVIDES, N. 1986a. Charged particle fluxes from planar magnetron sputtering sources. *Journal of Vacuum Science & Technology A: Vacuum, Surfaces, and Films,* 4**,** 196-202.

WINDOW, B. & SAVVIDES, N. 1986b. Unbalanced dc magnetrons as sources of high ion fluxes: Unbalanced magnetron ion-assisted deposition and property modification of thin films. *Journal of Vacuum Science & Technology A: Vacuum, Surfaces, and Films,* 4**,** 453-456.

WINTER, M. 2012. *Web Elements- Zirconium* [Online]. The University of Sheffield. Available: http://www.webelements.com/zirconium/ [Accessed 27-09-2013 2013].

WIRTANEN, G., SALO, S., HELANDER, I. M. & MATTILA-SANDHOLM, T. 2001. Microbiological methods for testing disinfectant efficiency on Pseudomonas biofilm. *Colloids and Surfaces B: Biointerfaces,* 20**,** 37-50.

XU, L.-C. & SIEDLECKI, C. A. 2012. Submicron-textured biomaterial surface reduces staphylococcal bacterial adhesion and biofilm formation. *Acta Biomaterialia,* 8**,** 72-81.

YAO, C., SLAMOVICH, E. B. & WEBSTER, T. J. 2008. Enhanced osteoblast functions on anodized titanium with nanotube-like structures. *Journal of Biomedical Materials Research - Part A,* 85**,** 157-166.

YAO, S. H., SU, Y. L., KAO, W. H., CHENG, K. W. & SU, C. T. 2011. Performance of nanolayer CrN/Ag coated cutting tools. *Surface Engineering,* 27.

YONGQIANG, W., XIAOXIA, C., XIUBO, T., CHUNZHI, G., SHIQIN, Y., ZHIQIANG, J. & LIANGJI, C. 2013. Effects of pulsed bias duty ratio on microstructure and surface properties of TiN films. *Vacuum,* 89**,** 185-189.

ZHANG, Y., CHENG, Y.-T. & GRUMMON, D. S. 2006. The influence of superelastic NiTi interlayers on tribological properties of CrN hard coatings. *Materials Science and Engineering: A,* 438–440**,** 710-713.

ZIEBUHR, W., HENNIG, S., ECKART, M., KRÄNZLER, H., BATZILLA, C. & KOZITSKAYA, S. 2006. Nosocomial infections by Staphylococcus epidermidis: how a commensal bacterium turns into a pathogen. *International Journal of Antimicrobial Agents,* 28, Supplement 1**,** 14-20.

ZIMMERMANN, R., ITURRIAGA, R. & BECKER-BIRCK, J. 1978. Simultaneous determination of the total number of aquatic bacteria and the number thereof involved in respiration. *Applied and Environmental Microbiology,* 36**,** 926-935.

ZUPANIC, F. 2010. Extracting electron backscattering coefficients from backscattered electron micrographs. *Materials Characterization,* 61**,** 1335-1341.

12 Abstracts and Presented Posters and Papers

12.1 SSBII 13 Port Sunlight October 2011

12.1.1 Reducing the infection in external pin fixation: Using ZrN/Ag surface-coatings

External bone fixation using pins is a method widely used to provide post-operative support and immobilisation in severe and/or comminuted fractures. The most frequent complication with external fixation is pin tract infection, usually caused by bacteria such as *Staphylococcus aureus* (including methicillin resistant *S. aureus*) and *Staphylococcus epidermidis,* both common of natural skin flora but are also important opportunistic pathogens (Chen *et al.*, 2006, Shirai *et al.*, 2009).

Using a Physical Vapour Deposition method called magnetron sputtering, objects can be coated with a thin film of material to produce a novel alloy. Using a 'reactive gas' (Nitrogen), hard wearing nitride coatings can be deposited. Combining the corrosion, scratch resistance and biocompatibility of zirconium nitride, with the antimicrobial efficacy of silver, displays a potential for reduction in pin tract infections. Coatings were deposited onto 10x10mm coupons of 316L medical grade stainless steel with a fine polish finish (R_a = 9.5 ± 2.4nm) for antimicrobial testing and silicon wafer (R_a = 1.0 ± 0.6nm) for coating characterisation. Microbiological assays performed included; retention assays using a live-dead cell viability stain, Tetrazolium violet redox dye assay to determine a contact kill, and zones of inhibition to display a leaching kill. Coating characterisation included Atomic Force Microscopy for surface topography, Scanning Electron Microscopy (surface/ structure properties) and Energy Dispersive X-Ray spectroscopy (composition) and Nano-scratch testing (adhesion properties). Microbiological tests confirmed that as silver content increased, their antimicrobial efficacy also increased. The highest silver gave a significant kill (>1 log), deeming it an ideal candidate for its desired use. Future work will involve testing novel antimicrobially active alloys in the presence of cells and a conditioning film.

Reducing the infection in external pin fixation: ZrN/Ag surface-coatings

David Wickens[1,2*], Stephen Lynch[3], Joanna Verran[1], Peter Kelly[2], Glen West[2], Kathryn Whitehead[1,2]
[1] Department Health Care Sciences, Manchester Metropolitan University, Chester St. Manchester M1 5GD UK *david.j.wickens@stu.mmu.ac.uk
[2] Surface Engineering Group, Manchester Metropolitan University, Chester St. Manchester M1 5GD UK
[3] School of Computing, Mathematics and Digital Technology, Manchester Metropolitan University, Chester St. Manchester M1 5GD UK

Introduction

External bone fixation using metal pins is a method widely used to provide post-operative support and immobilisation in severe fractures. The most frequent microbiological complication with external fixators is pin tract infection, usually caused by bacteria such as *Staphylococcus aureus* (including MRSA) and *Staphylococcus epidermidis,* both common microorganisms of natural skin flora. However, these microorganisms are also important opportunistic nosocomial pathogens.

Using a Physical Vapour Deposition method called magnetron sputtering, objects can be coated with a thin film of material to produce novel alloys. Combining the wear, scratch resistance and biocompatibility of zirconium nitride (ZrN), with the antimicrobial efficacy of silver (Ag) nanoparticles may create a putative antimicrobial surface which could result in the reduction of pin tract infections.

The aim of the work was to investigate the surface composition, properties and antimicrobial efficacy of ZrNAg at three concentrations of Ag.

Methods and Materials

For antimicrobial testing, coatings were deposited onto 10mmx10mm coupons of 316L medical grade stainless steel with a fine polish finish (R_a = 9.5 ± 2.4nm) and for coating characterisation silicon wafer (R_a = 1.0 ± 0.6nm).

The Magnetron sputtering rig used for the coatings was a Teer Coatings UDP350 in an unbalanced, closed field magnetic arrangement utilising a reactive Ar-N atmosphere. Applying 1.5kW to the Zr target, 30V substrate bias and varying the power of the Ag target at 70W, 150W and 230W produced coatings with different concentrations of silver.

Coating characterisation was undertaken including Atomic Force Microscopy (surface topography) Scanning Electron Microscopy (surface/structure properties), Energy Dispersive X-Ray spectroscopy (composition) and Nano-scratch testing (adhesion properties).

Microbiological assays performed included retention assays using a LiveDead® cell viability stain, tetrazolium violet (NBT) redox dye assay to determine a contact kill, and zones of inhibition to display a leaching kill.

Results

Table 1: EDX analysis of the ZrNAg coatings demonstrating Ag content in relation to magnetron power.

Power (W)	Ag (at.%)	StDev
70	0.45	0.63
150	15.54	1.76
230	29.76	0.22

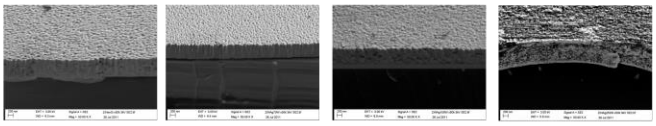

Fig.1: SEM fracture morphology (x50,000 mag) on Si wafer: **a)** ZrN, **b)**ZrN/0.45±0.63 at.%Ag, **c)** ZrN/15.54 ± 1.76 at.% Ag and **d)** ZrN/29.76 ± 0.22 at.% Ag demonstrating loss of columnar morphology as Ag content increases

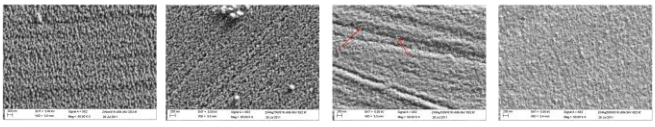

Fig. 2: SEM surface morphology (x50,000 mag) on stainless steel: **a)** ZrN, **b)** ZrN/0.45 ± 0.63 at.%Ag, **c)** ZrN/15.54 ± 1.76 at.% Ag (Ag nanoparticles indicated) and **d)** ZrN/29.76±0.22 at.% Ag demonstrating visible nanoparticles embedded in the ZrN matrix (indicated 'c')

Fig. 3: ZrN nano-scratch length (2mm) displaying first coating defect (Blue) and full delamination (Green)

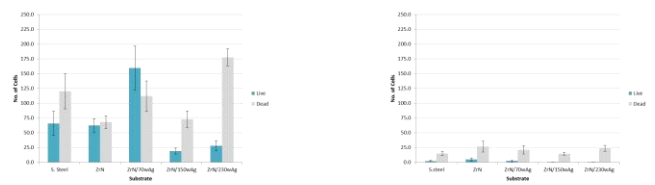

Figure 4: Retention assay cell counts demonstrating the number of Live:Dead® cells:
a) *S. aureus* and **b)** *S. epidermidis.* A decrease in viable cells is observed as Ag content increases. A significantly (P=0.03) smaller amount of *S. epidermidis* cells were present on all surfaces.

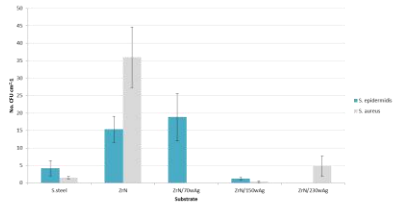

Figure 5: NBT assay cell counts demonstrating the contact kill of *S. aureus* and *S. epidermidis.* A decrease in viable colonies of both bacteria is observed as Ag content increases.

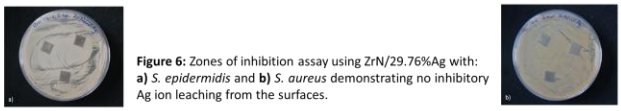

Figure 6: Zones of inhibition assay using ZrN/29.76%Ag with: **a)** *S. epidermidis* and **b)** *S. aureus* demonstrating no inhibitory Ag ion leaching from the surfaces.

Discussion

SEM demonstrated the morphology of the surfaces to be columnar in structure. The structure became amorphous as the silver content increased (Figure 1). The coating followed the topography of the underlying substrata e.g. surface scratches of the stainless steel (Figure 2). Silver nanoparticles were visible on the surfaces (Figure 2c) highlighted by the red arrows. CSM scratch test analysis showed the ZrN coating to have a poor adhesion and a brittle structure which would need to be improved for this material to be a potential candidate for a biomaterial coating (Figure 3).

LiveDead® staining displayed a 1 log difference in non-viable: viable cells with increased silver content (29.76 ± 0.22 at.% Ag) of the surfaces (Figure 4). Following contact assays, it was found that as the silver content increased, antimicrobial efficacy increased (Figure 5). No leaching of Ag ions was observed from the surfaces (Figure 6).

Conclusion

Microbiological tests confirmed that as silver content increased, as did the coatings antimicrobial efficacy. The highest silver content gave a significant kill (>1 log), deeming it a potential candidate for further study. Characterisation displayed a columnar structure and scratch testing portrayed brittle structure with poor adhesion.

Further work

Future work will involve investigation into the adhesion properties (using metallic interlayers and morphology of ZrN and ZrNAg. Other nanocomposite nitride/ silver alloys will be tested for scratch resistance and antimicrobial efficacy. Leaching of Ag ions will be quantitatively determined using ICP-AES. Following research into the materials, the most suitable will be applied to fixation pins and tested. Work will also involve testing the novel antimicrobially active alloys in the presence of cells and a conditioning film.

References & Acknowledgements

Chen, W., Y. Liu, et al. (2006 Biomaterials **27: 5512**
Shirai, T., H. Tsuchiya, et al. (2009). Journal of Biomedical Materials Research Part B: Applied Biomaterials **91B: 373**
Acknowledgements: CSM instruments for scratch and hardness testing. The authors gratefully acknowledge support from the EPSRC-funded Bridging the Gaps: Nano-Info-Bio project, grant reference EP/H000291/1

12.2 SGM Spring 2012 Meeting: March 2012

12.2.1 Zirconium nitride/silver alloys in the design of antimicrobial, fixation pin surface coatings

External bone fixation using pins is widely used to provide post-operative support and immobilisation in severe fractures. The most frequent complication with external fixation is pin tract infection, usually caused by *Staphylococcus aureus* (including MRSA) and *Staphylococcus epidermidis.*

Using magnetron sputtering objects can be coated with a thin film of material. Using nitrogen, hard wearing nitride coatings can be deposited. Combining the scratch resistance and biocompatibility of zirconium nitride, with the antimicrobial efficacy of silver, reveals a potential for reduction in pin tract infections. The coatings were deposited onto 10x10mm coupons of fine polished 316L medical stainless steel (R_a≈10nm) for antimicrobial testing and silicon wafer (R_a≤1.0nm) for coating characterisation. Microbiological assays included; retention assays (LiveDead™ stain), respiratory assays, and zones of inhibition. Coating characterisation included Atomic Force Microscopy, Scanning Electron Microscopy, Energy Dispersive X-Ray spectroscopy, and Nano-scratch testing. Microbiological tests confirmed that as silver content increased so did the antimicrobial efficacy. The highest silver content gave a significant kill, deeming it a potential candidate for its desired use.

Zirconium nitride/silver nanocomposites in the design of antimicrobial fixation pin surface coatings

David Wickens[1,2*], Stephen Lynch[3], Joanna Verran[1], Peter Kelly[2], Glen West[2], Kathryn Whitehead[1,2]
[1] School of Health Care Sciences, Manchester Metropolitan University, Chester St. Manchester M1 5GD UK *david.j.wickens@stu.mmu.ac.uk
[2] Surface Engineering Group, Manchester Metropolitan University, Chester St. Manchester M1 5GD UK
[3] School of Computing, Mathematics and Digital Technology, Manchester Metropolitan University, Chester St. Manchester M1 5GD UK

Introduction

External bone fixation using stainless steel pins is a method widely used to provide post-operative support and immobilisation in severe fractures. The most frequent microbiological complication with external fixation is infection of the pin tract. This is most commonly caused at the pin entry site by opportunistic pathogens of the body's natural flora, such as *Staphylococcus aureus* (including MRSA) and *Staphylococcus epidermidis*. Inevitably, if a surface is exposed, bacteria will adhere to the surface, therefore methods of elimination at the cell-surface interface are of importance for biomedical devices.

Using a physical vapour deposition method called magnetron sputtering, objects can be coated with a thin film of material to produce novel nanocomposites. Combining the wear, scratch resistance and biocompatibility of zirconium nitride (ZrN), a hard wearing ceramic used in the cutting tool industry, with silver (Ag), creates a putative antimicrobial nanocomposite.

The aim of the work was to investigate the surface composition, properties and antimicrobial efficacy of ZrN/Ag at three concentrations of silver.

Experimental

For antimicrobial testing, coatings were deposited onto 10 mm x 10 mm coupons of 316L medical grade stainless steel with a fine polish finish (R_a = 10 ± 2 nm) and for coating characterisation silicon wafer (R_a = 1.0 ± 0.6 nm).

The Magnetron sputtering rig used for the coatings was a Teer Coatings UDP350 reactively sputtering (Ar-N atmosphere). Applying 1.5 kW to the Zr target, a 30 V substrate bias and varying the power of the Ag target (70 W, 150 W and 230 W) produced coatings with different concentrations of silver. Coating characterisation was undertaken, including scanning electron microscopy/electron backscattering (surface & structure properties), and Energy Dispersive X-Ray spectroscopy (composition).

Microbiological assays performed included retention assays, submersing the samples in a cell suspension of a known concentration for 1 hour. Following a standardised rinse, LiveDead® cell viability stain was applied and the retained cells were counted. The nitro-tetrazolium violet (NTV) redox dye assay was used to determine a contact kill by adding a known amount of cells to the surface and following drying (1 h) and incubation in solid media (submersed) the respiring colonies were marked with violet (reduction of the tetrazolium). Zones of inhibition assays displayed any leaching inhibition occurred from the silver, by placing the surfaces onto a bacterial lawn. Microorganisms used were *Staphylococcus aureus* NCTC 8532 and *Staphylococcus epidermidis* NCTC 11047

Results & Discussion

Table 1: EDX of the ZrN/Ag coatings demonstrating the silver content in relation to applied magnetron power.

Power (W)	Ag (at.%)	StDev
70	0.5	0.6
150	15.5	1.8
230	29.8	0.2

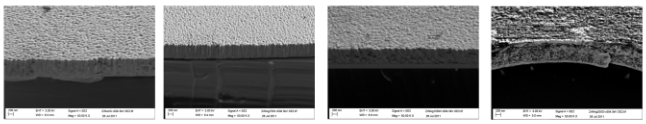

Fig.1: SEM fracture morphology (x50,000 mag) on Si wafer: **a)** ZrN, **b)** ZrN/0.5 at.% Ag, **c)** ZrN/15.5 at.% Ag and **d)** ZrN/29.8 at.% Ag, demonstrating loss of columnar morphology as the silver content increases.

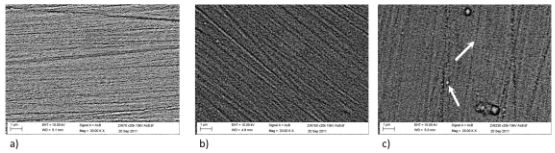

Fig. 2: Backscattered surface morphology (x 20,000 mag) on stainless steel: **a)** ZrN/0.5 at.% Ag, **b)** ZrN/15.5 at. % Ag and **c)** ZrN/29.8 at.% Ag, demonstrating silver nanoparticles (brighter phase, indicated on (c) embedded in the ZrN matrix.

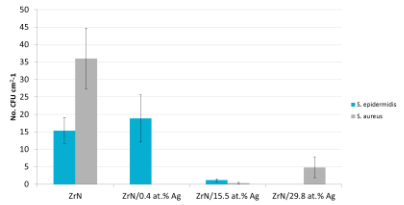

Fig. 3: NBT assay cell counts demonstrated an effective contact kill of *S. aureus* and *S. epidermidis.* A decrease in viable colonies of both bacteria was observed as the silver content increased.

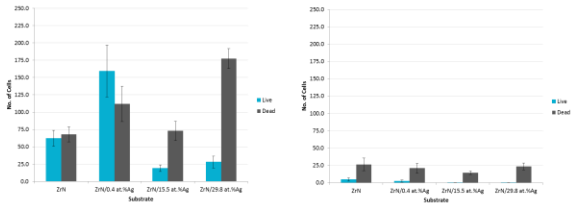

Fig. 4: Retention assay cell counts demonstrating the number/ratio of Live:Dead® cells:
a) *S. aureus* and **b)** *S. epidermidis.* A decrease in viable cells was observed as Ag content increased. Significantly *(p* =0.03) less *S. epidermidis* cells were retained on all of the surfaces.

- The surfaces were deposited in a columnar structure, that became increasingly dense as the silver content increased (Figure 1).
- The silver segregated as nanoparticles within the ZrN matrix and were visible on the surfaces following electron backscattering (Figure 2c).
- NTV assays demonstrated a contact kill occurrence. The number of respiring colonies on the surface reduced as the silver content increased (Figure 3).
- LiveDead® staining of attached cells displayed a 1 log kill difference in cell numbers retained between microorganisms for the 15.5 and 29.8 at.% Ag coatings (Figure 4).
- Significantly less *S. epidermidis* cells were retained on the surfaces compared to *S. aureus* (Figure 4).
- No zones of inhibition were observed (results not presented), however, leaching of silver from the surfaces has not been ruled out and can be quantified using inductively coupled plasma atomic emission spectroscopy (ICP-AES).

Conclusion

Coatings displayed a columnar deposition with nanoparticulate silver content seen on the electron backscattering images. Microbiological tests confirmed that as the silver content increased, so did the antimicrobial efficacy. Both the 15.5 and 29.8 at.% silver content coatings gave a significant kill with the LiveDead. The NTV assay showed a decrease in respiring colonies for both microorganisms apart from *S. epidermidis* on 0.4% at.% silver content.

Future Work

- Test the surfaces for toxicity against human inflammatory cells.
- Introduce conditioning films (blood, fibrinogen) to the surfaces.
- Use 5 cyano-2,3-d,(ptolyl) tetrazolium chloride fluorescent stain to determine cell respiration in comparison to LiveDead staining.
- ICP-AES to investigate the leaching of silver ions.
- Introduce titanium nitride/ silver (TiN/Ag) coatings and compare them against the ZrN/Ag.

Acknowledgements

The authors gratefully acknowledge support from the EPSRC-funded Bridging the Gaps: Nano-Info-Bio project, grant reference EP/H000291/1

12.3 IBBS Antimicrobial Strategies for Biofilm Control September 2012

12.3.1 Antimicrobial Zirconium Nitride Silver Nanocomposite Coatings to Combat External Fixation Pin Infection

Zirconium and its ceramic alloys are sometimes used in medical implants due to their good biocompatibility along with excellent hardness and corrosion resistance. These coatings may be used in knee and hip arthroplasties since oxidised Zirconium coatings demonstrate increased wear resistance compared to standard stainless steel components. External bone fixation systems face similar obstacles as medical implants with the added predicament of being highly infection prone around the pin entry site; a biologically critical interface between the non-sterile and sterile environments outside and inside the body respectively. Combining zirconium nitride with silver gives the potential for a surface with the aforesaid surface properties along with antimicrobial and solid lubricious properties.

Magnetron sputtering was used to achieve such coatings; a physical vapour deposition system reactively co-sputtering zirconium and silver to produce the nanocomposite thin film. Due to silver nitride being thermodynamically unstable the silver forms as nanoparticles within the ZrN matrix.

Coatings were produced on 316L polished stainless steel analysed for chemical composition, structure, surface topography and hardness. Using *Staphylococcus aureus* and *Staphylococcus epidermidis* microbiological methods tested for antimicrobial leaching, bacterial surface contact kill and the effect of surface topography on cell retention combined with survival of the biofilm using LiveDead™ staining.

Results demonstrated that addition of silver to the coatings decreased the amount of viable cells. No antimicrobial leaching of silver was observed from any of the surfaces. *S. aureus* was retained in higher numbers than *S. epidermidis*, however both organisms decreased in viability for the silver containing nanocomposites. These coatings have demonstrated the potential to be used on external fixation pins to reduce pin tract infections.

Zirconium nitride/silver nanocomposites in the design of antimicrobial fixation pin surface coatings

David Wickens[1,2*], Stephen Lynch[3], Joanna Verran[1], Peter Kelly[2], Glen West[2], Kathryn Whitehead[1,2]

[1] School of Health Care Sciences, Manchester Metropolitan University, Chester St. Manchester M1 5GD UK *david.j.wickens@stu.mmu.ac.uk
[2] Surface Engineering Group, Manchester Metropolitan University, Chester St. Manchester M1 5GD UK
[3] School of Computing, Mathematics and Digital Technology, Manchester Metropolitan University, Chester St. Manchester M1 5GD UK

Introduction

External bone fixation using stainless steel pins is a method widely used to provide post-operative support and immobilisation in severe fractures. With external fixation pin tract infection is the most frequent microbiological complication. This is most commonly caused at the pin entry site by opportunistic pathogens; *Staphylococcus aureus* (including MRSA) and *Staphylococcus epidermidis*. Methods of elimination at the cell-surface interface are of high importance for biomedical devices. Using a physical vapour deposition method for example magnetron sputtering, objects can be coated with a thin film of material to produce novel nanocomposites. Combining zirconium nitride (ZrN), with silver (Ag), creates a dual purpose nanocomposite with hard wearing and antimicrobial properties.

Aim

Investigate the surface properties and antimicrobial efficacy of ZrN/Ag nanocomposite coatings with two concentrations of silver for potential use on external fixation pins.

Experimental

Microbiological assays performed included retention assays, submersing the samples in a cell suspension of a known concentration for 1 hour. Following a standardised rinse, LiveDead® cell viability stain was applied and the retained cells were counted. A nitro-tetrazolium violet (NTV) redox dye assay was used to determine a contact kill by adding a known amount of cells to the surface and following drying (1 h) and incubation in solid media the respiring colonies were identified as violet following reduction of the tetrazolium stain. *Staphylococcus aureus* NCTC 8532 and *Staphylococcus epidermidis* NCTC 11047 were used in these studies. Coatings were deposited onto 10 mm x 10 mm coupons of 316L medical grade stainless steel with a fine polish finish (R_a = 10 ± 2 nm). The Magnetron sputtering rig used was a Teer Coatings UDP350.

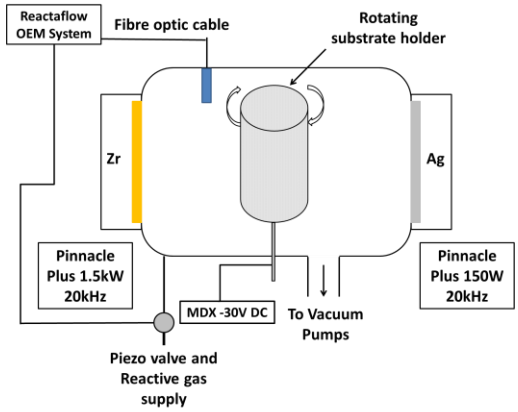

Fig. 1: Schematic diagram displaying the setup of the magnetron sputtering rig.

Results & Discussion

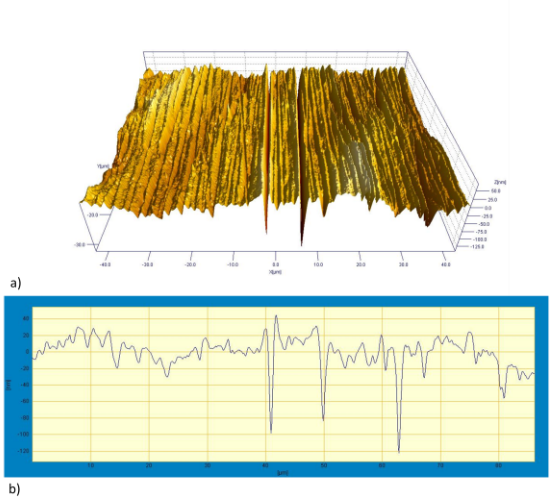

Fig. 2: a) 3D white light profilometry image of the stainless steel surface demonstrating the surface topography. **b)** A line profile of the scan shows the peaks and valleys of the surface across a single plane.

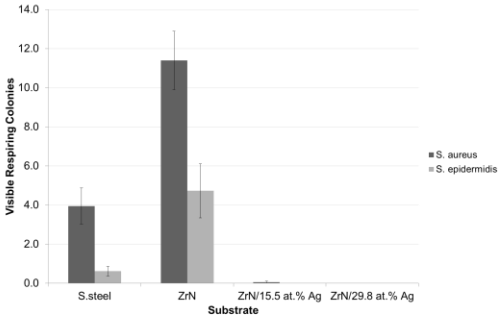

Fig. 3: NBT assay cell counts demonstrated an effective contact kill of *S. aureus* and *S. epidermidis*. A decrease in viable colonies of both bacteria was observed as the silver content increased.

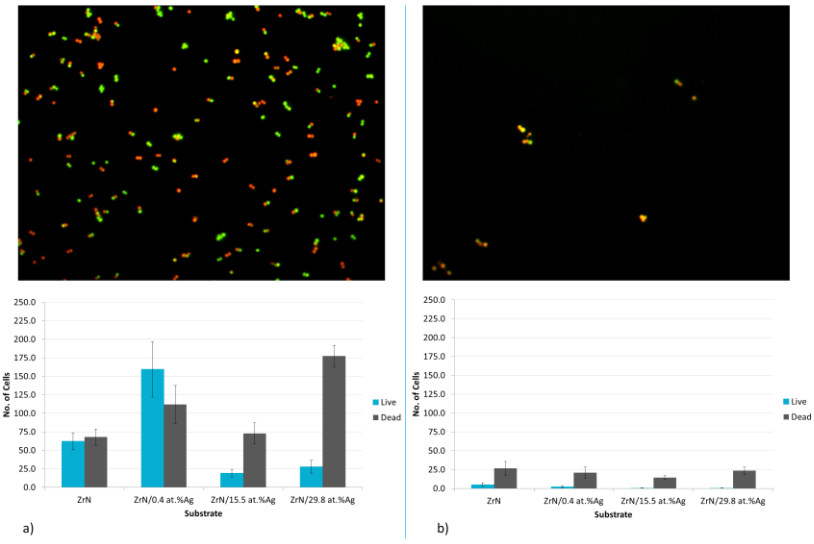

Fig. 4: Retention assay cell counts demonstrating the number/ratio of Live:Dead® cells:
a) *S. aureus* and **b)** *S. epidermidis*. A decrease in viable cells was observed as Ag content increased. Significantly *(p* =0.03) less *S. epidermidis* cells were retained on all of the surfaces. The images above demonstrate the density and distribution of the cells retained on the surface. Green indicates viable cells and red indicates bacteria with compromised cell membranes (dead).

Summary

- The microtopography of the surface did not affect the pattern of bacterial retention although surface features were large enough for the bacteria to reside and alter the retention characteristics (Figure 2).
- Respiratory assays demonstrated a contact kill. Visible respiring colonies on the surface were absent as the silver content of the surfaces was increased (Figure 3).
- LiveDead® staining of retained cells displayed a 1 log kill difference in cell numbers retained between microorganisms for the silver coatings (Figure 4).
- Significantly less *S. epidermidis* cells were retained on the surfaces compared to *S. aureus* (Figure 4).

Acknowledgements

The authors gratefully acknowledge support from the EPSRC-funded Bridging the Gaps: Nano-Info-Bio project, grant reference EP/H000291/1

EPSRC Engineering and Physical Sciences Research Council

12.4 SGM Spring Conference March 2013

12.4.1 Zirconium Nitride Silver Nanocomposite Coatings to Combat External Fixation Pin Infection

External bone fixation is a frequently applied medical procedure for rehabilitating severe fractures. The pins used require strict cleaning regimes at the entry site. However, the pin sites are still putative ports for conceivable pathogenic microbial infection. The study aim was to potentially combat and reduce pin tract infections (PTI) using zirconium nitride silver coatings; investigate the coating characteristics, determine the antimicrobial properties against *Staphylococcus aureus* and *Staphylococcus epidermidis* using LiveDead™ and CTC staining, and demonstrate the coatings biocompatibility against human cells (U-937 monocyte inflammatory cell line).

Zirconium Nitride (ZrN) is a hard wearing compound possessing corrosion resistance, thus giving it biomaterial potential. Combining with silver gives the coating potential for a multifunctional surface with antimicrobial characteristics. Magnetron sputtering was used to reactively co-sputter zirconium and silver, to produce nanocomposite thin films with a range of silver concentrations.

Addition of silver to the coatings increased antimicrobial efficacy towards the Staphylococci. No antimicrobial leaching of silver was observed from any of the surfaces, however *S. aureus* was retained in higher numbers than *S. epidermidis*. The bacteria were reduced by 1-log when added to the U-937 cells. These coatings have demonstrated potential to be used on external fixation pins to reduce PTI's.

Zirconium nitride/silver nanocomposites in the design of antimicrobial fixation pin surface coatings

David Wickens[1,2*], Stephen Lynch[3], Joanna Verran[1], Peter Kelly[2], Glen West[2], Kathryn Whitehead[1,2]

[1] School of Health Care Sciences, Manchester Metropolitan University, Chester St. Manchester M1 5GD UK *david.j.wickens@stu.mmu.ac.uk
[2] Surface Engineering Group, Manchester Metropolitan University, Chester St. Manchester M1 5GD UK
[3] School of Computing, Mathematics and Digital Technology, Manchester Metropolitan University, Chester St. Manchester M1 5GD UK

Introduction

External bone fixation using stainless steel pins is a method widely used to provide post-operative support and immobilisation in severe fractures. With external fixation pin tract infection is the most frequent microbiological complication. This is most commonly caused at the pin entry site by opportunistic pathogens; *Staphylococcus aureus* (including MRSA) and *Staphylococcus epidermidis*. Methods of elimination at the cell-surface interface are of high importance for biomedical devices. Using a physical vapour deposition method for example magnetron sputtering, objects can be coated with a thin film of material to produce novel nanocomposites. Combining zirconium nitride (ZrN), with silver (Ag), creates a dual purpose nanocomposite with hard wearing and antimicrobial properties.

Aim

Investigate the surface properties and antimicrobial efficacy of ZrN/Ag nanocomposite coatings with two concentrations of silver for potential use on external fixation pins.

Experimental

Microbiological assays performed included retention assays, submersing the samples in a cell suspension of a known concentration for 1 hour. Following a standardised rinse, LiveDead® cell viability stain was applied and the retained cells were counted. A nitro-tetrazolium violet (NTV) redox dye assay was used to determine a contact kill by adding a known amount of cells to the surface and following drying (1 h) and incubation in solid media the respiring colonies were identified as violet following reduction of the tetrazolium stain. *Staphylococcus aureus* NCTC 8532 and *Staphylococcus epidermidis* NCTC 11047 were used in these studies. Coatings were deposited onto 10 mm x 10 mm coupons of 316L medical grade stainless steel with a fine polish finish (R_a = 10 ± 2 nm). The Magnetron sputtering rig used was a Teer Coatings UDP350.

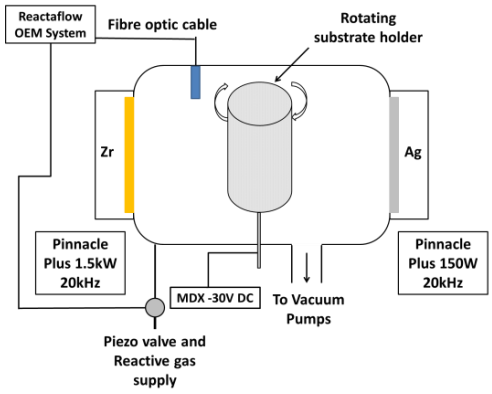

Fig. 1: Schematic diagram displaying the setup of the magnetron sputtering rig.

Results & Discussion

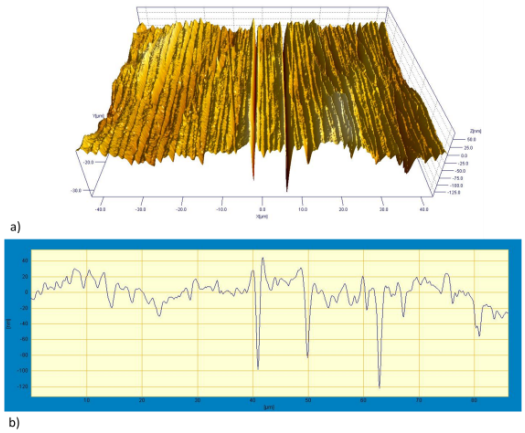

Fig. 2: a) 3D white light profilometry image of the stainless steel surface demonstrating the surface topography. **b)** A line profile of the scan shows the peaks and valleys of the surface across a single plane.

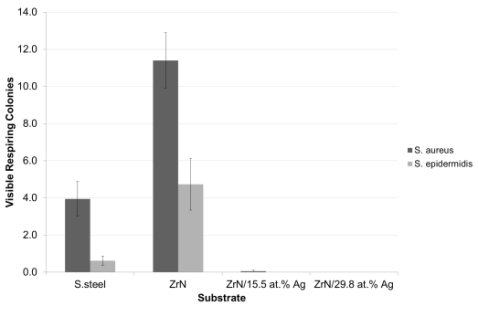

Fig. 3: NBT assay cell counts demonstrated an effective contact kill of *S. aureus* and *S. epidermidis*. A decrease in viable colonies of both bacteria was observed as the silver content increased.

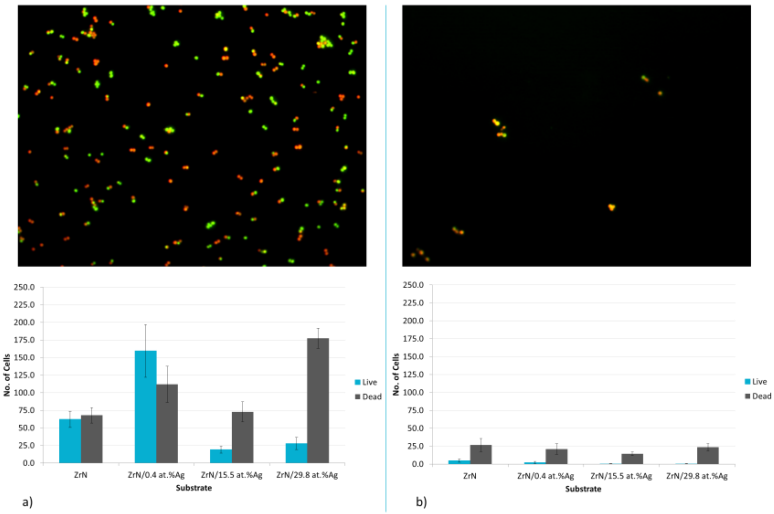

Fig. 4: Retention assay cell counts demonstrating the number/ratio of Live:Dead® cells:
a) *S. aureus* and **b)** *S. epidermidis*. A decrease in viable cells was observed as Ag content increased. Significantly (p =0.03) less *S. epidermidis* cells were retained on all of the surfaces. The images above demonstrate the density and distribution of the cells retained on the surface. Green indicates viable cells and red indicates bacteria with compromised cell membranes (dead).

Summary

- The microtopography of the surface did not affect the pattern of bacterial retention although surface features were large enough for the bacteria to reside and alter the retention characteristics (Figure 2).
- Respiratory assays demonstrated a contact kill. Visible respiring colonies on the surface were absent as the silver content of the surfaces was increased (Figure 3).
- LiveDead® staining of retained cells displayed a 1 log kill difference in cell numbers retained between microorganisms for the silver coatings (Figure 4).
- Significantly less *S. epidermidis* cells were retained on the surfaces compared to *S. aureus* (Figure 4).

Acknowledgements

The authors gratefully acknowledge support from the EPSRC-funded Bridging the Gaps: Nano-Info-Bio project, grant reference EP/H000291/1

12.5 EMRS Strasbourg May 2013

12.5.1 Zirconium Nitride Silver Nanocomposite Coatings to Combat External Fixation Pin Infection

External bone fixation is a frequently applied medical procedure for rehabilitating severe fractures. The pins used require strict cleaning regimes at the entry site. However, the pin sites are still putative ports for conceivable pathogenic microbial infection. The study aim was to potentially combat and reduce pin tract infections (PTI) using zirconium nitride silver coatings; investigate the coating characteristics, determine the antimicrobial properties against Staphylococcus aureus and Staphylococcus epidermidis using LiveDead™ and CTC staining, and demonstrate the coatings biocompatibility against human cells (U-937 monocyte inflammatory cell line).

Zirconium Nitride (ZrN) is a hard wearing compound possessing corrosion resistance, thus giving it biomaterial potential. Combining with silver gives the coating potential for a multifunctional surface with antimicrobial characteristics. Magnetron sputtering was used to reactively co-sputter zirconium and silver, to produce nanocomposite thin films with a range of silver concentrations.

Addition of silver to the coatings increased antimicrobial efficacy towards the Staphylococci. No antimicrobial leaching of silver was observed from any of the surfaces, however S. aureus was retained in higher numbers than S. epidermidis. The bacteria were reduced by 1-log when added to the U-937 cells. These coatings have demonstrated potential to be used on external fixation pins to reduce PTI’s.

12.6 Stevens Biomaterials Conference June 2013 New Jersey USA

12.6.1 Zirconium nitride/silver nanocomposites used in the design of antimicrobial external fixation pin coatings

External bone fixation is a method widely used to provide post-operative orthopaedic support and immobilisation in severe and/or comminuted fractures. The pin entry site creates a critical interface, potentially allowing infection by bacteria including Staphylococcus aureus and Staphylococcus epidermidis. Both species, which are indigenous skin flora, are known nosocomial opportunistic pathogens.

Magnetron sputtering is a highly versatile physical vapour deposition system. Reactively co-sputtering zirconium and silver can be used to produce the nanocomposite thin films. Due to silver nitride being thermodynamically unstable, the silver forms atomic state nanoparticles (<100nm) within the zirconium nitride coating matrix.

The objectives of this project were to produce coatings with high mechanical strength and wear resistance and develop antimicrobial coatings for potential use on medical devices, particularly external fixation pins.

Coatings were produced on medical grade 316L polished stainless steel and analysed for chemical composition, film morphology, surface topography, hardness and wear. Antimicrobial testing of the thin films was carried out using Staphylococcus aureus (NCTC 8532) and Staphylococcus epidermidis (NCTC 11057). Methods included zones of inhibition, the respiratory evaluation of colonies on the surfaces, LiveDead staining and CTC-DAPI fluorescence staining. The effect of surface properties on microbial retention was determined using retention assays. The antimicrobial efficacy

of the coatings was also investigated in the presence of medically important conditioning films, using the above techniques.

Results demonstrated that with the addition of silver to the coatings no inhibitory leaching of silver was observed from any of the surfaces following the zone of inhibition assays. However, there was a decreased amount of respiring bacterial colonies following contact with the surface. The effect of topographical properties on cell retention demonstrated that S. aureus was retained in higher numbers than S. epidermidis. Both organisms decreased in viability when in contact with the silver containing surfaces; however, the coating with the highest amount of silver present was not always the most effective. This suggests there could be a threshold for the maximum activity of the silver, or there are differences in distribution of the silver particles on the surface (to be investigated). In the presence of relevant conditioning films, the antimicrobial contact kill was reduced.

These coatings have demonstrated the potential to be used on external fixation pins to reduce pin tract infections. The nanocomposite coatings, provides a more hard wearing, scratch resistant surface than medical grade 316L stainless steel. These preferred tribological properties combined the antimicrobial efficacy potentially makes for a highly desirable surface. This may have future applications in the design of hard wearing, antimicrobial surfaces targeted towards potential use on external fixation pins.

Zirconium nitride/silver nanocomposites used in the design of antimicrobial external fixation pin coatings

David Wickens[1,2*], Glen West[2], Stephen Lynch[3], Joanna Verran[1], Peter Kelly[2], Kathryn Whitehead[1,2]
[1] School of Health Care Sciences, Manchester Metropolitan University, Chester St. Manchester M1 5GD UK *david.j.wickens@stu.mmu.ac.uk
[2] Surface Engineering Group, Manchester Metropolitan University, Chester St. Manchester M1 5GD UK
[3] School of Computing, Mathematics and Digital Technology, Manchester Metropolitan University, Chester St. Manchester M1 5GD UK

Introduction

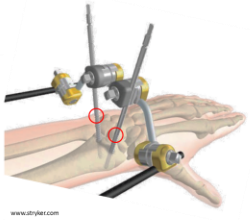

Fig. 1: Infection occurs most commonly at the pin entry site, indicated in red.

- External bone fixation using stainless steel pins is widely used to provide post-operative support and immobilisation in severe fractures.
- Pin tract infection is a major issue commonly caused at the pin entry site by opportunistic pathogens (Figure 1), particularly ***Staphylococcus aureus*** (including MRSA) and ***Staphylococcus epidermidis***.
- Medical grade stainless steel has been coated with novel nanocomposites, combining zirconium nitride (ZrN), with silver (Ag) to create a coating with both hard wearing, and antimicrobial properties.

Aim

To investigate the surface characteristics and antimicrobial efficacy of ZrN/Ag nanocomposite coatings.

Methodology

Microbiological assays

- *Staphylococcus aureus* NCTC 8532 and *Staphylococcus epidermidis* NCTC 11047 were used.
- Retention assay using acridine orange staining.
- LiveDead staining on retained cells on the surface.
- Nitro-tetrazolium violet (NTV) redox dye assay (to assess contact kill) following drying (1 h).
- Horse blood and bovine serum albumin (10% v/v) were dried to the surfaces to produce *in vitro* conditioning films (10 µL) and investigate their effect on antibacterial properties of the surfaces.

Surfaces

- The Magnetron sputtering rig used was a Teer Coatings UDP350 (Figure 2).
- Coatings were deposited onto 10 mm x 10 mm coupons of 316L medical grade stainless steel with a fine polish finish (R_a = 10 ± 2 nm).
- Power to the silver target was varied between 90 – 160 W to achieve contents of 6, 15, and 25 at. % Ag.

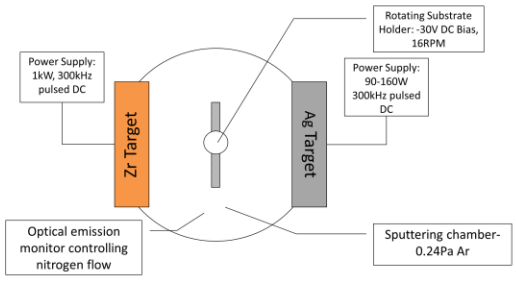

Fig. 2: Schematic diagram of the Teer UDP 350 Magnetron sputtering rig. Targets were 100 x 300 mm dimension and were 99.5% and 99.9% purity for Zr and Ag respectively.

Results

•The ZrN structure became more dense as the silver content increased (Figure 4) and the silver coatings increased in hydrophobicity in comparison to pure ZrN with the most hydrophobic being ZrN/ 15 at. % Ag (Figure 5).
•Coverage was reduced on all of the coated samples for *S. aureus* and just the silver coatings for *S. epidermidis* (Figure 3).
•Fewer *S. epidermidis* cells were retained on the surfaces compared to *S. aureus* (Figure 3 & 6).
•Respiring colonies on the surface were reduced in number as the silver content of the surfaces increased. Addition of a conditioning film reduced the efficacy of the silver (Figure 7).
•Increased silver lead to a decrease in "Live" cells on the surface (Figure 6).
•The surfaces did not leach silver at inhibitory concentrations towards the bacteria screened (Results not shown).

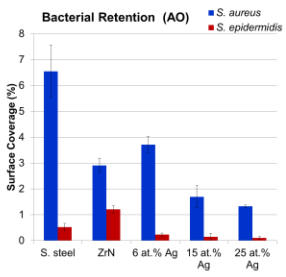

Fig. 3: Percentage surface coverage of the bacterial cells following a retention assay and acridine orange staining.

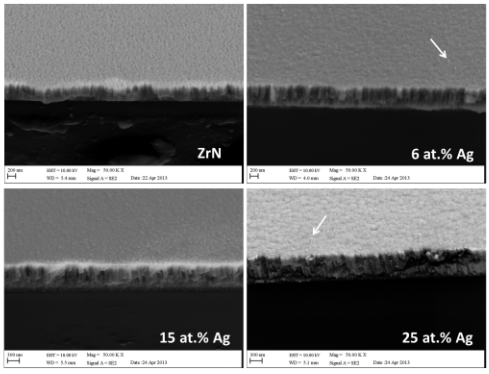

Fig. 4: SEM Fracture sections demonstrating the coating structure. Silver nanoparticles can be observed within the coatings (White arrows).

Fig. 5: Hydrophobicity of the five investigated coatings. Hydrophobicity is measured as a ΔG_{iwi} value. Negative values correspond to surfaces being hydrophobic.

Substrate	S. Steel	ZrN	6 at. % Ag	15 at. % Ag	25 at. % Ag
ΔG_{iwi}	-60.8	-39.6	-70.0	-77.2	-53.0
Std. Deviation	± 17.6	± 20.1	± 12.1	± 13.9	± 10.7

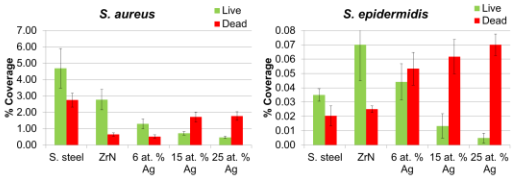

Fig. 6: LiveDead® assays displaying viable cells in green and dead cells in red.

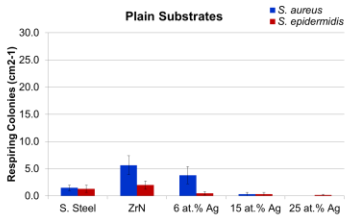

Fig. 7a: NTV assay colony counts following 24h incubation.

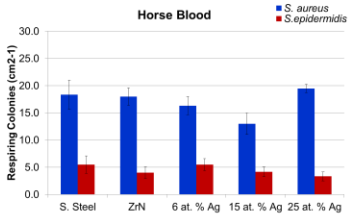

7b: NTV assay with a horse blood conditioning film.

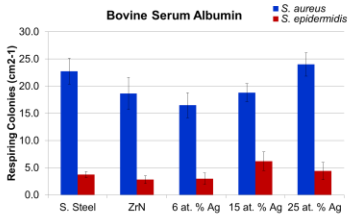

7c: NTV assay with a Bovine Serum Albumin Conditioning Film

Conclusion

ZrN/Ag nanocomposite coatings were produced and displayed a successful contact kill towards *S. aureus* and *S. epidermidis*. These hard wearing coatings display potential to be used to combat pin tract infection.

Acknowledgements

The authors gratefully acknowledge support from the EPSRC-funded Bridging the Gaps: Nano-Info-Bio project, grant reference EP/H000291/1

Wickens, D. J., West, G., Kelly, P. J., Verran, J., Lynch, S. and Whitehead, K. A. (2012) 'Antimicrobial activity of nanocomposite zirconium nitride/silver coatings to combat external bone fixation pin infections.' *Int J Artif Organs*,

12.7 International Journal of Artificial Organs: June 2012

Wickens, D. J., West, G., Kelly, P. J., Verran, J., Lynch, S. & Whitehead, K. A. 2012. *Antimicrobial activity of nanocomposite zirconium nitride/silver coatings to combat external bone fixation pin infections*. International Journal of Artificial Organs, 35, 817-825.

12.7.1 Antimicrobial activity of nanocomposite zirconium nitride/silver coatings to combat external bone fixation pin infection

During external fixation, temporary implants are used to penetrate the skin, muscle and bone to support severely fractured bones. This creates a biologically critical interface at the site of entry, which potentially allows a risk of infection. The aim of this study, therefore, was to investigate potential antimicrobial nanocomposites to combat infection.

Magnetron sputtering was used to produce zirconium nitride/silver nanocomposite coatings, which were prepared at two different silver concentrations of 15 at.% and 30 at.%. These coatings were characterised for morphology, chemical composition and antimicrobial activity, in comparison to pure zirconium nitride and stainless steel. Staphylococcus aureus and Staphylococcus epidermidis were used as in vitro test organisms in a range of antimicrobial assays; retention of the bacteria on the surfaces using LiveDead™ staining; the use of a metabolic redox dye to indicate any contact kill and zone of inhibition assays to indicate any leaching of inhibitory silver ions. Antimicrobial tests demonstrated a significant kill when the bacterial cells came in contact with the coatings containing silver at both 15.5 at.% and 29.8 at.%. No inhibitory leaching from the surfaces occurred. These surfaces demonstrate potential for use as antimicrobial fixation pin coatings.

Int J Artif Organs 2012; 35 (10): 817-825 DOI: 10.5301/ijao.5000156

ORIGINAL ARTICLE

Antimicrobial activity of nanocomposite zirconium nitride/silver coatings to combat external bone fixation pin infections

David J. Wickens[1,2], Glen West[2], Peter J. Kelly[2], Joanna Verran[1], Stephen Lynch[3], Kathryn A. Whitehead[1,2]

[1] School of Healthcare Sciences, Manchester Metropolitan University, Manchester - UK
[2] School of Engineering, Manchester Metropolitan University, Manchester - UK
[3] School of Mathematics, Computing & Digital Technology, Manchester Metropolitan University, Manchester - UK

ABSTRACT

During external fixation, temporary implants are used to penetrate the skin, muscle and bone to sup- port severely fractured bones. This creates a biologically critical interface at the site of entry, which potentially allows a risk of infection. The aim of this study, therefore, was to investigate potential antimicrobial nanocomposites to combat infection.

Magnetron sputtering was used to produce zirconium nitride/silver nanocomposite coatings, which were prepared at two different silver concentrations of 15.5 at.% and 29.8 at.%. These coatings were characterized for morphology, chemical composition, and antimicrobial activity in comparison to pure zirconium nitride and stainless steel. Staphylococcus aureus and Staphylococcus epidermidis were used as in vitro test organisms in a range of antimicrobial assays; retention of the bacteria on the surfaces and their survival using LiveDead™ staining; the use of a metabolic redox dye to indicate a contact kill and zone of inhibition assays to indicate leaching of inhibitory silver ions. Antimicrobial tests demonstrated a significant kill when the bacterial cells came in contact with the coatings containing silver at both
15.5 at.% and 29.8 at.%. No inhibitory leaching from the surfaces occurred. These surfaces demon- strate potential for use as antimicrobial fixation pin coatings.

KEY WORDS: *Pin-tract infection, Anti-infective agents, External fixators, Zirconium nitride, Silver, Nanocomposites*

Accepted: June 30, 2012

INTRODUCTION

Due to their invasive nature, implanted devices are prone to infection. Biomaterial infections, particularly bacterial implant infections, are of significance in medicine and with the use of implants increasing dramatically, methods to prevent and reduce infection are of interest (1-2). The failure of medical implants to resist colonization by pathogens and the frequency of infection depends upon many factors. These include the presence of bacteria in proximity to the implant, surrounding tissue necrosis, and the surface characteristics and material type used for the construction of the medical implant (1). The most common infections are caused by opportunistic pathogens, such as *Staphylococcus spp*. which are part of the body's natural flora. It was stated by Harris and Richards (2) that *Staphylococcus aureus* infections are more common in metal biomaterials while *Staphylococcus epidermidis* are more frequently associated with polymeric biomaterials. However, *S. epidermidis* is the second

DOI: 10.5301/ijao.5000156

most prevalent pathogen isolated from metal implant infections (2-4).

External fracture fixation is a method used to treat fractures that are severely comminuted or open to the environment. The system uses an external framework consisting of a frame support surrounding the limb, which acts as an anchor point for threaded bone pins that are screwed into the fractured bone (5). However, the nature of external fixation presents an intermedullary interface between the external biomaterial (non-sterile) and internal muscle and bone (sterile). The pin site of entry is constantly open and cannot heal, thus creating a critical interface, constraining the protective nature of the skin and the natural healing process that the body relies on.

Pin tract infections are the most medically important complication in stainless steel external fixation systems, with the frequency of infection between 2% and 30% (6). It has been stated by Parameswaran et al (7) that throughout their four year investigation, which included 285 external fixation subjects, 32 (11.2%) were infected. According to Mahan et al (8) out of 214 external fixation pins (42 total patients), following removal, 160 (74.8%) were found to be harboring bacteria on the tips, yet this did not always result in an infection. They discovered that 90% of the pins were contaminated with *S. epidermidis*, followed by *S. aureus* with 37.5% of all pins culturing positive.

The most effective method of eliminating a pin tract infection as stated by many authors is the removal of the device, followed by an aggressive course of systemic and/or local antibiotics (2, 4, 9). Others have suggested that the severity of the infection will indicate whether removal is required or antibiotic therapy is sufficient to eliminate the infection. The production of novel antimicrobial coatings is a potential method to combat pin tract infections.

Surface coatings and production

Zirconium nitride is a hard wearing compound used in industry to improve the life of cutting and forming tools, as well as being a decorative coating in some cases due to its gold appearance (10-12). In addition to having an excellent mechanical strength, zirconium nitride has been recognized as a potential biomaterial due to its corrosion resistance and chemical stability as well as good biocompatibility and low cytotoxicity (11, 13-15). However, its use as a biomaterial to combat pin tract infections, to the authors' knowledge, is novel.

Silver is used as a broad spectrum antimicrobial in ion and salt form, for example as silver sulphadiazine, silver nitrate and as metallic silver in medical and health products to increase hygiene and reduce infection. Metallic silver has been incorporated into wound dressings, which has displayed, *in vitro* and *in vivo*, a broad spectrum antimicrobial activity towards many microorganisms associated with wound infection (1, 16-17). There are several theories addressing the mechanism by which silver ions cause bacterial cell death, which differ depending upon the organism type, cell physiology, strain, and methods used. Many authors have described multiple changes in cell physiology when treated with silver, involving silver ions binding to proteins and enzymes in the cell wall, cell membrane and peptidoglycan (16, 18-23). Rai et al (23) described silver ions as having a high affinity for bacterial cell membranes, tissue proteins, nuclear membrane and respiratory enzymes, the latter resulting in inhibition of respiration and replication. This may be explained since Kim et al (17) suggested that a positive charge may be required for antimicrobial efficacy, which also allows attraction between the positively charged ions and the negative polarity of the cell membrane of some bacteria.

Magnetron sputtering is a physical vapor deposition (PVD) technique which uses the concept of an electrical field and a magnetic field interacting under a reduced pressure inert gas atmosphere to produce and control a partially ionized gas phase, known as a plasma. For the deposition of compound films, e.g., metal nitrides, a reactive gas is introduced (nitrogen in this case) in a process known as reactive sputtering (25). This paper describes deposition of zirconium nitride co-sputtered with silver. As silver nitride is thermodynamically unstable, the coating is deposited with a segregation of the silver in nanoparticulate form (<100 nm) (19) embedded in the zirconium nitride matrix. The aim of the investigation was to develop a durable antimicrobial coating for metallic implant applications using reactive magnetron sputtering.

MATERIALS AND METHODS

Surfaces

Medical grade 316 L stainless steel coupons (Aalco, Bolton, UK) (10 x 10 mm) with a fine polish finish (R_a =

10 ± 2 nm) were used as the underlying substratum and thus also as a control for microbiological testing. Coatings were also deposited onto highly polished silicon wafers (WRS Materials Spring City, PA, USA), cut into 10 × 10 mm coupons to determine the benchmark surface topography. Both stainless steel coupons and silicon wafers were cleaned using methanol and a clean fibre-free paper towel (TEXMET® 1000; Buehler, IL, USA), prior to sputtering.

Deposition of nanocomposite thin films

To produce the coatings for this study, adaptions were made to a method by Kelly et al (12). Coatings were deposited in a Teer Coatings UDP 350 magnetron sputtering system in a closed field, unbalanced magnetic configuration (13). Targets of 99.5% pure zirconium (300 × 100 × 10 mm) and 99.5% pure silver (300 × 100 × 3 mm), respectively, were sputtered in a pure argon nitrogen atmosphere. Prior to deposition, the substrates were sputter-cleaned in an argon plasma (0.4 Pa) for 10 min at -600 V DC. Throughout the sputtering procedure the zirconium target was powered with 1.5 kW pulsed DC power (20 kHz 90% duty) and the silver target with applied powers of 150 W and 230 W (20 kHz 90% duty) to obtain the two different silver concentrations in the deposited films. The sputter-coating procedure took place in a 0.24 Pa argon atmosphere with a -30 V DC substrate bias. The flow rate of nitrogen during reactive sputtering was controlled via the optical emissions monitoring technique using the intensity of zirconium optical emissions in the plasma as a control signal to generate the correct coating composition (12). To maintain a coating thickness of the order of one micron, deposition times were varied between 50 min and 19 min depending upon the power delivered to the silver target.

Thin film analysis

Energy Dispersive X-Ray Spectroscopy (EDX)

EDX was performed on the samples to determine the chemical composition of the coatings (Edax Trident, Leicester, UK) using an EDAX Sapphire Si (Li) detector, and quantified using a standardless ZAF algorithm. The chemical composition was calculated as an atomic percentage (at.%), giving the percentage of the atom relative to the total number of atoms in the scan.

Scanning Electron Microscopy (SEM)

Scanning electron microscopy was used to obtain images of the morphology and structure of the coatings using a Zeiss Supra VP40 field emission gun scanning electron microscope (FEG-SEM). Electron backscattered images (EBS) were obtained from the samples to visualise any silver particle distribution (Zeiss, Supra VP40, Germany).

Atomic Force Microscopy (AFM)

Two- and three-dimensional images along with roughness parameters were obtained using an atomic force microscope (Quesant Instruments, CA, USA) operated in contact mode using a force constant of 0.12 Nm^{-1} and a silicon nitride tip. Scans were made of the stainless steel and silicon wafer substrates to measure benchmark topographies. Scans for both the silicon and stainless steel substrates, with the ZrN coating and ZrN/Ag coatings containing 15.5 at.% and 29.8 at.% silver were performed. Scan sizes were 20 μm^2 and 1 μm^2 for the stainless steel and silicon wafer samples, respectively. Three replicate scans were performed on three separate coupons. R_a roughness parameters were taken from all scans of all substrates and the average value calculated.

Microbiology

Preparation of microorganisms for antimicrobial assays

Sterile brain heart infusion (BHI) broth (100 mL) was inoculated with *S. aureus* NCTC 8532 or *S. epidermidis* NCTC 11057. These were incubated overnight in an orbital incubator at 37°C for 24 hours at 130 RPM. Cultures were removed from incubation and the cells were washed by centrifuging at 3600 x *g* for 10 minutes. The supernatant was removed and the cells were re-suspended in sterile distilled water. Cells were diluted to an optical density (OD) of 1.0 ± 0.05 at 540 nm using a spectrophotometer (Jenway 6305; Bibby Scientific, Essex, UK), using sterile distilled water as a blank. Counts were taken using a serial dilution method to calculate the average colony forming units per mililiter (CFU/ml).

Respiratory activity of microorganisms

This method was adapted from Barnes et al (26) to determine the antimicrobial effect of the surfaces when in contact

with the microorganisms. Cells were prepared as previously stated and a dilution was chosen for the assay containing between 10^5 and 10^6 CFU/ml (27). The diluted suspension was deposited onto each coupon (10 µL) and put into a class 2 microbiological cabinet (Safelab Systems, Bristol, UK) for 1 hour to dry. Following drying, the coupons were placed in a Petri dish and 25 mL brain heart infusion agar that had been cooled to 50°C was used to overlay the inoculated samples (Oxoid, Basingstoke, UK), then incubated for 24 hours at 37°C. Following incubation, each plate was flooded with 2 mL of 0.3% filter sterilized nitro tetraozolium violet (Sigma-Aldrich, St Louis, MO, USA) and incubated for 6 hours at room temperature. Actively respiring colonies were visible on the coupons as dark violet colonies, which were counted for quantitative data and photographs were taken for qualitative data.

LiveDead™ Staining

LiveDead™ staining was carried out following a bacterial retention assay (adapted from Whitehead et al 2005 (28)) in order to determine the effect of the surfaces on bacterial cell retention, along with the antimicrobial activity of the thin films. Substrata were cleaned with ethanol and sterile distilled water and then dried in a class II air flow cabinet before use. The coupons were attached to the bottom of a glass Petri dish with double sided tape, and then the cell suspension (30 mL) was poured over the samples into the glass Petri dishes. The dishes were incubated for one hour at 37°C without agitation. Samples were removed using sterile forceps and rinsed once, gently with 5 cm^3 distilled water, with the bottle at a 45° angle, and a 3 mm nozzle (29). The samples were mounted onto glass slides for air drying in a class II microbiological flow cabinet for 45 min before staining. Prepared BacLight bacterial viability LiveDead™ stain (LiveDead™, BacLight™ bacterial viability kit; Invitrogen, Paisley, Scotland) (2.5 µL) was applied to the samples. Both stains had been individually diluted to a 1:40 stain: water ratio. The stain was left to dry (15 min) in the dark without rinsing, to be viewed immediately.

Viable (green) and non-viable (red) cells were counted using an epifluorescence microscope (Nikon Eclipse E 600, Surrey, UK), through a mounted F-View II black and white digital camera (Soft Imaging System Ltd, Helperby, UK, supplied by Olympus, Hertfordshire, UK) using a Cell-F Image analysis program (Olympus, Hertfordshire, UK). Viable cells fluoresced green while the non-viable cells, with a compromised membrane, fluoresced red. The samples were observed under 100x and 1000x (oil immersion) magnification (Leica Type F immersion oil, Wetzlar, Germany).

Zones of inhibition (ZoI)

ZoI were carried out to assess any leaching of silver from the nanocomposite films. One hundred microliters of standardized cell suspension (OD of 1.0 at 540 nm) was spread onto a brain heart infusion agar plate using a sterile glass spreader. The coated stainless steel coupons (10 × 10 mm) were sterilized by wiping with 70% ethanol and water and air drying. Sterile forceps were used to transfer the coupon to the agar where it was placed with the coating face down on to the bacterial lawn. The agar plates were incubated overnight for 24 h at 37°C. Any zones of inhibition were measured around the coupons using an electronic micrometer (Mitutoyo CD-6”CP, Japan).

Statistical analysis

All statistical analysis was performed using Microsoft Excel. Two-tailed distribution *T*-Tests with two sample homoscedastic variance or ANOVA (single factor) analysis of overall variance were carried out on the data. Results were reported as the mean ± standard error. Differences in statistical data were considered to be significant when $p \leq 0.05$ (29).

RESULTS

Following EDX analysis, the atomic silver contents of the two zirconium nitride/silver coating compositions were found to be 15.5 at.% and 29.8 at.% for the applied target powers of 150 W and 230 W, respectively. The zirconium nitride chemically consisted of a stoichiometric ratio of zirconium to nitrogen throughout all coatings tested (data not presented). High magnification SEM imaging (20,000x) of the cross sections of fractures demonstrated that the thin films were columnar in structure and that the columnar element reduced as the silver content increased (Figs. 1a-c). The 29.8 at.% silver coating displayed a clear difference in structure with no evidence of columnar deposition; the coating was more granular in appearance (Fig. 1c). Electron backscattering revealed a uniform chemical composition for zirconium nitride (Fig. 2a) while the co-sputtered ZrN and Ag were deposited in a heterogeneous structure, with silver nanoparticles em-

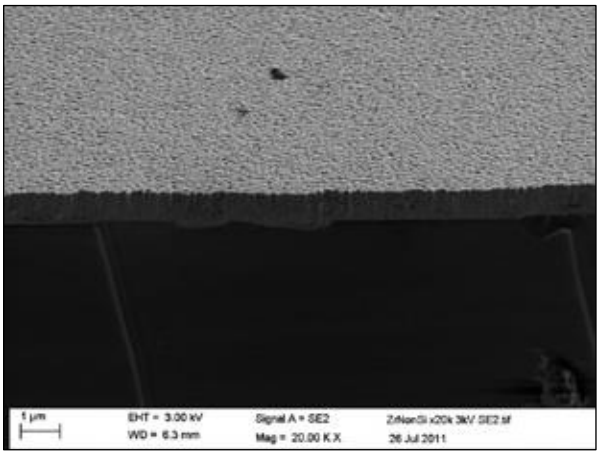

a

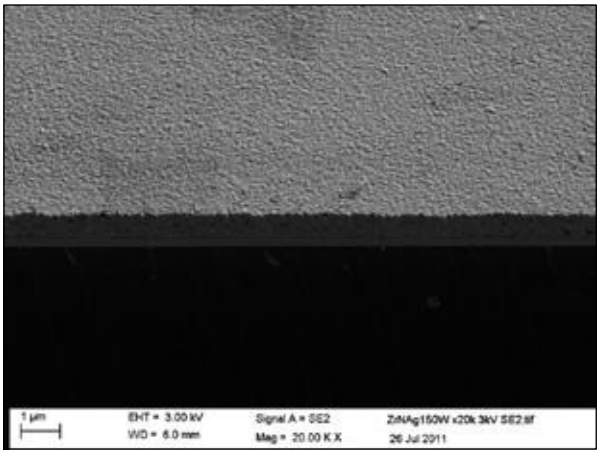

b

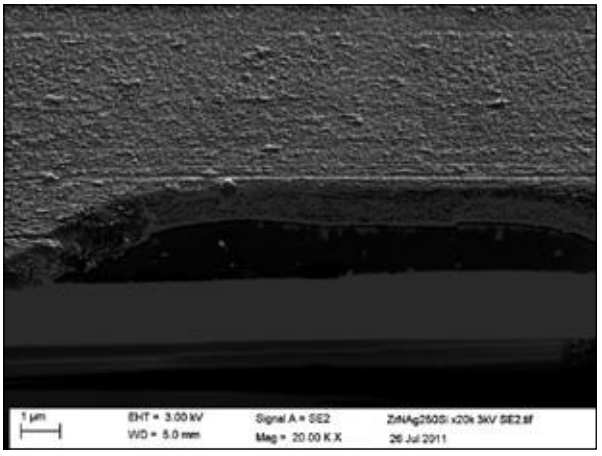

c

Fig. 1 - *SEM images of coating fractures displaying the structure of the thin films* **a)** *ZrN,* **b)** *ZrN/ 15.5 at% Ag,* **c)** *ZrN/ 29.8 at% Ag. Coatings demonstrated a columnar formation which became more granular as the silver content increased.*

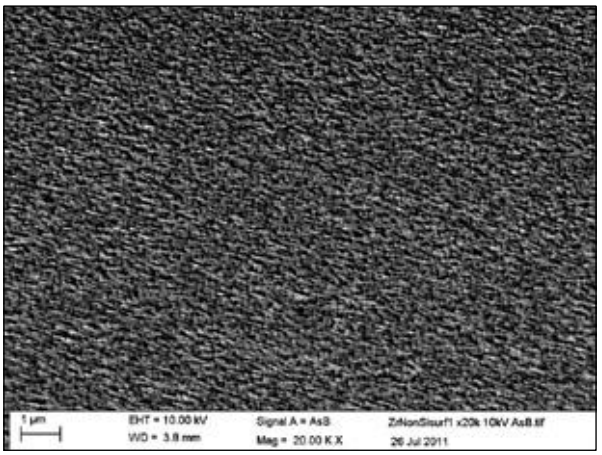

a

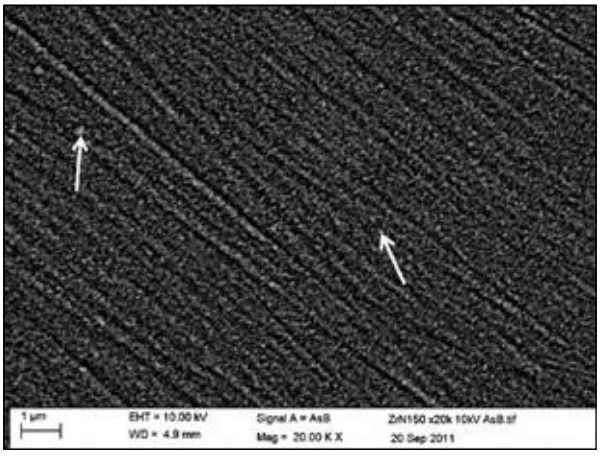

b

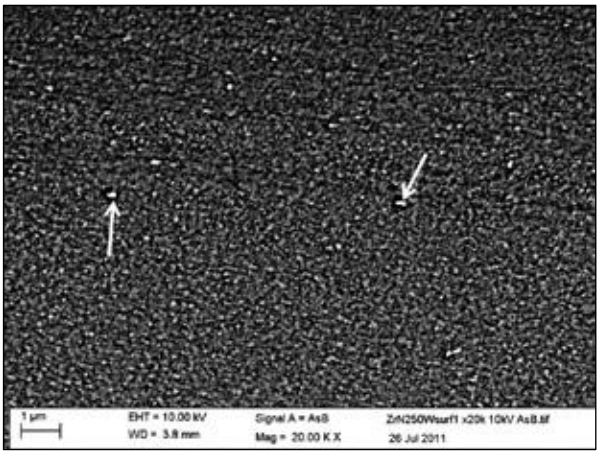

c

Fig. 2 - *Backscattered electron images of the coated surfaces* **a)** *ZrN,* **b)** *ZrN/ 15.5 at% Ag,* **c)** *ZrN/ 29.8 at% Ag. Silver nanoparticles were visible as bright spots within the images (indicated on* **b**&**c**).

 ISSN 0391-3988

Fig. 3 - *AFM imaging of the coated surfaces* **a)** *Stainless steel,* **b)** *ZrN,* **c)** *ZrN/ 15.5 at% Ag, d) ZrN/ 29.8 at% Ag demonstrating the coating followed the underlying surface features. Nanotopographies were evident for the coated surfaces* **(b-d)** *(Note: the z scales vary for each image).*

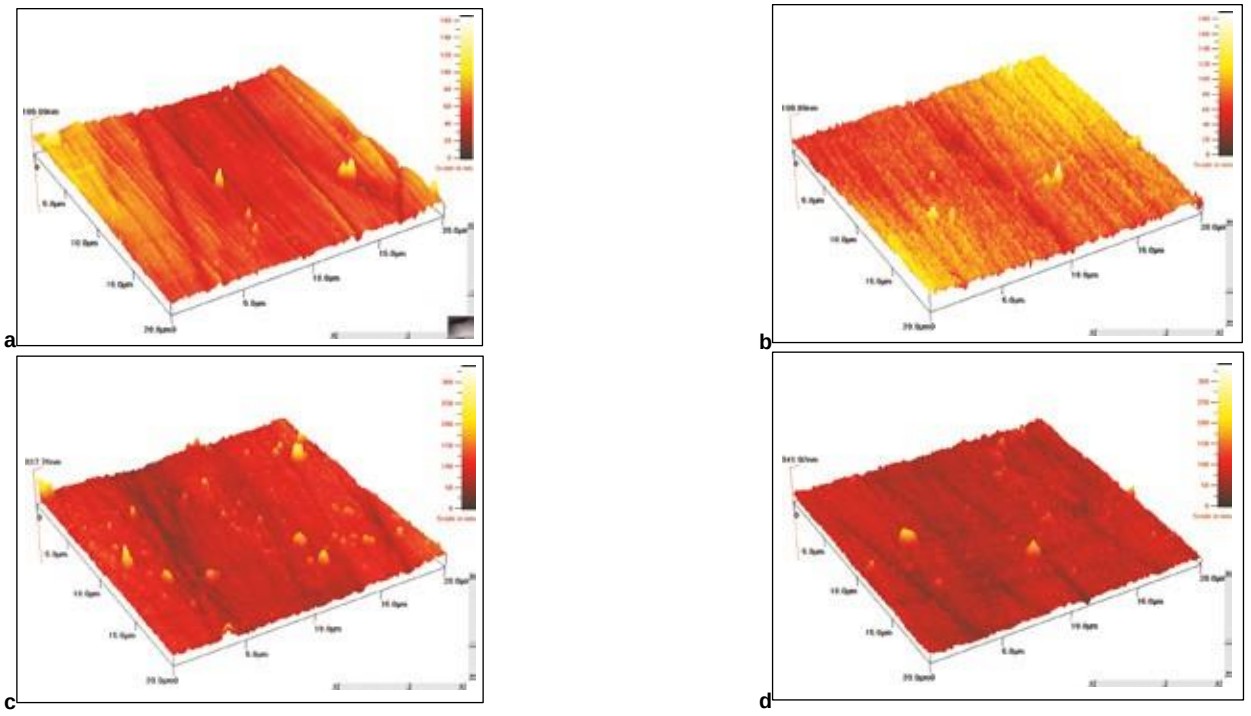

bedded in a pure ZrN matrix (Figs. 2b-c). This was observed due to heavier elements (in this case the silver) displaying a brighter image phase, so that the silver particles were observed in the images as bright spots throughout the overall coating.

The AFM images and data demonstrated that the ZrN (Fig. 3b) and ZrN/Ag (Figs. 3c-d) coatings followed the topographical features of the underlying stainless steel (Fig. 3a). The thin films were analyzed on the stainless steel substrata since this would be the material for use in external fixation pin coatings. The uncoated stainless steel presented significantly lower average roughness values ($p<0.05$) when compared to the coated samples (Tab. I). When the stainless steel surface was compared to the coated surfaces it was evident that although the underlying microtopography of the substratum was observed the coated surfaces also displayed nanofeatures (Figs. 3a-d). The ZrN/15.5 at.% Ag coating surface displayed protruding particles (Fig. 3c), and when compared with the coating containing 29.8 at.% Ag, the presence of the protrusions increased. These protrusions within the coating were larger particles of silver but with a range of sizes and shapes (Fig. 3d).

Microbiological analysis

As the silver content increased in the coatings it was demonstrated that the respiring colonies on the surface significantly decreased ($p<0.05$) in relation to the pure ZrN (Fig. 4). Both species of microorganisms appeared to survive better on the ZrN than the stainless steel surfaces. No leaching of inhibitory silver ions was observed for any of the coatings (data not presented).

A higher total number of dead to live *S. aureus* cells were present on all surfaces than was observed for the *S. epidermidis* samples, and the coated samples displayed a trend of

TABLE I - RA VALUES OF THE SUBSTRATE SURFACES

Substrate	Average R_a Value (nm)
Stainless steel	9.5
ZrN	13.2
ZrN/15.5 at.% Ag	13.1
ZrN/29.8 at.% Ag	11.9

The data demonstrate an increase in roughness between coated and uncoated samples but little difference between the different coating compositions.

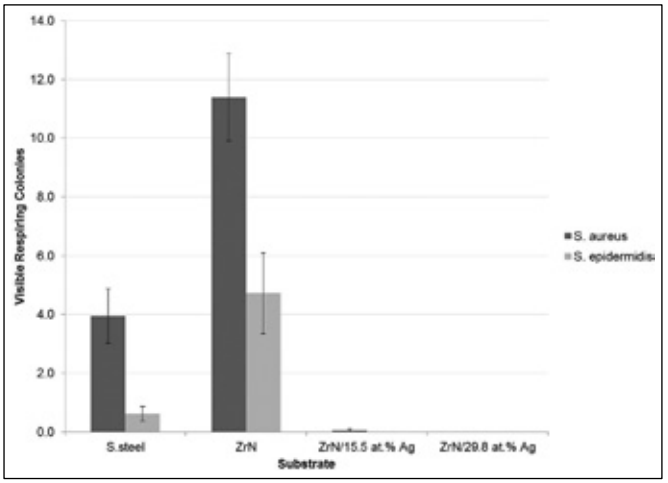

Fig. 4 - *Respiratory dye assay after one hour contact demonstrating a decrease in the number of visible respiring colonies on the surfaces containing silver over the stainless steel and the zirconium nitride.*

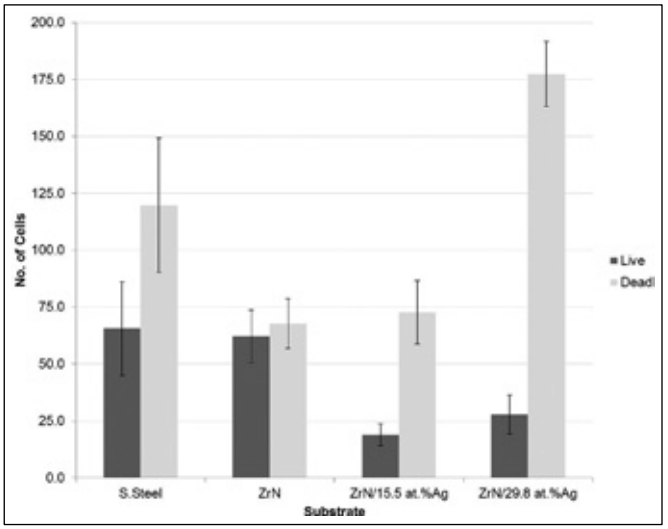

a

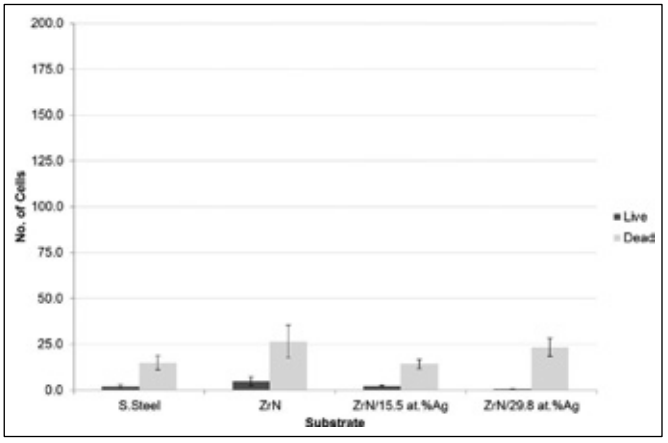

b

Fig. 5 - *Number of living to dead cells following LiveDead™ staining. A decrease in the number of living cells and an increase in the number of dead cells was observed for the coatings containing silver against both* **a)** *S. aureus and* **b)** *S. epidermidis.*

increasing dead cells as the silver content increased (Fig. 5a). Although the total number of cells retained on the surfaces was lower for *S. epidermidis* than *S. aureus* a higher number of dead to live cells for all the coatings was also observed (Fig. 5b). As with the *S. aureus* the number of dead cells increased with increasing silver concentration.

DISCUSSION

Substrata

The ZrN coatings, in all cases, had a stoichiometric composition. Backscattered electron SEM images showed that the silver was deposited as particles within the ZrN matrix, due to silver nitride being thermodynamically unstable, which resulted in deposits forming as nanoparticles within the zirconium nitride matrix (30). SEM cross-section images of the coatings indicated that the nanocomposite films comprised of columnar structures, which changed to a more dense structure as the silver content increased. It is not fully known why this structural difference occurs when the silver content is high; this will be investigated further in future work. Potential methods for altering the structure could be to change the process gas pressure, or to increase the substrate bias voltage, potentially giving a nanocomposite structure with increased density and altering the coating properties (31-33).

AFM analysis of the ZrN and ZrN/Ag coatings in relation to the underlying bare substratum of the stainless steel indicated that the presence of the coatings increased the roughness of the surface. However, coating images taken from the AFM on the stainless steel substrates showed that no surface features exceeded 1 µm in width. A surface topography of similar sizes to microbial dimensions might protect the cells from stresses such as shear forces at the air:solid:liquid interface (34). Surface features could arise from production processes during the manufacturing of the material. The roughness of the coatings increased as

the silver content increased, which is probably due to the silver particles protruding from the zirconium nitride surface, visible on the AFM scans of the coatings.

Microbiology

A redox dye (Tetrazolium Violet) was used to indicate respiring colonies on a surface after a contact time of one hour (26). Results showed a decrease in the number of colonies to zero for both of the silver-containing coatings. However, a decrease was also observed on the bare stainless steel substratum. In this case, when spread onto the stainless steel surface the cell suspension would not distribute across the surface area but remained in a single droplet. Cells will therefore have dried in a smaller area, resulting in a reduction of separate colonies. The increase in silver content reduced the viable cell counts of both microorganisms tested. The ZrN/Ag with a silver content of 29.8 at.% displayed on average no viable colonies for the *S. epidermidis* and *S. aureus*, after an initial deposition of around 5×10^4 cells onto the surfaces.

The zone of inhibition assays demonstrated that the surfaces did not leach silver ions into the surrounding area, inhibiting the growth of the microorganisms. These results agree with a similar investigation by Kelly et al (12), however, leaching of silver ions cannot be entirely ruled out; the concentration of silver may be at sub-inhibitory levels. The nature of the LiveDead™ staining kit is to stain all of the cells green using SYTO-9, while propidium iodide dominantly over-stains any cells in the population with a compromised cell membrane with a red stain (35). Following retention assays, LiveDead™ staining displayed a significant kill of both *S. aureus* and *S. epidermidis* as the silver concentration increased. The literature suggests that *S. epidermidis* tends to colonize polymer biomaterials more while *S. aureus* prefers metal substrates (2, 36-38), which may explain the higher number of *S. aureus* cells were retained on the surface.

CONCLUSIONS

Magnetron sputtering was used to reactively deposit zirconium nitride and zirconium nitride/silver coatings onto stainless steel with two different concentrations of silver. Silver nanoparticles were observed in the ZrN/Ag coatings. Although the nanotopography of the surface was altered by the coatings, this did not alter the microbial cell retention. *S. aureus* cells were retained on the surfaces in numbers one log higher than *S. epidermidis*. An increase in silver concentration led to a significant decrease in cell survival; the antimicrobial action of the silver in these coatings appears to require contact with the cell surface.

Financial Support: The authors gratefully acknowledge support from the EPSRC-funded Bridging the Gaps: Nano-Info-Bio project, grant reference EP/H000291/1.

Conflict of Interest Statement: The authors have no potential conflicts of interest in relation to this scientific work.

Address for correspondence:
Dr. Kathryn Whitehead
John Dalton East, Manchester Metropolitan University
Chester Street
Manchester, M1 5GD United Kingdom
e-mail: k.a.whitehead@mmu.ac.uk

REFERENCES

1. Chen W, Liu Y, Courtney HS, et al. *In vitro* anti-bacterial and biological properties of magnetron co-sputtered silver-containing hydroxyapatite coating. Biomaterials. 2006;27(32): 5512-5517.
2. Harris LG, Richards RG. Staphylococci and implant surfaces: a review. Injury. 2006;37(2)(Suppl 2):S3-S14.
3. Darouiche RO. Treatment of infections associated with surgical implants. N Engl J Med. 2004;350(14):1422-1429.
4. Coester LM, Nepola JV, Allen J, Marsh JL. The effects of silver coated external fixation pins. Iowa Orthop J. 2006;26: 48-53.
5. Taylor CJ. Correction of General Deformity with the Taylor Spatial Frame Fixator. http://www.jcharlestaylor.com/tsflitera- ture/01TSF-mainHO.pdf Accessed June 6, 2012.
6. Massè A, Bruno A, Bosetti M, Biasibetti A, Cannas M, Gallinaro P. Prevention of pin track infection in external fixation with silver coated pins: clinical and microbiological results. J Biomed Mater Res. 2000;53(5):600-604.

7. Parameswaran AD, Roberts CS, Seligson D, Voor M. Pin tract infection with contemporary external fixation: how much of a problem? J Orthop Trauma. 2003;17(7):503-507.
8. Mahan J, Seligson D, Henry SL, Hynes P, Dobbins J. Factors in pin tract infections. Orthopedics. 1991;14(3):305-308.
9. Trampuz A, Zimmerli W. Diagnosis and treatment of in- fections associated with fracture-fixation devices. Injury.
2006;37(2)(Suppl 2):S59-S66.
10. Pilloud D, Dehlinger AS, Pierson JF, Roman A, Pichon L.
Reactively sputtered zirconium nitride coatings: structural, mechanical, optical and electrical characteristics. Surf Coat Technol. 2003;174-175(0):338-344.
11. Aouadi SM, Debessai M, Filip P. Zirconium nitride/silver nanocomposite structures for biomedical applications. J Vac Sci Technol B. 2004;22(3):1134-1140.
12. Kelly PJ, Li H, Benson PS, et al. Comparison of the tribo- logical and antimicrobial properties of CrN/Ag, ZrN/Ag, TiN/ Ag, and TiN/Cu nanocomposite coatings. Surf Coat Technol.
2010;205(5):1606-1610.
13. Monaghan DP, Teer DG, Laing KC, Efeoglul, Arnell RD. Depo- sition of graded alloy nitride films by closed field unbalanced magnetron sputtering. Surf Coat Technol. 1993;59(1-3):21-25.
14. Okazaki Y, Ito Y, Kyo K, Tateishi T. Corrosion resistance and corrosion fatigue strength of new titanium alloys for medical implants without V and Al. *Mat Sci Eng A- Struct*. 1996;213 (1-2):138-147.
15. Brugnoni C, Lanza F, Macchi G, et al. Evaluation of the wear resistance of ZrN coatings using thin layer activation. Surf Coat Technol. 1998;100-101(0):23-26.
16. Kertzman Z, Marchal J, Suarez M, et al. Mechanical, tribo- logical, and biocompatibility properties of ZrN-Ag nanocom- posite films. J Biomed Mater Res A. 2008;84A(4):1061-1067.
17. Kim JS, Kuk E, Yu KN, et al. Antimicrobial effects of silver nanoparticles. Nanomedicine. 2007;3(1):95-101.
18. Necula BS, Fratila-Apachitei LE, Berkani A, Apachitei, Duszczyk J. Enrichment of anodic MgO layers with Ag nanoparticles for biomedical applications. J Mater Sci Mater Med. 2009;20(1):339-345.
19. Allaker RP. The use of nanoparticles to control oral biofilm formation. J Dent Res. 2010;89(11):1175-1186.
20. Sondil, Salopek-Sondi B. Silver nanoparticles as antimicrobial agent: a case study on E. coli as a model for Gram-negative bacteria. J Colloid Interface Sci. 2004;275(1):177-182.
21. Pal S, Tak YK, Song JM. Does the antibacterial activity of silver nanoparticles depend on the shape of the nanopar- ticle? A study of the Gram-negative bacterium Escherichia coli. Appl Environ Microbiol. 2007;73(6):1712-1720.
22. Edwards-Jones V. The benefits of silver in hygiene, per- sonal care and healthcare. Lett Appl Microbiol. 2009;49(2):
147-152.
23. Schierholz JM, Lucas LJ, Rump A, Pulverer G. Efficacy of silver-coated medical devices. J Hosp Infect. 1998;40(4):
257-262.
24. Rai M, Yadav A, Gade A. Silver nanoparticles as a new generation of antimicrobials. Biotechnol Adv. 2009;27(1):
76-83.
25. Schiller S, Goedicke K, Reschke J, Kirchhoff V, Schneider S, Milde F. Pulsed magnetron sputter technology. Surf Coat Technol. 1993;61(1-3):331-337.
26. Barnes BI, Cassar CA, Halablab MA, Parkinson NH, Miles RJ. An in situ method for determining bacterial survival on food preparation surfaces using a redox dye. Lett Appl Microbiol. 1996;23(5):325-328.
27. Kelly PJ, Whitehead KA, Li H, Verran J, Arnell R. The influ- ence of silver content on the tribological and antimicrobial properties of ZrN/Ag nanocomposite coatings. J Nanosci Nanotechnol. 2011;11(6):5383-5387.
28. Whitehead KA, Colligon J, Verran J. Retention of microbi- al cells in substratum surface features of micrometer and sub-micrometer dimensions. Colloids Surf B Biointerfaces.
2005;41(2-3):129-138.
29. Whitehead KA, Verran J. The effect of surface proper- ties and application method on the retention of Pseudo- monas aeruginosa on uncoated and titanium-coated stainless steel. Int Biodeterior Biodegradation. 2007;60(2):
74-80.
30. Pierson JF, Wiederkehr D, Billard A. Reactive magnetron sputtering of copper, silver, and gold. Thin Solid Films.
2005;478(1-2):196-205.
31. Thornton J. Influence of apparatus geometry and deposition conditions on the structure and topography of

thick sput- tered coatings. J Vac Sci Technol. 1974;11(4):666.
32. Miao L, Jin P, Kaneko K, Terai A, Nabatova-Gabain N, Tane- mura S. Preparation and characterization of polycrystalline anatase and rutile TiO thin films by rf magnetron sputtering. Appl Surf Sci. 2003;212-213:255-263.
33. Window B, Savvides N. Charged particle fluxes from pla- nar magnetron sputtering sources. J Vac Sci Technol A.
1986;4(2):196-202.
34. Whitehead KA, Verran J. The effect of surface topography on the retention of microorganisms. Food Bioprod Process.
2006;84(C4):253-259.
35. Williams SC, Hong Y, Danavall DCA, et al. Distinguishing between living and nonliving bacteria: Evaluation of the vital stain propidium iodide and its combined use with molecular probes in aquatic samples. J Microbiol Methods. 1998;32(3):
225-236.
36. Vuong C, Otto M. Staphylococcus epidermidis infections.
Microbes Infect. 2002;4(4):481-489.
37. Ziebuhr W, Hennig S, Eckart M, Kränzler H, Batzilla C, Kozitskaya S. Nosocomial infections by Staphylococcus epi- dermidis: how a commensal bacterium turns into a pathogen. Int J Antimicrob Agents. 2006;28 Suppl 1:14-20.
38. Montanaro L, Campoccia D, Arciola CR. Advancements in molecular epidemiology of implant infections and future per- spectives. Biomaterials. 2007;28(34):5155-5168.

12.8 Colloids and Surfaces B: Biointerfaces April 2013

Skovager, A., Whitehead, K., Wickens, D., Verran, J., Ingmer, H. & Arneborg, N. 2013. *A comparative study of fine polished stainless steel, TiN and TiN/Ag surfaces: Adhesion and attachment strength of Listeria monocytogenes as well as anti-listerial effect.* Colloids and Surfaces B: Biointerfaces, 109, 190-196.

12.8.1 A comparative study of fine polished stainless steel, TiN and TiN/Ag surfaces: Adhesion and attachment strength of Listeria monocytogenes as well as anti-listerial effect

Magnetron sputtering was used to produce nanocomposite TiN and TiN/Ag coatings on stainless steel surfaces. The surface chemistry (EDX), physicochemical properties (contact angles), topography and roughness parameters (WLP and AFM) of the fine polished stainless steel (FPSS), TiN and TiN/8.6 at.% Ag surfaces were examined. Real-time initial adhesion of two Listeria monocytogenes strains (EGDe and 64) to the three surfaces was determined under flow conditions, and their attachment strength after adhesion was measured using atomic force microscopy (AFM). The anti-listerial properties of the surfaces were determined using LIVE/DEAD staining. Our results demonstrate that FPSS, TiN and TiN/8.6 at.% Ag possessed different surface properties, which may influence both attachment strength and anti-listerial properties. There were no significant ($p > 0.05$) differences in the initial adhesion of the two L. monocytogenes strains to the three different surfaces. Attachment studies showed that the two L. monocytogenes strains did not attach to FPSS under wetted conditions. However, both strains attached to TiN and TiN/8.6 at.% Ag surfaces, although with less strength to TiN/8.6 at.% Ag than to TiN surfaces. The TiN/8.6 at.% Ag surface showed marked anti-listerial properties as compared with FPSS and TiN. Initial adhesion, attachment strength and anti-listerial properties were found to be strain dependent.

Colloids and Surfaces B: Biointerfaces 109 (2013) 190–196

Contents lists available at SciVerse ScienceDirect

Colloids and Surfaces B: Biointerfaces

journal homepage: www.elsevier.com/locate/colsurfb

A comparative study of fine polished stainless steel, TiN and TiN/Ag surfaces: Adhesion and attachment strength of Listeria monocytogenes as well as anti-listerial effect

Anne Skovager[a], Kathryn Whitehead[b], David Wickens[d], Joanna Verran[b], Hanne Ingmer[c], Nils Arneborg[a,*]

[a] Department of Food Science, Food Microbiology, Faculty of Science, University of Copenhagen, Denmark
[b] School of Healthcare Science, Faculty of Science and Engineering, Manchester Metropolitan University, UK
[c] Department of Veterinary Disease Biology, Faculty of Health and Medical Sciences, University of Copenhagen, Denmark
[d] School of Engineering, Faculty of Science and Engineering, Manchester Metropolitan University, UK

article info

Article history:
Received 24 January 2013
Received in revised form 21 March 2013
Accepted 27 March 2013
Available online 8 April 2013

Keywords:
Fine polished stainless steel
TiN/Ag coatings Initial adhesion Attachment strength Listeria monocytogenes Anti-listerial effect

abstract

Magnetron sputtering was used to produce nanocomposite TiN and TiN/Ag coatings on stainless steel surfaces. The surface chemistry (EDX), physicochemical properties (contact angles), topography and roughness parameters (WLP and AFM) of the fine polished stainless steel (FPSS), TiN and TiN/8.6 at.% Ag surfaces were examined. Real-time initial adhesion of two Listeria monocytogenes strains (EGDe and 64) to the three surfaces was determined under flow conditions, and their attachment strength after adhesion was measured using atomic force microscopy (AFM). The anti-listerial properties of the surfaces were determined using LIVE/DEAD staining.

Our results demonstrate that FPSS, TiN and TiN/8.6 at.% Ag possessed different surface properties, which may influence both attachment strength and anti-listerial properties. There were no significant ($p > 0.05$) differences in the initial adhesion of the two L. monocytogenes strains to the three different surfaces. Attachment studies showed that the two L. monocytogenes strains did not attach to FPSS under wetted conditions. However, both strains attached to TiN and TiN/8.6 at.% Ag surfaces, although with less strength to TiN/8.6 at.% Ag than to TiN surfaces. The TiN/8.6 at.% Ag surface showed marked anti-listerial properties as compared with FPSS and TiN. Initial adhesion, attachment strength and anti-listerial properties were found to be strain dependent.

1. Introduction

Listeria monocytogenes is a food-borne pathogen causing listeriosis in susceptible consumer groups [1] and is exceptionally able to persist in food processing environments [2]. Ready-to-eat (RTE)-food products are high risk products with respect to contamination by L. monocytogenes, because they are not further heat treated before consumption [2]. In food processing environments, L. monocytogenes has been isolated from high shear environments, such as vats and pipes in milk processing environments [3–5], and cooking facilities, flow lines, and RTE-food production drains in meat processing environments [6]. One approach to limit the presence of L. monocytogenes on processing equipment could be using surfaces with a combination of different properties; limiting initial adhesion of L. monocytogenes to the surfaces under flow conditions, limiting the strength of attachment of adhered L. monocytogenes to the surface, and exerting antimicrobial activity.

Titanium nitride (TiN) is known to be a hard, low friction, wear resistant coating material applied in cutting and forming tools [7–10]. Furthermore, TiN coated implants have been found to significantly reduce the presence of bacteria (oral microorganisms, Pseudomonas aeruginosa, Staphylococcus aureus) on their surfaces [11–13]. Silver (Ag), silver nanoparticles and silver-containing surfaces are well known to have antimicrobial properties [10,14–17]. Some mechanisms of the silver ions are thought to include structural changes of the cell wall of bacteria and interactions with thiol groups in proteins and enzymes and interruption of DNA replication due to damage of the DNA [18,19]. Anti-listeria activity has been observed when applying textiles deposited with silver [20] and when applying silver nanoparticles as an antimicrobial agent on stainless steel surfaces [15]. Incorporation of silver into TiN coatings offers the potential to modify these separate surface properties in order to obtain a hard wear-resistant material with antimicrobial properties, which may be applied in biomedical or

* Corresponding author at: Department of Food Science, Food Microbiology, Fac- ulty of Science, University of Copenhagen, Rolighedsvej 30, 1958 Frederiksberg C, Denmark. Tel.: +45 35 33 32 66; fax: +45 35 33 32 14.
E-mail address: na@life.ku.dk (N. Arneborg).

food processing industries. TiN/Ag coatings, with different silver concentrations, are produced by magnetron deposition [17,21]. The surface characteristics of TiN and TiN/Ag coatings have been examined to some extent [16,17,21]. An increase in silver concentration (0.0–16.7 at.%) of TiN/Ag coating was found to marginally reduce surface hardness (27.3–10.6 GPa). In addition, a marginal decrease in friction coefficient was found with a similar increase in silver content [16]. Retention and antimicrobial properties of TiN and TiN/Ag have been evaluated for some microorganisms. At a higher concentration, silver in TiN/Ag coatings significantly reduced the amount of viable (NBT assay) P. aeruginosa and S. aureus cells compared to TiN coatings [16]; the degree of reduction being dependent on the silver concentration [10]. The silver concentration also influenced the surface characteristics, such as nanotopography (surface features, grain size) and physicochemistry [17,21]. The anti-listerial properties do not yet appear to have been tested for TiN and TiN/Ag coated surfaces.

Previously, real-time initial adhesion at a single-cell level of different L. monocytogenes strains to fine polished stainless steel (FPSS) under flow conditions has been determined by using a flow perfusion system and fluorescence microscopy [22]. To the best of our knowledge, this has not, as yet, been done for TiN and TiN/Ag surfaces. Furthermore, when the L. monocytogenes cells have adhered to a surface, it would be of great relevance to observe how easy they are removed from the surface in order to evaluate the effect of differences in nanoscale surface properties on listerial attachment. One of the most advanced methods for determination of attachment strength utilizes atomic force microscopy (AFM), that measures the strength of bacterial cell attachment to a surface, or the ease of removal from a surface, with high force resolu- tion [23–25]. Only limited studies have been done on attachment strength of L. monocytogenes by the use of AFM, and the strength of attachment of L. monocytogenes to TiN and TiN/Ag surfaces by use of AFM has, as yet, not been examined.

In this work, we have made a combined study of the initial adhesion rate and attachment strength of two L. monocytogenes strains to FPSS, TiN and TiN/Ag surfaces, as well as the anti-listerial properties of these surfaces.

2. Materials and methods

2.1. Preparation of fine polished stainless steel coupons

Fine polished stainless steel (SS 304) (Outo Kumpu, Sheffield, UK) was cut into coupons (7.5 cm × 3.5 cm) using a guillotine. The steel coupons were soaked and rinsed in acetone overnight, after which they were rinsed in 96% alcohol for 5 min. Finally, the steel coupons were rinsed with distilled water and air dried for 20–24 h.

2.2. Production of TiN and TiN/8.6 at.% Ag surfaces

Magnetron sputtering was used to produce nanocomposite TiN and TiN/Ag films on the stainless steel surfaces. Before magnetron sputtering, stainless steel coupons were cleaned using methanol and a clean fibre-free paper towel (Buehler, TEXMET® 1000, IL, USA), then dusted using a compressed air duster (Electrolube, Leicestershire, UK) to remove any remaining physical contaminants.

To produce the coatings a method was followed from a previously published article [16]. The sputtering rig used was a Teer Coatings UDP 350 magnetron sputtering system in a closed field unbalanced magnetic configuration. The chamber was pumped down until a vacuum below 1.1×10^{-3} Pa was achieved. Argon gas (99.99% purity) was introduced into the chamber using a mass flow controller (MKS Instruments, Altrincham, UK). The substrates were sputter cleaned by increasing the chamber pressure to 0.4 Pa and applying power to the substrate holder, 150 W 150 kHz for 10 min. Throughout the sputtering procedure the titanium target (99.95% purity) was driven with 1.5 kW pulse DC power with a 20 kHz pulse and the silver target (99.99% purity) with powers of 120 W to get silver concentrations in the deposited films. The sputter coating procedure took place at 0.24 Pa argon atmosphere with the nitrogen delivered for the nitride coating at 60% in relation to full metal signal using a reactive sputter controller following the optical emission signal of the titanium plasma. The samples were attached to the magnetron substrate holder (18 cm × 8 cm) using kapton tape (Agar Scientific, Essex, England). The substrate holder was placed in the magnetron sputtering chamber with the samples facing away from the titanium target and rotated at 16 rpm throughout deposition.

2.3. Characterization of solid surfaces

2.3.1. Energy dispersive X-ray spectroscopy (EDX)

The coatings were characterized in terms of structures and compositions using scanning electron microscopy (SEM – Zeiss Supra VP40) and energy dispersive X-ray spectroscopy (EDX – Edax, Trident Leicester, UK) using an EDAX Sapphire Si (Li) detector, and quantified using a standardless ZAF algorithm. The chemical composition was calculated as an atomic percentage (at.%), giving the percentage of the atom relative to the total number of atoms in the scan [26].

2.3.2. White light profilometry (WLP)

Images of the surface topography (x101) were taken using a MicroXAM (phase shift) surface mapping microscope (ADE corporation, XYZ model 4400 mL system) with an AD phase shift controller (Omniscan, Wrexham, UK). Analysis was carried out using extended range vertical scanning interferometry. The image analysis system used was MAPVIEW AE 2.17 (Omniscan, Wrexham, UK).

2.3.3. Atomic force microscopy (AFM)

Roughness parameters and images were obtained using an AFM (Explorer, Veeco Instruments, Cambridge, UK) operated in contact mode. Silicon nitride, pyramidal shaped tips with front and back angles of 35° were used for the topography measurements with a force constant defined by the manufacturer as 0.05 N/m. Averages of the roughness measurements were taken from replicate 5 /Lm × 5 /Lm samples using a scan rate of 20.03 /Lm/s. A pixel resolution of 300 was used.

2.3.4. Contact angle measurements

The hydrophobicity was indirectly measured by using the sessile drop technique. The surface hydrophobicity (Φ_{Giwi}) as described by van Oss (1995) was calculated based on contact angle measurements using a Goniometer (KRUSS GMBH, Hamburg, Germany), two polar solvents (HPLC grade water (BDH, UK) and formamide (Normapur, St Helens, UK) and one nonpolar solvent (1-bromonapthalene, Acros Organics, Belgium) (Table 1). Further details of the methodology and calculations can be found in Szlavik et al. [27]. Each contact angle value is based on six replicate measurements.

2.4. Strains and growth conditions

Two L. monocytogenes strains, EGDe and 64587/35 (strain 64), were used. EGDe is a commonly used laboratory strain obtained from Werner Goebel (Biozentrum) [28], whereas 64587/35 was isolated from processing equipment and obtained from Susanne Knøchel (University of Copenhagen, IFV) [29]. Each strain was

Table 1
Atomic surface composition (%) of FPSS, TiN and TiN/8.6 at.% Ag. Mean values (±standard deviation) are based on triplicate measurements on EDX.

Atomic (at.) composition (%)	FPSS	TiN	TiN/8.6at.%Ag
C	5.9 (±0.7)		
O	2.9 (±0.2)		
Si	0.6 (±0.1)		
Cr	16.6 (±0.6)		
Fe	63.5 (±0.9)		
Ni	10.5 (±0.0)		
Ti		62.9 (±0.9)	53.4 (±0.7) N
37.1 (±0.9)			32.0 (±0.4) Ag
8.6 (±0.1)			

maintained on Tryptone Soya Agar (TSA) (Oxoid) at 5 °C and inoculated into 100 mL Tryptone Soya Broth (TSB) (Oxoid). The strains were grown overnight (22 ± 1 h) at 37 °C with agitation (225 rpm). The cell culture was harvested by centrifugation (5000 rpm, 5 min) and washed once in 0.85% NaCl (Merck) or MilliQ water. The optical density at 600 nm (OD_{600}) was adjusted to 1.0.

2.5. Initial adhesion assay

2.5.1. Bacterial staining

Cells were stained by adding 3 /LL SYTO9 (LIVE/DEAD BacLight™ Bacterial Viability kit, Molecular Probes, Invitrogen) and 10 /LL glucose pr. mL cell suspension. The suspension was mixed thoroughly by vortexing and incubated at room temperature in the dark for 20 min. The stained cells were centrifuged (10 min, 5000 rpm) and suspended in 0.15 M NaCl to an OD_{600} of 0.1 ± 0.005. This OD value corresponded to a cell density of approx. 1.5×10^8 CFU/mL, as measured by cell counts on TSA of the stained cells. These data indicate that, although the cells were stained with the DNA binding dye SYTO9, they were viable (data not shown).

2.5.2. Flow perfusion system and fluorescence microscopy

The same setup and procedure as described by Skovager et al. [22] was used. In brief, CoverWell Perfusion chambers (622503, PC3L-0.5, CoverWell, Grace Bio-Labs, Inc) were glued (Super attach, Loctite, Henkel Norden AB) on the solid surfaces. Silicone tubes (Watson Marlow Alitea) were glued on the inlet (ID:1.6 mm; wall: 1.6 mm) and outlet (ID: 4.8 mm; Wall: 1.6 mm) of the perfusion chambers. The solid surface coupons with the perfusion chambers were placed under the fluorescence microscope (Axioscope, Carl Zeiss; lamp: TI 6A, Carl Zeiss) equipped with a digital camera (CoolSNAP, Photometrics), connected to a computer. The camera was controlled by the software RSImage (Photometrics). A 10× objective was used (Zeiss, Fluar, 10 × 0.50, ∞/0.17). The perfusion chamber, inlet and outlet, was connected to an inlet and outlet pump (Perimax 16/1, Spetec) via tubes (silicone, blue/blue, Dobbelpumpenschlauch, ID: 1.651 in., wall: 0.065 in.).

After activation of the pumps, the surface was focused in the middle of the chamber under the microscope and fluorescent images were captured after 30 s, 3 min, 5 min, 10 min, 15 min and 20 min of perfusion. For each image, cells were excited for 0.5–2 s (excitation filter BP450-490; dichroic filter FT510 and emission filter LP520) visualizing the green cells. For each strain and type of surface, three biological replicates were carried out on differ- ent surfaces. Wall shear stress was set to 0.10 Pa corresponding to a flow rate of 0.75 mL/min. Image analysis of adhered cells was determined by use of the software ImageJ (Free software, http://rsbweb.nih.gov/ij/) and calculation of initial adhesion rate (IAR) (cells/cm^2 min) was performed by linear regression (Excel, Microsoft Office 2007) [22].

2.6. Determination of cell attachment strength to surfaces by AFM

10 /LL of bacterial cell suspension were added to the test surfaces and dried on the surfaces for 1 h in a microbiological Class II safety hood at room temperature. The same principle, AFM, and tips as described by Verran et al. [25] and Whitehead et al. [17] was used for determination of strength of cell attachment to the test surfaces. For the strength of attachment measurements, the AFM was operated in contact mode. Before/after each experiment the spring constant of the cantilever was determined using AFM software. Using AFM, the measurements were carried out at a rate of 20.03 /Lm/s at a screen size of 10 /Lm × 10 /Lm.

The test surface, with dried cells, was positioned on the AFM. A dry scan of the sample was taken to ensure the presence of cells in the area of analysis. 100 /LL of HPLC water (BDH, UK) was placed on the sample. To determine the ease of cell removal, scans were carried out with increasing force applied to the cantilever tip. Following each scan the number of bacteria remaining on the surface was counted to indicate the additional detachment of cells from the surface with increased force. The number of bacteria remaining was calculated as a percentage of those present initially for each scan, to enable comparison between substrata. Each value of cells remaining on the surface was based on scans of three replicate surfaces.

A perpendicular measurement of the force applied to the cantilever was obtained from force distance curves. The cantilever deflection was converted to a force using Hooke's law. To determine the lateral force of the interaction of the cantilever tip with the cell, the methodology provided by Deupree and Schoenfish was used [24]. Each lateral force value was based on two force curves on triplicate surfaces.

2.7. Determination of antimicrobial activity of surfaces by LIVE/DEAD staining

10 /LL of cell suspension was dried on the test surfaces for 1 h. Hereafter, the cells were stained with 2 /LL of staining solution (10 /LL propidium iodide (PI) +40 /LL SYTO9 + 450 /LL water, LIVE/DEAD BacLight™ Bacterial Viability kit Molecular Probes – Invitrogen) for 5 min.

Cells were focused and visualized by Epifluorescence microscopy (Nikon Eclipse E600, Surrey, UK) using a 100× objective (Nikon Eclipse E600, Surrey, UK). The principle of live-dead staining is that all cells are stained with SYTO9, but cells with a damaged cell wall/dead cells are penetrated by and additionally stained with PI, giving a red colour in contrast to the green of live cells [30]. The coverage area of total cells (i.e. green cells) on the surface were observed using filter B2-A (510–560 nm), whereas the coverage area of dead cells (i.e. red cells) on the surface were observed using filter G2-A (590–650 nm). Subsequently, the dead cell coverage % was calculated. For the same field of view, two images were captured; i.e. one with each filter. Ten fields of view were examined per surface. Two repeated experiments were made per L. monocytogenes strain, with 3 replicates of each surface.

2.8. Statistical analysis

Statistical analysis of IAR and % dead cell coverage were carried out using one-way ANOVA, and multiple comparisons between groups were made using LSD (Least significant difference) test in the SAS software (SAS Institute, Inc.). Probabilities below 0.05 were considered significant.

Table 2
Surface properties of FPSS, TiN and TiN/8.6 at.% Ag. Surface parameters (electron acceptor parameter, γ_s^+; electron donor parameter, γ_s^-; Lifshitz-van der Waal component, γ_s^{LW}; hydrophobicity, ΔG_{iwi}) are calculated on the basis of six replicate surface contact angle measurements using three solvents (water, formamide and 1-bromonaphthalene) and are given as mean value ± standard deviation. Roughness parameters (arithmetic average height parameter, R_a; standard deviation of the z height, R_q) are given as mean values ± standard deviation of three replicate measurements on AFM.

Surface	Surface hydrophobicity parameters [mJ/m^2]				Roughness parameters (AFM) [nm]		Peak/valley features (WLP) [/Lm]	
γ_s^{LW}		γ_s^-	γ_s^+	ΔG_{iwi}	R_a	R_q	Depth (min − max)	Width (min − max)
FPSS	36.3 ± 3.7	2.6 ± 1.0	0.3 ± 0.4	−68.9 ± 10.4	5.6 ± 1.8	7.1 ± 2.4	0.0010–0.15	0.16–9.68
TiN	41.4 ± 1.4	38.9 ± 10.1	1.9 ± 0.9	11.4 ± 12.7	13.2 ± 3.5	16.9 ± 4.4	0.0012–0.18	0.16–7.90
TiN/8.6 at.% Ag	39.4 ± 2.8	57.2 ± 10.7	0.9 ± 1.2	39.2 ± 17.1	15.1 ± 7.9	25.3 ± 10.7	0.0015–0.18	0.16–6.61

3. Results

3.1. Solid surface chemistry

The TiN and TiN/8.6 at.% Ag surfaces were made by magnetron deposition. EDX was used to determine the chemical composition of the three surfaces. The three surfaces showed markedly different surface chemistry. The FPSS surface was composed of C (5.9%), O (2.9%), Si (0.6%), Cr (16.6%), Fe (63.5%) and Ni (10.5%). The surface composition of the FPSS, coated with Ti and N (TiN), was 62.9% Ti and 37.1% N. The surface composition of FPSS sputtered with Ti, N and Ag (TiN/8.6 at.% Ag) were 53.4% Ti, 32.0% N and 8.6% Ag (Table 1).

3.2. Physicochemical properties of solid surfaces

To characterize the physicochemical properties of the surfaces, mean contact angle measurements, when applying water, formamide and 1-bromonaphthalene, respectively, were performed on FPSS (93.3 ± 1.3°; 72.5 ± 3.2°; 35.4 ± 9.2°), TiN (28.3 ± 9.8°; 0.0 ± 0.0°; 20.8 ± 5.1°) and TiN/8.6 at.% Ag (16.6 ± 7.7°; 24.2 ± 9.9°; 39.4 ± 8.5°). The calculated surface components (Table 2) are based on these contact angle measurements. The γ_s^{LW} components of all three surfaces were determined to be in the same range. All surfaces had higher electron donating ($-\gamma_s^-$) than accepting ($-\gamma_s^+$) properties. The electron donating properties varied between the surfaces, where TiN/8.6 at.% Ag (57.2 ± 10.7 mJ/m^2) had the highest, and FPSS (2.6 ± 1.0 mJ/m^2) the lowest, electron donating capability (Table 2). The electron accepting properties of the different surfaces were in a similar low range (0.3–1.9 mJ/m^2) (Table 2). FPSS was considered to be partly hydrophobic (ΔG_{iwi}: −68.9 mJ/m^2), whereas TiN (ΔG_{iwi}: 11.4 mJ/m^2) and TiN/8.6 at.% Ag (ΔG_{iwi}: 39.2 mJ/m^2) were considered hydrophilic (van Oss, 1995) (Table 2).

3.3. Surface topography

The surface topography was examined by use of AFM and WLP (Fig. 1). The scratches in the FPSS were easy to visualize by use of AFM (Fig. 1A–C), and the topography differed markedly from the TiN and TiN/8.6 at%Ag surfaces. The TiN surface had a more evenly distributed granulated topography

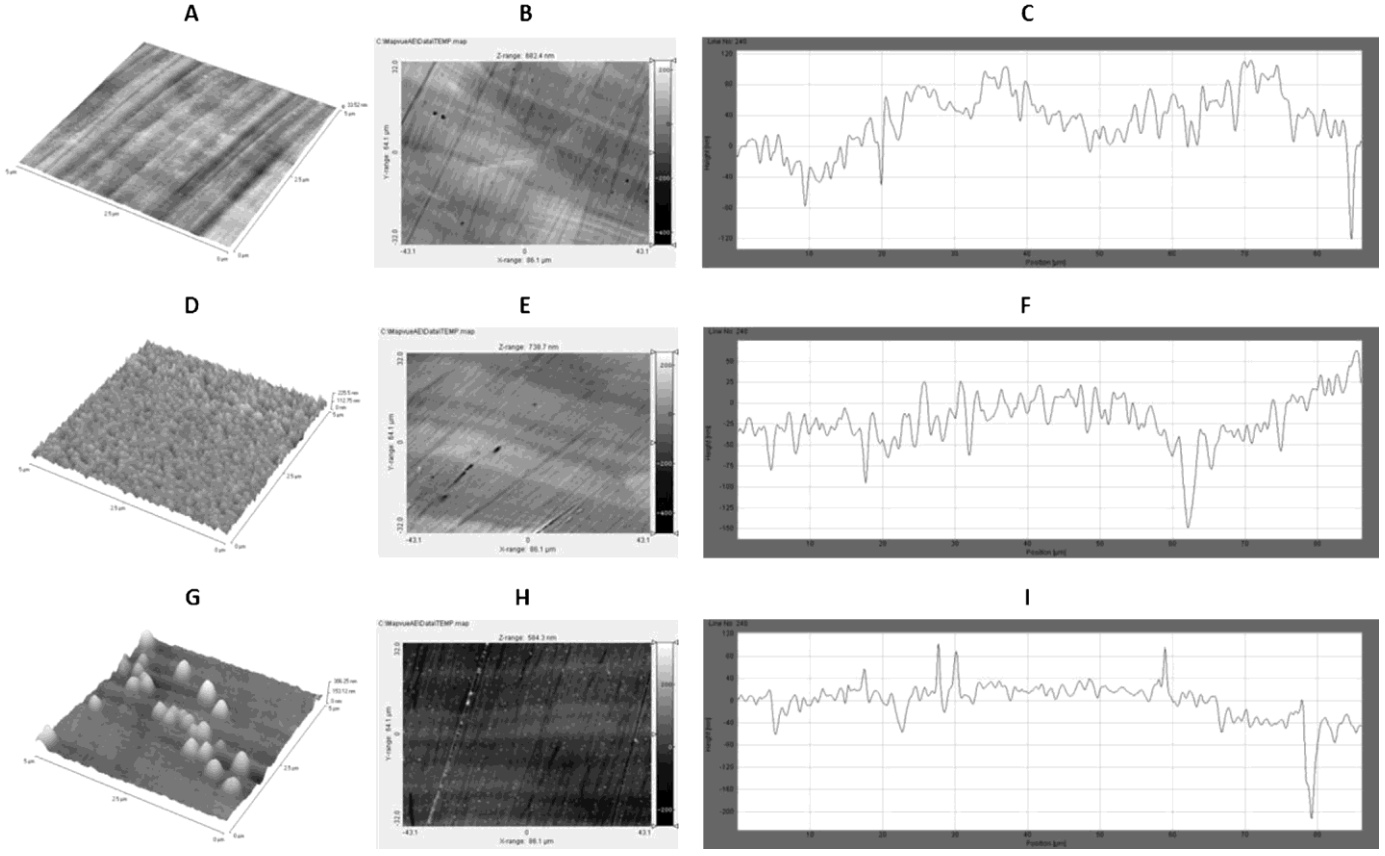

Fig. 1. 3D and 2D AFM images of FPSS (A and B), TiN (D and E) and TiN/8.6at.% Ag (G and H) demonstrating surface features. Line profiles of FPSS (C), TiN (F) and TiN/8.6 at. % Ag (I) based on white light profilometry (WLP).

(Fig. 1D). The TiN/8.6 at.% Ag surface had a topography similar to TiN (Fig. 1G), but small globules of Ag were present on the surface (small white dots in Fig. 1H). Furthermore, for FPSS, the size spans of the peak/valley depth (0.0010–0.15 /Lm) and width (0.16–9.68 /Lm) were smaller and larger, respectively, than those of TiN (0.0012–0.18 /Lm; 0.16–7.90 /Lm) and TiN/8.6 at.% Ag (0.0015–0.18 /Lm; 0.16–6.61 /Lm) surfaces (Table 2). Additionally, the roughness parameters (R_a and R_q) of FPSS (R_a: 5.6 ± 1.8 nm; R_q: 7.1 ± 2.4 nm) were markedly smaller than those of TiN (R_a: 13.2 ± 3.5 nm; R_q: 16.9 ± 4.4 nm) and TiN/8.6at%Ag (R_a: 15.1 ± 7.9 nm; R_q: 25.3 ± 10.7 nm) surfaces; the values of the two latter surfaces being in the same range (Table 2).

3.4. Initial adhesion of Listeria monocytogenes

Determination of real-time initial adhesion under flow conditions of the two different L. monocytogenes strains to the three different surfaces with different surface properties was possible by use of the method described by Skovager et al. [22]. It should be noted that it was necessary to use 0.15 M NaCl as solute, instead of water, due to auto-fluorescence of the surface.

Initial adhesion experiments showed that there was a tendency for the two L. monocytogenes strains (EGDe and 64) to adhere better to FPSS than to TiN and TiN/8.6 at.% Ag. This difference, however, was not significant ($p > 0.05$) (Table 3). For all three tested surfaces, strain 64 adhered better to all surfaces than strain EGDe (Table 3). High standard deviations were observed for IAR on TiN/8.6 at.% Ag surfaces, which may be due to uneven distribution of silver on the surface (Fig. 1G).

3.5. Attachment strength of L. monocytogenes strains

As the flow perfusion system used in the present study is a closed system, it was not possible to determine attachment strength by use of AFM directly after cells had adhered under flow conditions.

Table 3
Initial adhesion rates (IAR) [cell × 10^5/(min cm^2)] of two L. monocytogenes strains to fine polished stainless steel (FPSS), Titanium nitride (TiN) and Titanium nitride silver (TiN/8.6 at.% Ag) surfaces under flow conditions. Values with different capital letters in superscripts, within a row, were significantly different ($p < 0.05$). Values are means of three adhesion experiments (±standard error of the mean).

Initial adhesion rates (IAR) [cells × 10^5/(min cm^2)]			
Strain	FPSS	TiN	TiN/8.6 at.% Ag
EGDe	4.99 ± 0.19^{BA}	4.27 ± 0.12^{B}	4.27 ± 1.21^{B}
64	5.86 ± 0.19^{A}	5.55 ± 0.53^{A}	5.35 ± 0.69^{BA}

However, both L. monocytogenes strains dried on the surfaces under static conditions could be visualized by a dry AFM scan. Interestingly, when the FPSS was wetted and set point 0 was applied, no cells were observed on FPSS (data not shown), indicating that all cells were very easily removed from the FPSS, and that the attachment to FPSS was very weak. In contrast, both L. monocytogenes strains still attached to the TiN and TiN/8.6 at.% Ag surfaces after the first wet scan (set point 0/first run).

Observing triplicate surfaces (TiN or TiN/8.6 at.% Ag), the detachment of cells by increased lateral force (F_{lat}) varied considerably, resulting in large standard deviations (Fig. 2). It is assumed that this variation may be due to local variation in topography; charge distribution, and/or uneven charge distribution of the surface. Nevertheless, averaging the data from the three replicates gave a rough indication of the differences in attachment strength of the cells between the surfaces.

More EGDe cells were removed from the TiN/8.6at.% Ag sur- face compared to the TiN surface, when the same lateral force was applied (Fig. 2 A and C), indicating that the EGDe strain stuck less to silver containing surfaces than to surfaces without silver. Similar results were observed for strain 64 (Fig. 2B and D), although the difference was less pronounced.

The EGDe strain attached more strongly to TiN than strain 64 (Fig. 2A and B), when increased lateral forces were applied.

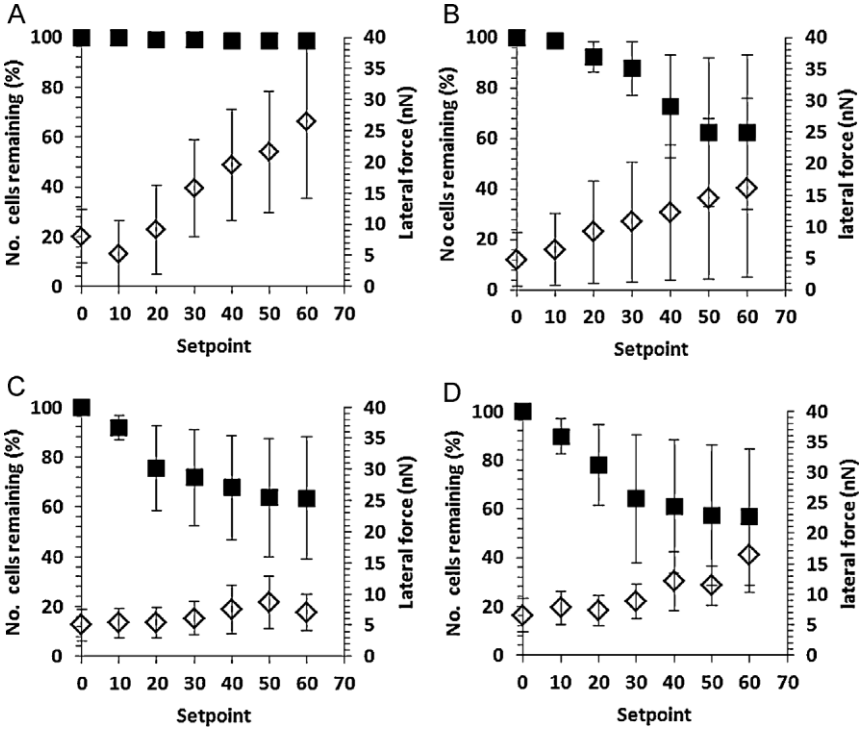

Fig. 2. Number of remaining cells (━) of L. monocytogenes strains EGDe (A and C) and 64587/35 (B and D) at increased lateral forces (♦) on TiN (A and B) and TiN/8.6 at.% Ag (C and D) surfaces. Each mean lateral force value for each set point/run is based on two force curves on triplicate surfaces. Each value of the cells remaining on the surface is based on triplicate surfaces. Error bars indicate standard error of the mean.

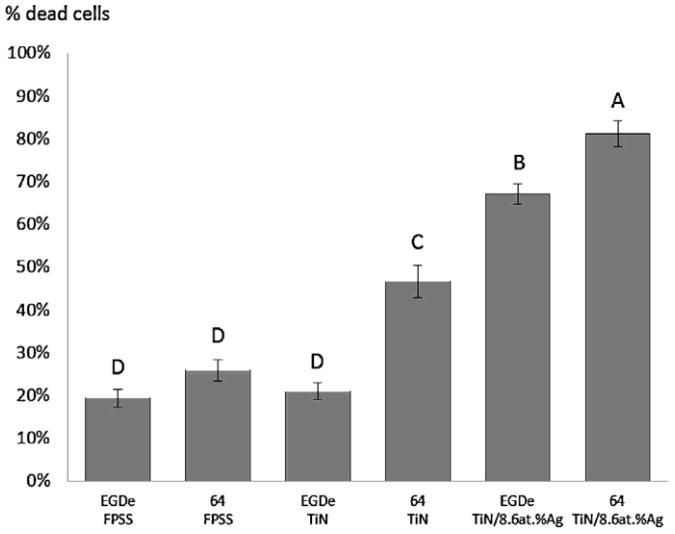

Fig. 3. Anti-listerial effect of FPSS, TiN and TiN/8.6 at. % Ag surfaces on L. monocytogenes strains EGDe and 64587/35 (64), measured by use of LIVE/DEAD BacLight™ Bacterial Viability kit. Mean dead cell coverage values [%] are based on two biological replicates on ten replicate images from triplicate surfaces. Error bars indicate standard deviations. Values with different capital letters were significantly different ($p < 0.05$).

Furthermore, slightly higher forces were applied to remove the same amount of 64 cells from the TiN/8.6 at.% Ag surface as compared with the removal of EGDe cells (Fig. 2C and D), suggesting that strain 64 attached better to TiN/8.6 at.% Ag than strain EGDe.

3.6. Antimicrobial activity of solid surfaces

The anti-listerial effect of the surfaces was determined by use of LIVE/DEAD backlight Viability kit on the different surfaces (Fig. 3). Although dead cells of both L. monocytogenes strains were observed on the FPSS surface (EGDe: 19.3 ± 2.0% dead cells; 64: 25.8 ± 2.4% dead cells), this surface possessed no marked anti-listerial activity as compared with the other two surfaces. This rather high level of dead cells on the FPSS may be due to the harvest of cells in the stationary growth phase and/or the drying of cells on the sur- face. The coverage of dead EGDe cells on TiN was not significantly different ($p > 0.05$) from that of the FPSS surface. However, significantly ($p < 0.05$) more dead cells of strain 64 (46.6 ± 3.8%) than of strain EGDe (20.9 ± 14.3%) were found on TiN. The TiN/8.6at.%Ag surface had a significantly ($p < 0.05$) higher antimicrobial effect on both strains (EGDe: 67.0 ± 2.4%; 64: 81.1 ± 3.1%) than TiN and FPSS, with strain 64 being the more susceptible strain.

4. Discussion

The process of bacterial adhesion to solid surfaces is often divided into two distinct phases: i.e. reversible and irreversible adhesion [24]. In this paper we define initial adhesion to be the reversible adhesion phase, that is the short period of time when a bacterium approaches and comes into contact with a surface by e.g. electrostatic and Lifshitz-van der Waals forces. Furthermore, we define attachment to be the irreversible adhesion phase, that is the phase where a bacterium strengthens its attachment to a surface by e.g. covalent and hydrogen bonding forces. It should be noted that adhesion of L. monocytogenes to solid surfaces might involve extracellular structures, such as flagella [31]. Since, however, L. monocytogenes only produces flagella at growth temperatures below 37 °C [31], this phenomenon is not considered to be of any importance in the present study.

The surface material of food processing equipment may be the first line of defence against contamination of foods, by providing, first, inhibition of initial adhesion, and subsequently a decrease in attachment strength (or retention) of adhered bacteria, and finally antibacterial activity towards attached bacteria. Many studies have included one or two of these phenomena in combination [11,16,17,32–35], but combined, and thus comparative, studies of all three phenomena seem to be lacking. This study is the first of its kind to use all three of these approaches to characterize the interactions between L. monocytogenes and FPSS, TiN and TiN/8.6% Ag surfaces.

Both silver and titanium nitride surfaces influence initial adhesion and retention of various bacteria [11,17,32,36]. For example, silver coatings reduce the adhesion of Escherichia coli, P. aeruginosa and S. aureus to orthopaedic external fixation pins, whilst the opposite is seen for Staphylococcus haemolyticus [36]. In the present study, we have demonstrated that TiN and TiN/8.6 at.% Ag, as compared with FPSS, have a tendency to decrease the initial adhesion under flow conditions of two foodborne pathogenic L. monocytogenes strains (EGDe and 64). This difference, however, is not significant, thereby suggesting that the flow conditions and the strain specificity may be more important than the surface characteristics for determining adhesion under flow conditions. Katsikogianni and Missirlis [37] also found that increasing shear rates might decrease the predictability of adhesion of S. epidermidis in relation to the thermodynamic theory of adhesion.

It is well known that initial adhesion of L. monocytogenes to solid surfaces is strain dependent [4,22,38,39]. This phenomenon was also observed for all the surfaces investigated in the present study; i.e. strain 64 adhered better to all three surfaces than strain EGDe. The strain dependency could be due to different surface characteristics of the two different L. monocytogenes strains [22]. Strain EGDe has a significantly larger cell size, less hydrophobic characteristics, and more electron donating properties than strain 64 [22]. All three solid surfaces in the present study have more electron donating than accepting properties (Table 2), and thus more repulsive interactions may occur between EGDe and the surfaces.

In the present study, both L. monocytogenes strains readily detach from the FPSS surface, but not from the TiN and TiN/8.6 at.% Ag surfaces, upon contact with water. Most interestingly, these results indicate that under wet conditions, FPSS may be preferred over the two other surfaces as to detachment of adhered L. monocytogenes cells. Despite the lower roughness values (R_a and R_q) of FPSS (Table 2), as compared with TiN and TiN/8.6 at.% Ag surfaces, this observation may be due to the bigger peak/valley width span of FPSS, resulting in a poorer fit of the single cells in the valleys and thus smaller cell-surface contact area, whereby less attractive interactions may occur [34]. Furthermore, when water (hydrophilic) is added, partly hydrophobic repulsive interactions may occur with the FPSS surface, and the water may more easily withdraw the cells from the FPSS surface than from the hydrophilic TiN and TiN/8.6 at.% Ag surfaces.

Both L. monocytogenes strains attach more strongly to TiN than to TiN/8. at.% Ag surfaces. The difference was, however, more pronounced for strain EGDe (Fig. 2). Similar results were also observed for S. aureus, when comparing attachment strengths to TiN and TiN/16.7 at.% Ag surfaces [17]. Differences in attachment strength may be due to differences in surface topography. Increased silver content does not change the roughness parameters (R_a and R_q) markedly (Table 2), but results in an increased size and height of surface nanotopographies, where the features become larger and more rounded [13,21]. The L. monocytogenes cells may therefore have more difficulty in aligning and fit into the dimensions of the surface fractures of TiN/8.6 at.% Ag, resulting in weaker attachment due to less contact area between the cells and the surface. Furthermore, the more electron donating (γ_s^-) properties of TiN/Ag

surfaces found in the present study (Table 2) may result in more repulsive interactions with the electron donating L. monocytogenes strains. Finally, the much more hydrophilic TiN/8.6 at.% Ag surface (Table 2) may to a higher extent repel the more hydrophobic L. monocytogenes cells, resulting in weaker attachment.

The attachment strength of L. monocytogenes to stainless steel, when applying different shear stress in a radical flow chamber, has previously been found to be strain dependent [4]. Differences in attachment strength to TiN and TiN/16.7 at.% Ag, using AFM, have been found at species level between P. aeruginosa and S. aureus, where attachment of S. aureus was stronger than for P. aeruginosa [17]. In the present study, the average attachment strength of L. monocytogenes was found to be strain dependent (Fig. 2). The less hydrophobic EGDe strain [22] retains better to the hydrophilic TiN than the more hydrophobic strain 64, whereas the less elec- tron donating strain 64, compared to strain EGDe, attaches in a marginally higher number to the TiN/8.6 at.% Ag surface possessing the highest electron donating capabilities. Additionally, the dimen- sions of the bacterial cell as well as the topographical dimensions influence retention [23,35]. Previously, it has been found that the smaller S. aureus cells were better retained on the smaller nanoto- pographical features of TiN surfaces, whilst the larger P. aeruginosa cells attached better to the rougher surface with larger grain size of TiN/Ag4.6% and TiN/Ag16.7% [17]. This agrees with our findings that the larger cell size of EGDe may be better attached within the big- ger valley width span of TiN, whereas the smaller 64 strain may fit better to the smaller valley with span of the TiN/8.6 at.% Ag surface.

Both Ag and TiN/Ag surfaces are known to possess antimicrobial properties [10–12,14–17]. However, the bacteriostatic or bacteri- cidal effect of silver may depend on the size and shape of the silver particles as well as their distribution density in the surrounding matrix [16]. Force modulation (FM) indicated that the silver forms heterogeneous islands within the TiN matrix, which may influence the antimicrobial properties of TiN/Ag surfaces [21]. An increase in silver concentration of TiN/Ag coatings was found to alter both the surface topography and the physicochemistry as well as the antimi- crobial properties against S. aureus [10,16]. To date, the anti-listerial effects of TiN and TiN/Ag surfaces have not been determined. We find a clear anti-listerial effect of TiN/8.6 at.% Ag for both L. mono- cytogenes strains (Fig. 3). Therefore, from an anti-listerial point of view, TiN/8.6 at.% Ag surfaces are preferable over FPSS and TiN sur- faces.

Strain 64 is more susceptible to the TiN/8.6 at.% Ag surface than the EGDe strain, which could be due to the fact that strain 64 attaches better than strain EGDe to the TiN/8.6 at.% Ag surface, thereby being in closer contact with the antimicrobial silver. More- over, the smaller cell size of strain 64 may enhance the cell-surface contact area to the anti-microbial silver. Surprisingly, strain 64 is also slightly susceptible to TiN surfaces. In general, Ti and N are not considered anti-microbial, and future studies are required to eluci- date this observation. It should be noted, however, that PI-stained cells are cells with damaged cell membranes that may still be able to recover, as observed for P. aeruginosa in contact with primarily TiN surfaces [16].

In conclusion, the three solid surfaces investigated in this study possess different chemical composition, physicochemical proper- ties and topographical features, which influence both attachment strength and antimicrobial properties, but not initial adhesion. The initial adhesion, attachment strength, and anti-listerial effect are strain dependent, probably due to different surface characteristics of the two strains. Although the two L. monocytogenes strains adhere to all three surfaces, our results suggest the preference of FPSS over TiN and TiN/Ag as a food contact material under wetted condi- tions, as the two strains under these conditions are fully removed from this surface. However, FPSS possesses no marked anti-listerial properties. The TiN/Ag surface is clearly more anti-listerial than the

TiN surface, and in combination with the fact that the attachment strength of L. monocytogenes cells to TiN/Ag seem lower than to TiN, these data indicate its potential use as food contact material under dry conditions.

Acknowledgements

This work was supported by the Danish Research Council for Technology and Production Science, grant no. 274-08-0291. We would like to thank Professor Susanne Knøchel for providing L. monocytogenes strains for the study.

References

[1] V. Velusamy, K. Arshak, O. Korostynska, K. Oliwa, C. Adley, Biotechnol. Adv. 28 (2010) 232.
[2] A. Lianou, J.N. Sofos, J. Food Prot. 70 (2007) 2172.
[3] S. Doijad, S.B. Barbuddhe, S. Garg, S. Kalekar, J. Rodrigues, D. D'Costa, S. Bhosle, T. Chakraborty, Food Control 22 (2011) 1900.
[4] S. Perni, T.G. Aldsworth, S.J. Jordan, I. Fernandes, M. Barbosa, M. Sol, R.P. Ten- reiro, L. Chambel, I. Zilhão, B. Barata, A. Adrião, M. Leonor Faleiro, P.W. Andrew, G. Shama, Int. J. Food Microbiol. 116 (2007) 384.
[5] I.M.M. Silva, R.C.C. Almeida, M.a.O. Alves, P.F. Almeida, Int. J. Food Microbiol. 81 (2003) 241.
[6] B. Gudbjörnsdóttir, M.-L. Suihko, P. Gustavsson, G. Thorkelsson, S. Salo, a.-M.
Sjöberg, O. Niclasen, S. Bredholt, Food Microbiol. 21 (2004) 217. [7] D.S. Rickerby, R.B. Newbery, Vacuum 38 (1988) 161.
[8] P. Kelly, R. Arnell, Vacuum 56 (2000) 159.
[9] J. Musil, P. Karvankova, Surf. Coat. Technol. (2001) 101.
[10] P.J. Kelly, H. Li, P.S. Benson, K.A. Whitehead, J. Verran, R.D. Arnell, I. Iordanova, Surf. Coat. Technol. 205 (2010) 1606.
[11] A. Scarano, M. Piattelli, G. Vrespa, S. Caputi, A. Piattelli, J. Oral Implantol. 29 (2003).
[12] B. Groessner-Schreiber, M. Hannig, A. Dück, M. Griepentrog, D.F. Wenderoth, Eur. J. Oral Sci. 112 (2004) 516.
[13] K.A. Whitehead, T. Deisenroth, A. Preuss, C.M. Liauw, J. Verran, Colloids Surf. B: Biointerfaces 82 (2011) 483.
[14] H. Jiang, S. Manolache, A.C.L. Wong, F.S. Denes, J. Appl. Polym. Sci. 93 (2004)
1411.
[15] E.A. Araújo, N.J. Andrade, L.H.M. da Silva, P.C. Bernardes, A.V.N. de, C. Teixeira, J.P.N. de Sá, J.F.Q. Fialho, P.E. Fernandes, J. Food Prot. 75 (2012) 701.
[16] P.J. Kelly, H. Li, K.A. Whitehead, J. Verran, R.D. Arnell, I. Iordanova, Surf. Coat.
Technol. 204 (2009) 1137.
[17] K.A. Whitehead, H. Li, P.J. Kelly, J. Verran, J. Adhes. Sci. Technol. 25 (2011) 2299. [18] J.R. Morones, J.L. Elechiguerra, A. Camacho, K. Holt, J.B. Kouri, J.T. Ramírez, M.J.
Yacaman, Nanotechnology 16 (2005) 2346.
[19] M. Rai, A. Yadav, A. Gade, Biotechnol. Adv. 27 (2009) 76.
[20] E. Chadeau, N. Oulahal, L. Dubost, F. Favergeon, P. Degraeve, Food Control 21 (2010) 505.
[21] K.A. Whitehead, P. Kelly, H. Li, J. Verran, J. Vac. Sci. Technol. B: Microelectron.
Nanometer. Struct. 28 (2010) 180.
[22] A. Skovager, K.A. Whitehead, H. Siegumfeldt, H. Ingmer, J. Verran, N. Arneborg, Int. J. Food Microbiol. 157 (2012) 174.
[23] K.A. Whitehead, D. Rogers, J. Colligon, C. Wright, J. Verran, Colloids Surf. B: Biointerfaces 51 (2006) 44.
[24] S.M. Deupree, M.H. Schoenfisch, Langmuir 24 (2008) 4700.
[25] J. Verran, A. Packer, P.J. Kelly, K.a. Whitehead, J. Adhes. Sci. Technol. 24 (2010)
2271.
[26] D.J. Wickens, G. West, P.J. Kelly, J. Verran, S. Lynch, K.A. Whitehead, Int. J. Artif.
Organs 00 (2012) 1.
[27] J. Szlavik, D.S. Paiva, N. Mørk, F. van den Berg, J. Verran, K. Whitehead, S. Knøchel, D.S. Nielsen, Int. J. Food Microbiol. 152 (2012) 181.
[28] M.H. Larsen, B.H. Kallipolitis, J.K. Christiansen, J.E. Olsen, H. Ingmer, Mol. Micro- biol. 61 (2006) 1622.
[29] M. Harmsen, M. Lappann, S. Knøchel, S. Molin, Appl. Environ. Microbiol. 76 (2010) 2271.
[30] Molecular-Probes, Molecular Probes Inc., (2004).
[31] S. Vatanyoopaisarn, A. Nazli, C.E. Dodd, C.E. Rees, W.M. Waites, Appl. Environ.
Microbiol. 66 (2000) 860.
[32] M. Hjelm, L.R. Hilbert, P. Møller, L. Gram, J. Appl. Microbiol. 92 (2002)
903.
[33] K.A. Whitehead, J. Colligon, J. Verran, Colloids Surf. B: Biointerfaces 41 (2005)
129.
[34] K.A. Whitehead, J. Verran, Food Bioprod. Process. 84 (2006) 253.
[35] J. Verran, A. Packer, P. Kelly, K.A. Whitehead, Int. J. Food Microbiol. 141 (Suppl) (2010) S134.
[36] M.A. Wassall, M. Santin, C. Isalberti, M. Cannas, S.P. Denyer, J. Biomed. Mater.
Res. 36 (1997) 325.
[37] M.G. Katsikogianni, Y.F. Missirlis, J. Mater. Sci. 21 (2010) 963.
[38] R. Gamble, P.M. Muriana, Appl. Environ. Microbiol. 73 (2007) 5235. [39] N.I.A. Silva, P. Teixeira, J. Food Prot. 71 (2008)
1379.